(73)

Seasonal Measurements of Nonmethane Hydrocarbons (NMHC) in a Sub-tropical Evergreen Forest in Southern China

by

John. J. Graham, Jr.

A.B. Chemistry
Harvard University, 1991

Submitted to the
Department of Earth, Atmospheric and Planetary Sciences
in partial fulfillment of the requirements
for the degree of

Doctor of Philosophy
in Atmospheric Science

at the

Massachusetts Institute of Technology
June 1998

Signature of Author: _____

Department of Earth, Atmospheric and Planetary Sciences
May 1, 1998

Certified by: _____

Ronald G. Prinn
TEPCO Professor of Atmospheric Chemistry
Thesis Supervisor

Accepted by: _____

Thomas Jordan
Head, Department of Earth, Atmospheric and Planetary Sciences

Seasonal Measurements of Nonmethane Hydrocarbons (NMHC) in a Sub-tropical Evergreen Forest in Southern China

by

John J. Graham, Jr.

Submitted to the Department of Earth, Atmospheric and Planetary Sciences
on May 1, 1998 in Partial Fulfillment of the Requirements
for the Degree of Doctor of Philosophy in
Atmospheric Science

ABSTRACT

Terrestrial ecosystems have long been recognized as important sources of reactive hydrocarbons. One ecosystem type that has not previously been investigated is the subtropical evergreen forest category found in Southern China. To begin a study of this ecosystem, we conducted two campaigns. First, bi-monthly air samples were collected in stainless steel canisters over a 15 month period at Dinghushan Biosphere Reserve (DHSBR) in Guangdong, China and analyzed at MIT using capillary gas chromatography with flame ionization detection. DHSBR is both mountainous and covered 79% by forest and experiences hot, wet summers and cool, dry winters. Much of the dominant subtropical vegetation in DHSBR is representative of the natural vegetation in a vast area of interior Southern China (23-32° N, 100-120° E), while the occasional tropical vegetation is representative of the natural vegetation of coastal Southern China. Seasonal variations in both isoprene and terpene concentrations were observed at DHSBR. Maximum isoprene mole fractions reached 7 ppb in the late summer afternoon compared to wintertime maximums of 0.1 ppb. Second, an in situ study was conducted during the summer of 1996. In addition to hourly NMHC samples, measurements of carbon monoxide (CO), nitrogen oxides (NO_X), Photosynthetically Active Radiation (PAR), temperature, relative humidity, wind velocity and daily rainfall were recorded. A study using a vegetation enclosure was also performed in order to estimate NMHC emissions from the individual major tree species in the forest reserve. The resulting isoprene emission estimate for this ecosystem was 8.6 ± 6.1 mg C m^{-2} h^{-1}. Using these measurements, we have assessed the sensitivity of the emissions of isoprene to environmental variables and ecosystem speciation and the importance of these emissions to regional photochemistry. Estimates of atmospheric hydroxyl radical concentrations were made from the observed decay of reactive hydrocarbons, yielding $5.7 \pm 2.8 \times 10^6$ molecules cm^{-3}. Measurement of many hydrocarbons in addition to CO, NO_X and wind information allowed identification of several characteristic air mass types observed during the in situ campaign.

Thesis Supervisor: Ronald G. Prinn
Title: TEPCO Professor of Atmospheric Chemistry

Acknowledgments

First and foremost I wish to thank my advisor Ron Prinn for providing me with the resources necessary to complete this thesis. I was given a high degree of freedom in my research, which enabled me to mature as a scientist at my own pace, learning and growing from mistakes along the way. Thank you for your patience Ron!

Second, I salute my Chinese colleagues for their assistance and perseverance throughout the process. Professors Huang Zhongliang, Kong Guohui, Wang Gengchen and Wang Mingxing each contributed significantly to my work. More important still is Bai Juanhui. Without his friendship and hard work I would have been lost.

A significant part of my education came through interactions with other students here at MIT. My labmates and officemates Gary Kleiman, Stephanie Shaw and Jin Huang all contributed to my experience as friends and colleagues. And how could I forget my only summer UROPer Deborah Rhodes. In addition, I want to thank the support staff: Linda Kubrick, Mark Pendleton and Anne Slinn.

Equally important are the many people who helped keep my life in perspective and enriched the non-academic part of my stay at MIT. Rosario and Jesse, Jeff and Brett: thank you for your support and for putting up with my very occasional fits of insanity.

Finally, I want to thank my family for their encouragement and support. In particular, John saw to the day to day. I really did finish this time mom, honestly!

In memory of
Lunetta Churchill McMore

Table of Contents

List of Figures

List of Tables

Chapter 1: Introduction

1.1 Preface

In the past several decades, atmospheric science has enjoyed a boom, fueled in part by heightened public awareness of several environmental issues. Concerns over such problems as changing climate, greenhouse gases, the stratospheric ozone hole, photochemical smog and deforestation of rain forests have spurred much interest in the chemistry of the earth's atmosphere. Scientists have noted that trace gas concentrations including methane, carbon monoxide and nitrous oxide are rising. Man has been implicated in this atmospheric change since the trends have their origins in the beginning of the industrial revolution of the last century. We have impacted the trace gas budget significantly through deforestation, biomass burning, land use changes including planting crops and using nitrogen based fertilizers and any number of industrial activities. One primary issue with the increase of trace gases concerns the oxidizing capacity of the atmosphere. If this change causes a decrease in the oxidizing capacity, the atmosphere will lose the ability to attack and destroy substances released to it. This would be particularly important for stratospheric ozone as more Hydrochlorofluorocarbons (HCFCs) would reach the stratosphere and for climate as the methane lifetime would increase.

We must attempt to understand the complex chemistry of the atmosphere so that we may know how our continued influence will contribute to the ever-present changes in the air above us. As a first step, we need to break down the chemistry into manageable parts, focusing on individual pieces of the puzzle. Then we may put things back together to get a picture of the broad scheme. Scientists have therefore looked at individual and grouped gases for this purpose including nitrogen oxides (NO_x), ozone (O_3), carbon monoxide (CO), carbon dioxide (CO_2), methane (CH_4), sulfur gases, and non-methane hydrocarbons (NMHC) to name some of the important species of interest.

They have also investigated specific regions over the globe since regional variations are very substantial. This thesis provides results and interpretation of an observational study in an ecosystem type and region never previously investigated. It focused on biogenic hydrocarbons but included anthropogenic NMHC, CO and NO_x.

1.2 Biogenic Nonmethane Hydrocarbons

1.2.1 Impacts of Biogenic NMHC on Tropospheric Chemistry

In this thesis I chose to focus on the tropospheric chemistry of NMHC, particularly those derived from biogenic sources. These compounds play a significant role in shaping the composition of the troposphere. Measurements in Europe show from 11% to 34% of total NMHC in the atmosphere are due to natural processes (Anastasi et al., 1991). Fehsenfeld et al. (1992) and Altshuller (1983) estimate that roughly 60% of NMHC emitted in the US are from natural sources. The mix of compounds varies greatly between anthropogenic and natural emissions, and the reactivities of the mixes differ. Although these northern hemispheric areas have been studied in greatest detail, they do not constitute the greatest source regions for natural NMHC emissions in the world. That distinction belongs to the tropics. Guenther et al. (1995) report tropical woodlands account for half of all natural volatile organic compound (VOC) emissions. Additionally, natural emissions are highly weighted toward the summer months (Yokouchi et al., 1983; Jobson et al., 1994; Goldstein et al., 1995). Therefore, we expect that during the high emission summer months natural emissions will play a particularly important part in tropospheric chemistry.

Many areas of atmospheric chemistry are affected by these natural compounds: tropospheric ozone levels, OH radical concentrations, CO concentrations, organic nitrate reservoirs and organic aerosols. A complex relationship exists between ozone and natural NMHC in the troposphere centering around levels of NO_x. Depending on the particular circumstance, NMHC can act as net sources or sinks for ozone (Peterson and Tingey, 1980). Ozonolysis of alkenes like isoprene and terpenes acts as a sink but in the

presence of sufficient NO_x, the interaction is such that a net production of ozone occurs. When NO_x concentrations are roughly 4-7 parts per billion (ppb), model results predict a doubling of ozone concentrations from 50 to 100 ppbv with inclusion of natural NMHC chemistry versus the base case with only anthropogenic NMHC (Trainer et al., 1987). Jacob and Wofsy (1988) report that vegetative NMHC emissions in the tropics account for increased canopy ozone levels of 30-40 ppbv. Other predictions of NMHC effects on ozone concentrations range from 10-30 percent increases over levels where natural emissions are not included (Mackenzie et al., 1991; Lopez et al., 1987; McKeen et al., 1991). Roberts et al. (1983) and Altshuller (1983) find that NMHC have a minimal effect on ozone production in the troposphere. It is agreed that NO_x levels must be above a threshold for ozone production to occur. Otherwise, the RO_2 radicals will react with themselves instead of converting NO to NO_2. The photolysis of NO_2 results in a $O(^3P)$ which may combine with molecular oxygen to form ozone. Self-reaction of RO_2 also serves to suppress OH radical concentrations which would be produced by the $NO + RO_2$ reaction.

Oxidation of NMHC also influences OH radical concentrations (Darnall et al., 1976; Robinson 1978; Logan et al., 1981; Kasting and Singh, 1986) . OH reacts with all alkanes in addition to other hydrocarbon species like alkenes which also have appreciable reactions rates with ozone. Increases in NMHC concentration in the atmosphere may lead to decreases in OH and thereby decrease the atmosphere's capacity to oxidize other compounds (Fehsenfeld et al., 1992, Young et al., 1997). This oxidation by OH helps to clean the atmosphere. NMHC also affect the concentration of OH indirectly through CO. Eventually, NMHC may end up as CO which is a significant sink for OH radical (Zimmerman et al., 1978; Cofer et al., 1982; Gregory et al., 1986; Hatakeyama et al., 1991). Hatakeyama et al. (1991) estimate that CO production from NMHC equals that derived from methane and exceeds that from fossil fuel combustion. They estimate that 25% of tropospheric CO is derived from the oxidation of NMHC. With its high atmospheric concentrations, CO serves to control OH levels in the

atmosphere. When model chemistry included isoprene oxidation, it was found that CO levels increased by 10 and 31% for latitudes 45° N and 15° N respectively (Fehsenfeld et al., 1992). Jacob (1988) found that isoprene degradation in the tropics enhanced CO levels by 20 to 70 ppb.

Many have investigated the potential for increased aerosol concentration due to tropospheric reactions of biogenic hydrocarbons since aerosols influence the radiation budget both directly and through their role as cloud condensation nuclei. Most found that the levels of organic aerosols are detectable but insignificant, on the order of 1% of the aerosol loading (Yokouchi and Ambe, 1985; Shaw et al., 1983; Altshuller 1983). Nonetheless, Hoffmann et al. (1997) find high potential aerosol yields from monoterpenes and point to sesquiterpenes as being important for further analysis. Fehsenfeld et al.(1992) state that significant levels of aerosol derived from terpene oxidation could contribute to background haze with sufficiently high terpene concentrations. These findings are echoed by other researchers as well (Hatakeyama et al., 1989; 1991; Pandis et al., 1991).

In addition, hydrocarbons may react to form organic nitrates like peroxyacetyl nitrate (PAN) which acts to store NO_x and transport it over large distances (Aiken et al., 1982; Brewer et al., 1983; Lopez et al., 1989; Grosjean et al., 1992). This interaction creates problems for those trying to control ozone levels by limiting local NO_x emissions. Hydrocarbons can also have an effect on the nitrogen budget through the reaction of isoprene and NO_3 which is especially important at night (Skov et al., 1992). Furthermore, organic acids may be produced as a result of the atmospheric chemistry of NMHC yielding acidic rainfall (Jacob and Wofsy, 1988; Kotzias et al., 1990; Hov et al., 1991; Hoffmann et. al., 1997).

Other negative impacts have been noted by Moller (1988) and Juttner (1986), claiming pollution from tropospheric hydrocarbon reactions results in forest damage in Germany. Hov et al. (1989) mention that NMHC act as greenhouse gases but their concentrations compared to methane are small so this effect is negligible. Perhaps a

positive reaction of hydrocarbons, especially in the lower stratosphere, is the scavenging of chlorine (Greenberg and Zimmerman, 1984; Rinsland et al., 1987). The chlorine abstraction of a hydrogen is an order of magnitude faster than OH but its concentration in the troposphere is 1000 times less. Even so, modeling efforts by Singh and Kasting (1988) show that as much as 40% of NMHC oxidation in the troposphere and 90% of NMHC oxidation in the stratosphere (10-20 km) is caused by Cl atoms. Once in the lower stratosphere, the importance of the chlorine reaction overtakes that of OH. One final point that Enhalt et al. (1985) and Greenberg et al. (1990) make deals with using hydrocarbons as tracers for vertical motion. Specifically, short-lived hydrocarbons in the upper troposphere signal fast vertical motions have taken place.

In summary, vegetative NMHC emissions may significantly impact the chemistry of the troposphere primarily through complex interactions with ozone and OH. Model results predict that isoprene oxidation in particular may decrease OH atmospheric levels by a factor of 5 for low NO_x conditions, which could affect the local lifetimes of almost all other reactive species (Fehsenfeld et al. 1992). Nitrate, aerosol and CO budgets may all be influenced by the presence of vegetative NMHC.

1.2.2 Literature Survey of Recent NMHC measurements

While searching the literature, it became apparent that some regions of the globe have received less attention than others. Our interests lie primarily in natural contributions of hydrocarbons to the atmosphere and therefore to remote areas versus urban ones. Many authors have demonstrated that natural emissions are governed by such factors as light intensity and temperature (Arnts et al., 1981; Yokouchi and Ambe, 1984; Juuti et al., 1990; Fehsenfeld et al., 1992). Other important factors include season, relative humidity, wind speed and type and age of vegetation. Based on this knowledge, it seems reasonable to break observations down by ecological region. Table 1.2.1 shows this. It represents much of the recent work done in NMHC measurements by the major scientific groups across the globe. This review is not exhaustive but studies not listed here are primarily concentrated in the United States or in urban areas.

Figure 1.2.1 Times Atlas of the World Vegetation Type Classification

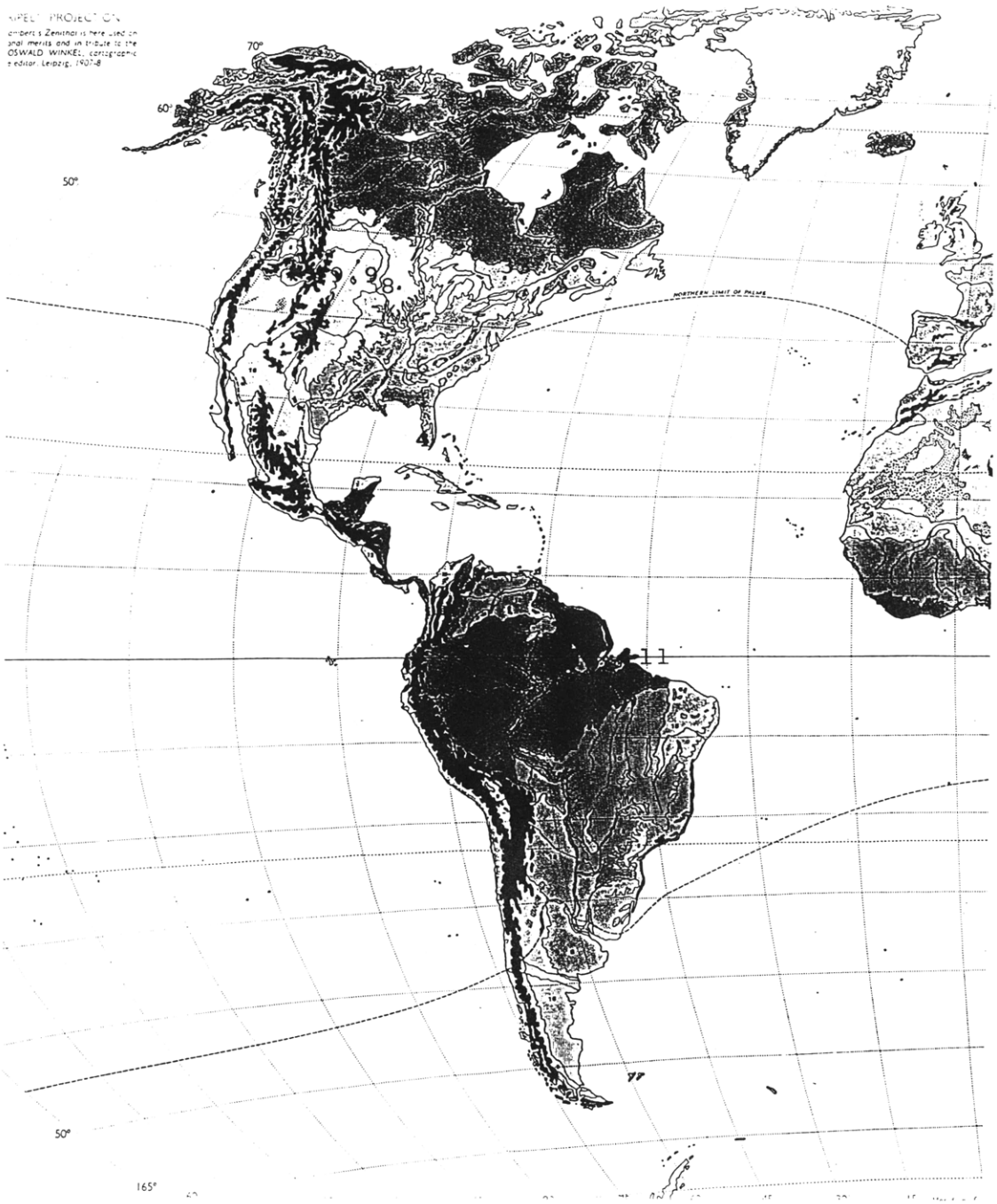

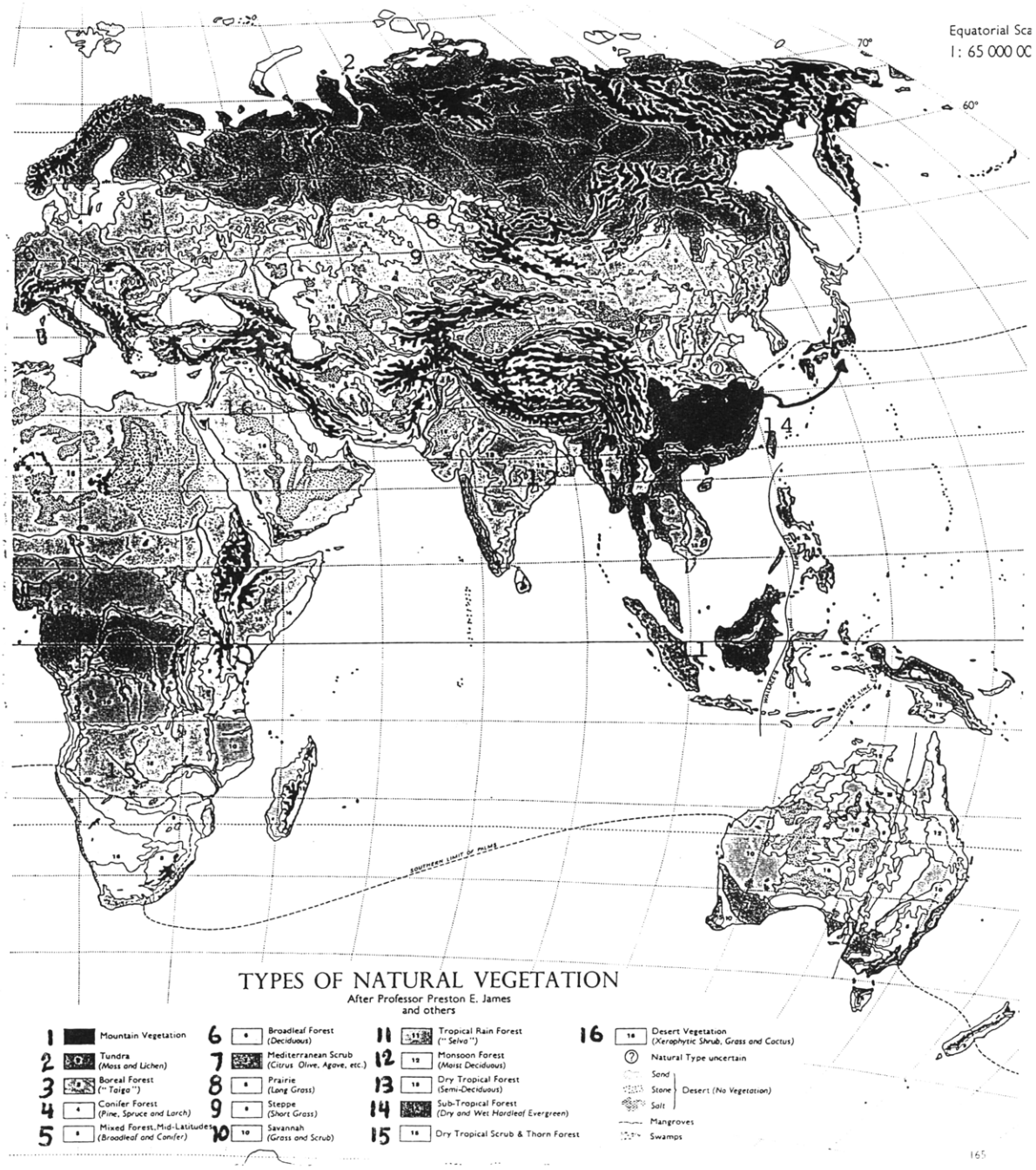
Equatorial Sca
1: 65 000 00
70°
60°
TYPES OF NATURAL VEGETATION
After Professor Preston E. James
and others
1 Mountain Vegetation
2 Tundra (Moss and Lichen)
3 Boreal Forest (" Taiga ")
4 Conifer Forest (Pine, Spruce and Larch)
5 Mixed Forest, Mid-Latitudes (Broadleaf and Conifer)
6 Broadleaf Forest (Deciduous)
7 Mediterranean Scrub (Citrus Olive, Agave, etc.)
8 Prairie (Long Grass)
9 Steppe (Short Grass)
10 Savannah (Grass and Scrub)
11 Tropical Rain Forest (" Selva ")
12 Monsoon Forest (Moist Deciduous)
13 Dry Tropical Forest (Semi-Deciduous)
14 Sub-Tropical Forest (Dry and Wet Hardleaf Evergreen)
15 Dry Tropical Scrub & Thorn Forest
16 Desert Vegetation (Xerophytic Shrub, Grass and Cactus)
? Natural Type uncertain
Sand
Stone
Salt
Desert (No Vegetation)
Mangroves
Swamps
165

Table 1.2.1 Summary of NMHC measurements performed over the past two decades grouped by vegetation type. Listed are detection method, column used and species reported.

Vegetation	Lead Author	Year	Sampling Location(s)	Hydrocarbons	Detector /Column Type
Broadleaf Forest	Cao	1997	Eastern England	isoprene,monoterpenes	GC-FID, MS
(Deciduous)	Geron	1997	Southeastern US	isoprene	GC-FID
	Klemp	1997	Black Forest in SW Germany	C2-C5	GC-FID / Porapak QS
	Kramp	1997	Black Forest in SW Germany	C5-C8	GC-FID / DB-5
	Fuentes	1996	Southern Ontario, Canada	C3-C12	GC-FID, MS / HP-1
	Guenther	1996	Tennessee	isoprene	GC-FID, RGD / DB-1
	Fuentes	1995	Southern Ontario, Canada	C3-C12	GC-FID, MS / HP-1
	Boudries	1994	Brittany, France	C2-C9	GC-FID / PLOT (Al2O3/KCl)
	Khalil	1992	near Baton Rouge, LA	C2-C7,isoprene,monoterpenes, aromatics	GC-FID, MS
	Martin	1991	Pennsylvania	isoprene	GC-FID / DB-1
	Bufler	1991	Welzeim Forest, F.R.G.	monoterpenes	GC-MS / DB 1301, UCON 50
	Kanakidou	1988	Auch, France(SW)	C2-C6, isoprene	GC-FID / PLOT
	Trainer	1987	Scotia, Pennsylvania	C2-C5,isoprene	
	Lamb	1985	Pennsylvania	isoprene, TNMHC	GC-FID / SE-30
			Atlanta, Georgia	isoprene, a-Pin	GC-FID / SE-30
	Tille	1985	Western Europe	C2-C5	GC-FID / Spherosil XOB 075
Mixed Forest Mid-latitude	Gong	1997	White Face Mnt., NY	C2-C10	GC-FID / Rtx-1
Broadleaf and Conifer	Hagerman	1997	Southeastern US	isoprene,monoterpenes	GC-FID
	Hov	1997	Europe	C2-C7, aromatics	GC-FID
	Guenther	1996	Southeastern US	isoprene, monoterpenes	GC-FID, MS, RGD / Unibeads 3S,DB-1
	Solberg	1996	Various European	C2-C7	GC-FID / PLOT (Al2O3/KCl)
	Goldan	1995	Southeastern US	C3-C10,isoprene,monoterpenes	GC-FID / DB-5
	Goldstein	1995	Massachusetts	C2-C6	GC-FID / PLOT (GS-Alumina)
	Goldstein	1995	Massachusetts	C2-C6	GC-FID / PLOT (GS-Alumina)
	Lindskog	1994	Rorvik, Sweden	C2-C5	GC-FID
	Simon	1994	Landes, France	monoterpenes	GC-FID, MS / SP-5
	Hov	1992	Birkenes, Norway	C2-C4	GC-FID / Aluminum Oxide
	Hov	1991	Birkenes, Norway	C2-C4	GC-FID / Aluminum Oxide
	Mowrer	1991	Rorvik, Sweden	C2-C5	GC-FID / PLOT
	Clement	1990	Duchesnay Forest, Quebec	monoterpenes	GC-FID, MS / DB-5
	Juttner	1988	Southern Black Forest	monoterpenes, aromatics, C7-C9	GC-MS
	Riba	1987	Landes , France	monoterpenes	GC-FID
	Juttner	1986	Southern Black Forest	monoterpenes	GC-MS
	Hov	1983	Norway	monoterpenes	GC-FID/Ucon LB 550X-33 SCOT
Mediterranean	Arey	1995	S. Coast Air Basin, CA	isoprene,monoterpenes	GC-FID, MS / DB-5, HP-5
Scrub	Parrish	1992	Point Arena, CA	C2-C5	GC-FID
	Arey	1991	Central Valley, CA	monoterpenes	GC-FID, MS / DB-5, HP-5
	Pierotti	1990	California	monoterpenes	GC-FID, PID
	Singh	1988	Moffett Field, CA	isoprene, C2-C5	GC-FID/Phenyl isocyanate Porasil C

Vegetation	Lead Author	Year	Sampling Location(s)	Hydrocarbons	Detector /Column Type
Sub-Tropical	Khalil	1990	Chengdu, Sichuan China	C2-C4	GC-FID
Hardleaf Evergreen	Yokouchi	1988	Tsukuba, Japan	isoprene, monoterpenes	GC-FID, MS / OV-1
	Yokouchi	1983	Tsukuba, Japan	monoterpenes	GC-FID, MS /5% Silicone DC-200
Mountain	Das	1992	Gulmarg, India	isoprene, monoterpenes	Photoionization (PI) / SE-30
	Aiken	1987	Catherine Peak, NM	C2-C3	GC-FID / Phenylisocyanate
	Roberts	1985	Rocky Mnts., Colorado	monoterpenes	GC-FID, GC-MS / SE-30,SE-54
	Roberts	1983	Niwot Ridge, Colorado	monoterpenes	GC-FID / SE-30
	Shaw	1983	Soviet Georgia	Isoprene,monoterpenes,TNMHC	GC-FID, MS / OV-101
	Holdren	1979	Moscow Mnt., Idaho	isoprene, monoterpenes, aromatics	GC-FID, MS / SE-30,
Monsoon Forest	Ayers	1988	Northern Australia	C2-C4, isoprene, benzene	GC / FID
Prarie	Konig	1995	Austria	isoprene,monterpenes	GC-FID, MS / DB-5
Conifer Forest	Bottenheim	1997	L. Fraser Valley, B.C. Canada	C2-C6	GC-FID / PLOT (Al2O3/KCl)
	Beverland	1996	Scotland	isoprene,monoterpenes,TNMHC	GC-FID
	Bottenheim	1995	Southern Canada	C2-C6	GC-FID/Phenyl isocyanate Porasil C
	Montzka	1993	Western Alabama	isoprene, benzene	GC-FID / DB-5
	Lamb	1986	Washington	isoprene	GC-FID / SE-30
	Lamb	1985	Washington	monoterpenes	GC-FID / SE-30
	Lonneman	1978	Florida	C2-C10	GC-FID
Tropical Rain Forest	Davis	1994	Amazon (also Alabama)	isprene, monoterpenes	GC-FID
	Rudolph	1992	Republic of the Congo	C2-C5, aromatics	GC-FID / PLOT, DB-56 Porapak QS
	Zimmerman	1988	Ducke Forest Reserve, Brazil	C2-C10,isoprene,monoterpenes,aromatics	GC-FID
	Rasmussen	1988	Amazon Basin	isoprene	GC-FID / DB-1
	Bonsang	1987	Guyana	C2-C6	GC-FID / n-Octane on Porasil
	Gregory	1986	Guyana	isoprene	GC-FID
	Cronn	1982	Borneo	monoterpenes, aromatics	GC-FID / SE-30
Boreal Forest	Beine	1996	Alaska	C2-C5	GC-FID
	Blake	1994	eastern Canada	C2-C10	GC-FID / PLOT (Al2O3/KCl), DB-1
	Jobson	1994	Fraserdale, Ontario Canada	C2-C5, isoprene	GC-FID / PLOT (Al2O3/KCl)
	Janson	1992	Jadraas, Sweden	monoterpenes	GC, ion trap detection
Tundra and Polar	Laurila	1996	Northern Finland	C2-C5	GC-FID / PLOT (Al2O3/KCl)
	Jobson	1994	Northwest Territories, Canada	C2-C6	GC-FID / PLOT (Al2O3/KCl)
	Blake	1992	Arctic and sub-Arctic	C2-C5, isoprene	GC-FID / GS-Q, PLOT
	Doskey	1992	Barrow, Alaska	C2-C10	GC-FID / GS-Q, DB-1
	Rudolph	1992	Antarctic	C2-C5	GC-FID
	Rudolph	1989	Antarctica	C2-C3	GC-FID
	Rasmussen	1983	Barrow, Alaska	C2-C3, aromatics	GC
	Rasmussen	1980	Antarctica	C2	GC

Vegetation	Lead Author	Year	Sampling Location(s)	Hydrocarbons	Detector /Column Type
Marine	Blake	1997	Northwest Pacific	C2-C10	GC-FID
Environments	Clarkson	1997	Near New Zealand/Antarctica	C2-C5	GC-FID/Phenyl isocyanate Porasil C
	Blake	1996	Atlantic and Pacific	C2-C6, aromatics	GC-FID / PLOT (Al2O3/KCl)
	Greenberg	1996	Mauna Loa, Hawaii	C2-C10	GC-FID/Phenyl IC-Porasil C, DB-1
	Heikes	1996	S. Atlantic \ W. Indian Ocean	C2-C4	
	Donahue	1993	Central Pacific	C2-C5	GC / PLOT (Al2O3/KCl)
	Plass-Dulmer	1993	Atlantic	C2-C4	GC-FID / Porapak QS
	Greenberg	1992	Mauna Loa, Hawaii	C2-C10	GC-FID/Phenyl IC-Porasil C, DB-1
	Koppmann	1992	Atlantic 40N-30S	C2-C10	GC-FID / Porapak QS, DB5
	Bonsang	1991	Hao Atoll, South Pacific	C2-C5	GC-FID / PLOT (Al2O3/KCl)
	Simo	1991	Western Mediterranean	C19-C32, PAHs	GC-FID / SE-54
	Bonsang	1990	Amsterdam Is. Indian Ocean	C2-C5	GC-FID / PLOT (Al2O3/KCl)
	Greenberg	1990	E. Pacific W. Coast of N.A.	C2-C5, aromatics	GC-FID
	Rudolph	1990	Atlantic Ocean	C2-C5	GC-FID / Porapak QS
	Hov	1989	N. Atlantic Norwegian Arctic	C2-C5	GC-FID / PLOT
	Bonsang	1988	Intertropical Indian Ocean	C2-C6	GC-FID / N-Octane Porasil C
	Rudolph	1988	Atlantic Ocean (aircraft)	C2-C5	GC-FID / Porapak Q, DB-1
	Singh	1988	Eastern Pacific	E3, Pa, Pe, inB,	GC-FID/Phenyl isocyanate Porasil C
	Bonsang	1985	Mediterranean and Red Seas	C2-C6	GC-FID / N-Octane Porasil C
	Cofer	1982	Atlantic Ocean	TNMHC	GC-FID / Porapak Q
	Cronn	1982	South China Sea, Java Sea	C2-C5	GC-FID / n-Octane on Porasil C
	Enhalt	1982	Atlantic Ocean (aircraft)	C2-C5	GC-FID
	Singh	1982	Eastern Pacific Ocean	C2-C5	GC-FID/Phenyl isocyanate Porasil C
	Rudolph	1981	North Atlantic	C2-C5	GC-FID / Spherosil XOB 075
	Eichmann	1980	Tasmania-Indian Ocean	C9-C28	GC-FID
	Eichmann	1979	North Atlantic	C9-C28	GC-FID / OS 138SCOT,WCOT
	Brooks	1973	Gulf of Mexico	C2-C3	GC-FID / Porapak Q
	Lamontagne	1973	North and South Pacific	C2-C4, aromatics	
Savannah	Donoso	1996	Venezuela	C2-C6	GC-FID / PLOT (Al2O3/KCl)
	Guenther	1996	Republic of South Africa	isoprene,monoterpenes	GC-FID, MS
	Hao	1996	Zambia	C2-C6	GC-FID / HP-1, DB-1, GS-Q
	Greenberg	1985	Kenya	C2-C10, isoprene, aromatics	GC-FID

We have based our classification of vegetation type on the map from the Times Atlas of the World (Figure 1.2.1). They break down natural world vegetation types into sixteen possible categories, twelve of which we have identified with reported observations. In some instances we were uncertain as to the proper categorization since exact study positions were not given and map resolution was not high. Other issues arose when the vegetation studied did not fit the description of the climax vegetation type from the map. For example, in the southeastern US a region classified as Broadleaf Forest might have a stand of pine which was studied. Two of the four remaining classifications should contribute relatively little to the natural NMHC budget: Steppe and Desert. Many researchers expect that emissions from trees and shrubs far surpass those from grasses and crops (Evans et al., 1982; Anastasi et al., 1991). Lamb et al. (1987) estimate that crops represent less than 3% of biogenic hydrocarbon emissions in the United States. The other two types, Dry Tropical Forest and Dry Tropical Scrub & Thorn Forest may have appreciable emissions and cover a significant area in the southern hemisphere and Indian subcontinent (Guenther et al, 1996b).

Observations from the broad-leaved forests of the United States and Europe tend to concentrate on either smaller hydrocarbons (less than six carbons) or the larger terpene compounds with the hemi-terpene isoprene being common to both groups. Isoprene has been shown to be a major constituent of deciduous tree hydrocarbon emissions (Lamb et al., 1985; Khalil and Rasmussen, 1992). These studies were conducted primarily to obtain information regarding biogenic emission rates and hydrocarbon distribution (Tille et al., 1985; Lamb et al., 1985; Kanakidou et al., 1989; Bufler and Wegman, 1991). Martin et al. (1991) focus on diurnal isoprene concentrations and isoprene oxidation products. Experiments in southern Canada conducted by Fuentes et al. (1996) showed very low isoprene and terpene concentrations in early spring, increasing appreciably into the late summer. Diurnal variation was also noted with isoprene showing afternoon maxima and nighttime minima and terpenes displaying the reverse trend.

Many observations from mountainous regions were obtained in the US as well. Two records from Asian sites are also noted. Roberts et al. (1983; 1985) and Holdren et al. (1979) concentrate on terpenes. They find that terpenes exist in measurable concentrations within the forest canopy (up to 16 ppb) where they may have significant influence on the local tropospheric chemistry. Outside the canopy the concentrations tend to be below detection limits and contribute little to the chemistry. In Soviet Georgia, Shaw et al. (1983) find terpene concentrations of 4 ppb or less and indicates they play a small role in the formation of atmospheric aerosols. A unique paper is from Das (1992) who performed measurements with a photoionization detector, whose high sensitivity eliminates the need for preconcentration.

Researchers report many measurements from the mid-latitude mixed forests of Europe. Like a majority of other measurements, two typical fractions exist: terpenes or smaller hydrocarbons. Research here focused on diurnal (Riba et al., 1987; Clement et al., 1990) and seasonal (Juttner, 1988; Hov et al., 1991; Hov, 1992) trends in NMHC concentrations. Juttner (1986; 1988) also gives attention to biogenic and anthropogenic organic pollutants in the Black Forest. Recent studies have been published from the northeastern US in New York (Gong and Demerjian, 1997) and Massachusetts (Goldstein et al., 1995 a, b). Isoprene concentrations in New York showed the expected diurnal variation and the seasonal maximum occurred during late June. Goldstein et al. (1995a) report biogenic emissions of three species (ethene, propene and 1-butene) with emission ratios of 4:2:1. They also report seasonal cycles of background light alkanes and acetylene reveal a winter maxima and summer minima, which is attributed to seasonal variation in OH as opposed to source variation. The summer:winter ratio for the hydroxyl radical is inferred from the data set to be 9:1 (Goldstein et al, 1995b).

Tropical rain forests may be the most productive regions for biogenic NMHC. Data exists from around the globe for this vegetation type, though it is concentrated in South America. Isoprene dominates the reactive mix of hydrocarbons in these regions (Cronn and Nutmagul, 1982; Gregory, 1986; Zimmerman et al., 1988; Rasmussen and

Khalil, 1988). Diurnal and vertical distributions are observed. Both Rudolph et al. (1992b) and Jacob and Wofsy (1990) note that biomass burning in the dry season greatly enhances the NMHC concentrations found in the tropics. Jacob and Wofsy (1990) attribute rain-out as a factor in addition to the fact that little burning occurs during the wet season.

The polar regions exhibit some of the lowest biogenic emission rates for NMHC. Primary interest here concerns the relative importance of NMHC transport from lower latitudes to local emissions. Rudolph et al. (1989) attribute local emissions to oceanic sources for Antarctica. They find short-lived compounds, like alkenes, tend to vary as one would expect from the local source. Transport from low latitudes dominates the seasonal cycle for alkanes on the other hand. Blake et al. (1992) add that oil drilling can contribute significant amounts of hydrocarbons to the Arctic troposphere. They observed air parcels having a hydrocarbon mix including isoprene attributed to boreal forests and hydrocarbons associated with natural gas leakage and fossil fuel burning. This demonstrates the influence of long-range transport on the local tropospheric hydrocarbon concentrations. Jobson et al. (1994) show decreasing concentrations of light NMHC from winter to spring. The relative and absolute concentrations of these species agreed well with reported data from other arctic sites, indicating homogeneous air masses. This is most likely due to the low winter OH concentrations increasing compound lifetime.

Lonneman et al. (1978) and Lamb et al. (1986; 1987) offer results from conifer forests. Lonneman found that local biogenic hydrocarbon emissions in Florida were not significant enough to greatly affect the tropospheric chemistry during a three day period in May. In the US northwest, Lamb et al. (1985) showed reasonable agreement in α-pinene fluxes determined by enclosure and gradient profile techniques. More recently, measurements in British Columbia provide evidence that anthropogenic NMHC emissions can dominate tropospheric chemistry near urban areas (Bottenheim et al., 1995, 1997).

Arey et al. (1991, 1995), Singh et al. (1988) and Pierotti et al. (1990) discuss hydrocarbons from the Mediterranean scrub classification. All of those studies were performed in California. Results of the Arey et al. (1995) study suggest that ozone control strategies must focus on reductions of both NO_x and anthropogenic NMHC. Even though biogenic NMHC emissions in the California basin represent only ten percent of the total, combined with current levels of NO_x, they could produce ozone concentrations which exceed the National Ambient Air Quality Standard. It is insufficient to control anthropogenic NMHC. We found only one study each for the monsoon forest (Ayers and Gillett, 1988) and Prairie vegetation (König et al., 1995) types.

In the earliest listed study from savannah (Greenberg et al., 1985), the authors conclude that NMHC mixing ratios during the dry season in remote regions resemble those measured over oceans. Concentrations near populated areas approached NMHC concentrations of other remote areas. Several more recent studies have been published (Donoso et al, 1996, Guenther et al., 1996b, Hao et al., 1996), filling an important gap in measurements, as tropical savannahs cover significant portions of Africa, South America and Australia. Guenther confirms that the significant measured NMHC fluxes from vegetation in African savannahs agree reasonably with those predicted by global emission models. Relatively high alkene concentrations, including isoprene in remote Venezuela are attributed to biogenic sources. Heightened alkane levels are seen downwind from petroleum sites as expected (Donoso et al., 1996).

The boreal zone of northern latitudes represents more than 10% of the earth's landmass (Blake et al., 1994). Based on the findings of Janson (1992) that NMHC concentrations in a boreal region were of the same magnitude as those found in conifer forests of more southern latitudes, we conclude this region is an important place for further study. Since 1992, other researchers have reported measurements (Jobson, et al., 1994, Blake et al., 1994, Beine et al, 1996). Blake et al. (1994) confirm the dominance of isoprene as a sink for OH during biomass burning episodes (which elevate levels of

many other NMHC). Seasonal trends are noted by Jobson et al. (1994). Isoprene concentrations were above the detection limit from April through October, with a maximum during the summer. Other light NMHC showed highest levels during the winter months.

Another region which may contribute significant amounts of NMHC to the troposphere is the sub-tropical evergreen forest of China. This vegetation type is also found in Japan, Australia and New Zealand. Yokouchi and Ambe (1988) found significant levels of isoprene (1 ppbv) and α-pinene (2 ppbv) in Japanese agricultural areas similar to China's sub-tropical forest. They do not include smaller hydrocarbons in their analysis. Khalil et al. (1990) have studied bio-gas generators and rice paddies in China for evidence of hydrocarbon emissions but focus on methane and rule out heavier hydrocarbons as having significant sources from the generators.

The major group of the measurements we have listed in Table 1.2.1 are derived from various marine locales. Studies in these remote regions, with no local anthropogenic influences, are desirable to establish true background levels in the atmosphere. From the table, it is clear that researchers place emphasis on the smaller hydrocarbons in these regions. This is due to the relative ease of detecting and separating light hydrocarbons, in addition to their appreciable lifetimes and concentrations relative to heavier species. Analysis has shown that the ocean is saturated with these hydrocarbon species relative to the atmosphere (Bonsang et al. 1988; 1990; 1991). Their observations imply an oceanic source for hydrocarbons. Measurements from our laboratory confirm this picture and point to diurnal variability as well, which implies that photosynthetic processes may be responsible (Donahue and Prinn, 1993).

Sampling on board ships or from aircraft are especially important for obtaining an accurate picture of spatial hydrocarbon distribution. The advantage over land measurements is that the equipment is mobile. Observations taken over a broad area can give latitudinal distributions of compounds. Such distributions point toward major sources in the Northern Hemisphere which could be attributed to either anthropogenic

or land based influences. North-South gradients are noted by Cofer (1982) and Singh and Salas (1982). One disadvantage for ship observations occurs when looking for seasonal variations. It is clearly difficult to sample from the same place over the course of a season while floating in a boat! In situ sampling from aircraft presents similar problems since the sample pre-concentration step often takes tens of minutes; planes cover a large distance over that time period.

From the observations it is evident that measurements of NMHC are particularly sparse in Asia, Africa and the southern hemisphere in general relative to the northern hemisphere. Some representative reported NMHC concentrations are listed in

Table 1.2.2a Reported Measurements of Isoprene and Terpenes in ppbv

Location	Isoprene	α-Pinene	β-Pinene	d-limonene	Δ^3-carene
Houston, Tx[a]	0.79	0.22-0 67	0.40		
Moscow Mnts, Idaho[a]		0.113	0.086	0.010	0.064
Rural N. Carolina[a]		0.23-0.43			
Whiteface Mnt., NY[a]		0.4 (0.1-4.0)	2.4 (0.5-3.10)	2 2(0.2-15 0)	6 4(0.5-24.0)
Niwot Ridge, Colorodo[a]	0.63/0.11*	0.14/0.07*	0.07/0.07*		0.05/0.03*
Norway[a]		1.17-1.84	0.33-2.17		
North Carolina[a]		8.0	1.8		0 5
Idaho[a]		0.3	0.3	0 3	<0.1
Panama[a]	0.6				
Washington[a]	6.0				
Brazil[a]	2.40		0 27		.024
Brazil[b]	2.04	0.10	0 03		0 01
Nigeria[b]	1.21	0.06	<0 01		<0 01
Kenya[b]	0 04	<0.01	<0 01		<0.01
SW United States[c]	0 90/6 3+	0 75/0.30+	0.40/0.17+		
Candor, N. Carolina[d]	2 00	0.225	0 130	0.069	
Centreville, Alabama[d]	4.23	0.160	0.136	0 024	
Oak Grove, Miss[d]	2.238	0.271	0 304	0.063	
Yorkville, Georgia[d]	1.96	0 071	0 206	0 046	
Rome, Italy[e]		1.5	0.18	0 04	
Georgia Forest[e]	1.4	0.8	0.43	0 08	0 90

[a]Greenberg and Zimmerman (1984) * summer/winter
[b]Zimmerman et al. (1988)
[c]Goldan et al. (1995) + nighttime/daytime
[d]Hagerman et al. (1997)
[e]Fehsenfeld et al. (1992)

Table 1.2.2b Reported Measurements of Selected NMHC in ppbv

Location	Ethane	Ethene	Acetylene	Propane	n-Butane	n-Pentane	Benzene
Indonesia[a]	0.58	0.81	0.07				
Brazil[a]	1.55	1.4	0.65	0.33	0.78		0.37
Niwot Ridge, CO[a]	2.24	0.46	0.70	1.27	0.51	0.19	0.24
Pawnee Grasslands[a]	5.27	1.82	0.61	1.76	0.61		0.58
Atlantic-Equatorial[a]	0.73-1.0	0.08-0.5	0.07-0.28	0.1-0.26	0.03-0.18	0.01-0.06	
Pacific 10°N-20°S[a]	0.27-0.34	0.07-0.11	0.09-0.33	0.2-0.31	0.3-0.30	0.26-0.36	
Pacific 17°N-11°S[a]	0.50-2.70	0.20-4.00	0.20-1.05	0.16-0.84	0.08-0.18	0.01-0.16	0.04-1.86
North Atlantic[a]	1.0-1.9	0.02-0.51	0.08-0.30	0.13-0.45	0.03-0.25	0.02-0.30	
Pacific 20-32°S[a]	0.94-2.4	0.05-0.12	0.37-0.46	0.39-0.80	0.51-0.66	0.24-0.30	
Brazil[b]	0.98	0.97	0.30	0.37	0.09	0.07	0.08
Nigeria[b]	0.73	0.29	0.20	0.10	0.04	0.03	0.07
Kenya[b]	0.65	0.33	0.58	0.11	0.08	0.04	0.16
SW United States[c]				2.75/1.2[+]	0.62/0.30[+]	0.24/0.09[+]	0.13/0.10[+]

[a]Greenberg and Zimmerman (1984)
[b]Zimmerman et al. (1988)
[c]Goldan et al. (1995) [+] nighttime/daytime

Table 1.2.2a for terpenic compounds and 1.2.2b for some other commonly quantified hydrocarbons. The original compilation of observations in 1992 pointed to three main vegetation types warranting further study: savannahs, boreal forests and sub-tropical hardleaf evergreen. In the past several years, NMHC measurements have been published characterizing the first two types. It appears that our choice of the third type was fortuitous as the gap in published NMHC data still exists. Our NMHC measurements comprise the first major data set reported for the major biome of southern China.

1.3 Overview of Research Presented in this Thesis

The primary goal of this work is to assess through multi-gas measurement the influence of biogenic NMHC on the local tropospheric chemistry in China's sub-tropical biome. With the help of the Chinese Academy of Sciences (CAS), we identified a suitable site in southern China to pursue our NMHC study. The Dinghushan Biosphere Reserve is part of a network of research installations maintained by the CAS

(Figure 1.3.1). We traveled to Dinghushan in June of 1994 to confirm feasibility and performed an exploratory study from June 12 through June 15. Based on the results of this preliminary study, we implemented a flask sampling campaign in June 1995 to elucidate seasonal variations in NMHC at Dinghushan. This effort was overlapped by our intensive phase of in situ measurements which covered July and August of 1996. In addition to NMHC measurements, we obtained data on other trace gases: carbon monoxide and nitrogen oxides. Meteorological measurements included hourly values of temperature, humidity, and local wind velocity, plus daily total rainfall. Photosynthetic radiation (PAR) was also monitored.

We focus on measurements of hydrocarbons having two to ten carbon atoms, with particular interest in isoprene and terpenes as these compounds have short lifetimes due to their high reactivity (on the order of hours to days). Biogenic emission fluxes are calculated from bag enclosure measurements and compared to fluxes derived using a simple column loss approach. Analysis of loss frequency for most measured NMHC and CO show that the biogenic species dominate the chemistry in the region. We include alkanes and other longer lived hydrocarbons to provide information on air mass origin in addition to broadening the data base of global concentrations and trends. Hydrocarbon concentration and OH reactivity ratios are used to investigate the atmospheric processing of pollution plumes. These same plumes enable us to estimate OH radical concentrations in the forest.

Figure 1.3.1 Map of China indicating the location of the CAS observational stations. Dinghushan Biosphere Reserve is number 23. Notice also the relative proximity of Guangzhou (GZ), Hong Kong (HK) and Zhaoqing (ZQ).

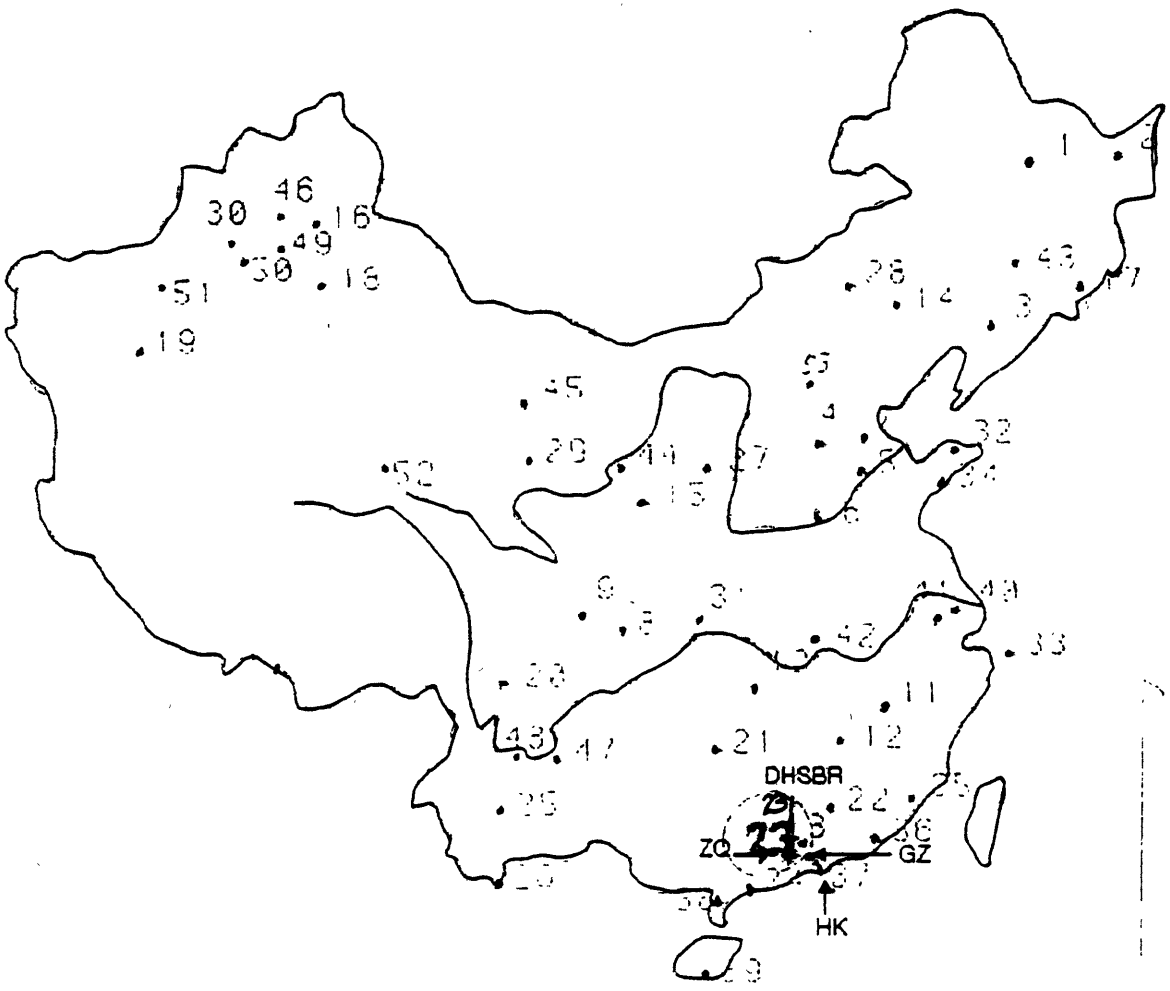

Chapter 2: Flask Sampling Campaign

2.1 Climate at the Dinghushan Biosphere Reserve

2.1.1 Geography and Circulation

The Dinghushan Biosphere Reserve (DHSBR) is located in Guangdong Province, southern China near the Tropic of Cancer (23°09'21"-23°°11'30" N and 112°30'39"-112°33'41" E). The reserve lies in the low mountains and hilly lands of the Dayunwu Mountain Range which runs from northeast to southwest. Within the reserve, the terrain declines from the northwest to the southeast. Unlike roughly two thirds of other regions near the Tropic of Cancer dominated by desert or semi-desert conditions, this area's unique climate and geographic location give rise to a climax vegetation of tropical-subtropical forest. Monsoon circulation during the summer months causes southeast and southwest winds to prevail, bringing warm and humid air masses to DHSBR from the Pacific Ocean and the South China Sea. Typhoons commonly occur during summer and fall. As these air masses reach the mountains of the region, they rise, resulting in heavy rainfall. Wintertime circulation is characterized by northeast and east winds, often bringing dry, cold air. Climatic observations were conducted over the twelve year period from 1975 to 1986. We compare later our summertime 1996 in situ campaign and prior year flask campaign results for temperature, PAR, rainfall and relative humidity to this climate record.

2.1.2 Measured Climate Variables

Temperature

The mean annual temperature is 20.9 °C with a mean maximum in of 28.1 °C in July and a mean minimum of 12 °C in January. During July and August 1996 the mean temperature was 26.2 °C and 26.4 °C respectively with ranges of 22-32 °C and 23-31.5 °C (Figure 2.1.1). This compares to the temperature record means of roughly 28.1 °C

and 27.6 °C. Measured values for the mean minimum/maximum monthly temperatures for July and August were 23.9/28.9 and 23.7/28.3 versus historical values of 24.3/32.7 °C and 24.2/32.5 °C. The summer of 1996 was slightly cooler than normal for Dinghushan. Temperatures recorded along with flask samples over the prior year are typical for the region (Figure 2.1.2). Hourly temperatures were obtained during the intensive campaign using a mercury thermometer with 0.2 degree gradations.

Relative Humidity

Relative humidity is high and fairly constant year round in Dinghushan. The mean annual relative humidity is 81.5%, with a high of 86.5 % in March and a low of 73.5% in December. Average relative humidity during summer 1996 was over 88%. Lowest recorded relative humidity over the period was 48% (Figure 2.1.1). Seasonal values for relative humidity (Figure 2.1.2) are consistent with the long-term record. As might be expected, clouds frequently fill the skies allowing less than 4 hours of daily sunshine from February through April. Hourly values of relative humidity were calculated using wet and dry bulb temperatures obtained from a motorized sling psychrometer with a 0.2 degree reading accuracy.

Rainfall

The mean annual rainfall observed from 1975 to 1986 was 1,956 mm. The wet season, with mean monthly rainfall exceeding 200 mm, occurs from April through September, May being wettest at 312 mm per month. November through January define the dry season with monthly rainfall means under 50 mm, December being driest with a 22 mm monthly mean. Over summer of 1996, DHSBR experienced greater than average precipitation. Monthly values for July and August were 282.5 and 339.4 mm respectively (Figure 2.1.1). These were roughly 30-50 mm greater than the average monthly means recorded but well within the maximum monthly mean values (>400 mm) observed over the twelve year period. We experienced over forty mm of rain for four

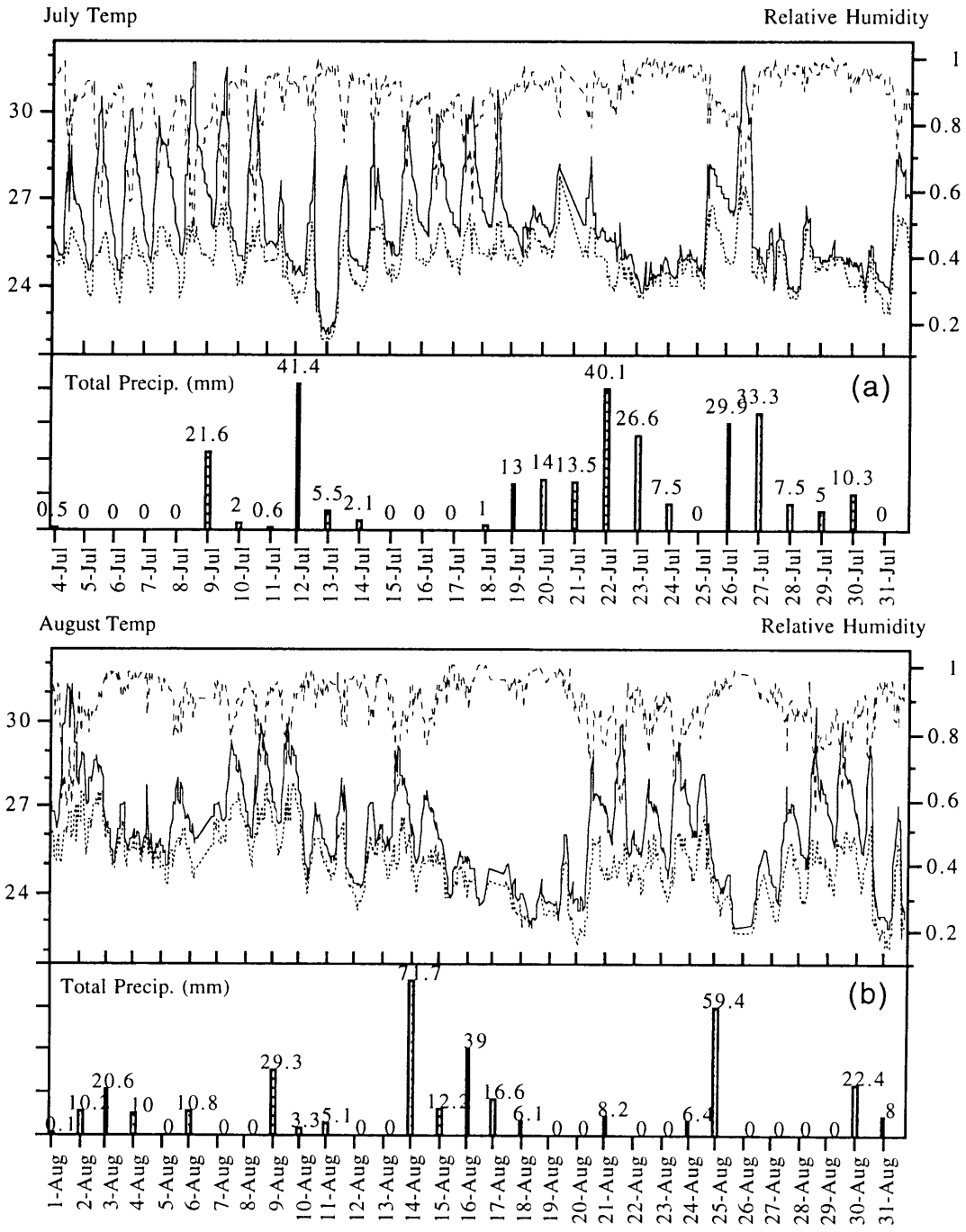

Figure 2.1.1 Values for July (a) and August (b) temperature (solid line) and wet bulb temperature (dashed) are given as the lower two curves. Relative humidity (dashed) is shown at the top. The bar graph displays daily totals of precipitation.

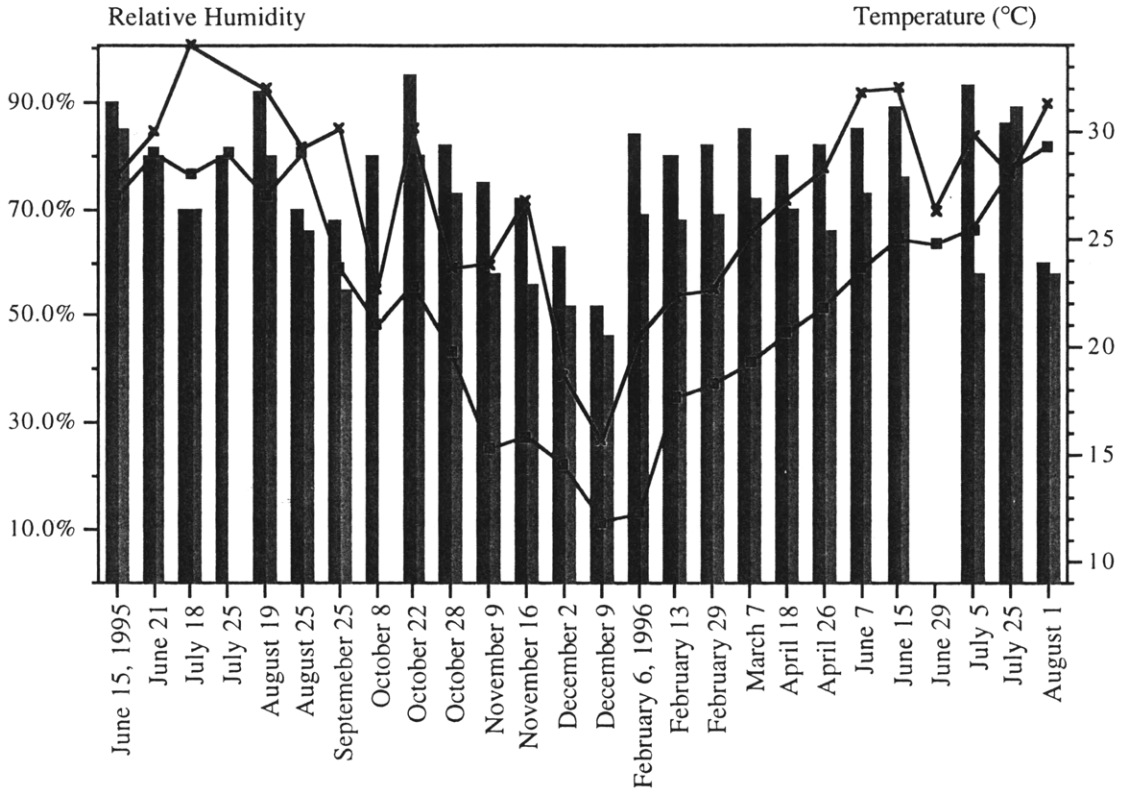

Figure 2.1.2 Temperature and Relative Humidity recorded at the time of flask sampling for the seasonal campaign. The left bar is the 8 AM and the right is the 2 PM measurement of RH. Morning temperature is given by the box points and afternoon temperature uses crosses.

days over the course of the summer; this is more than some monthly totals during the dry winter months!

Local Wind Velocity

Local wind velocity was measured once per hour using a handheld anemometer accurate to 0.05 m/s and 10° in the horizontal plane. In general, wind was out of the north or east quadrants during the daytime and from the south or west at night. In the immediate vicinity of the sampling site, this trend meant downslope wind during the morning and afternoon and upslope in the evening hours. Mean wind speeds vary from 1-3 m/s, being most windy during the spring months.

PAR

Photosynthetic Active Radiation (PAR) in the 400 to 700 nm waveband was recorded using a LI-190SA Quantum Sensor (LI-COR, inc.) and a strip chart recorder.

The instrument uses a cosine corrected response to obtain the correct flux density of solar radiation through a planar surface. Absolute calibration is +/- 5% traceable to the U.S. National Institute of Standards and Technology. Data were collected for twelve hours on most days starting at 7 AM and ending at 7 PM near sundown. Twenty complete days in July and twenty-three in August were used to obtain daily average totals of PAR. Full sun sky over a one hour period would yield roughly 2 mmol $s^{-1}m^{-2}$ (1 μmol = 6.02 X 10^{17} photons = 1 μEinstein). Daily averages of 0.89 and 0.71 mmol s^{-1} m^{-2} were seen in July and August. The true average is somewhat lower than this since those days not represented in the data are missing generally due to inclement weather. Maximum sunlight hours occurred between 11 AM and 3 PM during July with slightly lower maximum daily values in August between 12 and 2 PM. Figure 2.1.3 displays the entire PAR record.

2.2 Flask Sampling Campaign

In June 1994 we went to Dinghushan to assess the feasibility of the site for our research. We took twenty flask samples over a four day period and analyzed the air for NMHC at MIT the following month. The samples were taken primarily between 6 AM and 6 PM as these were the times of expected highest isoprene concentrations. Over thirty NMHC were identified using a Gas Chromatograph with a Flame Ionization Detector (GC-FID) instrument and knowledge of individual NMHC retention times on our system. Biogenic gases identified included isoprene, α-pinene and Δ-3 carene (Figure 2.2.1). Terpene concentrations were found in the 50-450 parts per trillion (ppt) range and isoprene in a 60-600 ppt interval. Using the diurnal trend of isoprene as a guide, we decided that the optimal flask sampling time would be at 6 AM and 2 PM as these were roughly the times of the extremes. In practice, the sampling times for the flask campaign occurred at 8 AM and 2 PM. Sample frequency was roughly four flask collections per month, taken on two days separated by approximately one week.

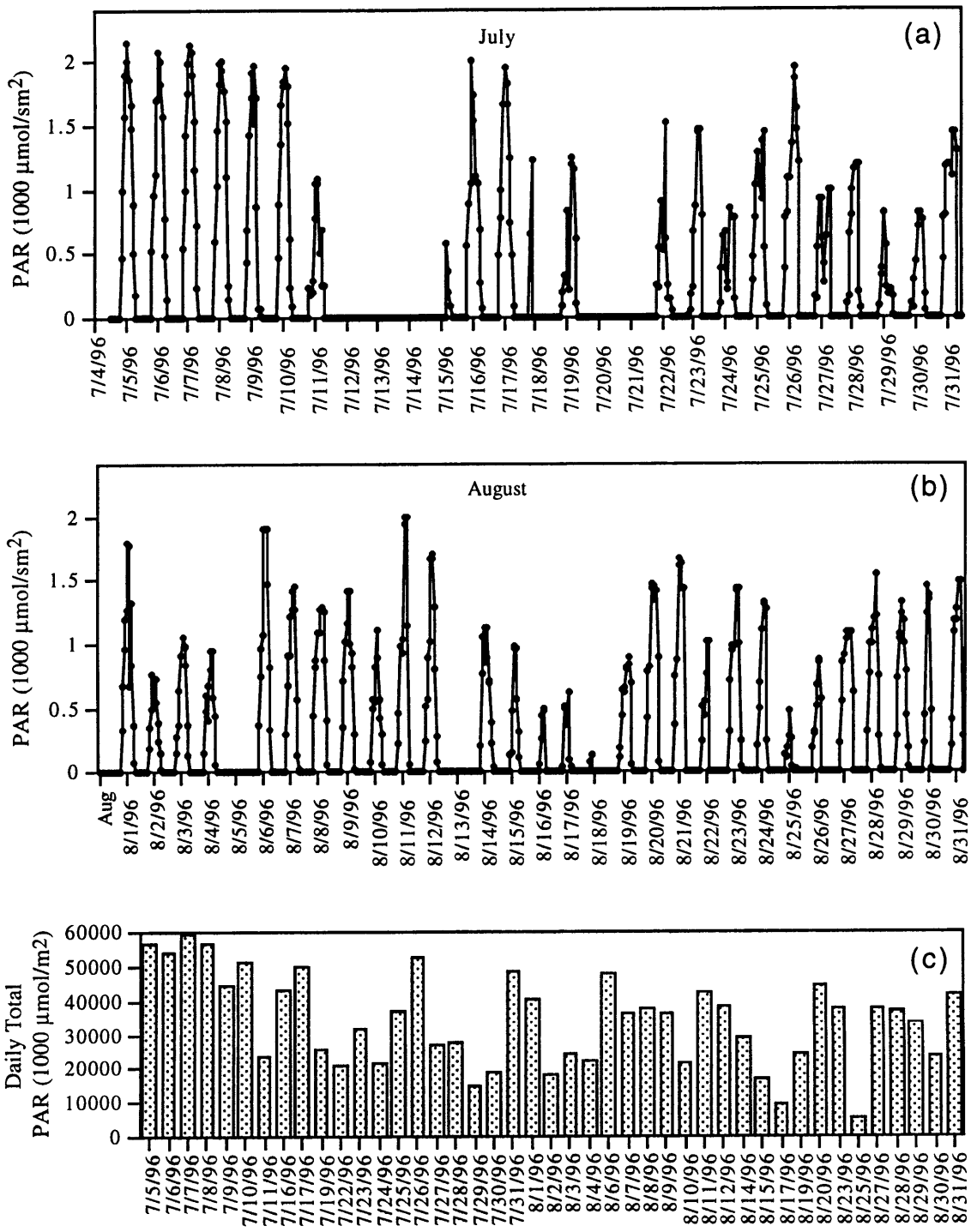

Figure 2.1.3 PAR values are shown in (a) and (b) for the months of July and August respectively. Data were unavailable for days without peaks. Integrated PAR for days with complete sunrise to sunset measurements is given in the final graph (c).

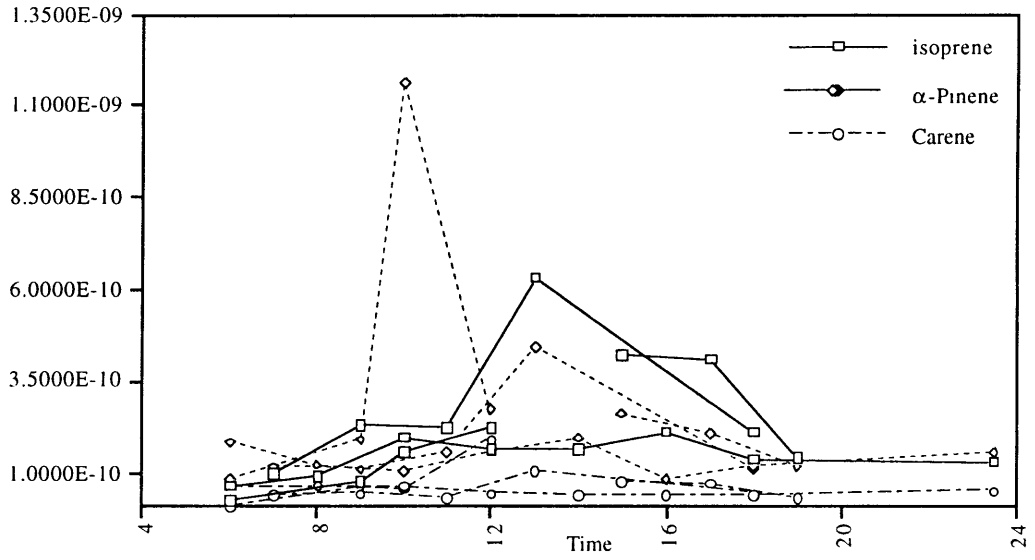

Figure 2.2.1 Isoprene, α-Pinene, and Δ-3-carene concentrations obtained from the preliminary flask sampling study performed over four days at Dinghushan Biosphere Reserve in June 1994.

2.2.1 Flask Campaign: Experimental

Flask measurements were obtained over a fifteen month period from June 1995to August 1996, with the intent to identify seasonal patterns in NMHC concentrations at Dinghushan. Stainless steel flasks (0.8 l) fitted with Nupro SS-4H4 Bellows sealed valves were cleaned on a devoted manifold system. Flasks were hooked to the manifold and then pumped to six Torr with a mechanical vacuum pump. Next, flasks were pressurized with zero air to roughly 40 psig and subsequently evacuated as above. After flushing three times, flasks were pumped down to ~300 mTorr using a cryogenic vacuum pump and then capped. In China, the prepared flask was attached by a 30 cm 1/4" OD stainless steel line to a battery powered model MB-158 Metal Bellows pump. The air inlet used a Teflon filter attached to the pump inlet with a 10 m 1/4" OD Teflon line. A tee with purge valve and pressure gauge was placed on the outlet side, one branch to purge and the other to fill the tank (Figure 2.2.2). The filling procedure was as follows: first the line was flushed with the purge valve open for 3 minutes, then it was

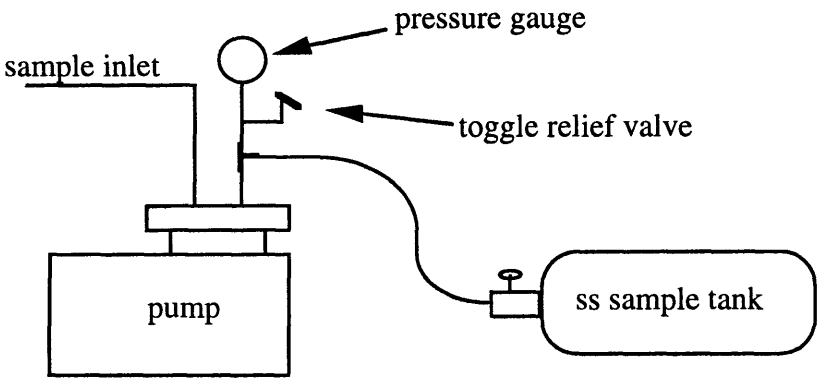

Figure 2.2.2 Canister sampling assembly showing the toggle switch which allows flushing of the dead volume to the sample tank valve prior to filling.

pressurized to 40 psig and released several times to completely flush the line to the cylinder. Once the line was cleaned, the tank valve was opened and filled with air to almost 40 psig. About 90 seconds is required to fill the tank.

Flasks filled through April 1996 were analyzed within three weeks of their collection time. Those flasks collected while the chromatographic equipment was in China were analyzed as much as 6 months after their collection time. It should be noted that prior to June 29, tanks were sampled as described in the previous paragraph. The final four flask samples were taken through the same sample line used in the intensive phase. The site for the bulk of the flask samples was roughly on the other side of the mountain from the intensive sampling laboratory which could potentially explain the heightened levels seen at the intensive-phase site for the biogenic gases. Alternatively, it could simply be due to higher emissions in the mid to late summer.

Analysis of the flask air was performed at MIT using a flame ionization detector (FID) in a Hewlett Packered 5890A gas chromatograph (GC). Hydrogen carrier gas (2.27 cc min^{-1}) was used, with flows of 360 cc min^{-1} zero air, 21 cc min^{-1} nitrogen and 33 cc min^{-1} make-up hydrogen to the detector. Initially, the flask was attached to a pressure regulator and the sample line. A vacuum pump on the outlet side of a mass flow

controller (Tylan, Inc.) emptied the sample line of air up to the closed Whitey valve on the flask. This line, including an Ascarite II (NaOH) trap for CO_2 and H_2O removal, was then flushed with tank air for five minutes at a rate of almost 30 ml per minute. With the flow established, the 1 cc collection loop was immersed in liquid argon for sixteen minutes, resulting in a collected sample volume of 435 cc. Switching of a 6-port Valco valve followed by desorption of the sample by immersing the sample loop in room temperature water allowed the sample to travel to a low volume 0.32 ID fused silica cryofocus loop (also cooled with liquid Argon).

At run start, the gases were again volatilized with immersion in water and sent directly to a dual in-line column set-up. The first, a WCOT 50 m x 0.32 mm CP-Sil 5CB (D_f=1.2 μm polydimethylsiloxane) column separated the light NMHC in clumps which were further separated on a 14 meter section of a 0.32 OD PLOT column with Al_2O_3/KCl stationary phase (Chrompack) . Essentially, the temperature program and column combination were designed to allow separation of NMHC with two to ten carbons without using sub-ambient temperatures often employed by other researchers to separate the lightest species. Cryogens are often used in gas chromatography to achieve sub-ambient temperatures. Our preliminary experience at the site in Dinghushan made it clear that low cryogen consumption was essential since supplying the laboratory site with cryogens was difficult. We determined later that this trap and column set-up would not be robust enough to handle hourly NMHC measurements of very humid air as required in the intensive phase. The temperature profile included an initial three minute period at 35 °C. This enabled ethane and ethene separation on the PLOT column. Next, temperature ramped 12 degrees per minute to 65 °C then holding for one minute. The final two ramps of 10 degrees per minute brought the oven temperature to 150 °C, held it for three minutes, and finally increased it to 200 °C and held it for seven minutes Total run time was thirty minutes. A sample chromatogram of a standard run is given to show system separation performance (Figure 2.3.3). Over the

Figure 2.2.3 Standard Analysis of tank 5200 performed on the 5890a GC system. Retention times and peak identification are listed below.

Compound	Retention Time (min.)
a. Ethane	2.669
b. Ethene	2.729
c. Propane	3.222
d. Propene	3.980
e. 2-methylPropane	4.575
f. Butane	4.873
g. 1-Butene	6.160
h. 2-methylPropene	6.495
i. cis-2-Butene	6.834
j. Pentane	7.838
k. cycloPentane	7.951
l. 1-Pentene	9.437
m. cycloHexane	10.847
n. Hexane	11.038
o. Isoprene	11.339
p. 1-Hexene	12.363
q. 3-methylHexane	13.370
r. Heptane	13.805
s. cycloHeptane	14.196
t. Benzene	14.612
u. 1-Heptene	14.995
v. Octane	16.760
w. cycloOctane	17.963
x. Toluene	18.461
y. 1-Octene	18.725
z. Nonane	20.870
aa. α-Pinene	21.315
bb. 1-Nonene	22.075
cc. Δ-3-Carene	23.244
dd. Decane	23.702
ee. Sabinene	24.628
ff. γ-Terpinene	24.797
gg. d-Limonene	24.910
hh. 1-Decene	25.038
ii. Myrcene	26.782
jj. Undecane	27.965

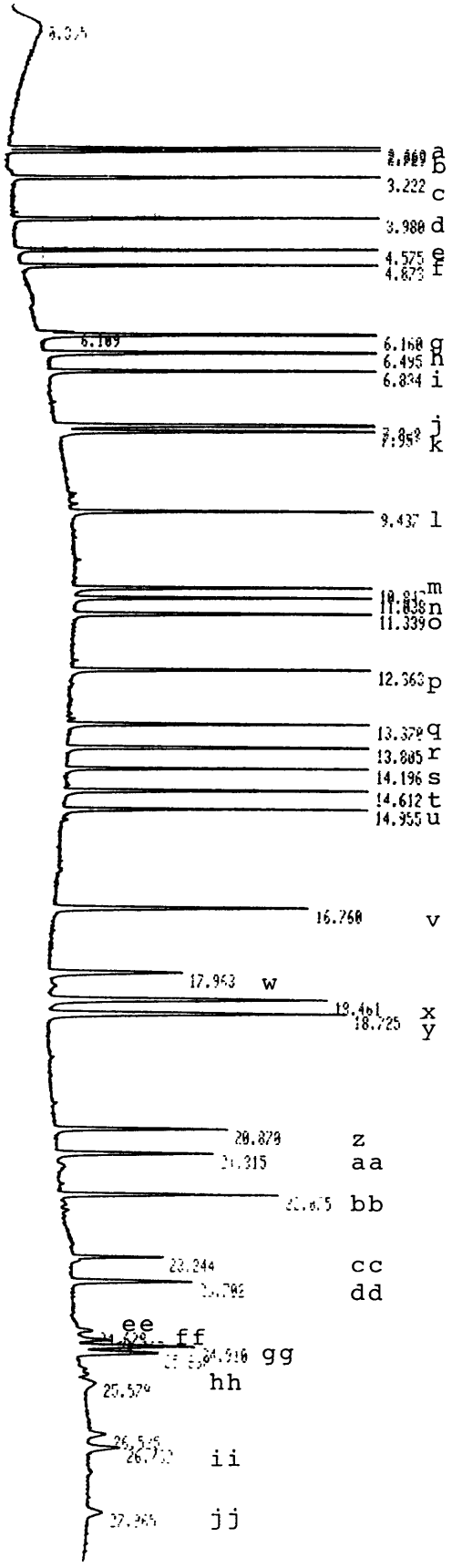

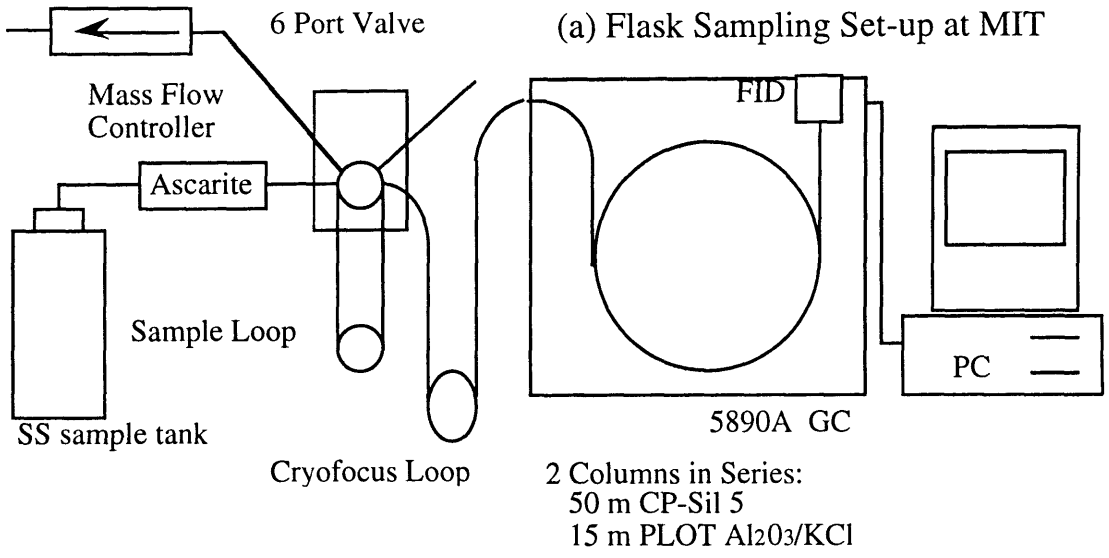

(b) In-Situ Set-up at Dinghushan Biosphere Reserve

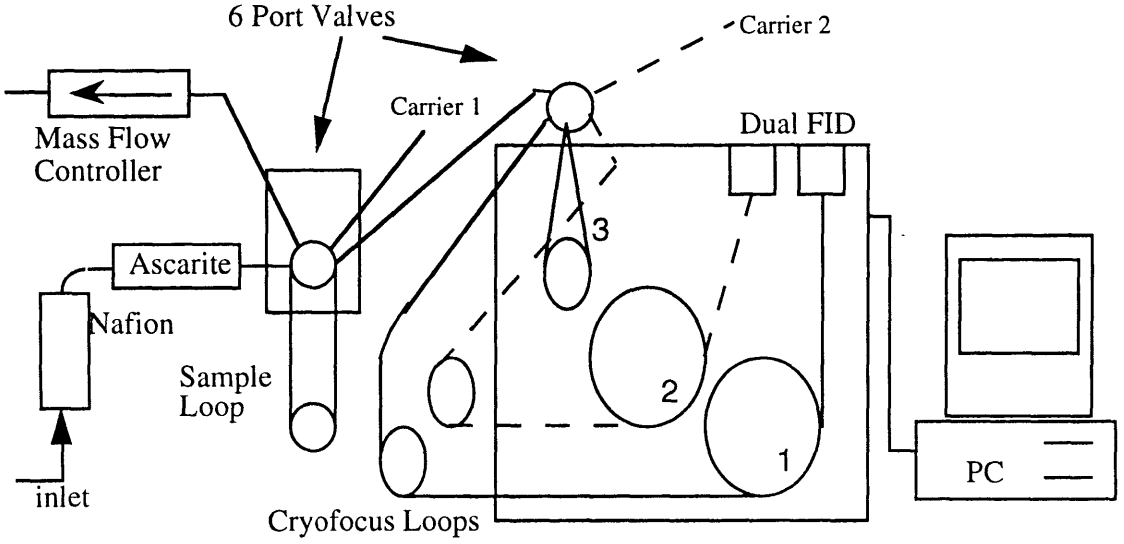

Column 1: 50 m PLOT Al_2O_3/Na_2SO_4
Column 2: 60 m CP-Sil 5
Precolumn (3): 1 m PLOT

Figure 2.2.4 (a) gives the schematic for the hydrocarbon system at MIT. (b) shows the dual column system used in the intensive phase in China. The primary difference between the two set ups is series versus parallel columns requiring one detector for the former and two for the latter.

course of the year, some column degradation occurred and minor changes to the temperature profile were required. Some samples suffered from coelution of peaks which required minor alterations in temperature programming to correct. The final twelve samples (the last six sample pairs) were analyzed using the setup detailed in the intensive phase. Figure 2.2.4 diagrams both hydrocarbon analysis systems.

2.2.2 Flask Campaign: Calibration

Instrument calibration and peak identification were performed by using standard mixtures and permeation devices produced in our lab as described in the Appendix. Signal output was recorded and integrated on an HP-3393A integrator. In general, we ran two to three samples from each tank and took the average peak area for quantification. Often a standard addition run was performed to assist in identification of later peaks as retention time shifts were common after the first half of the run (which affected compounds retained longer than benzene). Standard samples were diluted by UHP N_2 and then treated as tank samples. Most reported peaks were calibrated by using a corresponding standard peak except for those few which were not in our standards. These peaks were quantified by the RMR technique as explained in the Appendix.

2.2.3 Flask Campaign: Results

Correlations between all compounds were performed. Two major groups of hydrocarbons had similar trends (showing intercorrelations > 0.85). The first group consisted of primarily alkanes including 2-methylbutane, pentane, cyclopentane, 2-methylpentane, 3-methylpentane, 2,2-dimethylbutane (and coeluting peak(s)), 2,3-dimethylbutane (and coeluting peak(s)). Propane and 2-methylpropane showed similar trends. The second group was made up of alkenes with a few larger alkanes including: the four butene isomers, five pentene isomers, 1-hexene, 1-heptene, octane, nonane, 3-methylhexane, hexane, and cyclohexane. Ethylbenzene and 2-methyl-2-butene were correlated with both major groupings. Isoprene, α-pinene and camphene had low correlation (<0.5) with most, if not all other compounds we identified. There were

correlations on the order of 0.8 between the various terpenes. We interpret these correlations as some evidence that our identifications are correct as we would not expect the variations in biogenic gases to mirror those from other sources.

Many researchers have reported seasonal trends in light NMHC in the boundary layer (Greenberg et al, 1996; Boudries et al., 1994; Jobson et al., 1994; Goldstein et al., 1995; Klemp et al., 1995). Such trends are influenced by factors like seasonal variations in source strength, sink strength and mixing patterns. Gases with relatively high emission year round exhibit maxima during the winter and minima during late summer. The variation in mixing ratio is due in large part to changes in OH levels due to seasonal differences in humidity and sunlight. Primary loss mechanisms for light alkanes involve oxidation by OH radicals. The effect is most pronounced at high latitudes where OH variability is greatest. Goldstein et al. (1995) estimate this variation in northern midlatitudes at almost an order of magnitude. Our data set despite being at lower latitudes still shows some evidence of this seasonal trend. With only sparse sampling over one year, in addition to high variability and local pollution events, we cannot however make any definitive statements about the seasonal trends of light alkanes at Dinghushan.

Table 2.2.1 Carbon monoxide concentrations obtained from flask samples.

Sample time	CO concentration (ppb)
June 7 AM	785
June 7 PM	627
June 15 AM	733
June 15 PM	661
June 29 AM	156
June 29 PM	343
July 5 AM	220
July 5 PM	121
July 25 AM	766
July 25 PM	196
August 1 AM	163
August 1 PM	305

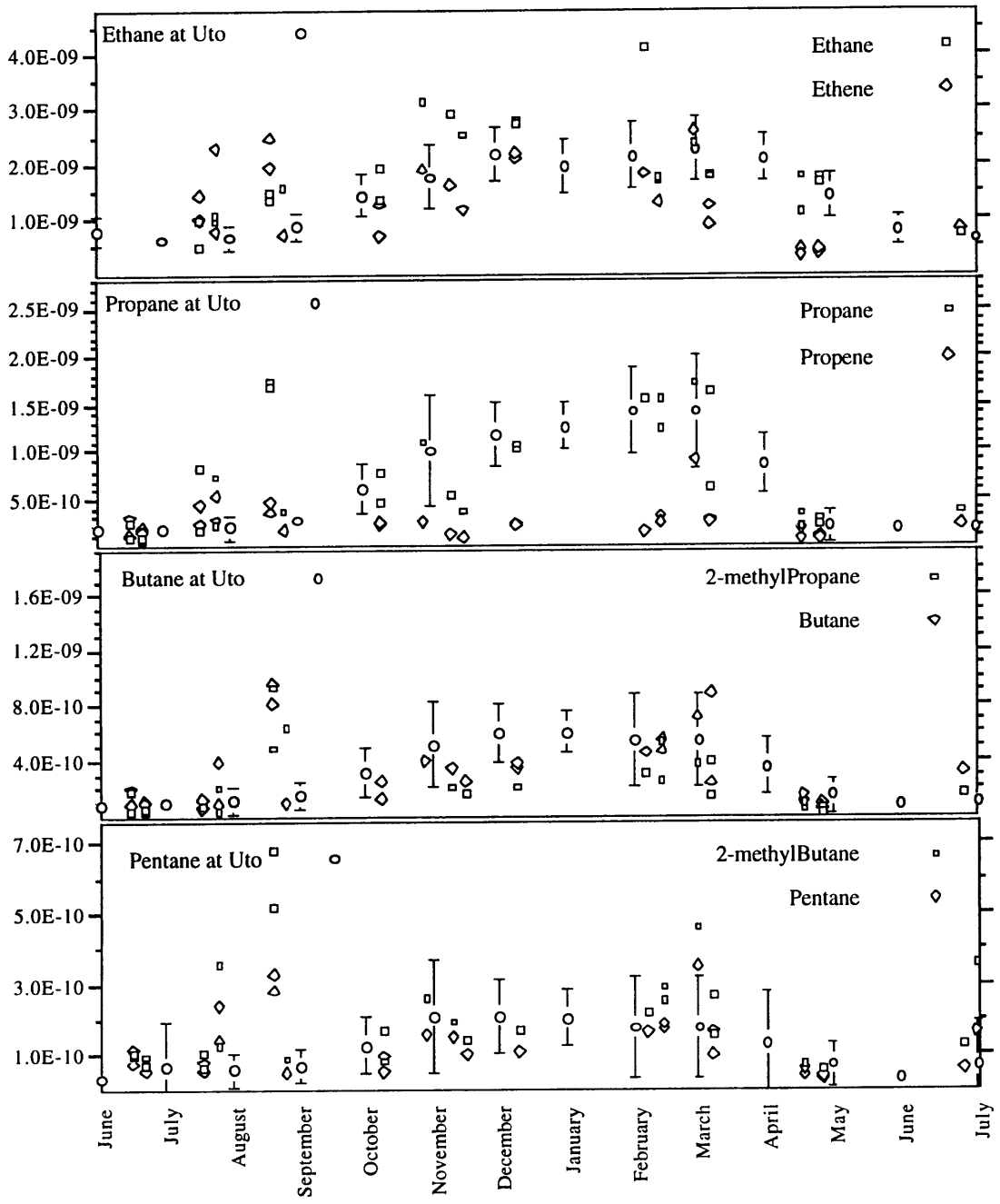

Figure 2.2.5 Light hydrocarbon canister measurements (plotted as square and diamond) with pollution events filtered out. Pollution events were determined by high CO (above 200 ppb), high acetylene (above 0.3 or 0.8 ppb depending on season) or high light alkanes (any alkane above 5 ppb). All data points were removed for samples qualifying as polluted. Also plotted (circles) are seasonal means and averages obtained at Uto in the Baltic Sea (Laurila and Hakola 1996) for four species. The trends at Dinghushan show reasonable agreement.

For most of the flask data, there is no consistent way to distinguish between background and polluted air masses, most likely due to difference in the pollution sources. Three methods were used to determine unpolluted samples: low carbon monoxide, low acetylene and/or alkane levels in the low to sub ppb range. From June 7, 1996 to August 1, 1996 there are CO data which clearly point out times of pollution (Table 2.2.1). Atmospheric CO is derived primarily from combustion or atmospheric processing of hydrocarbons. Based on the observations of CO during June 1996 one can conclude that air masses with levels of CO above 200 pbb are most likely polluted. Some use atmospheric levels of acetylene as a tracer for pollution as its main source comes from combustion of fossil fuels or biomass burning. Levels below 0.3 ppb may be considered to be clean air (Klemp, et al. 1997). Data from acetylene seasonal trends in Massachusetts (Goldstein et al., 1995) indicate background variations as given by the 10th percentile value in the data set to be approximately 0.3 ppb or less during summer and 0.8 ppb during winter. The 10th percentile value is determined by ordering all measurements by concentration, multiplying the total number of sample points by 0.1, and then finding the value corresponding to that measurement (the median is the 50th percentile). The intensive campaign data show levels of acetylene at roughly 335 ppt for the lowest 10% of measurements, which we interpret to be clean air. It seems reasonable to label flask air samples having higher values than 0.3 ppb during the summer and above 1 ppb in the winter as potentially polluted. Air containing alkane concentrations near or greater than 10 ppb may also be termed polluted with some confidence. With these criteria, we have attempted to remove pollution events from the flask data set to reveal a background trend for the light hydrocarbons (Figure 2.2.5).

Laurila and Hakola (1996) report results from flask measurements taken at Utö which is an island in the Baltic sea (59° 47' N, 21° 23'E). Three hundred seven samples were taken over the course of 1993 and 1994 yielding average values with standard deviation plotted as error bars in Figure 2.2.5. A seasonal cycle is apparent in the data with a maximum concentration seen in winter and minimum in summer. Concentrations

build into March for ethane whereas the maximum value for pentane is reached in February. The more reactive light hydrocarbons decline to the low summer levels earlier than ethane but all show a major drop between April and May. Hydrocarbon levels recover in late July into August, building to peak concentrations the following spring. Others have reported similar trends, with the more reactive hydrocarbons reaching winter peak levels earlier and declining faster in the spring (Boudries et al., 1994; Jobson et al., 1994; Bottenheim and Shepherd, 1995; Goldstein et al., 1995b). These results from North America and Europe agree not only qualitatively but also quantitatively, yielding similar ranges for maxima and minima.

The results of my seasonal measurements agree somewhat well with those obtained at Utö both in magnitude and monthly trend. Light alkane concentrations build into March with lower values seen in May. Build up is observed in the late summer. Butane and pentane both show less variation with season when compared with the Utö averages. This could be a result of the higher average OH values and lower seasonal OH variation. Propene behavior is seen to differ from that of the alkanes displaying somewhat higher mixing ratios during the summer months over the winter. This could be due to biogenic contribution in the warm season. 1-butene also shows a similar summer increase. Both alkenes have been reported to have biogenic sources (Goldstein, et al., 1995; Laurila and Hakola, 1996). The levels of ethene measured in China tend to be higher than those reported by others.

Other gases we measured, isoprene and monoterpenes, have primarily biogenic sources. Their emission rates show strong temperature dependence. An experiment conducted with a Monterey pine showed concentrations of α-pinene and β-pinene measured inside an enclosure to be 3 ppbv at 10 °C and roughly 12 ppbv at 30 °C (Juuti, 1990). Those figures agree with Hatakeyama et al.'s (1991) assertion that a thirty degree increase in average temperature will result in an order of magnitude increase in terpene emissions. Unlike terpenes, which are emitted continuously, isoprene is primarily emitted during daylight hours. Isoprene levels, therefore, tend to be maximum

during the late afternoon. Light intensity also influences isoprene emission (Guenther et al. 1993). Several researchers have found it useful to plot isoprene concentrations versus temperature to demonstrate the relationship between increasing temperature and increasing emission rates. These trends are summarized in Table 2.2.2. The slopes have good agreement, hovering around 0.07, which translates roughly into a doubling of concentration in the air for every 4 °C temperature change. The two slopes of 0.056 may be a result of difference in sampling location relative to emission source and to the effects of light on emissions. Another factor maybe the local chemistry, with higher OH radical or O_3 levels causing slope variations. Local meteorology and the time of sample during the day may also affect the slope. Differences in intercepts reflect the differences in concentration from site to site. Using the data from our seasonal flask measurements, we obtained a slope of 0.072 which closely mirrors other published results (Figure 2.2.6). According to Fehsenfeld et al.(1992), at a given temperature, isoprene emission

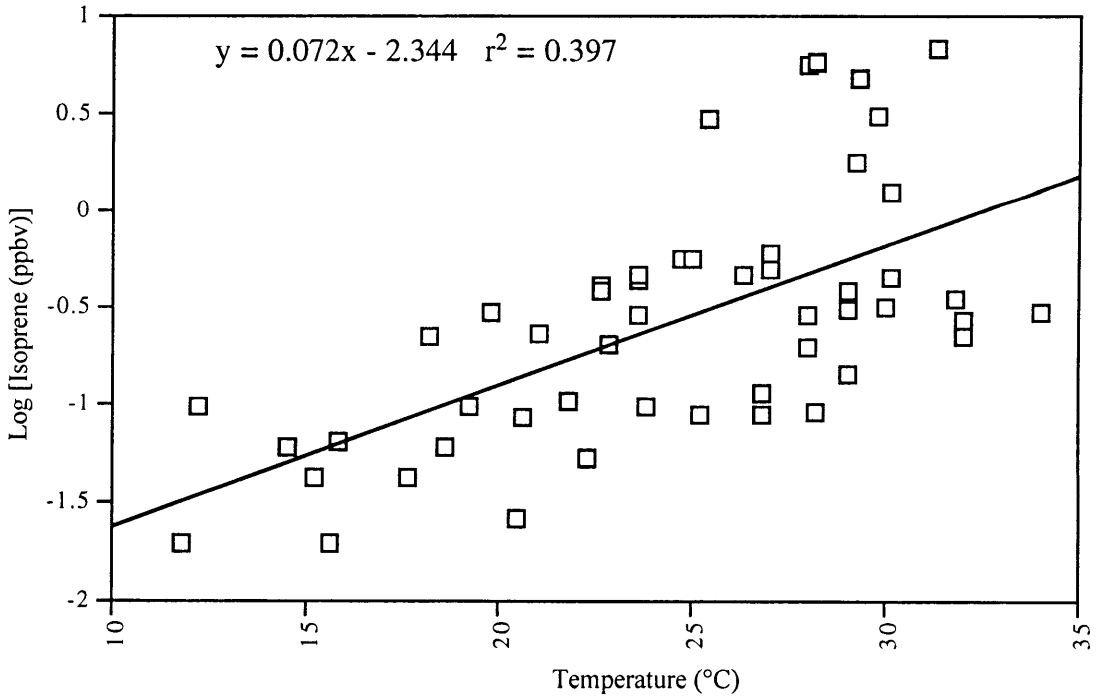

Figure 2.2.6 Log Isoprene concentration versus Temperature for all flask measurements June 1995 to August 1996. Slope of the linear fit agrees with those reported in the literature, though the correlation coefficient is low.

Table 2.2.2 Temperature dependency of isoprene (is) concentrations of the form log [is] = slope*T (°C) + intercept

Location	Slope	Intercept
Fraserdale, Ontario[a]	0.071	-1.4
Western Alabama[b]	0.076	0.012
Scotia, Pennsylvania[b]	0.076	0.019
Whiteface Mountain, NY[c]	0.070	-2.68
Whiteface Mountain, NY[c]	0.056	-1.92
Southern US[d]	.056202	-1.3784
Centreville, Alabama[d]	0.066	-1.6019
Dinghushan, China[e]	0.072	-2.344

[a] Jobson et al. (1994)
[b] Goldan et al. (1995)
[c] Gong and Demerjian (1997)
[d] Hagerman et al. (1997)
[e] This work

will rise with increasing temperature until saturation is reached between 1000 to 1500 μmol m^{-2} s^{-1}. Reported isoprene levels average 3-4 ppbv in the tropics and subtropics (Jacob 1988, Yokouchi 1988).

Terpene concentrations are reported to vary an order of magnitude diurnally. Yokouchi (1983) records daytime α-pinene values of 0.25 ppbv increasing to 2.5 ppbv at night. Janson (1992) cites similar results with daytime terpene concentrations ranging from 0.01-0.5 ppbv and nighttime values of 0.2-8 ppb. Likewise, measurements by Riba et al.(1987) vary from 0.5 to 4 ppbv. Those researchers attribute this variation to increased atmospheric stability and decreased levels of OH radical and ozone at night. Less mixing occurs during evening hours.

Seasonal variations follow temperature trends, with summertime having highest NMHC levels and winter showing lowest. Representative terpene[winter/summer] differences measured include [<.001 / 0.3] ppbv (Roberts et al., 1983), [0.02 / 0.2] ppbv (Juttner 1988), and [<0.05 / 0.6] (Yokouchi et al., 1983). Isoprene concentrations are greatly reduced during winter months when both temperature and daylight hours are at minima. Fehsenfeld et al. (1992) predict winter vegetative NMHC emissions to be

roughly 5% those found during peak summer production in the United States. The seasonal data obtained from Dinghushan show maximum summer isoprene levels to be in the low ppb range with winter minima two orders of magnitude lower. Terpene trends are not as pronounced but do show minima in December and February with higher and more variable results in the summer months.

Two other variables mentioned, wind speed and relative humidity have minimal effects on the emission rates. Yokouchi et al. (1983) claim that average winds < 3 m/s do not appreciably decrease α-pinene concentrations. It is possible that slight decreases in concentration due to advection could be offset by slight increases in emission. Relative humidity has been shown to correlate with isoprene emission rates. Both Guenther et al. (1991) and Fehsenfeld et al. (1992) report that a 10% increase in relative humidity leads to a 1-3% increase in isoprene emission rates. No consistent variation is noted for terpenes. Lamb et al. (1995) report positive correlations between ambient relative humidity and α-pinene concentrations. They also note results of enclosure studies that show wet branch emission fluxes are an order of magnitude higher than dry branch fluxes at the same temperature.

2.2.4 Flask Campaign: Interpretation

Measurements of light alkanes can be used to determine the photochemical history of an air mass. Once emitted, the fate of atmospheric trace species is determined by atmospheric processes including chemical destruction and mixing with other air masses. Knowledge of relative concentrations of hydrocarbons in an air mass can provide information about the degree of chemical processing that has occurred between emission and measurement since primary chemical destruction of light hydrocarbons occurs through reaction with OH and the rates of reaction differ. The analysis that follows could be quite powerful when joined with knowledge of back trajectories.

Many researches have employed the technique of analyzing hydrocarbon ratios in air samples to examine photochemical aging (Rudolph and Johnen, 1990; Parrish et al.,

1992; Jobson et al, 1994; Blake et al., 1996; Greenberg et al., 1996). Following Greenberg et al. (1996), the time rate of change of an individual hydrocarbon may be expressed as:

$$\frac{d[HC]}{dt} = -k_{HC}[OH][HC] - k_m([HC] - [HC]_d) \qquad (2.2.1)$$

where

[HC] = mixing ratio of the hydrocarbon
t = time
$[HC]_d$ = mixing ratio of hydrocarbon in a diluting air mass
k_{HC} = rate constant for reaction of hydrocarbon and OH radical
k_m = an idealized mixing coefficient

In the limiting case where dilution effects are ignored (i.e. k_m=0) the hydrocarbon concentration can be expressed as:

$$[HC] = [HC]_o \exp\{-k_{HC}\int_0^t [OH]dt\} \qquad (2.2.2)$$

$$[HC] = [HC]_o \exp\{-k_{HC} < [OH] > t\} \qquad (2.2.3)$$

where

$[HC]_o$ = the initial hydrocarbon concentration
<[OH]> = the time average OH concentration
t = the time since the injection of hydrocarbon into the air parcel

Equation 2.2.2 defines what is meant by the photochemical age of an individual hydrocarbon based on OH oxidation. Since in general it is difficult to accurately know the time averaged concentration of OH, it is useful to compare the ratios of three hydrocarbons. It follows that the concentration ratio of two hydrocarbons (HC1, HC2) will be:

$$\ln\left(\frac{[HC2]}{[HC1]}\right) = \ln\left(\frac{[HC2]_o}{[HC1]_o}\right) - (k_{HC2} - k_{HC1})\langle[OH]\rangle t \qquad (2.2.4)$$

A similar equation can be expressed for HC3 and HC1. Combining the two equations of the form 2.2.4 for three hydrocarbons, the term <[OH]>t may be eliminated. The resulting equation is:

$$\ln\left(\frac{[HC3]}{[HC1]}\right) = M\left\{\ln\left(\frac{[HC2]}{[HC1]}\right)\right\} + B \qquad (2.2.5)$$

where the slope M is equal to

$$M = \frac{(k_{HC3} - k_{HC1})}{(k_{HC2} - k_{HC1})} \qquad (2.2.6)$$

and the intercept B is given by

$$B = \ln\left(\frac{[HC3]_o}{[HC1]_o}\right) - M\left\{\ln\left(\frac{[HC2]_o}{[HC1]_o}\right)\right\} \qquad (2.2.7)$$

For the limiting case where chemistry has no effect on the time evolution of ratios (inert species or reaction rates with OH = 0) and we assume k_m is constant (or an integrated average over time), and $[HC]_d$ is negligible, equation 2.2.1 will reduce to

$$\ln\left(\frac{[HC3]}{[HC1]}\right) = \ln\left(\frac{[HC2]}{[HC1]}\right) + \ln\left(\frac{[HC3]_o}{[HC2]_o}\right) \qquad (2.2.8)$$

The relationships between n-butane (HC3), propane (HC2) and ethane (HC1) for our seasonal measurements are graphed in Figure 2.2.7. The data are divided into four sets of points: the first and second are clean and polluted air samples (as determined by the criteria in section 2.2.3) obtained when local air flow was from any octant except the east or southeast. The third and fourth are clean and polluted air samples coming from

the east and southeast octants. The slope obtained using all points regardless of octant wind direction or polluted/clean classification was 1.07 with an r-squared value of 0.64. The plotted regression line with a slope of 1.47 and r-squared value of 0.834 was obtained by excluding data points from the east/southeast which demonstrated pollution. Table 2.2.3 gives a summary of results for the slopes and r-squared values reported by investigators in the last decade. The slopes agree somewhat well with one another which is surprising in that the measurements come from a variety of locations. The slopes are also quite different from the theoretical slope (from equation 2.2.6) obtained if chemistry is the only mechanism for loss of hydrocarbons in an air parcel. This slope is in the vicinity of 2.6 depending on the temperature chosen, as reaction rates have temperature dependence. Clearly, this assumption that the time evolution of concentration ratios with a parcel will follow the chemistry line is faulty. The deviations are due primarily to the effects of mixing on a parcel's hydrocarbon mixing ratios. The chemistry slope has dependency on the temperature chosen in addition to the experimentally determined rate constant. Parrish et al. (1992) estimate the uncertainty in

Table 2.2.3 Summary of recent results for the slope of ln [Butane] / ln [Ethane] versus ln [Propane] / ln [Ethane]. Notice the range 1.42-1.68 is well below the theoretical slope calculated by time evolution of concentrations governed by kinetics alone.

Researcher	Slope	r squared
Rudolph and Johnen (1990)	1.66	0.89
Parrish et al. (1992)	1.47	
Jobson et al. (1994a)	1.68	0.95
Jobson et al. (1994b)	1.44	0.92
Bottenheim and Shepherd (1995)	1.42	0.69
Greenberg et a. (1996)	1.51-1.68	0.70-0.98
Blake et al. (1996)	1.6	0.63
Graham (this thesis)	1.47	0.83

the slope due to uncertainty in the rate constants to be within 7%. As mixing ratios approach detection limits, further errors can be introduced into calculating photochemical age of an air parcel.

For each point on Figure 2.2.7, the ratio pair may be used to get the relative photochemical age of the alkanes in the air parcel. First, an arbitrary point in the upper right hand corner of the plot representing the initial parcel hydrocarbon ratio was chosen. This ratio is approximately 1.65:1 for propane:ethane and 1.46:1 for butane:ethane. That point is then used to plot the lines which give the time evolution of hydrocarbon ratios for the two limiting cases on the Figure (m= 1 for dilution and m = 2.58 for chemistry). The photochemical age is defined by equation 2.2.3 and by assuming [OH] = 1 x 10^6 molecules cm^{-3}, we can mark along the chemistry only line the chemical processing time required to reach a particular point along the line (which represents a particular ratio for propane:ethane and butane:ethane). To obtain the photochemical age of an air parcel from the butane to ethane ratio of a particular sample point, simply move horizontally (i.e. maintaining a constant butane:ethane ratio) until the chemistry slope is reached. Since we have guessed at the initial emission ratio, and have marked the photochemical processing time on the chemistry line, by assuming chemistry alone has influenced the change in hydrocarbon ratio, we can read the photochemical processing time for a sample point from the chemistry line. The propane to ethane ratio is used in a like manner, following along a constant ratio vertically until the chemistry line is intersected. The crosses along the chemistry line give the photochemical age of the parcel. One could also calculate the age from equation 2.2.4 assuming the initial emission ratio and average [OH] are known. For most of our sample points, we get two different predictions of air mass age, implying either or initial ratio is incorrect or more likely, that mixing processes are also involved in changing hydrocarbon ratios in the air mass.

As discussed in Parrish et al. (1992), mixing of air parcels causes the measured ratios to lie above and to the left of the kinetic slope. The photochemical age of the

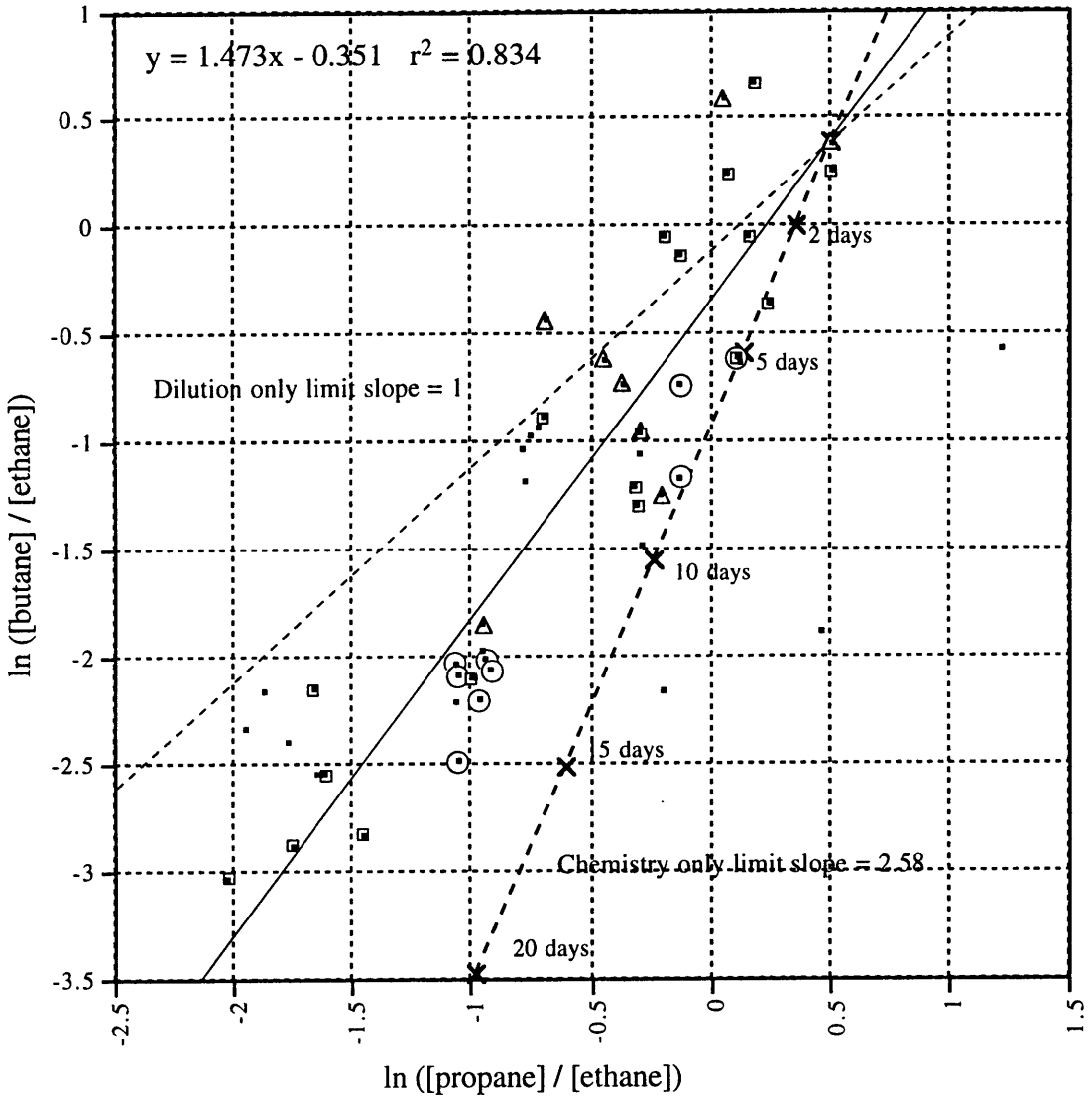

Figure 2.2.7 The relationship between the natural logarithms of butane:ethane and propane:ethane concentration ratios is plotted. Boxed points represent clean air with a local wind direction not from the east or southeast. Circled points are clean air from the east or southeast. Triangled points are polluted air from non east or southeast octant. Remaining points are polluted samples from the east or southeast. The linear regression line (solid) is fitted to encapsulated data points. An arbitrary point was chosen in the upper right hand corner as the theoretical initial emission ratio. Lines are displayed to show the bounds of chemistry or dilution only processes. The crosses along the chemistry line give time in days required to reach that pair of ratios. These times were calculated using equation 2.2.4 with <[OH]> assumed to be 10^6 cm^{-3}.

mixed parcel will lie somewhere between the age of the two original parcels. From the point of view of one parcel, if the other parcel has higher ratios (i.e. hydrocarbons more recently emitted) then the apparent age of the parcel will be less than the true age of the parcel. The two ratios will give different indications of parcel age, with the calculated age from the less reactive species being closer to the actual age of the original parcel. In the case where a more dilute, aged parcel is mixed in, the age calculated from the more reactive species will lie closer to the true age of the original parcel.

Some of the uncertainty for calculating ages can be removed by comparing two species with like reaction rates with OH, for example, n-butane and i-butane. The kinetic slope at 298 K for these two species ratioed to ethane is 0.91. For this case, the slopes of the two theoretical limits for dilution only or for chemistry only nearly coincide. The dilution only slope is unity by equation 2.2.8. If we assume that the initial emission ratios of these two compounds are nearly uniform, then when one parcel mixes with another, the difference in apparent photochemical age from both compounds will be similar. The dilution effect yielding different photochemical ages is therefore minimized.

The data for n-butane and i-butane are plotted in Figure 2.2.8. We have broken the data into two distinct sets (plotted as circles and squares). The slopes for both regression lines agree well with that expected from chemistry, demonstrating that the effects of dilution on the ratios has been minimized. By inspection of Figure 2.2.8 and the ratios of i-butane:n-butane for each data point, it is apparent that iso-butane levels are sometimes higher relative to n-butane than would be expected. Generally, the range of ratios is reported in the literature to be 0.4-0.6. Indeed, for the in situ measurements discussed later, these expected ratios hold up. For the seasonal data, the majority of points (squares) are clustered around the commonly reported range with an average value of 0.55 and standard deviation of 0.09. The other group (circles) has iso-butane levels an average of 1.13 times those of n-butane with the standard deviation equaling 0.23. This would seem to imply that some of the air samples had different emission sources from those seen over the summer of 1996. Ordinarily both isomers are reported

to have similar sources with the normal isomer about twice as prevalent. From the seasonal data, it seems there must be some other source which contributes an uncharacteristically high level of isobutane. The air samples having this higher ratio are considered polluted by our methods with local winds blowing anywhere from 0° (N) to 180° (S) but not from the west. It should also be noted that the ratios of n-butane and propane to ethane are both greater in my measurements than others reported in the literature. This is most likely due to the prevalence of propane fuel use in China. Butane and ethane are both contaminants of the liquid propane used there, with butane having the higher concentration of the two.

One would expect the plots to have the air masses with the most recent emissions to lie in the upper right hand corner. All of the results from previous papers we have cited have ethane being more concentrated than the butanes and propane. This may be in part due to the relative distance the sampling sites were from the sites of emission. It seems clear that a fair number of my samples suffered from recent injections of light hydrocarbons as the propane and the butanes had higher levels than ethane. Bottenheim and Shepherd (1995) and Jobson et al. (1994) show that winter measurements cluster in the upper right and summer measurements in the lower left. This reflects the influence of seasonal OH levels. Points in the lower left show older, more chemically processed air. Figure 2.2.7 does not show that exactly. The right most points above (0,0) are all from summer measurements. The points near (-0.25, -1.25) and the large cluster near (-1, -2) are primarily winter measurements and those points in the lower left are from late spring and summer. The April measurements are all in the lower left which makes sense since ethane is still at its high winter levels whereas the more reactive hydrocarbons have already started into their seasonal decline.

Several papers have been published in the 1990's which investigate the uses of equation 2.1.1 through models (McKeen et al, 1990, 1993, 1996). Significant simplifications used in our approach may be problematic. One is the assumption that k_m and $k_i \times$ [OH] are constants. Another, that the processes of mixing and chemistry are

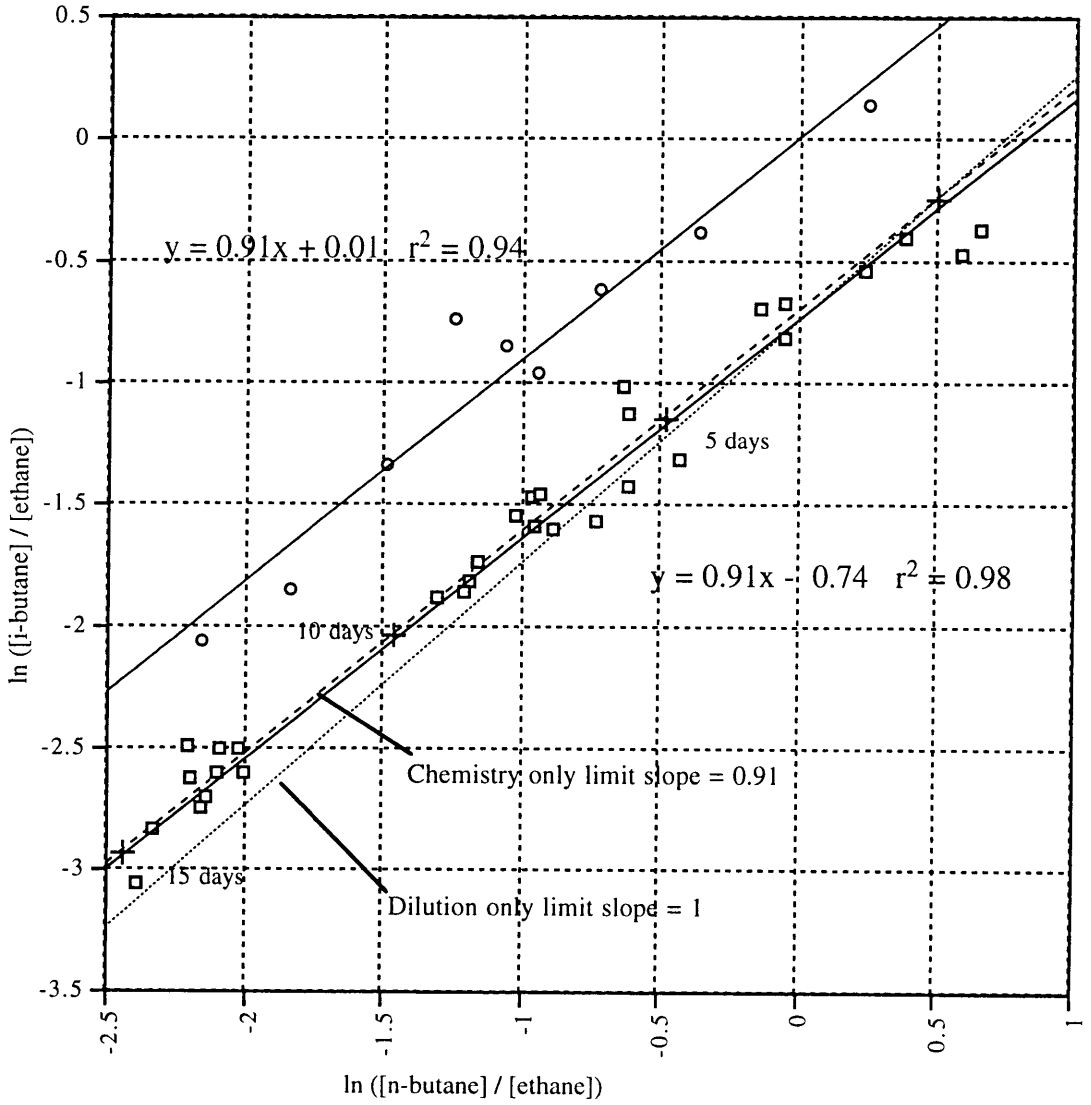

Figure 2.2.8 The relationship between the natural logarithms of i-butane:ethane and n-butane:ethane concentration ratio is plotted. The solid linear regression line is given for two sets of points. The squares represent air parcels with a mean i-butane to n-butane ratio of 0.55. The circles are points from air samples having a 1.13 average i-butane to n-butane ratio. It is likely that there are two distinct sources which account for the different ratio of butane isomers. An arbitrary point is used in the upper right hand corner to represent the initial emission ratios for the squares. The dashed lines show the expected bounded behavior due to mixing and chemistry. Crosses on the chemistry line give photochemical age values as determined from equation 2.2.4 with assumed <[OH]> to be 10^6 cm^{-3}.

separable, may not hold. Errors are also introduced by ignoring background concentrations, $[HC]_d$, in the analysis. Following the procedure in McKeen et al. (1996), we attempt to better quantify the relative effects of dilution versus chemistry to explain the deviations from the theoretical kinetic slope.

If we consider two species whose reactivity with OH is great enough such that the background levels of hydrocarbon ($[HC]_d$) are minimal in comparison to levels in polluted air, we can solve equation 2.2.1 for two hydrocarbons and combine the solutions to obtain

$$\ln\left(\frac{[HC1]}{[HC1]_o}\right) = \left(\frac{k_m + L_{HC1}}{k_m + L_{HC2}}\right)\ln\left(\frac{[HC2]}{[HC2]_o}\right) \qquad (2.2.9)$$

where L_i equals loss of species i due to reaction with OH and k_m is the mixing parameter. By plotting the ln values of two hydrocarbons, we may get the value of the slope of equation 2.2.9. Then a measure of the relative effects of photochemistry versus dilution can be derived using the relation between L_{HC1} and L_{HC2}. We want to solve the slope relation for the ratio k_m/L_{HC2} using $L_{HC1}/k_{HC1} = L_{HC2}/k_{HC2}$. This leads to

$$m \cdot (k_m + L_{HC2}) = k_m + rL_{HC2} \qquad (2.2.10)$$

where m is the slope from the log HC1 versus log HC2 plot and r is k_{HC1} / k_{HC2}. The desired ratio follows: $\frac{k_m}{L_{HC2}} = \frac{r-m}{m-1}$ (2.2.11)

We calculated three separate values for this ratio using the seasonal dataset. They are summarized in Table 2.2.4. Propane was plotted against i-butane, n-butane and n-pentane yielding three different values for the relative effects of mixing and chemistry ranging from 1.71 to 3.05 with an average of 2.4 (equation 2.2.11). This implies that mixing processes are almost 2.5 times more important than chemistry in determining the relative hydrocarbon mixing ratios we measured. If we weight the theoretical slopes of unity for mixing and 2.58 for chemistry by this ratio (about 30% chemistry and 70% mixing) we obtain a value of 1.46 for the expected slope of plotted hydrocarbon ratios which agrees with our value of 1.47 in Figure 2.2.7. It should be noted that the uncertainty from the reaction rates and measured quantities of roughly ± 0.30 for each ratio computed from equation 2.2.11 does not account for the variation seen for these three estimates.

Table 2.2.4 Summary of measurements to determine the relative importance of mixing versus chemical processes. The range of values is quite wide, likely due to the fact that our air mass origins were varied.

Plotted Species	Slope (m)	ratio of k_{OH} (r)	k_m/L_{HC2}
ln Propane v. ln i-butane	0.812	0.491	1.71
ln Propane v. ln n-butane	0.865	0.453	3.04
ln Propane v. ln n-pentane	0.794	0.292	2.44

In general we cannot assume that the background concentrations of hydrocarbons in the diluting air masses are negligible since we are in a terrestrial site with nearby population centers. This is especially true for the longer lived species. Equation 2.2.5 requires a background value to be subtracted from [HC1], [HC2] and [HC3] when k_m is non-zero. Depending on the relative atmospheric levels being measured in the sample and in the background air, the background term may be ignored. The subtracted background value is scaled by the factor $k_m / (k_m + L_{HC})$ which appears in the general solution to equation 2.2.1 when k_m is non-zero. The more reactive the species, the smaller the scaling factor, as the loss term in the denominator will start to outweigh the mixing term.

We can determine k_m from our analysis of the relative effects of dilution and chemistry. Table 2.2.4 gives us the ratio of k_m to the inverse lifetime of three separate hydrocarbons. Using the fact that the atmospheric lifetimes of alkanes are related through their reaction rates with OH, we can solve for the above scaling factor. To determine the scaling factor for ethane, we solve for k_m from Table 2.2.4; k_m equals the value in the last column divided by the lifetime of the hydrocarbon for each row. We need not know OH since it factors out of the scaling term, leaving $\# k_i / (\# k_i + k_{ethane})$ where # represents the number in the third column of the Table and k_i is the corresponding OH-hydrocarbon reaction rate constant. The values for the scaling of ethane background obtained for i-butane, n-butane and n-pentane are 0.91, 0.97 and 0.97 respectively. Inclusion of this background value for ethane results in the predicted

trendline lying between the pure chemistry and pure mixing slopes, just as our actual data does. As time increases, and ethane concentrations in the plume approach background values, the slope of the line will approach $(k_m + L_{n\text{-}butane}) / (k_m + L_{propane})$ (McKeen et. al., 1996). For our predicted values of k_m, the slope should eventually reach 1.13-1.27. The points in the lower left hand side of the Figure 2.2.7 appear to be bending away from the best fit slope for all points, perhaps as a result of this background effect.

Figure 2.2.9 displays all twenty-six days of flask measurements for thirty-nine hydrocarbons. Cyclopropane, ethane and ethene are missing a few early measurements. Acetylene was not always cleanly separated from a nearby unidentified peak so concentrations are not given for some samples. Cyclopentene, cis-2-pentene and trans-2- pentene are lacking some points for the winter flasks. Some other hydrocarbons were identified with less frequency depending on run conditions and levels of the hydrocarbons in the sample. Several of the hexane isomers are unreported as they coeluted with one another. 1-pentene and 2-methyl-2-pentene also coeluted. Limonene and sabinene were identified in some samples but analytical problems near the end of the run interfered with consistent data collection for those compounds.

Many of the samples showed heightened levels from some pollution source. September 25 and October 22 are good examples. Virtually all species reported show increased atmospheric levels on those days. The exclusively biogenic gases do not show the same consistent correlations as the other NMHC. In some cases, terpene concentrations seem to be higher when pollution events occur. February 29 seems a bit different than other days with elevated hydrocarbon levels. On that day, the xylenes, toluene, isopentane and the methylpentanes display significant differences between the AM and PM measurements which are not mirrored in the other species. This seems to point to a different source of pollution for that afternoon.

The data from our seasonal flask campaign is quite sparse, which makes it difficult to make any grand conclusions. There is evidence that the biogenic gases

including isoprene, the terpenes and propene have a seasonal cycle with highest levels seen during the summer and lower values observed during the colder winter months. The reverse trend is apparent for the light alkanes, as might be expected from the seasonal variations in OH levels. Unfortunately, the preponderance of polluted air samples decreases the usefulness of our data for determining background levels of hydrocarbons over the year. This may be due to immediately local pollution sources or could also be a result of the proximity of two major populations centers to the biosphere reserve: Guangzhou which is 86 kilometers to the east, and Zhaoqing, the provincial capital, which is 19 kilometers to the west.

Figure 2.2.9 Results of the flask measurement campaign at Dinghushan Biosphere Reserve from June 1995 through August 1996. Note the x-axis is not linear in time and the y-axis is a log scale of NMHC concentration (ppbv). The two curves reflect the morning measurement (squares-solid line) and afternoon measurement (diamonds-dotted line).

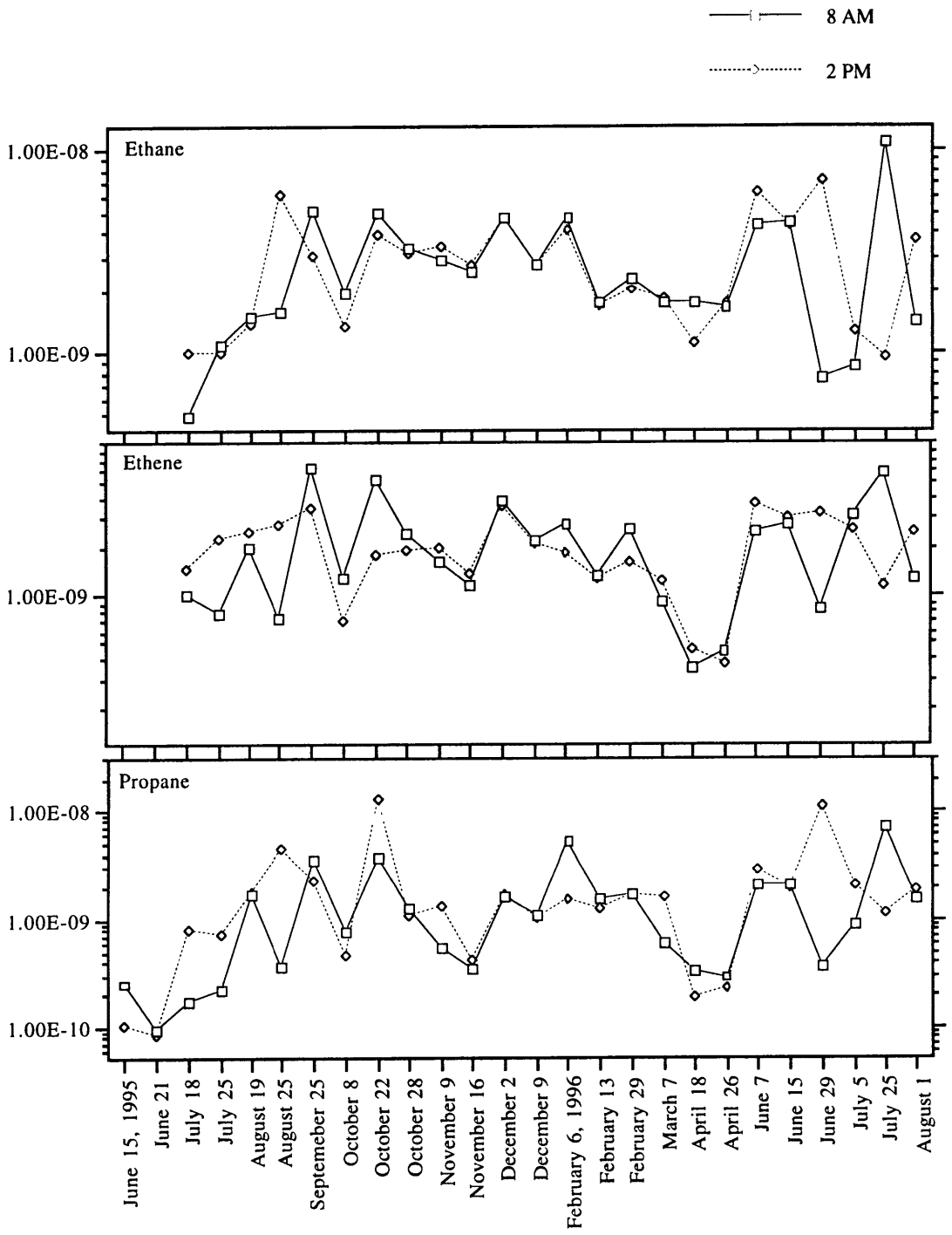

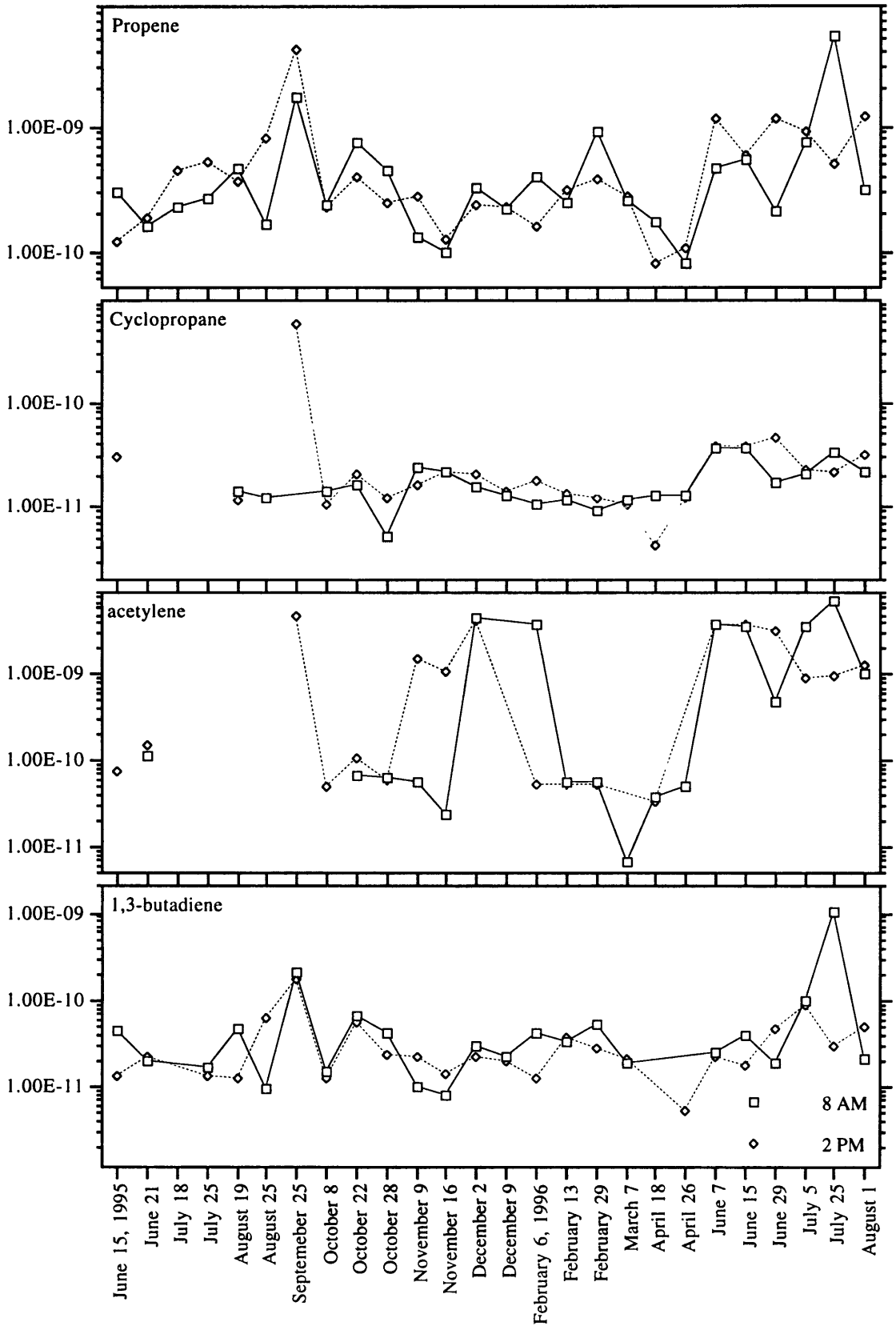
Propene
1.00E-09
1.00E-10
Cyclopropane
1.00E-10
1.00E-11
acetylene
1.00E-09
1.00E-10
1.00E-11
1,3-butadiene
1.00E-09
1.00E-10
1.00E-11
8 AM
2 PM
June 15, 1995
June 21
July 18
July 25
August 19
August 25
Septemeber 25
October 8
October 22
October 28
November 9
November 16
December 2
December 9
February 6, 1996
February 13
February 29
March 7
April 18
April 26
June 7
June 15
June 29
July 5
July 25
August 1

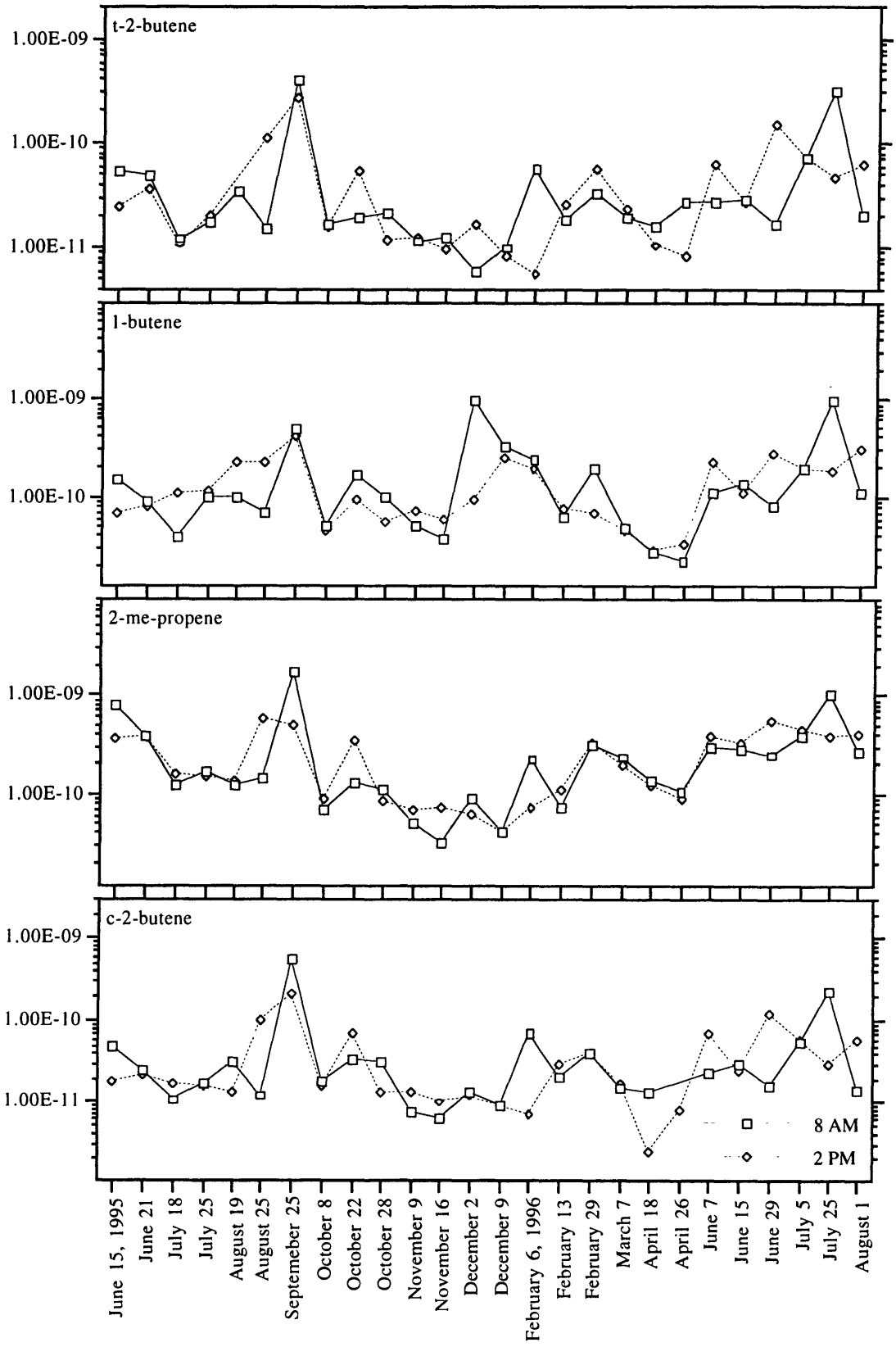
t-2-butene
1.00E-09
1.00E-10
1.00E-11
1-butene
1.00E-09
1.00E-10
2-me-propene
1.00E-09
1.00E-10
c-2-butene
1.00E-09
1.00E-10
1.00E-11
8 AM
2 PM
June 15, 1995
June 21
July 18
July 25
August 19
August 25
Septemeber 25
October 8
October 22
October 28
November 9
November 16
December 2
December 9
February 6, 1996
February 13
February 29
March 7
April 18
April 26
June 7
June 15
June 29
July 5
July 25
August 1

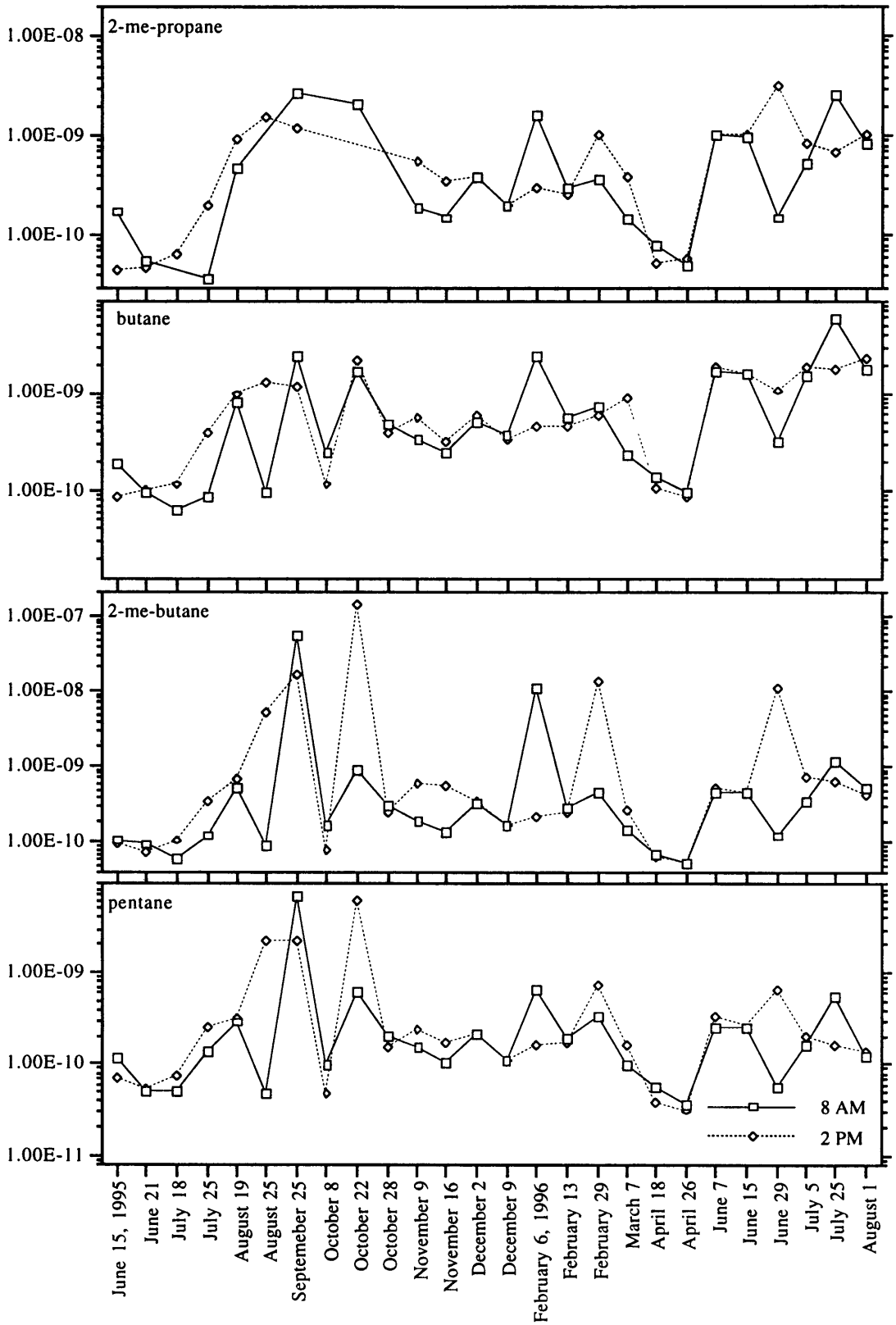
2-me-propane
1.00E-08
1.00E-09
1.00E-10
butane
1.00E-09
1.00E-10
2-me-butane
1.00E-07
1.00E-08
1.00E-09
1.00E-10
pentane
1.00E-09
1.00E-10
1.00E-11
8 AM
2 PM
June 15, 1995
June 21
July 18
July 25
August 19
August 25
Septemeber 25
October 8
October 22
October 28
November 9
November 16
December 2
December 9
February 6, 1996
February 13
February 29
March 7
April 18
April 26
June 7
June 15
June 29
July 5
July 25
August 1

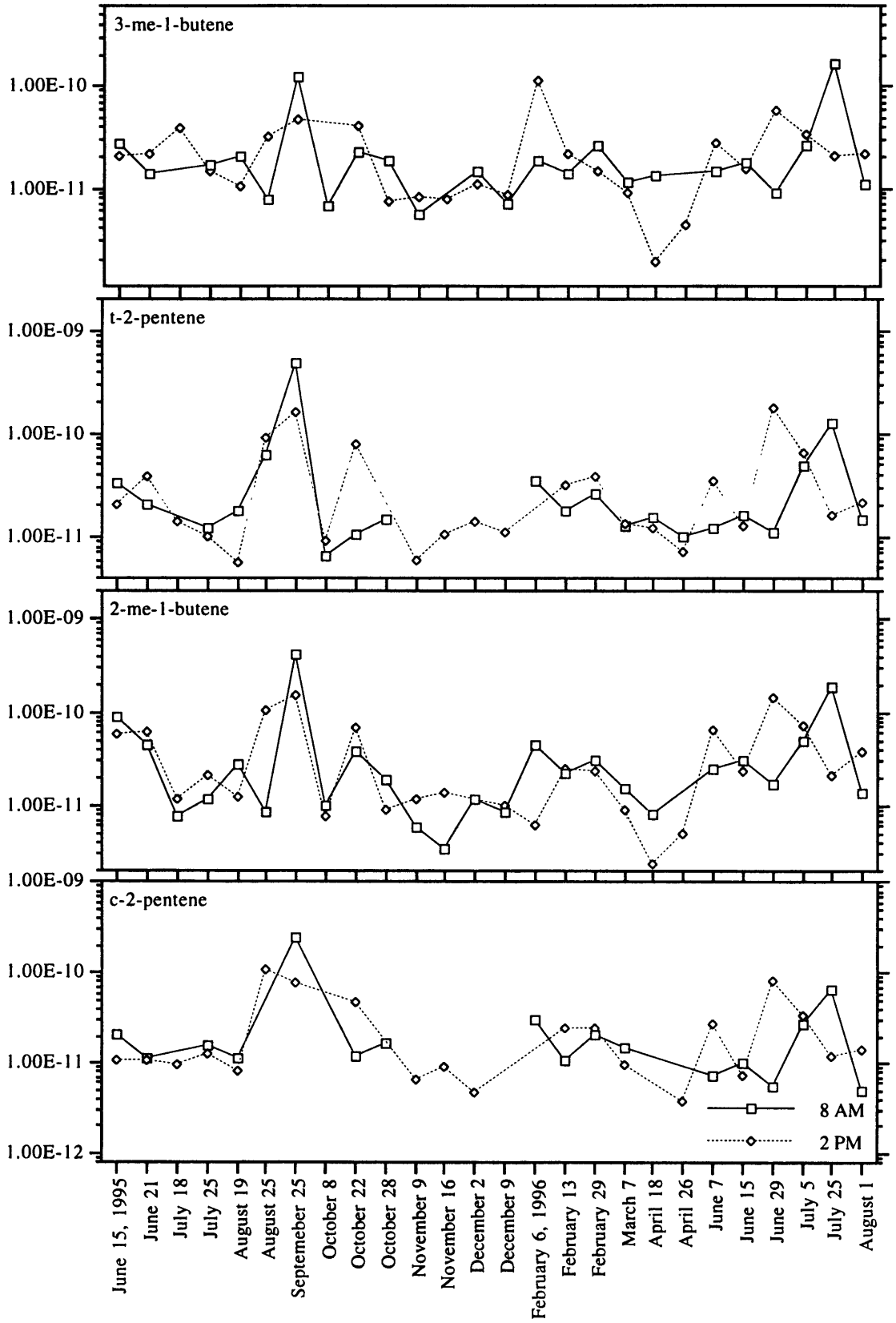
3-me-1-butene
1.00E-10
1.00E-11
t-2-pentene
1.00E-09
1.00E-10
1.00E-11
2-me-1-butene
1.00E-09
1.00E-10
1.00E-11
c-2-pentene
1.00E-09
1.00E-10
1.00E-11
1.00E-12
8 AM
2 PM
June 15, 1995
June 21
July 18
July 25
August 19
August 25
Septemeber 25
October 8
October 22
October 28
November 9
November 16
December 2
December 9
February 6, 1996
February 13
February 29
March 7
April 18
April 26
June 7
June 15
June 29
July 5
July 25
August 1

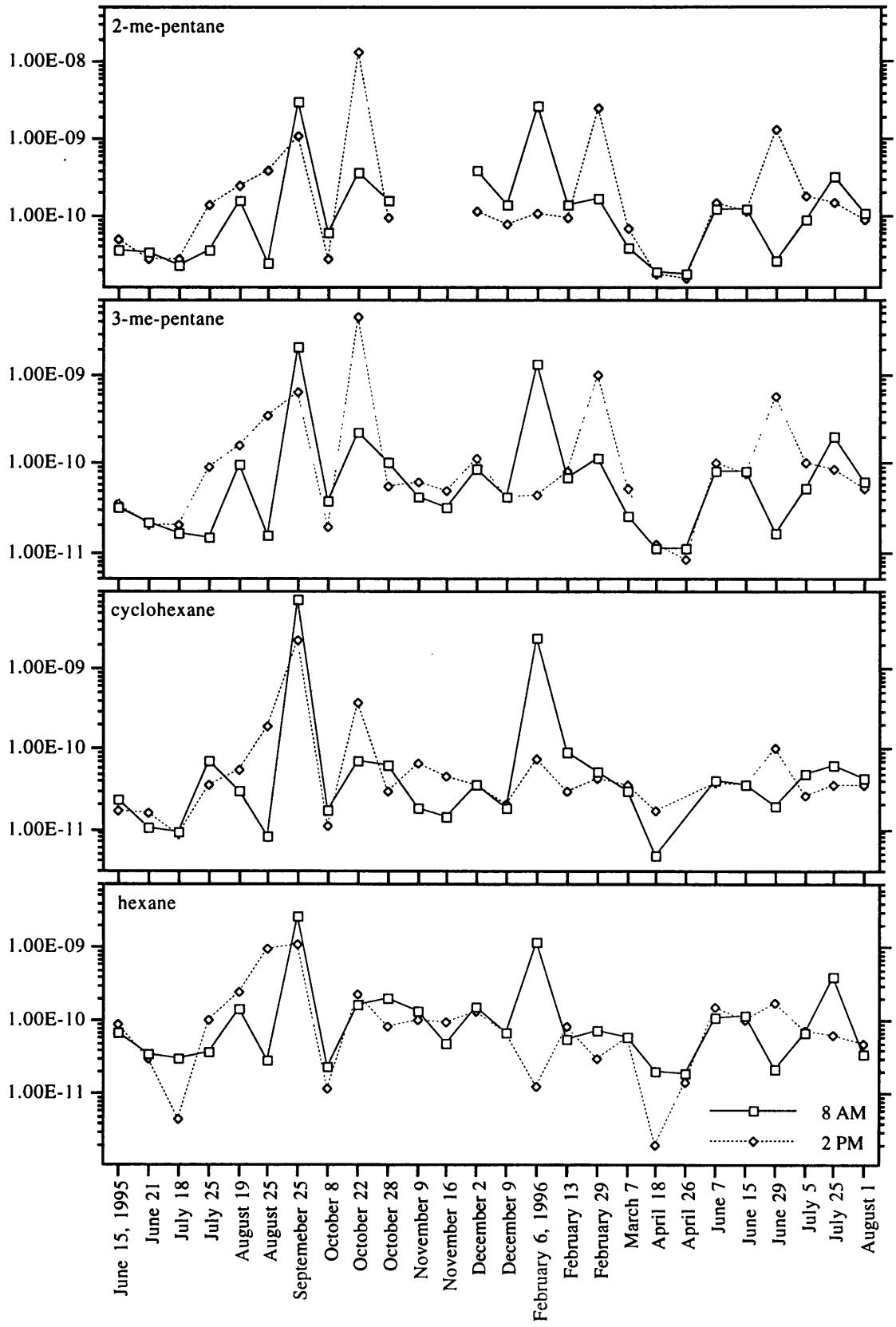
2-me-pentane
1.00E-08
1.00E-09
1.00E-10
3-me-pentane
1.00E-09
1.00E-10
1.00E-11
cyclohexane
1.00E-09
1.00E-10
1.00E-11
hexane
1.00E-09
1.00E-10
1.00E-11
8 AM
2 PM
June 15, 1995
June 21
July 18
July 25
August 19
August 25
Septemeber 25
October 8
October 22
October 28
November 9
November 16
December 2
December 9
February 6, 1996
February 13
February 29
March 7
April 18
April 26
June 7
June 15
June 29
July 5
July 25
August 1

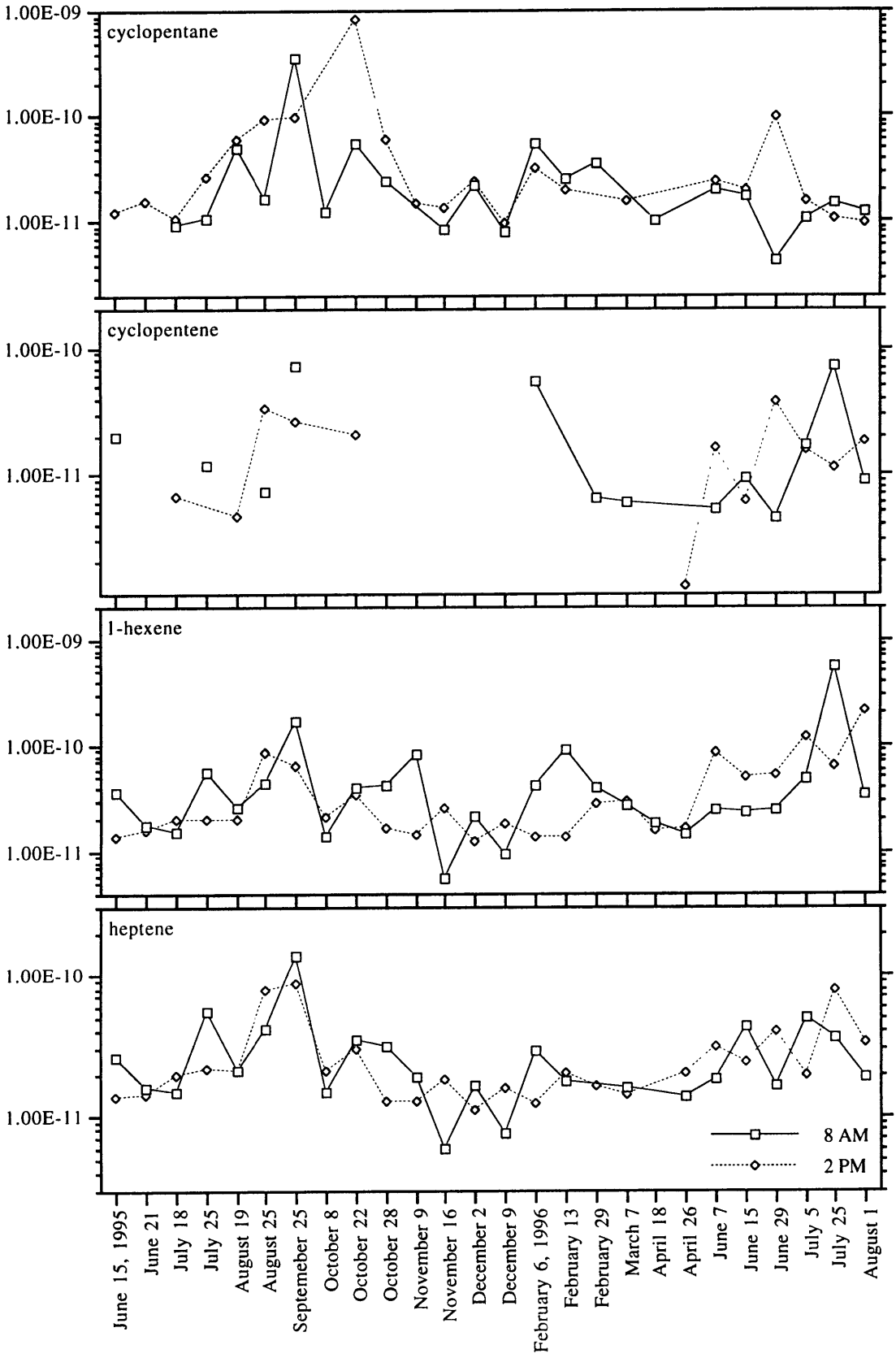
cyclopentane
1.00E-09
1.00E-10
1.00E-11
cyclopentene
1.00E-10
1.00E-11
1-hexene
1.00E-09
1.00E-10
1.00E-11
heptene
1.00E-10
1.00E-11
8 AM
2 PM
June 15, 1995
June 21
July 18
July 25
August 19
August 25
Septemeber 25
October 8
October 22
October 28
November 9
November 16
December 2
December 9
February 6, 1996
February 13
February 29
March 7
April 18
April 26
June 7
June 15
June 29
July 5
July 25
August 1

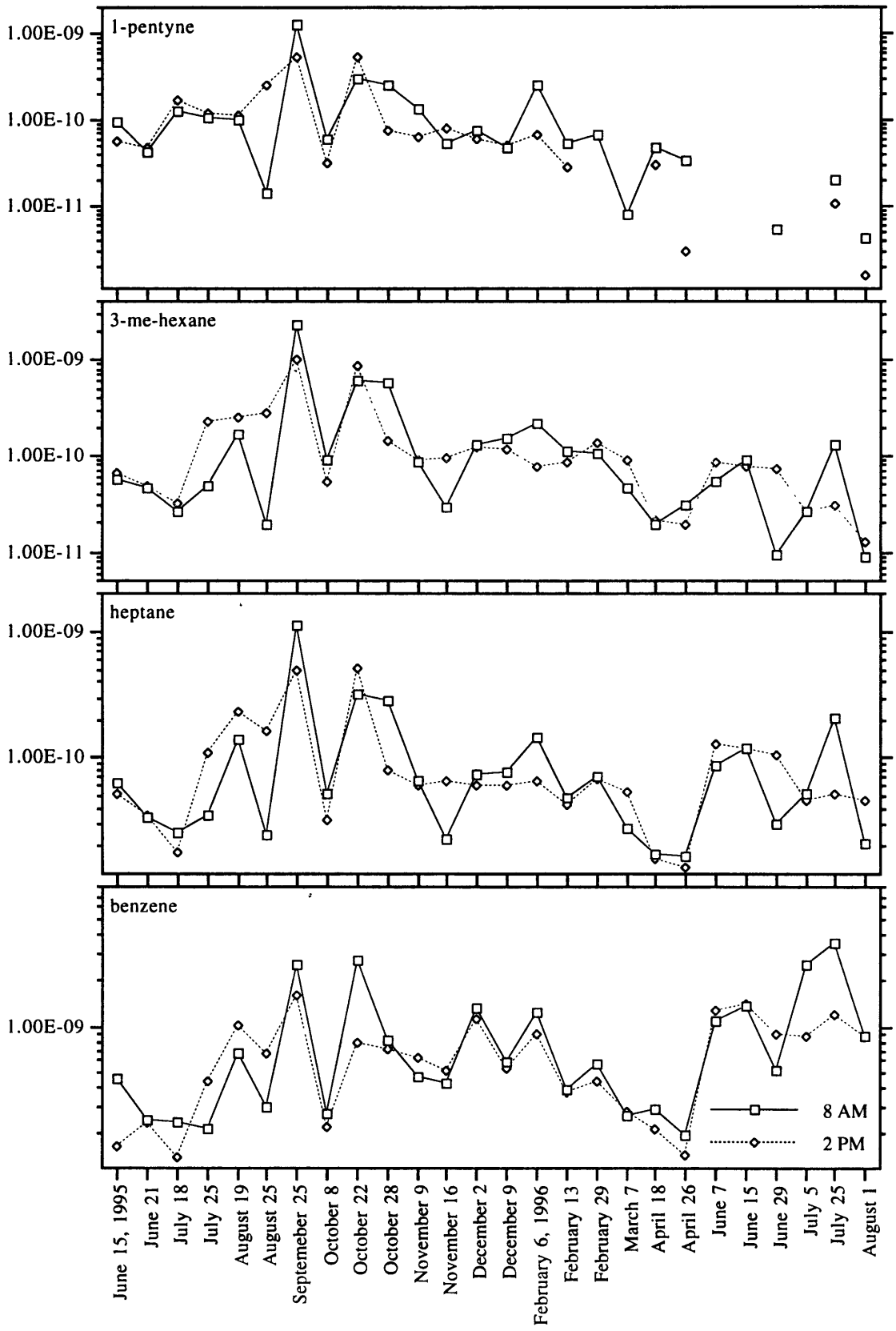
1-pentyne
1.00E-09
1.00E-10
1.00E-11
3-me-hexane
1.00E-09
1.00E-10
1.00E-11
heptane
1.00E-09
1.00E-10
benzene
1.00E-09
8 AM
2 PM
June 15, 1995
June 21
July 18
July 25
August 19
August 25
Septemeber 25
October 8
October 22
October 28
November 9
November 16
December 2
December 9
February 6, 1996
February 13
February 29
March 7
April 18
April 26
June 7
June 15
June 29
July 5
July 25
August 1

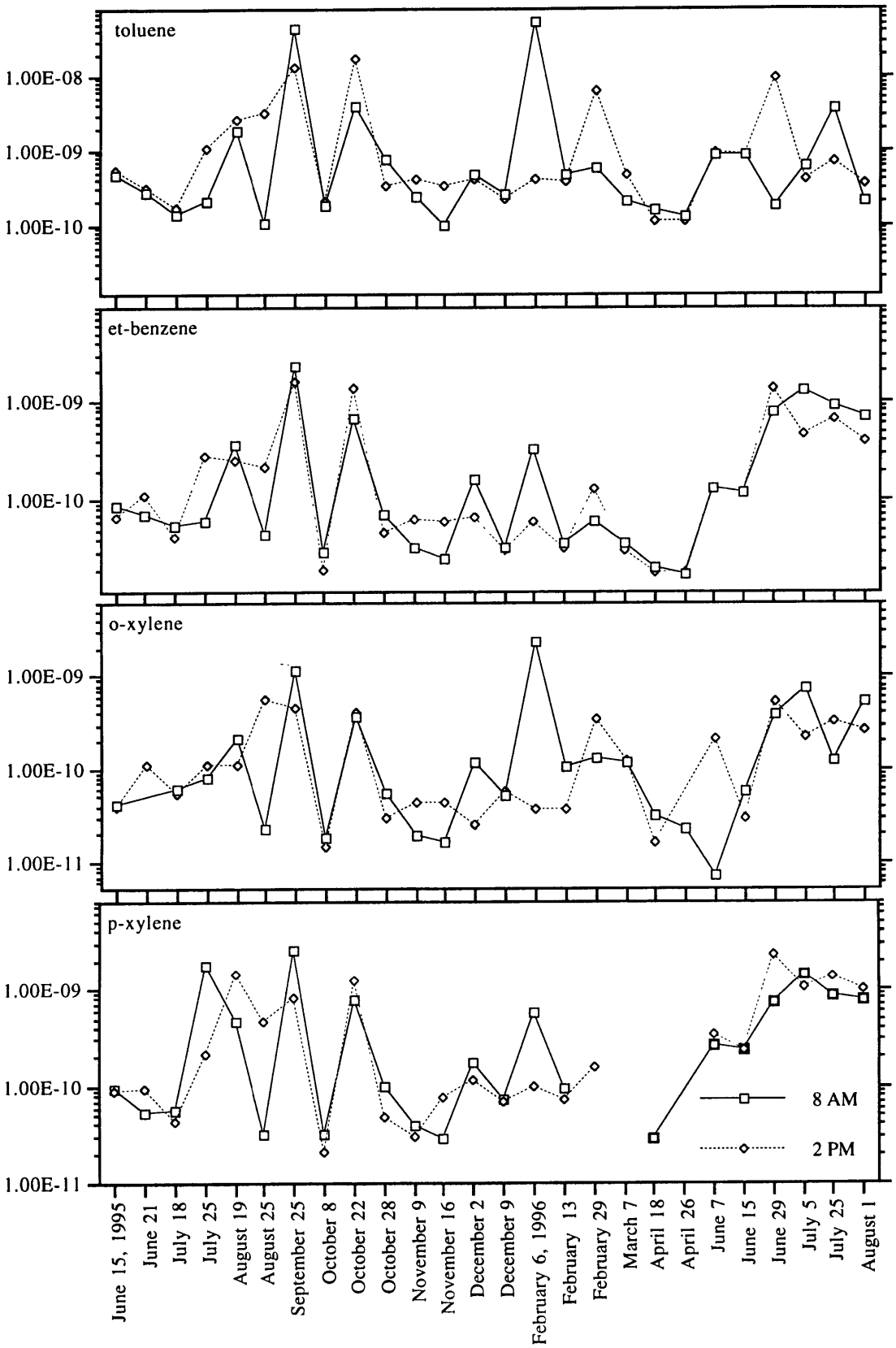
toluene
1.00E-08
1.00E-09
1.00E-10
et-benzene
1.00E-09
1.00E-10
o-xylene
1.00E-09
1.00E-10
1.00E-11
p-xylene
1.00E-09
1.00E-10
1.00E-11
8 AM
2 PM
June 15, 1995
June 21
July 18
July 25
August 19
August 25
September 25
October 8
October 22
October 28
November 9
November 16
December 2
December 9
February 6, 1996
February 13
February 29
March 7
April 18
April 26
June 7
June 15
June 29
July 5
July 25
August 1

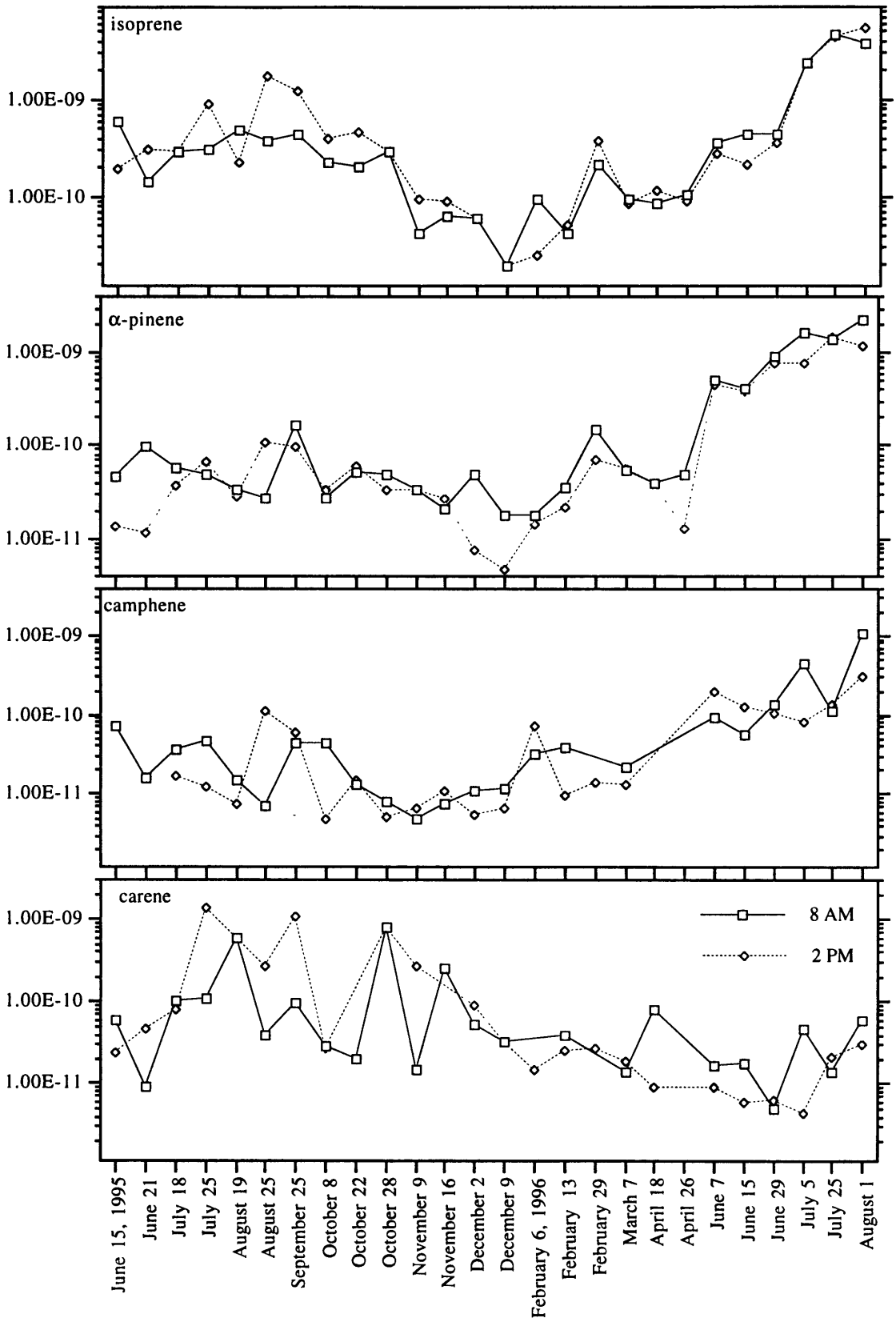
isoprene
1.00E-09
1.00E-10
α-pinene
1.00E-09
1.00E-10
1.00E-11
camphene
1.00E-09
1.00E-10
1.00E-11
carene
1.00E-09
1.00E-10
1.00E-11
8 AM
2 PM
June 15, 1995
June 21
July 18
July 25
August 19
August 25
September 25
October 8
October 22
October 28
November 9
November 16
December 2
December 9
February 6, 1996
February 13
February 29
March 7
April 18
April 26
June 7
June 15
June 29
July 5
July 25
August 1

Chapter 3: In situ Measurements

3.1 Intensive Phase: Experimental

The intensive phase of our campaign covered nine weeks from June 28 through August 31 in the summer of 1996. We sampled NMHC hourly using a dual FID set-up which enabled us to identify over 50 distinct NMHC. Information regarding NO/NO_2 concentrations was also obtained. For a two week period, we collected CO data. We also performed some simple bag enclosure measurements to estimate the emission rate of NMHC from local dominant vegetation.

Initially, we had two separate sample lines; the first was 1/4" OD stainless steel for the hydrocarbon system and the second a 1/4" OD FEP Teflon for the other gas measurements. Due to pump failure, we resorted to using one Teflon sample line from the evening of Julian day 191 on. The line was installed at the height of 10 meters, hanging off a branch in the lower canopy but at least four meters away from the nearest foliage. An inverted funnel with a Teflon particle filter was used at the inlet. The sample line was 35 meters long, and located upslope, to the west of the laboratory building. The slope was roughly 30°, which positioned the inlet above the canopy around the laboratory building and downhill from it, but below the canopy of the trees surrounding and uphill (See Figure 3.1.1). A small clearing was located just southeast of the sample funnel, and slightly to the east stood a temple complex.

Air samples were pulled down the sample line at roughly 8 liters per minute using a model MB-158 Metal Bellows pump. Hydrocarbon air samples were siphoned off of the main flow at a rate of 25 standard cubic centimeters per minute (sccm). The bulk of the flow was sent on to the NO_x, O_3 and CO detectors which required 2 liters per minute for their analyses. The remaining flow was vented through a tee with an 18 inch extension to ensure no room air was pulled back up the line to the instruments (Figure 3.1.2).

We initially used an automated sampling collection for the hydrocarbons through Julian day 183. The computer controlled cooling and heating cycles of both

sample and cryofocus loops were realized by raising and lowering the liquid gas level in the cryogenic tanks rather than physically moving the loops. This control was accomplished by installing the loops in a cryogenic cylinder which was in turn inserted into a bigger cryogenic tank. The opening at the lowest part of the insertion cylinder made the fluid connection between the two cylinders. The system was made air tight and closed after being filled with liquid gas. The gas was stored inside the tank at roughly 25 psig. By letting pressed gas enter and exhaust from the insertion cylinder, the liquid level, and hence loop cooling, was readily controllable. This process was governed by a level controller which sensed the level inside the tank via thermocouples positioned inside the tank. The computer instructed the level controller when to activate the pressure control solenoid valve to achieve the desired loop trapping temperature. The heat cycle was also initiated by the computer. The cartridge heater warmed the loop and simultaneously vaporized the liquid immersing the loop, causing a pressure increase which forced the liquid level lower.

The main body of the liquid level controlling system was designed with one cryogenic cylinder within another. The outer tank is commercially available (LN-30 Andonian Cryogenics, Inc., Waltham, MA) used without further modification. The inner cylinder or insertion port was specially designed and manufactured by the same company. The controlling mechanisms were all attached to the cylinder through its top flange: gas inlet, outlet, and loop, the solenoid valves, the level sensing thermocouples, the heating cartridge and all the electrical feedthrough. The loop was under constant cooling either by contact with liquid gas or with vapor in equilibrium with the liquid unless the heating sequence was enacted. The liquid gas in the closed system was stored under constant pressure regulated by relief valves with normal relief pressure in the 25-30 psig range. Our design has the advantage of being closed, reducing static loss of liquid. Also, the elevated vapor pressure causes the liquid temperature to rise to a higher value than that under normal atmospheric pressure upon the new equilibrium. These effects both save money on the expense of liquid coolant, the latter effect allowing the use of relatively cheap liquid nitrogen over liquid argon.

The internal cylinder contains the loops, serving as the working volume of the controlling system. It has an inner diameter of 0.75 inches for the length inside the

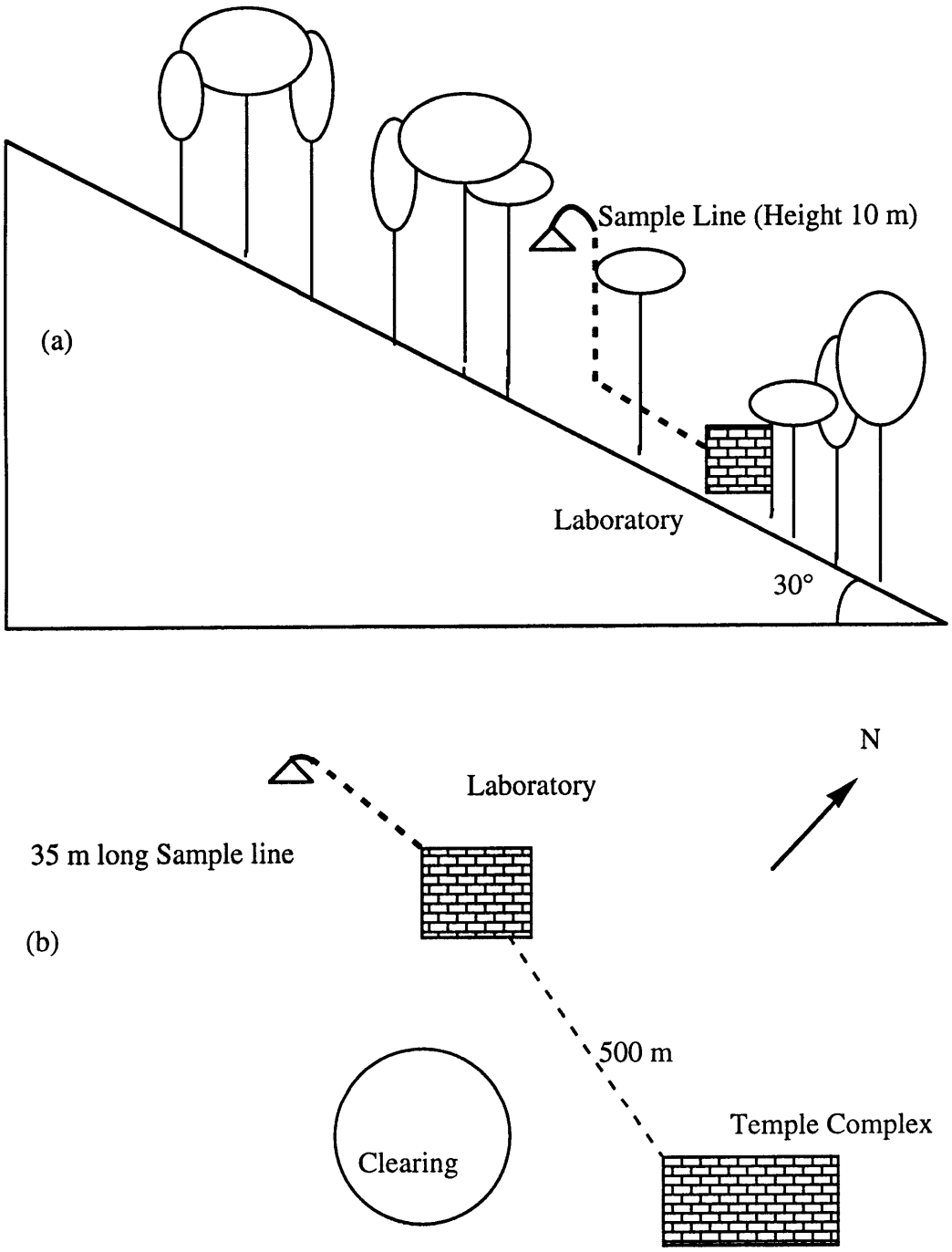

Figure 3.1.1 Schematic of the sampling site. The top figure (a) shows the slope from the sample inlet to the laboratory, highlighting the effect this had on the placement of the sample inlet within the canopy. The bottom figure (b) gives the general location of the temple complex in relation to the laboratory. The area called "clearing" isn't quite a clearing per se. It is an area where there was limited canopy overstucture such that wind coming from the southeast could potentially travel to the sample inlet without encountering foliage. This could be important in that deposition to the canopy can be significant.

outer tank and a slightly expanded bowl to physically mount the top flange through which the system communicates with the outside environment. A thinner internal diameter decreases the volume of working media when the same height of liquid level is required, hence reducing the time constant of the controlling cycle. The system works efficiently and quickly as a result.

Frequent cartridge heater failure (and limited replacement supply) prompted a return to manual sample collection using handheld dewars of liquid nitrogen. Collection using liquid nitrogen is far from ideal since trapping of unwanted oxygen may occur if the loop temperature is allowed to cool to that of liquid nitrogen. To avoid this, we held the sample loop above the level of the liquid nitrogen and monitored the loop temperature with a thermocouple. Constant collection temperature was impossible to maintain and was generally too low to quantitatively capture both ethane and ethene. After Julian day 197, we were able to use liquid argon which allowed efficient collection of all gases of interest.

Collection time was sixteen minutes after day 198 (previously 8-20 minute periods were used) with a flow rate of 25 sccm through a 0.39 cc inner volume stainless steel sample loop. Air was passed through a Nafion dryer and Ascarite II trap prior to collection to remove water and CO_2 respectively. A Tylan mass flow controller provided accurate measures of flow rate through the sample loop. After collection, the 6-port Valco valve was switched to inject placing the sample loop in-line with the carrier stream of the PLOT (Al_2O_3/Na_2SO_4) column. The sample went through a second Valco valve and entered a two meter piece of PLOT column used as a precolumn and means to separate light and heavy hydrocarbon fractions. During this time, the oven remained at a constant 120 ^oC. (This temperature was settled on by day 197 as the system had stabilized at that point. Prior to that, the temperature was different depending on carrier flow and retention capabilities of the precolumn). After three minutes, the second Valco valve was switched to inject, placing the precolumn in line with the carrier gas flow of the 60 m x 0.25 mm ID CP-Sil 5CB column. Light hydrocarbons passed completely through the precolumn during the three minutes and were cryofocused on 0.32 OD fused silica tubing. Heavy hydrocarbons remained in the precolumn and were subsequently flushed back out by the second carrier which traveled in reverse of the first. These compounds were trapped on a

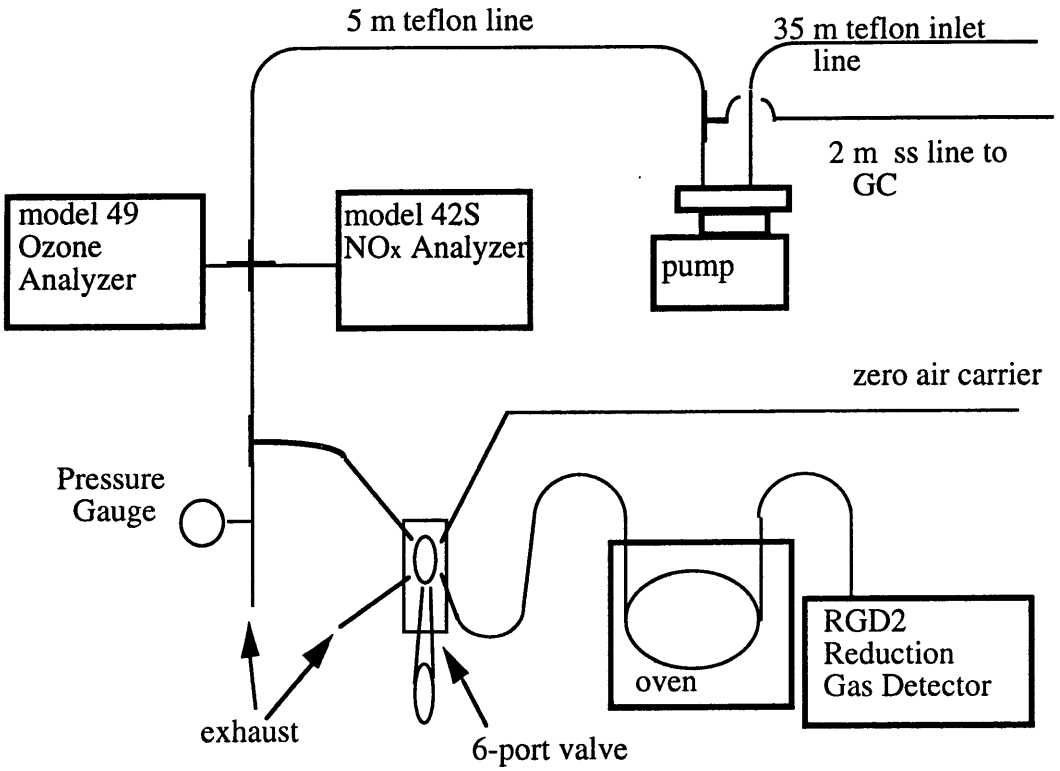

Figure 3.1.2 The inlet set up for trace gas measurements at Dinghushan. Flow was roughly 8 liters per minute, leading to residence time in the sample inlet line of 15 seconds maximum. Since the sample line volume is under one liter (calculated at 700 cm-3), the residence time is more likely about 6 seconds.

second fused silica loop. After 5 minutes elapsed, the loops were placed in a room temperature water bath. Figure 2.2.4b displays the setup. Temperature programming was used to provide reasonable peak separation for hydrocarbons on the respective columns. For three minutes, the temperature was held at 60 °C. This was followed by a 10 °C per minute ramp to 120 °C which was then held for one minute. Subsequent ramping at 4 degrees per minute brought the temperature to 160 °C, which was again held for one minute. A final 10 °C per minute ramp brought the oven to its maximum temperature, 200 °C where it remained for five minutes, yielding a 30 minute runtime.

3.2 Intensive Phase: Calibration

Calibration runs took two forms over the summer in China during the intensive phase. Initially, we used four permeation tubes for calibration: 2-methylbutane, 3-methyl-

Table 3.2.1 Summary of results for calibration runs of permeation tubes. The left hand column gives the day of the sample and other four columns show the corresponding normalized response for each individual species. The variation seen for the two lighter hydrocarbons is smaller than that seen for the heavier two. For twenty-five of twenty-eight measurements, the deviation is within 5% of the average over the five week period. Prior to day 199 there were problems transferring the heavy fraction. On days between 199 and 220 where values are missing, operator error prevented proper transfer of the compounds. After day 220, emission rates for the two heavy species became unstable. For ethylbenzene, a leak was discovered, which may also be responsible for its increased response over time. The final row gives the RMR response factor. Good agreement is seen for the two light hydrocarbons. The heavier hydrocarbons show significant difference. Since the response is from two separate detectors, there is no reason to expect that inter-detector response would be similar. Even so, the response factor for octane is similar in magnitude to that of the light alkanes.

Day	2-me-butane	3-me-pentane	octane	ethylbenzene
193.07	1.01	1.07		
195.13	0.97	0.96		
199.13	0.98	1.02	0.90	0.78
200.05	0.96	0.99	0.87	0.78
204.01	1.06	1.03		
205.13	1.03	1.04		0.93
206.22	0.96	0.97	1.16	0.81
207.18	1.02	1.02	1.05	0.86
208.14	1.00	1.00	0.92	0.97
209.21	1.01	1.01		0.90
210.21	0.99	0.98	1.10	0.90
211.13	1.00	1.00	1.01	0.95
212.21	0.99	1.00	1.18	0.90
213.17	0.96	0.95		0.88
214.21	1.01	1.01	1.00	1.00
215.13	0.99	1.00	1.11	1.07
216.14	1.05	1.05	1.02	1.12
217.05	1.04	1.04	1.01	1.08
218.01	1.01	0.99	0.95	1.05
219.21	0.97	0.96	0.95	1.19
220.21	0.96	0.95	0.96	1.26
221.22	1.11	1.11		
220.13	1.00	0.99	0.94	1.40
223.09	0.99	0.98		
224.08	0.94	0.91		
225.21	1.02	1.01		
226.09	1.00	1.01		
227.17	1.07	1.07		
average response factor	1.91E-12	2.04E-12	1.78E-12	1.03E-12

pentane, octane and ethylbenzene. The first two compounds eluted with the light hydrocarbons and the second pair with the heavy ones. We missed consistently transferring the heavy pair (octane and ethylbenzene) to the proper column until day 199. This meant that sometimes we did not obtain data for all of the heavy hydrocarbons during the initial period. Samples were obtained by direct injection of the sample loop (volume = 0.39 cc), bypassing the in-line traps. Using mass loss rate and flow rate over the permeation devices, one can obtain moles of each hydrocarbon injected. Relative Molar Response (RMR) was then used to obtain a calibration curve for the entire set of NMHC we identify. Peak areas of each sample run were calibrated using the calibration run for that day. If no calibration run was performed for a particular day, the average of the two nearest bracketing runs was used to find hydrocarbon concentrations.

Results from permeation tubes over the course of the summer are shown in Table 3.2.1. Most times the response from the instrument stayed within ten percent of the average response over the entire period. For the lighter hydrocarbons, the response was even more stable, within five percent. The RMR factor differed by only six percent between 2-methylbutane and 3-methylpentane. Variation on the heavy hydrocarbon detector was greater. This could be due to true variations at that detector. Generally we would expect day to day response variation to be related to changes in purity of carrier gas, make-up gas or zero air to the detector. Since the supplies of these gases were common to both detectors, it leads me to suspect a different source for the variation. The differences could be due in particular to changes in emission rate from the tubes.

One of the difficulties encountered in the field was the inability to properly regulate the storage temperatures. We recorded the temperature just prior to the actual sampling. The range of measured temperatures was within two degrees (from 27.5° C to 29.5° C). Mass loss was measured at those two extreme temperatures and at 28.5° C; the loss rate was essentially linear between the two extreme temperatures for the four hydrocarbons. The slope of the loss rate trends was increased with increasing molecular weight of the species. The rate of emission of ethylbenzene at the lower temperature was only 75% of that at the higher temperature. The low temperature rate of 2-methylbutane was 81% that of the high rate. Another possible factor responsible for the variations in

Table 3.2.2 Shown are the results of five standard runs each of tank 5199 and its daughter tank. The average area results are given in the second and third columns with standard deviations of the mother (5199) and daughter tanks in columns four and five. The final column compares twice the response difference to the average response to determine how the concentrations differ between tanks.

Compound	Average area response 5199	Average area response Daughter	Stdev M	Stdev D	2*(m-d)/(m+d)
Ethane	52732	52473	0.27%	2.39%	0.49%
Ethene	72856	72693	0.19%	1.14%	0.22%
Propane	61706	61164	0.41%	2.88%	0.88%
Propene	48335	47838	0.77%	1.75%	1.03%
2-mepropane	57625	56629	0.68%	2.62%	1.74%
Butane	55474	54491	0.44%	1.64%	1.79%
t-2-Butene	33272	32811	0.64%	0.94%	1.39%
1-Butene	60097	59681	0.38%	0.64%	0.69%
2-mePropene	60369	60079	0.51%	1.60%	0.48%
c-2-Butene	17237	17427	5.44%	2.30%	-1.09%
Pentane + CP	89278	89796	1.28%	4.15%	-0.58%
1-Pentene	30613	31080	4.50%	2.30%	-1.51%
Cyclohexane	41018	40199	2.48%	1.99%	2.02%
Hexane + Isoprene	92264	90864	1.28%	2.73%	1.53%
1-Hexene	35830	35180	2.02%	2.73%	1.83%
3-meHexane	28589	28522	5.01%	1.50%	0.24%
Heptane	37552	34449	1.45%	11.00%	8.62%
CycloHeptane	21129	21357	9.79%	2.81%	-1.07%
Benzene	39057	38390	3.74%	2.65%	1.72%
1-Heptene	23963	23558	9.34%	4.80%	1.71%
Octane	21306	19403	7.90%	11.44%	9.35%
cycloOctane	30230	27799	3.57%	5.56%	8.38%
Toluene	15614	15066	5.55%	2.70%	3.57%
1-Octene	30091	28110	3.04%	4.93%	6.81%
Nonane	15217	15247	26.22%	24.08%	-0.20%
α-Pinene	8078	8717	8.40%	33.84%	-7.61%
1-Nonene	20217	19062	14.93%	8.76%	5.88%
Camphene	27987	22205	10.03%	14.98%	23.04%
Carene	8652	8664	18.03%	44.22%	-0.15%
Decane	19466	11921	24.44%	52.23%	48.08%
Sabinene	11810	5848	37.63%	30.22%	67.53%
γ-Terpinene	30171	15941	33.95%	22.17%	61.72%
Limonene	26449	12992	55.05%	23.75%	68.24%

Table 3.2.3 Summary of response factors for standard calibration runs in Dinghushan. The top rows give the response of the 5199 daughter standard and the bottom show that of the permeation tubes. The light fraction permeation tube response values agree well with the average from the standard tank. The octane permeation tube response is 10% lower than the average obtained from the heavy hydrocarbon response from the standard.

Light fraction	Mole*RMR/area
Ethane	1.64E-12
Ethene	1.67E-12
Propane	1.62E-12
Propene	1.63E-12
2-mePropane	1.58E-12
Butane	1.58E-12
t-2-Butene	1.47E-12
1-Butene	1.74E-12
2-me-Propene	1.78E-12
c-2-Butene	1.68E-12
cycloPentane	1.65E-12
Pentane	1.63E-12
1-Pentene	1.72E-12
cycloHexane	1.66E-12
Hexane	2.02E-12
Isoprene	2.04E-12
1-Hexene	2.41E-12
3-methylHexane	2.96E-12
cycloHeptane	3.32E-12
Heptane	2.46E-12
Benzene	2.56E-12
1-Heptene	2.63E-12
Average all	1.97E-12
Average to Hexane	1.67E-12
2-methylButane PT	1.91E-12
3-methylPentane PT	2.04E-12

Heavy fraction	Mole*RMR/area
Toluene	1.98E-12
1-Octene	1.97E-12
Octane	1.98E-12
1-Nonene	2.22E-12
Nonane	2.12E-12
cycloOctane	1.78E-12
Myrcene	1.74E-12
1-Decene	2.30E-12
Decane	1.08E-12
Limonene	1.75E-12
Sabinene	1.67E-12
Undecane	2.25E-12
Average	1.90E-12
Octane PT	1.78E-12
ethylBenzene PT	1.03E-12

permeation tube response is the equilibration time in the sample line. The flow rate over the permeation tubes was 10 sccm with a volume of 300 cm^3 in the line. It may take longer than 90 minutes for equilibrium to be reached in the line, assuming that the temperature is stable for that long. Since the emission rates of heavier hydrocarbons were more sensitive to temperature variations, the changes in concentration in the sample line would also undergo greater change with varying storage temperatures. A long time constant for equilibrium might mean that the concentrations in the gas stream we sampled may have been due to a different temperature than that we were measuring at sample time.

In the middle of August, starting Julian day 226, we were able to use a daughter standard of MIT tank 5199. This daughter was prepared by filling a clean, evacuated stainless steel electropolished tank with standard gas. Upon return to MIT, the daughter tank was quantitatively compared to tank 5199 to obtain concentrations in the daughter. These results are given in Table 3.2.2. The majority (twenty-three of thirty-five) of compounds show less than two percent difference between area results based on the average value for five runs per tank. The daughter tank showed slightly greater variation from run to run. For the five compounds which showed especially poor agreement between tanks (greater than 10% difference), high variability was also seen from the individual runs. We believe this is due in part to significant peak broadening in the final minutes of the run in addition to column age effects. The three terpenes sabinene, γ-terpinene and d-limonene eluted as part of a quartet which was not always cleanly separated leading to higher standard deviations for those compounds. The large variations in the heaviest species indicate that our absolute concentration assignment for the daughter tank could be off by as much as 50%.

Comparison of the calibration data from the field campaign show reasonable agreement between permeation tube and daughter standard 5199 scales. The average RMR response in mole per area on the light hydrocarbon system was 1.98×10^{-12} for the two permeation tubes and 1.97×10^{-12} for the 22 NMHC in the standard. Looking at Table 3.2.3, we can see that for most lighter NMHC, the mole per area value hovers around 1.7×10^{-12}. This compares to 1.9×10^{-12} for the 2-methylbutane permeation tube. RMR is generally expected to agree within 10% of actual values, which these results roughly confirm. There seems to be a systematic variation from the ethane to 1-heptene, which has been noted by Sprengnether (1992). The differences between permeation tube average response and the standard tank response of the lighter hydrocarbons should cause an apparent jump down in concentration of roughly 10% when the calibration scale was switched on day 226. Indeed this is supported by the data. For the heavier hydrocarbons the RMR agreement is less secure. In part this may be due to the Nafion dryer. The dryer causes rearrangement and/or loss for some terpenes (especially the bridged varieties) which caused significant variations in response (Burns et al., 1983). Those species most

affected by this were not included in Table 3.2.3. The octane permeation tube does show agreement within 10% of the average response of the tank hydrocarbons. The low response from decane is a mystery though it agrees well with that from the ethylbenzene tube. We opted to calibrate the heavy fraction with the octane permeation tube prior to day 226 since the response seemed more in line with that obtained from the tank hydrocarbons.

For calibration runs in the field, standard gas was diluted and treated identically as whole air samples. We tried to perform one standard run each day. Atmospheric concentrations for hydrocarbons were calculated by comparison to the standard analysis for that day. For hydrocarbons not in the standard, RMR was used. Two back-to-back runs were performed to show that the traps did not significantly affect the results of the majority of compounds for standard runs (Table 3.2.4). On the light side, the largest deviations were seen for the last four eluting compounds. We surmise that these fluctuations are more a result of column performance variations and its effects on peak width later in the run rather than deleterious effects of the traps. The results from the heavy hydrocarbons are not as promising. As noted, the Nafion dryer disrupts analysis of terpenes. Some like camphene show losses as high as 80%. γ-terpinene concentrations seem to be enriched by a factor of 5. We have no reason to expect the traps would adversely affect the heavier alkanes like nonane and decane. It is entirely possible that some terpene fragments coelute with those species, causing the apparent increase in concentration shown in run 62880007 in Table 3.2.5.

Figures 3.2.1a and 3.2.1b summarize the results of all standard analyses from the final two weeks of August. For each specie, the average response is used to normalize each run. Error bars are one standard deviation obtained from the set of measurements. The earlier eluting compounds on each column gave more stable responses, varying less than 10% from day to day. Some of the later eluting (and heavier) species yielded response deviations greater than 30%. The worst offenders were terpenes, which is most likely the result of adverse interactions with the Nafion dryer. We can use the results of the standard variations as bounds for our measurement precision. In the field, precision seems much lower than in the relatively stable conditions at MIT.

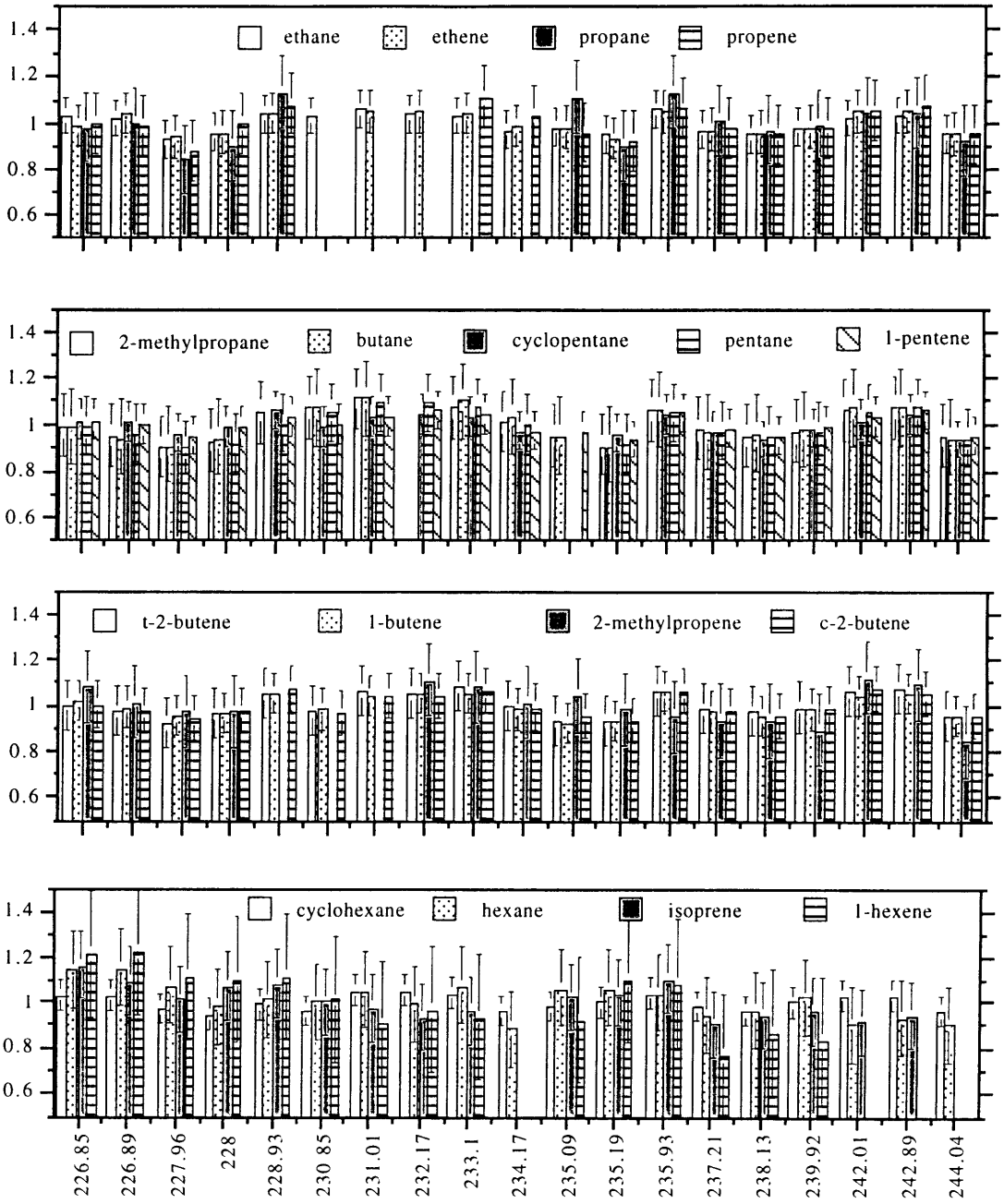

Figure3.2.1a Results of standard calibration samples over the period August 14-31. For each run, the peak area for individual compounds is normalized to the average area for that compound over the entire period. Error bars represent one sigma obtained from each data series. The x axes are given in Julian day and the y axes are normalized with one representing the average value.

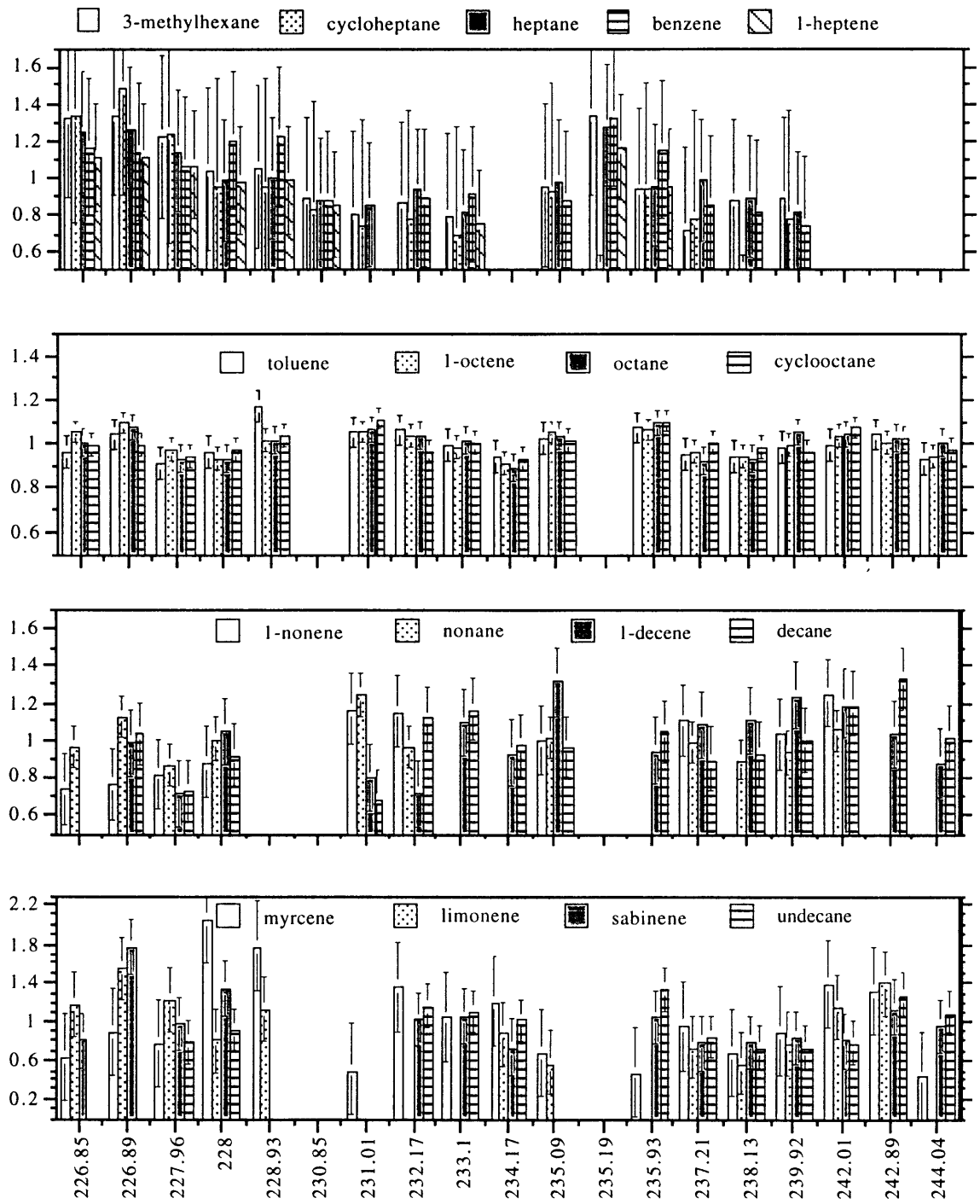

Figure 3.2.1b Results of standard calibration samples over the period August 14-31. For each run, the peak area for individual compounds is normalized to the average area for that compound over the entire period. Error bars represent one sigma obtained from each data series. The x axes are given in Julian day and the y axes are normalized with one representing the average value.

Compound	(a) 62272309	(b) 62280007	a/b
ethane	2579	2662	0.97
ethene	3502	3548	0.99
propane	2862	3076	0.93
propene	2246	2539	0.88
2-me-propane	2811	2900	0.97
butane	2729	2816	0.97
t-2-butene	1624	1702	0.95
1-butene	2936	2966	0.99
2-me-propene	2776	2802	0.99
c-2-butene	852	885	0.96
cyclopentane	2239	2297	0.97
pentane	2190	2243	0.98
1-pentene	1498	1573	0.95
cyclohexane	1958	1899	1.03
Hexane	1392	1302	1.07
Isoprene	2759	2922	0.94
1-hexene	1621	1606	1.01
3-methylhexane	1223	1049	1.17
cycloheptane	864	668	1.29
heptane	1531	1334	1.15
benzene	1718	1941	0.88
1-heptene	945	865	1.09
toluene	1151	1215	0.95
1-octene	1141	1095	1.04
octane	845	842	1.00
1-nonene	590	635	0.93
nonane	445	519	0.86
cyclooctane	538	560	0.96
α-pinene	216	129	1.67
camphene	873	188	4.66
myrcene	233	316	0.74
1-decene	322	374	0.86
decane	392	494	0.79
carene	172	135	1.28
γ-terpinene	210	1151	0.18
limonene	374	255	1.47
sabinene	351	458	0.77
undecane	220	256	0.86

Table 3.2.4 Comparison of two back to back standard runs. Run (a) was performed without any in-line traps. Run (b) used both the Nafion dryer and Ascarite trap. The final column gives the ratio of run a to run b. For most low molecular weight species the ratio is close to unity. Notable exceptions are 3-methylhexane to benzene. Those four compounds showed greater variability than the other light fraction species for the standard runs. The ratio for the terpenes show wide variation which is caused by the Nafion dryer. Camphene seems to be destroyed to a great extent, and may even be rearranged to γ-terpinene whose concentration seems to increase with the use of Nafion.

Some of these standard runs have no reported results for certain species. Runs performed from day 230 through 234 showed contamination of propane, with highest levels on the first day, decaying over the next four. Zero air runs were performed through this period and yielded concentrations over 3 ppbv at the start. Oddly, propane concentrations bracketing the zero air run were considerably lower. Ethene and propene showed contamination as well but the levels were lower and decreased more rapidly. Standard runs on day 234 and 244 lack the last seven peaks on the light hydrocarbon side due to instrumental problems in the later part of the run sequence. Injection errors occurred for runs on days 230 and 235 for the heavy fraction.

The dynamics of trap contamination are unclear. It is possible that depending on the hydrocarbon concentrations in the gas stream, flux into or out of the traps may occur. Zero air runs should give the maximum amount of contamination possible as there is very little hydrocarbon in the gas stream. Standard runs may exhibit some evidence of contamination if the dilution factor is sufficiently large. The contamination seen here occurs primarily as a result of high concentrations of hydrocarbons in ambient air passing through the traps. Zero air blank runs showed little evidence of significant contamination for the majority of species we measured. Several hours after a large pollution event the blanks showed levels of light hydrocarbons to be less than 15 ppt except for the period from 230 through 234 as discussed previously. For normal background levels, only 2-methylpropene gives consistent contamination peaks of roughly 180 pptv. Other light hydrocarbons show levels of contamination under 10 pptv from time to time. Since normal levels of those compounds are in the many hundreds of ppt, the effects are marginal.

Despite the potential contamination and removal of hydrocarbons by traps, they are necessary for effective chromatography. The PLOT column is highly sensitive to water vapor, which binds to the active sites and generally degrades the column. Separation capability is diminished and large retention time shift may occur, causing difficulty in peak identification. Removal of CO_2 is also important. Due to its high atmospheric concentration, CO_2 trapped in the sample loop can cause a pressure surge upon desorption. This surge decreases retention times of all species as the collected gas slug is quickly forced through the first several meters of column.

Standard addition runs were performed to investigate our ability to recover each hydrocarbon in our standard. Problems from the in-line traps and from our cryotrapping procedure should affect the standard addition runs just as if they were ambient air. While in a normal standard run we used zero air to dilute to atmospheric levels, for a standard addition, the dilution gas was whole air. By subtracting the response at the detector which should have been due to standard gases, we can compare the response due to whole air with that of the bracketing whole air samples. If we have perfect recovery, the standard addition concentrations with standard response removed should fall between the two bracketing runs assuming that atmospheric concentrations are either increasing or decreasing through the period or constant. It is possible that the mixing ratios of the ambient air for the middle standard addition run could be higher or lower than both bracketing runs. Results of these tests are shown in Figure 3.2.2a and Figure 3.2.2b.

Some compounds graphed in the Figures 3.2.2 a and b are not present in the standard and therefore can be used to ascertain the behavior of the background concentrations during the middle hour of the 3 hour standard addition test. The runs on day 228 (starting with 281937 on graph 3.2.2a) occur during the decay from a pollution event as evidenced by the high initial propane concentrations. Many of the five and six carbon species not in the standard show highest levels during the standard addition run. This is also true of some hydrocarbons in the standard. Most of the lightest compounds show decreasing levels over the three hours. Most species for the two experiments displayed in 3.2.2b show background hydrocarbon levels increasing over the period. The behavior of the cycloalkanes was peculiar. For cyclooctane, cycloheptane and cyclopentane, the hydrocarbon levels after standard subtraction were still far higher than expected from the bracketing runs. This could be due to incorrect mixing ratio assignments in the standard tank (ones that are slightly too low). Looking at the RMR values confirms this could be a possibility as they are a bit higher than the average values for other species with the same carbon number. Since the peak area due to the standard is as much as 20 times greater than that from the ambient air for the cycloalkanes, a minor change in concentration could account for a major difference as seen in the addition runs. It should be noted that cyclopropane, which is not in the standard, also shows this trend.

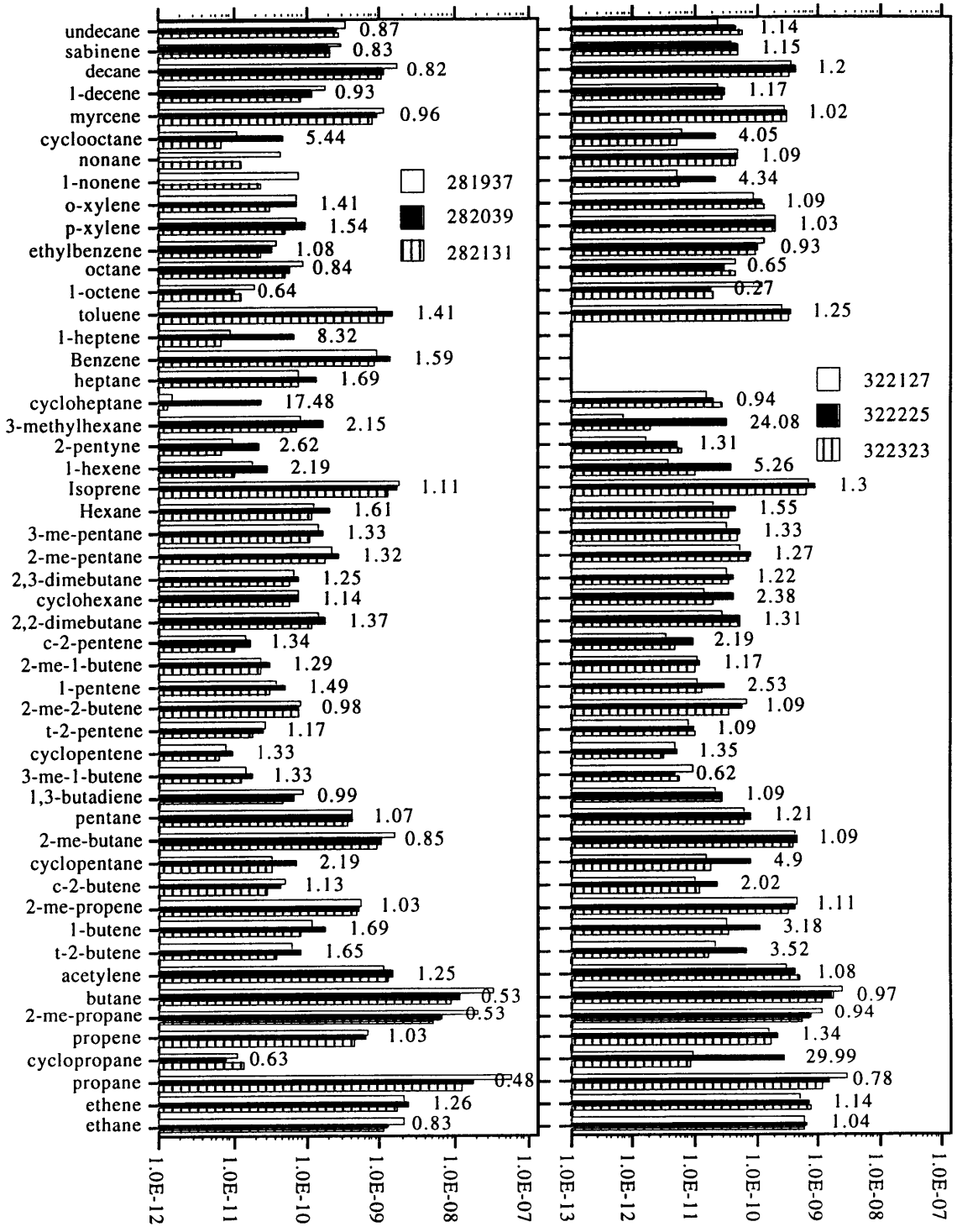

Figure 3.2.2a Results of standard addition runs are given. The middle, solid bar is the concentration of hydrocarbon in the ambient air calcualted by subtracting out the theoretical response from the standard gas. The outer bars are the concentrations from the bracketing ambient air runs. The ratio of the ambient air concentration fromthe addition run to the average of the two bracketing runs is given at the end of the bar for each species.

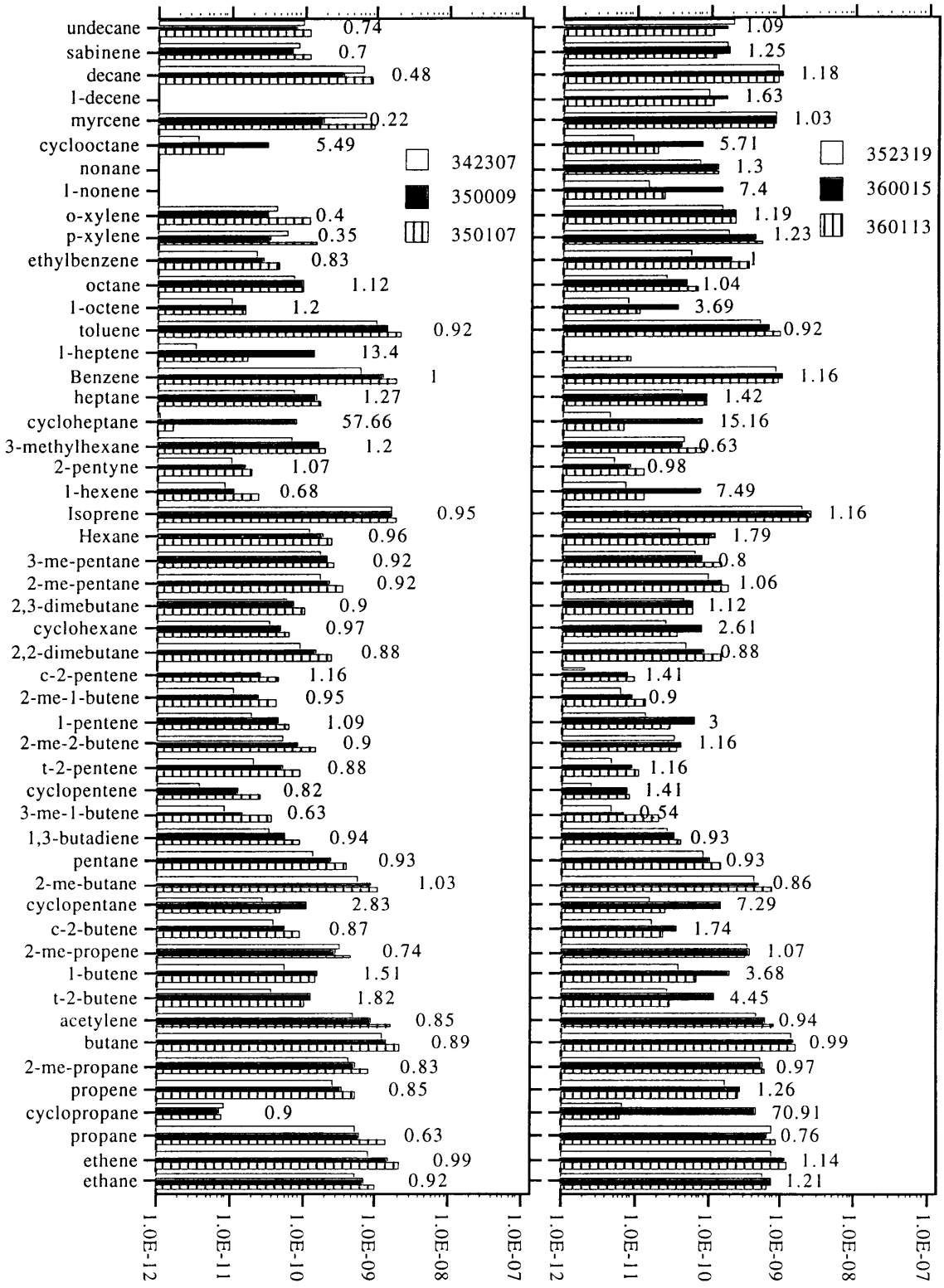

Figure 3.2.2b Results of standard addition runs are given as in Figure 3.2.2a.

For the majority of compounds, the trends are as expected with the middle bar in Figures 2.3.4a,b lying between the values of the two extremes.

3.3 Ancillary measurements

3.3.1 Nitrogen Oxides

NO and NO_2 measurements were performed using a model 42S chemi-luminescence low level NO-NO_2-NO_x analyzer (Thermo Environmental Instruments, Inc., MA). The gas phase reaction of nitric oxide and ozone produces a characteristic luminescence with an intensity proportional to the concentration of the nitric oxide. Decay of excited NO_2 molecules results in light emission.

$$NO + O_3 \longrightarrow NO_2^* + O_2 \qquad (3.3.1)$$

$$NO_2^* \longrightarrow NO_2 + h\upsilon \qquad (3.3.2)$$

In order to measure NO_2 in the sample stream, it must first be reduced to NO. Reduction is achieved by passing the sample through a Molybdenum converter heated to 325 °C.

$$3\,NO_2 + Mo \longrightarrow 3\,NO + MoO_3 \qquad (3.3.3)$$

The conversion reaction is near 100% efficient. The instrument cycles through three states: NO, NO_x and zero. In the NO mode, sample air is drawn directly to the reaction chamber. Reaction with ozone occurs and the resulting decay intensity is recorded as NO. By switching two solenoids, the instrument is put in the NO_x mode. Sample gas passes through the NO_2 converter and then proceeds to the reaction chamber. NO and NO_2 converted to NO then react and are detected as NO_x. In the zero mode, the sample bypasses the converter and is directed to a prereaction chamber. Nitrogen oxide reacts with ozone here (instrumental design is such that up to 200 ppb NO will react in the prereactor chamber, assuming no interferents). The NO-free sample air then passes to the reaction chamber where a zero reading is recorded. Every ten seconds the instrument

switches modes. The minimum detectable limit is 50 ppt for the instrument and zero drift is negligible since it is monitored and corrected for continuously.

Data were recorded once per hour starting on Julian Day 183. The instrument output is given as a continuously updated 5 minute average; each new 10 second measurement replaces the oldest one to yield a new average value. On day 196 the recording frequency was increased to once every ten minutes, thereby effectively capturing NO_x levels for every other five minute averaging period. We had two problems which make the data prior to day 231 useless as far as the absolute numbers are concerned. First, the initial full scale range was 200 ppb and span drift can be as much as 1% full scale per day. Second, calibration gas was not available to monitor performance until day 231.

Calibrations were performed by using a NIST traceable NO standard, having 50.5 ppm NO and < 0.5 ppm NO_2. The full scale was set to 20 ppb to better reflect the levels of NO_x seen in the forest. Using a model 146 dynamic gas calibration unit (Thermo Environmental Instruments, Inc., MA) we were able to properly calibrate our detector. The model 146 has Tylan mass flow controllers and an ozone generator which allowed us to dynamically dilute the NO standard down to 90% full scale to establish the span reading. Then, using gas phase titration, we created an NO_2 standard to calibrate that channel. Essentially, NO reacts with ozone in the model 146, creating NO_2. At the NO_x instrument, decreases in NO levels from the original value give the concentration of NO_2 levels which must be present in the airstream. This also allows the instrument to confirm the conversion efficiency of the Molybdenum converter. Care must by taken to supply the instrument with NO_x-free air. This was accomplished by using traps of Purifil, molecular sieves and iodated charcoal. Daily span and zero checks were performed. The first week required recalibration of the instrument every other day due to drift of roughly 10% from full scale. The second and final week had more stable results showing reasonable span and zero values. Figures 3.3.1a and 3.3.1b show the data obtained over the entire period. One can clearly see spikes in the data representing pollution events. For the last two weeks, there were three occasions where NO climbed above 40 ppbv. During each event, there was a corresponding rise in NMHC levels. The trends are particularly similar for toluene,

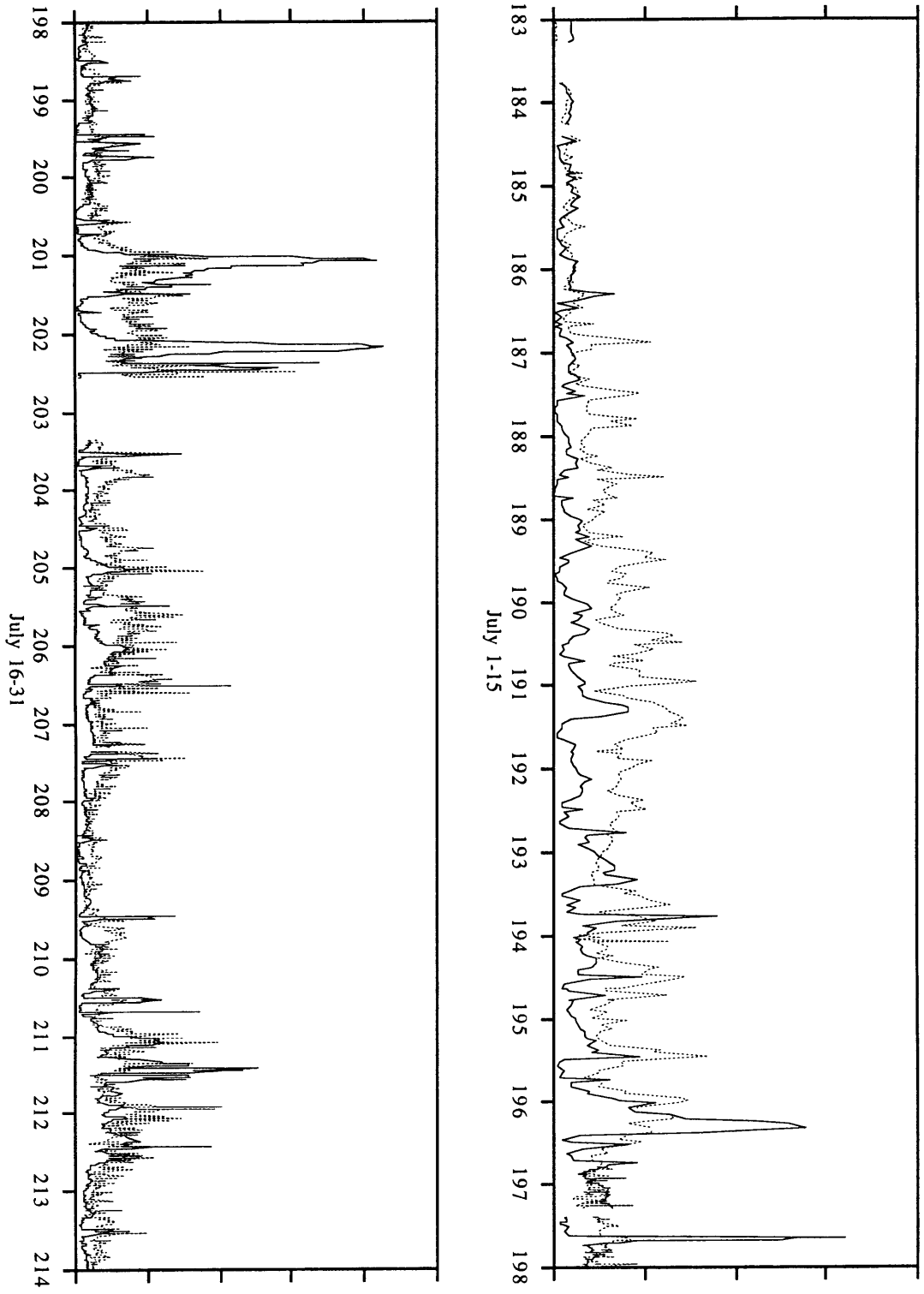

Figure 3.3.1a NOx plots for the month of July. Solid line is NO and dashed is NO_2. The absolute calibration scale was unavailable for this period.

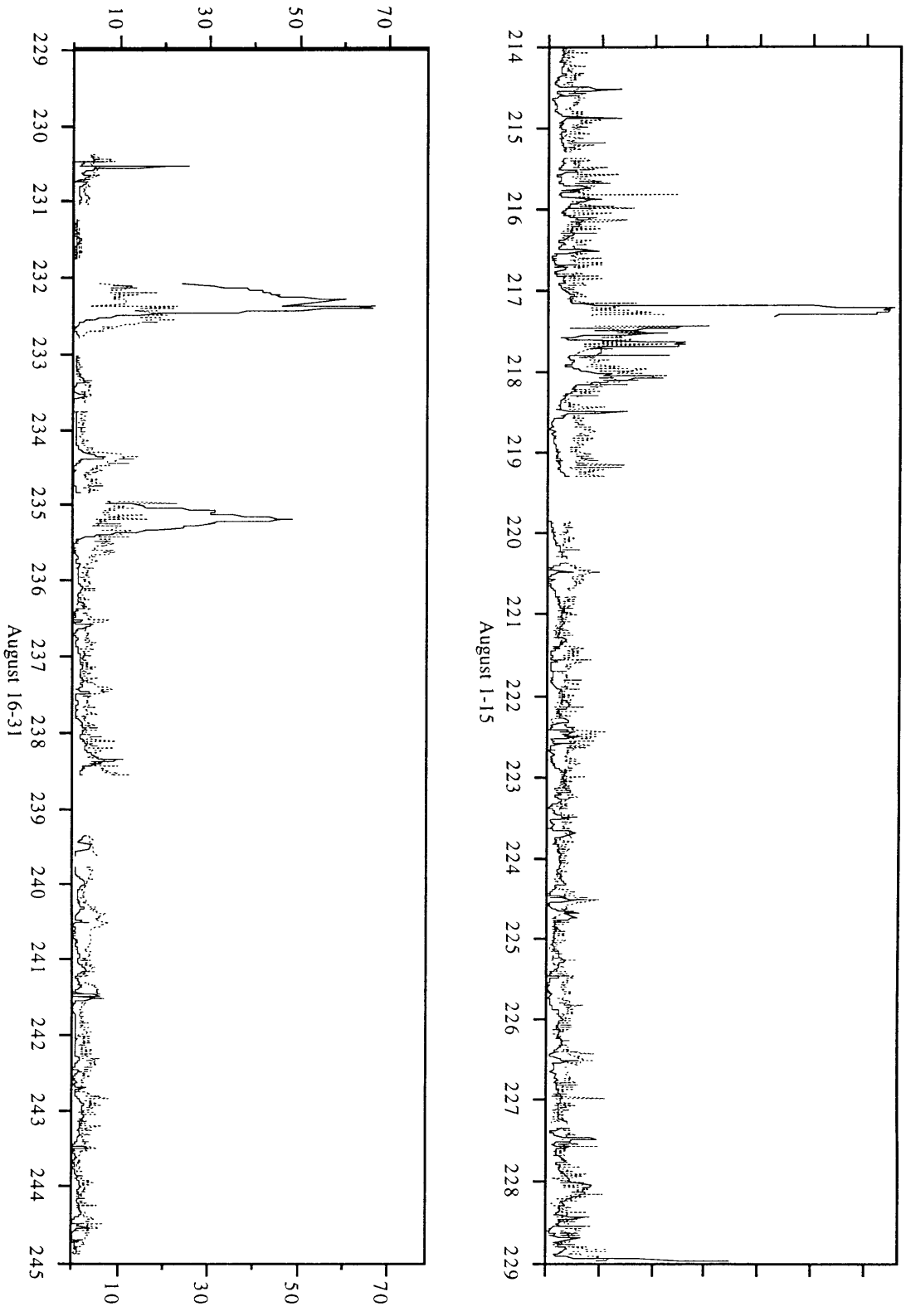

Figure 3.3.1b NO_x plots for the month of August. Solid line is NO and dashed is NO_2 The absolute calibration scale was unavailable for the first half of the month.

3-methylhexane and the six carbon alkane isomers like hexane, the methylpentanes and the dimethylbutanes.

3.3.2 Carbon Monoxide

Carbon Monoxide data were collected using a Trace Analytical RGD2 reduction gas detector. Detection occurs as a result of mercuric oxide reduction. A reduced gas passes over the heated mercuric oxide bed (280 °C), reacting to form mercury vapor as in the following reaction:

$$X\,(g) + HgO\,(s) \longrightarrow XO\,(g) + Hg\,(g) \quad (3.3.4)$$

where X represents any reduced gas. Downstream of the reaction bed, an ultraviolet photometer determines quantitatively the amount of Hg vapor in the airstream. The reaction of CO occurs with almost 100% conversion efficiency, so every mole of CO results in the creation of one mole of mercury vapor. The detector is linear over a range of approximately 100 mV (100 ppb per 2 cc sample), and can be corrected with a potentiometer to give linearity over a 500 mV range. A small linearity adjustment was required over the range of concentrations under which we operated (60-200 ppb) as confirmed by our calibration curve. The detection limit is one ppb per two cm^3 sample and response drift is negligible if the reaction bed temperature and flow rate are maintained constant.

Zero air passed over molecular sieves to remove water and organics was used as carrier gas. Carrier flow rate was set to thirty cm^3 min^{-1} and controlled by a flow restrictor. A Valco six port valve with a two cm^3 stainless steel sample loop was used to introduce whole air into the carrier stream. After valve switching, the sample passed through a three meter column of stainless steel 1/8" tubing packed with 5 Å molecular sieves. Oven temperature was maintained at a constant 90° C, giving adequate separation of the hydrogen and carbon monoxide peaks. The instrument was operated from July 7 through July 20 in the field. A severe storm on July 20 sent a power surge to the instrument which blew its fuse and damaged the heating mechanism for the reaction bed; subsequent measurements were not possible as a result.

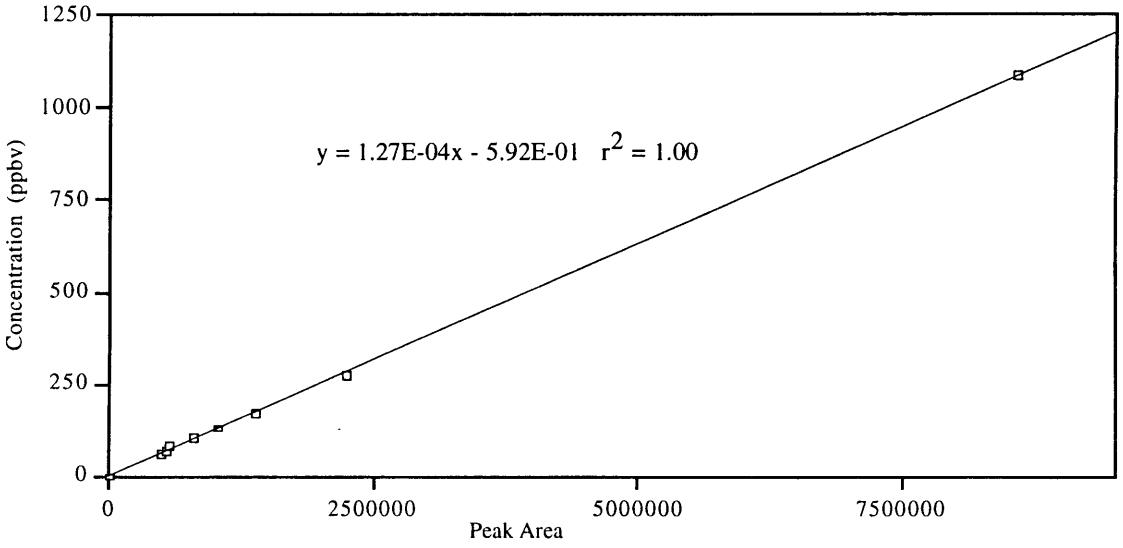

Figure 3.3.2. CO calibration curve showing detector linearity over the range of 50-1100 ppbv.

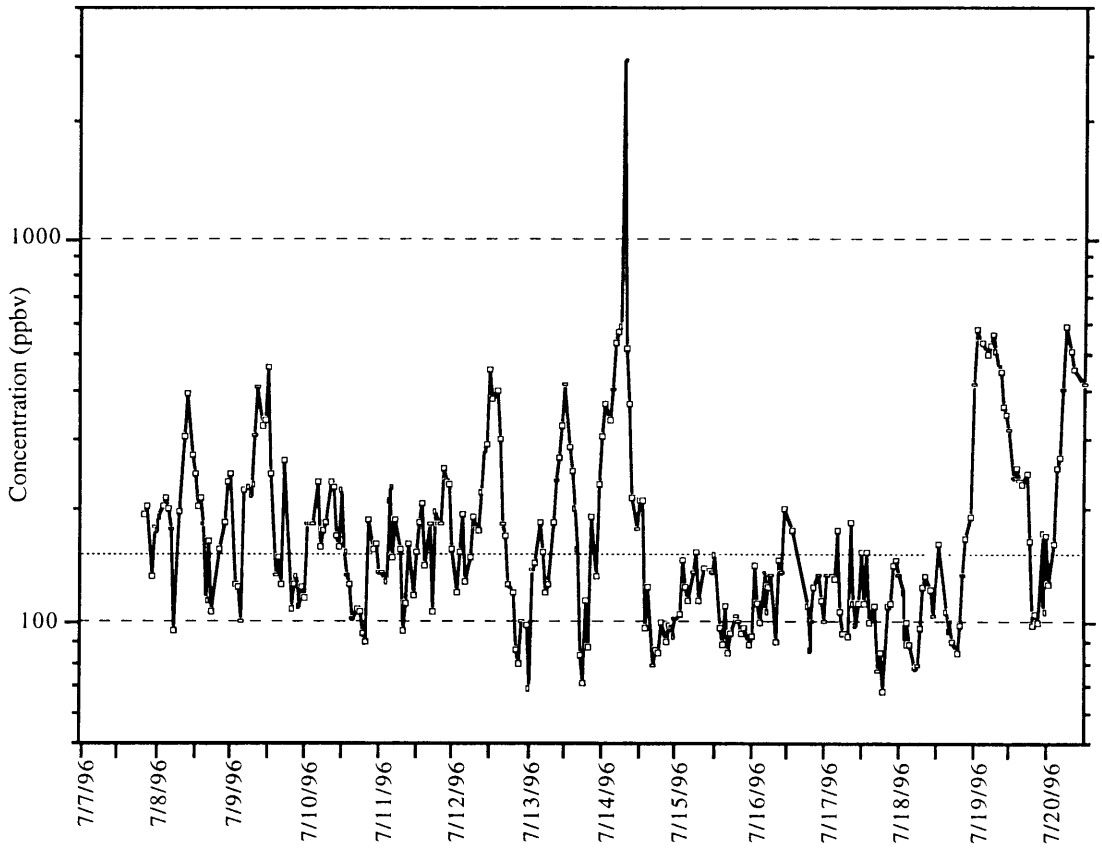

Figure 3.3.3. Data series for CO. Dotted line represents the median value of 152 ppbv.

Instrument calibration over the range of observed areas was achieved by dynamically diluting a 3.34 ppm CO NIST traceable standard with +/- 1% analytical certification. With the linearity potentiometer set at 0.9, linear responses were obtained over the span of interest (Figure 3.3.2) In general, instrument non-linearity may reach 5% at higher CO values without the linearity adjustment. Figure 3.3.3 gives the results over the two week period. By removing the pollution episodes, which were determined by averaging all data points minus one obvious outlier (2910 ppb) and excluding any point occurring outside of two sigma (2σ=230.2 ppb), we obtained an average background value for CO of 170 ppb. The median value for the 289 points was 152 ppb. An average value of 147 ppb was calculated by excluding those points within 5 hours of an obvious pollution episode. The final two numbers seem to be in reasonable agreement, and are taken as appropriate estimates of background CO over the two week sampling period. Instrumental precision is 5% of the measured concentration over the range of values we encountered.

3.4 NMHC Flux Measurements

3.4.1 Methods for Determining NMHC Fluxes from Vegetation

Three primary methods have been used for the determination of hydrocarbon fluxes from vegetation. They include enclosure, tracer, and micrometeorological techniques. The second two techniques are useful for flux determination over a wide area whereas the first relies on direct measurement from individual species.

The field enclosure technique makes use of a tedlar bag (or other inert enclosure) wrapped around a branch and the mass accumulation of hydrocarbons is determined from the difference in concentrations measured over time. This method is the easiest to employ and does not require fast response detectors but has several drawbacks. One problem is that stresses on the branch, like radical changes in CO_2 or H_2O concentration, may affect emission rates. In addition, the branch may be damaged while being handled and that may affect emission flux. It is also necessary to sample each species of tree in the area of interest since they exhibit different emission patterns. Once rates are determined for an individual branch, they must be extrapolated to the entire tree and then to the forest as a whole, which requires a detailed survey of tree species in the forest. Since leaf age has

been shown to play a role in emission rates, it is also necessary to sample different branches to get some average value (Isidorov et al., 1984, Lamb et al., 1987, Fehsenfeld et al., 1992).

A second technique uses an SF_6 tracer to aid in hydrocarbon flux determination. A known amount of tracer gas is released and then samples are taken downwind. Since tracer flux and downwind concentration are known along with downwind hydrocarbon concentration, one can work backward to find hydrocarbon fluxes. The assumption used is simple. If the tracer release accurately mimics hydrocarbon release from vegetation, then the downwind concentration ratios must equal the corresponding emission fluxes (Allwine 1985, Lamb et al, 1986, Arnts 1982).

The third technique relies on micrometeorologic surface layer theory. There are several interrelated methods that have been employed in the determination of gas flux from vegetation. Examples include Bowen ratio and flux-gradient methods. Knoerr and Mowry (1981) used the Bowen ratio or energy balance method to estimate hydrocarbon fluxes. This technique uses the relation: net radiation = latent heat exchange + sensible heat exchange + photosynthetic energy use. The terms on the right can all be expanded in terms of constants times gradients of water vapor, temperature, and CO_2 respectively. Vertical measurements of those variables are made and diffusivities of vapor, sensible and latent heat are assumed to be equivalent. Net radiation can also be measured directly and therefore the latent heat term can be determined. One can then estimate the flux of any compound of interest by comparing the calculated flux gradient of water vapor with the gradient of the trace gas compound of interest.

Gradient profile methods again use the flux relation: flux = K dC/dz where K is a vertical eddy diffusivity constant and dC/dz is the vertical gradient of the compound of interest. K can be determined from vertical wind speed and temperature profiles following the procedures outlined by Nieustadt (1978), Dyer (1974) and Benoit (1977) and summarized in Lamb et al. (1985). Similar expressions are used for heat and momentum fluxes which can be expressed in terms of nondimensional vertical profiles (based on vertical temperature and velocity profiles). Empirical expressions for the non-dimensional vertical profiles as a function of the Monin-Obukov length, z/L, have been developed by careful experiments by a number of investigators. The expressions differ depending on the

stability of the atmosphere. The original expressions for heat and momentum fluxes can then be solved for velocity and temperature as a function of z/L. Simultaneously solving those expressions iteratively to yield best fit profiles (with best fit coefficients related to K) will enable the determination of the diffusivities of heat and momentum. It is assumed that the eddy diffusivity of mass (for hydrocarbon of interest) is equivalent to the diffusivity of heat for all stability conditions. One thing to note: in forested regions, the vertical profiles of wind speed and temperature are displaced upward by an amount based on the tree height. It is necessary to make use of the zero-plane displacement height (d) which is an imaginary surface where fluxes become zero. Also, at a height of $d + z_o$ where z_o is the surface roughness, the wind speed should equal zero. All heights are therefore changed from z to (z-d) to incorporate this new parameter.

More recently, researchers have been using the Relaxed Eddy Accumulation method for computing trace gas flux from vegetation (Guenther et al., 1996b; Geron et al., 1997). Basically, three-dimensional winds are measured simultaneously with two sampling bags, one for updrafts and the other for downdrafts. The flux is obtained by taking the difference in concentrations between up and down air samples multiplied by the standard deviation of the vertical wind speed.

3.4.2 Dynamic Flow Through Experiments

Our original intention was to use a vertical gradient technique to estimate emissions of NMHC from the forest. The absence of a uniform fetch in the middle of the forest in addition to the relative sophistication of the technique led us to favor an enclosure method. By using a dynamic flow through the enclosure, we hoped to avoid some of the factors contributing to plant stress which traditional bag enclosures suffer from: increasing bag temperature and changing concentrations of CO_2 and H_2O within the bag. (Arey et al., 1995).

Our enclosure system consisted of a Teflon film bag supported on a stainless steel frame. The cylindrical frame was about 25 cm in diameter and 35 cm tall yielding a volume of just over 17 liters. We placed ambient air passed through a charcoal filter into a large tedlar (polyvinyl fluoride) bag enclosed by black polyethylene to prevent photochemical reactions. Other groups use true ambient air, making the assumption that

over the course of the experiment, the background concentrations will remain roughly constant. Then they collect background and emission samples simultaneously, the former from the inlet to the enclosure and the latter from the outlet. We preferred to have a separate reservoir both because we could be sure the concentrations were constant and also due to the difficulty we would have faced filling two sampling bags at once. The inlet of a battery powered metal bellows pump was connected to the background bag with the outlet hooked to a calibrated Matheson gas flow rotometer. As soon as the sampling bag was placed over the branch and secured with a cable tie, the sweep air was allowed to pass over the branch. The enclosure inlet was on one side of the bag and the outlet on the far side. Air flow was maintained at 4 liters per minute for almost 15 minutes until a steady state was reached. König et al. (1995) recommend at least 3 air exchanges to achieve steady state. Over the course of the following 6 to 8 minutes, two 0.8 liter black polyethylene covered tedlar bags with stainless steel valves were filled with air from the outlet. The internal temperature of the bag was monitored with a glass bulb thermometer secured along the bottom of the frame. Since all of our samples were taken from branches low in the canopy, the effect of direct sunlight on recorded temperature was not really an issue. Figure 3.4.1 displays the schematic for our enclosure system.

We performed measurements on three separate days, each time sampling from two different tree species. The background and sample air was analyzed with our GC system within two days of the sampling time. Our intention was to sample from the most

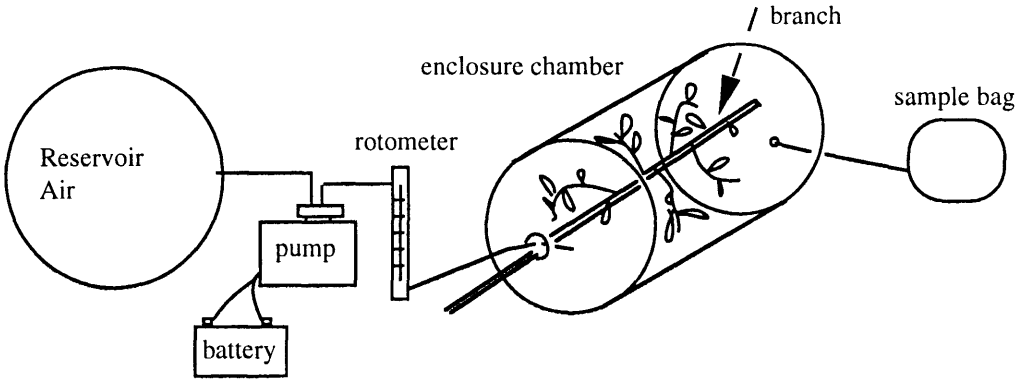

Figure 3.4.1 Schematic of our enclosure system. Sweep air was pumped from the reservoir through the rotometer into the enclosure. Tedlar sample bags were filled at the outlet on the opposite side from the inlet.

prevalent species in the forest, and indeed, we were able to obtain measurements from four of the top six species (Castanopsis chinensis, Schima superba, Aporasa yunnanensis and Cryptocarya concinna). The 100 m^2 region immediately surrounding the sample inlet contained two tree species (Aporosa yunnanensis and Acmena acuminatissima) represented in the most abundant species but their branches were out of our reach. Our initial pair of measurements came from two varieties (Sarcosperma larinum and Caryota ochlandra) of tree that had several plants in the vicinity of the sample inlet but were not major contributors to the forest biomass. By investigating those trees we hoped to not only get a representative sample from the region as a whole but also from the small subset where we were performing our in situ measurements. We did sample Aporosa yunnanensis from a different site. That species had ten trees in the neighborhood of our sample inlet in addition to its relative abundance in the forest as a whole. Table 3.4.1 lists information on the dominant vegetation in the vicinity of our laboratory at Dinghushan.

After each experiment was performed, we clipped the enclosed branch so that we could weigh the biomass both wet and dry. A Mettler balance was used before and after the leaves were dried in a 60 °C oven to determine mass. Prior to drying, the surface area of the leaves was calculated using a LI-COR model LI-3000 portable area meter, accurate to one hundredth of a cm^2. The results of these measurements as well as the internal enclosure temperature and expected incident PAR at the top of the canopy at the time of sampling are recorded in Table 3.4.2. The actual values for PAR came from the base of the mountain so they may not accurately reflect incident PAR, depending on the relative angle of the sun.

Isoprene emission rates (μg C g^{-1} h^{-1}) from individual branches were calculated using the following equation:

$$E = \frac{f(C_o - C_i)}{b} \qquad (3.4.1)$$

where

f = the sweep gas flow rate in cubic meters per hour
C_o = the isoprene concentration in μg per cubic meter in the outlet gas
C_i = the isoprene concentration in μg per cubic meter in the inlet gas
b = the dry foliar mass in grams

Error estimation can be made using a standard analysis. The random error in a quantity dependent upon several variables is given by

$$\sigma(F) = \sqrt{\sum_{i=1}^{N}\left(\frac{\partial F}{\partial X_i}\right)^2 (\sigma_i)^2} \qquad (3.4.2)$$

where

N = the number of variables
$\partial F/\partial X_i$ = the partial derivative of the function with respect to each X_i
σ_i = the standard deviation or error in each variable

In our case, we have four measured variables: two concentrations, one flow rate and one mass. We assume our concentration random error at most is ±10% and the same standard error is used for the rotometer. It is likely that both of these errors are less. The mass is measured accurately to 0.01 g. Table 3.4.3 shows the measured emission rate results and gives an example calculation based on the uncertainty in our measurements.

Species	Height (m)	age (yr.)	Leaf Ratio (%)	Biomass (Kg)	Biomass Ratio (%)	Mean DBH (cm)
Castanopsis chinensis*	23	235	0.92	32559.00	11.11	74.17
Schima superba*	24	85	2.54	29037.40	9.90	30.34
Aporosa yunnanensis*	25	22	7.97	11358.00	3.87	4.4
Acmena acuminatissima	26	30	3.48	12614.60	4.30	8.72
Cryptocarya concinna*	8.6	40	4.31	31331.04	10.69	11.58
Cryptocarya chinensis	7.6	40	2.72	11938.13	4.07	20.43
Species in 100 m^2 area	Height (m)	age (yr.)	number			DBH (cm)
Averrohoa carambola	14	120	2			45.2
Aporosa yunnanensis	6	20	10			7.9
Sarcosperma larinum*	6.5	15	2			5.5
Caryota ochlandra*	15	30	5			22
Acmena acuminatissima	7	35	1			28
Macaranga sampsoni	5	20	1			5.2

Table 3.4.1 The top half of this table shows information regarding the top six species by biomass in the broad region surrounding our laboratory at Dinghushan. These species account for almost 44% of the total biomass. Also note the leaf ratio with the greatest percentages corresponding to the smallest trees (by DBH). Since more of their mass is concentrated in the leaves, the leaf biomass ratio (leaf ratio times biomass) differs form the total biomass ratio listed. The six tree species within the 100 square meters containing the sample inlet are listed in the bottom half of the table. Only Acmena acuminatissima overlaps with the dominant species types. The asterisk indicates a sampled specie.

Table 3.4.2 Details from the dynamic enclosure experiments. The leaf surface area was measured before drying the leaves. Enclosure temperature and incident PAR at the canopy top are shown. Complete shading at the sampling sites implies significantly less PAR available to the enclosed leaves.

Species	Dry Weight (g)	Leaf Surface Area (cm^2)	Sample Temperature (°C)	PAR at Canopy Top ($\mu mol\ m^{-2}\ s^{-1}$)
Sarcosperma larinum	19.41	1316.19	29.2	491
Caryota ochlandra	14.07	1886.87	29.5	495
Schima superba	28.47	1117.85	28.0	479
Aporosa yunnanensis	11.12	1726.88	28.5	479
Cryptocarya concinna	23.57	2158.98	30.0	335
Castanopsis chinensis	35.62	2182.02	32.1	348

Table 3.4.3 Isoprene emission rates as calculated with equation 2.3.5 are given in the top half of the final column. The lower half of the table demonstrates our error analysis for Caryota ochlandra following equation 2.3.6. The emission rate error is based on equation 3.4.2.

Species	Concentration out ($\mu g\ m^{-3}$)	Concentration in ($\mu g\ m^{-3}$)	flow ($m^3\ h^{-1}$)	Dry Weight (g)	Emission rate ($\mu g\ m^{-2} h^{-1}$)
Sarcosperma larinum	6.71	2.76	0.24	19.41	0.05 ±0.01
Caryota ochlandra	215.78	2.59	0.24	14.07	3.64 ±0.52
Schima superba	4.16	0.94	0.24	28.47	0.03 ±0.01
Aporosa yunnanensis	3.87	1.13	0.24	11.12	0.06 ±0.01
Cryptocarya concinna	252.83	0.82	0.24	23.57	2.57 ±0.36
Castanopsis chinensis	6.44	0.82	0.24	35.62	0.04 ±0.01

Variable	X_i measured value	σ_i	$\partial F/\partial X_i$	$(\sigma_i \partial F/\partial X_i)^2$
C_o Sample Concentration	215.78 $\mu g\ m^{-3}$	21.58 $\mu g\ m^{-3}$	0.017	0.14
C_i inlet Concentration	2.59 $\mu g\ m^{-3}$	0.26 $\mu g\ m^{-3}$	0.017	0.00
f flow rate	0.24 $m^3 h^{-1}$	0.024 $m^3 h^{-1}$	15.15	0.13
b leaf biomass	14.07 g	0.01 g	0.26	0.00
				Total error $=(0.14+0.13)^{0.5}= 0.52$

Many reported rates in the literature are standardized to 1000 μmol m^{-2} s^{-1} for PAR and 30 °C temperature. Following the procedure recommended by Guenther et al. (1993), our results can also be standardized. Measurements are converted using the following equation:

$$I = I_s * C_L * C_T \tag{3.4.3}$$

where

I = isoprene emission rate at temperature T (K) and PAR flux L (μmol m^{-2} s^{-1})
I_s = isoprene emission rate at T_s = 30 °C and 1000 μmol m^{-2} s^{-1}
C_L = correction factor for PAR derived from measurements
C_T = correction factor for Temperature derived from measurements

The correction factors are defined by

$$C_L = \frac{\alpha C_{L1} L}{\sqrt{1+\alpha^2 L^2}} \tag{3.4.4}$$

and

$$C_T = \frac{\exp\left(\frac{C_{T1}(T-T_s)}{RT_sT}\right)}{1+\exp\left(\frac{C_{T2}(T-T_M)}{RT_sT}\right)} \tag{3.4.5}$$

with

α = 0.0027 ± 0.0016
C_{L1} = 1.066
R = 8.314 J K^{-1} mol^{-1}
C_{T1} = 95,000 J mol^{-1}
C_{T2} = 230,000 J mol^{-1}
T_M =314 K

We measured the temperature directly so the C_T factor is trivial to determine. The true PAR values incident at our branches is trickier to estimate. We know the approximate value of PAR at the top of the canopy. Estimates of the extinction of PAR within the canopy are given in Guenther et al. (1995) for a canopy with a leaf area index (LAI) of 5.

The index is determined as projected area coverage by foliage per ground area such that LAI of 5 implies 5 m^2 leaf area for a 1 m^2 surface area. A typical oak forest has an LAI of 5. Qualitatively, we can assume the Dinghushan forest to have a similar value. Based on those results, the PAR reaching lower levels in the canopy is a factor of 14.6 less than that of leaves at the top. If we assume our LAI is 5, we can calculate the appropriate standard emissions for our sampled species. Geron et al. (1994) use a different scheme for calculation PAR extinction within the canopy which predicts a factor of 10 decrease at the lowest level for an LAI of 5 and light extinction of 0.5. Their equation is

$$PAR_i = PAR \cdot \left(\exp\left\{ -E_L \cdot LAI\left[\frac{(2i-1)}{10} \right] \right\} \right) \qquad (3.4.6)$$

where

PAR_i = the PAR flux at canopy level i (ranging from 1 to 5 top to bottom)
E_L = the light extinction coefficient for PAR (0.28 to 0.84)
LAI = the ratio of m^2 of projected leaf area to m^2 of ground area

Using data from the Dinghushan Biosphere Reserve booklet (1993), we can get an alternative estimate of the extinction for PAR. They divide the canopy into three layers and list the energy absorbed at each level of the forest. The lowest level of the canopy where we sampled absorbs about 4% of the energy available from PAR. They estimate over 80% of the incoming radiation is absorbed in the topmost level of the canopy. Average effective radiation listed shows that 37 μmol photons m^{-2} s^{-1} reaches the lowest level which is just under 5% of the 766 μmol photons m^{-2} s^{-1} arriving at the top. We might therefore infer from these results that the LAI for Dinghushan should be greater than 5. Solving equation 3.4.6 for LAI given PAR_i = 0.05 PAR yields a value of 6.7 for the LAI. These values are reasonable in light of measurements in the Amazon (Jacob and Wofsy, 1990). For a LAI of 7 in the jungle, the radiation available at the lowest levels in the forest are 3% of those at the top. According to the Jacob and Wofsy (1990), 98% of the total isoprene emitted by the Amazon forest originates in the upper 10 meters of canopy. Now we may estimate L in equation 2.3.8 based on our measurement of PAR at

the canopy top and the approximate factor of 20 extinction. Our standardized values of emissions for isoprene are shown in Table 3.4.4 along with the correction factors calculated with equations 3.4.4 and 3.4.5.

Table 3.4.4 Standard emission rates at 303 K and 1000 μmol m^{-2} s^{-1} for our six sampled species at Dinghushan as calculated by equation 2.3.7. Correction factors for PAR (C_L) and Temperature (C_T) are shown. Rate is given as micrograms C per grams dry leaf mass per hour.

Species	Emission rate (μg g^{-1} h^{-1})	C_L	C_T	Standard Emission rate (μg g^{-1} h^{-1})
Sarcosperma larinum	0.05 ±0.01	0.07 ± 0.04	0.88 ± 0.18	0.8 ± 0.5
Caryota ochlandra	3.64 ±0.52	0.07 ± 0.04	0.91 ± 0.18	56.1 ± 37.7
Schima superba	0.03 ±0.01	0.07 ± 0.04	0.76 ± 0.15	0.5 ± 0.3
Aporosa yunnanensis	0.06 ±0.01	0.07 ± 0.04	0.81 ± 0.16	1.1 ± 0.7
Cryptocarya concinna	2.57 ±0.36	0.05 ± 0.03	1.00 ± 0.19	55.2 ± 37.1
Castanopsis chinensis	0.04 ±0.01	0.05 ± 0.03	1.21 ± 0.24	0.6 ± 0.4

Some typical standard emission values for isoprene range from 32-110 μg $g^{-1}h^{-1}$ for emitting species. Species with rates less than 0.5 μg $g^{-1}h^{-1}$ are considered non-emitters (Guenther et al., 1996c). König et al. (1995) report emission ranges for various oak varieties of 0.61-50.4 μg $g^{-1}h^{-1}$. Our values are near this range. Two species, Caryota ochlandra and Cryptocarya concinna, have appreciable emission rates while the other four would be considered very low emitters of isoprene. These results are by no means conclusive due to the number of assumptions we have made in addition to the fact that we only sampled one branch from each tree. Most measurements reported are an average of many separate experiments with different levels of PAR and temperature. The empirical relations used to calculate standard emissions were developed for a different group of tree species and may not be appropriate for those we sampled. Our estimates for PAR extinction are based on an average reported for the forest system at Dinghushan. Moreover, we sampled at several different locations within the forest and it is likely that the canopy overhead gave varied amounts of coverage from direct radiation.

Next we must estimate a biomass factor for the forest as a whole which we may multiply by our calculated emission rates to obtain an emission flux from the entire forest.

Since we did not measure this quantity directly, we must estimate it from available data and techniques. In their paper discussing global modeling of natural volatile hydrocarbons, Guenther et al. (1995) relate foliar density (g m^{-2}) to net primary productivity (NPP). For a tropical seasonal forest, the peak foliar mass is expected to be 60% of NPP. NPP for the monsoon evergreen broad-leafed forest is given in the Dinghushan Biosphere Reserve booklet (1993) as 2599 g m^{-2} $yr.^{-1}$. This compares to 2050 g m^{-2} predicted by Guenther et al. (1995) for this type of ecosystem. The peak foliar mass therefore for this forest is 0.6 x 2599 or 1559 g m^{-2}. As expected, this is quite large in comparison to some other forests. Often cited mid-latitude biomass density factors as calculated by Lamb et al. (1993) include 470 g m^{-2} for a deciduous forest and 650 g m^{-2} for a coniferous one. An alternate method for arriving at the foliar mass is by using the average specific leaf weight (SLW) and LAI. SLW was found to be 82.4, 72.8 and 60.4 g m^{-2} for the three canopy levels at Dinghushan. The product of SLW and LAI gives an estimate for the foliar mass. In our case, the sum of the three SLWs multiplied by our estimated LAI of 6.7 yields a biomass factor of 1445 g m^{-2}. This agrees quite well with our other estimate. Taking the average and standard deviation for these three estimates, we obtain a biomass factor of 1410 ± 170 g m^{-2}. Note that this value is the peak foliar mass.

Using the biomass factor, we can obtain an estimate for the isoprene emissions from the entire forest. The evergreen broad-leafed region we studied covered 125 hectares. We sampled four species where we know their biomass ratio in the forest. If we weight the emission rate times the biomass ratio, we obtain an average flux estimate of 6.1 ± 4.2 μg C $g^{-1}h^{-1}$ for the forest type representing over a third of the forest by biomass. Therefore, the isoprene flux during the summer months at Dinghushan was 1410 ± 170 g m^{-2} multiplied by the average emission rate giving 8.6 ± 6.1 mg C m^{-2} h^{-1}. Geron et al. (1997) list the results of several studies in the United States with a range of 0.07 to 9.33 mg C m^{-2} h^{-1}. The near zero value was obtained for evening, night and early morning fluxes whereas the maximum flux estimate came from a study in an oak grove. Oaks are known high isoprene emitters.

We also measured terpene fluxes during these experiments but the results are more uncertain due to analytical problems surrounding the Nafion dryer. Any α-pinene emitted was most likely removed by the dryer based on our standard runs and comparison of whole air runs with and without the dryer. Standard runs showed increases in γ-terpinene and sabinene concentrations and decreases in levels of limonene. Results for myrcene and camphene were inconsistent. That being said, we found detectable terpene emissions from four of the tree species sampled. Not surprisingly, the levels are generally smaller than those encountered in the literature. Equation 3.4.1 was used to calculate the fluxes and results are give in Table 3.4.5. The range for emissions is based on the results of standard runs, comparing the average response with and without the Nafion dryer. Camphene losses were about a factor of five, myrcene ranged from a gain of 50% to a factor of 2 loss. Sabinene showed close to a factor of two gain and γ-terpinene a factor as high as eight. To obtain a standard emission rate, we applied a general equation for terpene emission temperature dependence from Guenther et al. (1993)

$$M = M_s \cdot \exp(\beta(T - T_s)) \qquad (3.4.7)$$

where the subscript s represents the standard value and β is an empirically determined coefficient equal to 0.090 ± 0.025. The extrapolation to regional emissions for terpenes is less promising than with isoprene as we have biomass information on only two of the four

Species	Terpene	Emission rate ($\mu g\ g^{-1}\ h^{-1}$)	Standard rate ($\mu g\ g^{-1}\ h^{-1}$)
Sarcosperma larinum	camphene	0.02 ± 0.07	0.02 ±0.07
	myrcene	0.03± 0.03	0.03 ±0.03
Caryota ochlandra	myrcene	0.05± 0.05	0.05 ±0.05
Schima superba	camphene	0.09± 0.37	0.11 ±0.45
	γ-terpinene	0.32± 0.16	0.38 ±0.19
	sabinene	0.05± 0.03	0.06 ±0.03
Aporosa yunnanensis	camphene	0.02± 0.06	0.02 ±0.07
	myrcene	0.03± 0.03	0.04 ±0.04

Table 3.4.5 Terpene emission results from our enclosure study. The emission rate is calculated using equation 2.3.5. Uncertainties for the emission rates were determined by using the results of standard analyses which allowed quantification of the effects of the Nafion dryer on terpene peak areas. By using equation 3.4.7, the rates were converted to a standard rates at 303 K.

terpene emitters representing under 14% of the total biomass. If we assume that this is representative, we may use the same biomass factor 1410 ± 170 g m^{-2} to obtain emission rates. The percent biomass weighted emission rate for terpenes from Schima superba and Aporosa yunnanensis is 0.06 ± 0.07 μg g^{-1} h^{-1}. This leads to a flux of 0.08 ± 0.10 g C m^{-2} h^{-1}.

3.5 Intensive Phase: Results and Discussion

3.5.1 NMHC data summary

We were able to amass almost 1200 data points for many of the NMHC species identified during our intensive campaign. Figure 3.5.1 displays our entire data set minus those measurements we deemed questionable. Quite a number of issues were dealt with to sort out the good from the questionable data. Between Julian days 183 and 192 we discarded light hydrocarbon data from ethane to butane. Due to our inability to regulate the collection temperature, we saw high variability in the levels of light species. Rather than attempt to pick out those values that seemed reasonable, we chose to eliminate data from the entire period. Though it was not until day 197 that we started using liquid Argon, we did become proficient at regulating the collection temperature and therefore retain information on all species except for ethane between days 192 and 197. Pentane, cyclopentane and hexane all suffered from contamination apparently from a piece of Teflon tubing in the sampling line which was removed on day 192. Some species like methylcyclohexane and cycloheptane have significant gaps in their record as they periodically went below the detection limit of the instrument. The first five days for the heavy hydrocarbon fraction are without data as the transfer to the second chromatographic column was inconsistent. The next 10 day period had many points removed as it was clear that proper gas transfer had not occurred. Six different heavy species were seen to have contamination from the first hydrogen carrier gas. To address this, at day 219 we changed to a new tank and added an oxygen trap to the carrier gas line which led to a steep decrease in the concentrations obtained for cyclooctane, nonane, 1-decene, ethylbenzene and the xylenes. Curiously, the contamination did not appear in the zero air runs. Possibly some interaction between some contaminant in the carrier gas and whole air led to higher

concentrations of those compounds. The terpenes which are presented have only one week of data. For that particular week alone we did not use the Nafion dryer to dry the air sample and relied on Ascarite to do double duty as a remover of both CO_2 and H_2O.

We analyzed the graphed data for the median value, interquartile ranges and the outer decile values. That information is presented in box and whisker form (Figure 3.5.2). Some species show average concentrations above the 90th percentile. This is due to sample concentrations well above the median being averaged. One can clearly see that the light alkanes have wide ranges as a result of the local propane emissions. The isoprene numbers were obtained from data prior to Julian day 191 and the terpene information

Table 3.5.1 Summary of some commonly measured NMHC species from this study and three others. The number of samples for each study represented are 81 for the Amazon, over 600 for Massachusetts and roughly 20 for Canada. The median value is given in ppbv as are [interquartile ranges] when available.

Compound	This work	Amazon[a]	Massachusetts[b]	rural Canada[c]
ethane	1.27 [0.93-2.17]	1.17 [0.73-1.55]	1.227	0.90 / 0.85
ethene	1.41 [0.81-2.51]	1.24 [0.73-1.68]		0.11 / 0.18
acetylene	0.88 [0.52-1.51]	0.33 [0. 22-1.03]	0.243	0.09 / 0.19
propane	2.66 [1.35-5.78]	0.48 [0. 31-1.69]	0.461	0.08 / 0.33
propene	0.41 [0.24-0.83]	0.28 [0. 22-0.67]		0.05 / 0.04
i-butane	1.34 [0.78-2.95]	0.22 [0. 06-0.43]	0.079	0.01 / 0.10
n-butane	2.76 [1.57-5.98]	0.09 [0.09-0.66]	0.167	0.01 / 0.20
t-2-butene	0.04 [0.03-0.09]			0.00 / 0.01
1-butene	0.08 [0.04-0.16]			0.03 / 0.03 sum propyne
c-2-butene	0.03 [0.02-0.07]			0.06 / 0.04 sum i-butene
i-pentane	0.82 [0.60-1.12]	0.25 [0.06-1.00]		0.02 / 0.18
n-pentane	0.17 [0.10-0.31]	0.09 [0.06-0.23]	0.079	0.01 / 0.12 sum cyclopentane
isoprene	0.67 [0.25-2.06]	2.65 [1.39-3.38]		0.25 / 0.03
2-methylpentane	0.17 [0.11-0.24]	0.01 [0-0.05]		0.05 / 0.12
3-methylpentane	0.10 [0.06-0.15]	0.02 [0-0.05]		
hexane	0.07 [0.04-0.13]	0.03 [0.02-0.06]	0.022	0.03 / 0.04
benzene	0.87 [0.56-1.40]	0.10 [0.07-0.15]		
toluene	0.60 [0.39-0.99]	0.72 [0.33-2.67]		
ethylbenzene	0.03 [0.02-0.05]	0.02 [0-0.04]		
m + p-xylene	0.06 [0.04-0.10]	0.12 [0.02-0.59]		
o-xylene	0.05 [0.03-0.09]	0.03 [0.01-0.10]		
α-pinene	0.46 [0.32-0.79]	0.13 [0.09-0.18]		
camphene	0.13 [0.10-0.19]	0.04 [0.01-0.06]		

[a] Zimmerman et al. (1988) from July and August 1985

[b] Goldstein et al. (1995b) July 1993

[c] Bottenheim and Shepherd (1995) July 1991 for two sites.

Figure 3.5.1 NMHC mixing ratios by volume from Dinghushan during the summer of 1996. The horizontal axes are Julian day covering a span from June 28 (day 180) to August 31 (day 245) with the exception of the terpenes, which have data from the week of JD 220. The vertical axes are log scale mixing ratio (by volume). Calibration from day 180 to 225 was performed by permeation tubes and Relative Molar Response (RMR). An MIT produced standard tank, daughter 5199, was used for calibration from day 226 forward. This allowed direct calibration of over thirty NMHC with the balance calibrated using RMR. Conversion to the NCAR(NIST) calibration scale is achieved by using ratios in Table B.3 in the Appendix. Many of the lightest hydrocarbons lack data during the first several weeks as sample preconcentration was performed using liquid nitrogen vapor rather than submersion of the sample loop in liquid Argon. Stable temperatures were difficult to maintain with the vapor technique. Contamination from supplied GC gases prevented accurate concentration determination for many of the heaviest species prior to day 219 at which point we added more in-line traps and replaced the carrier gases.

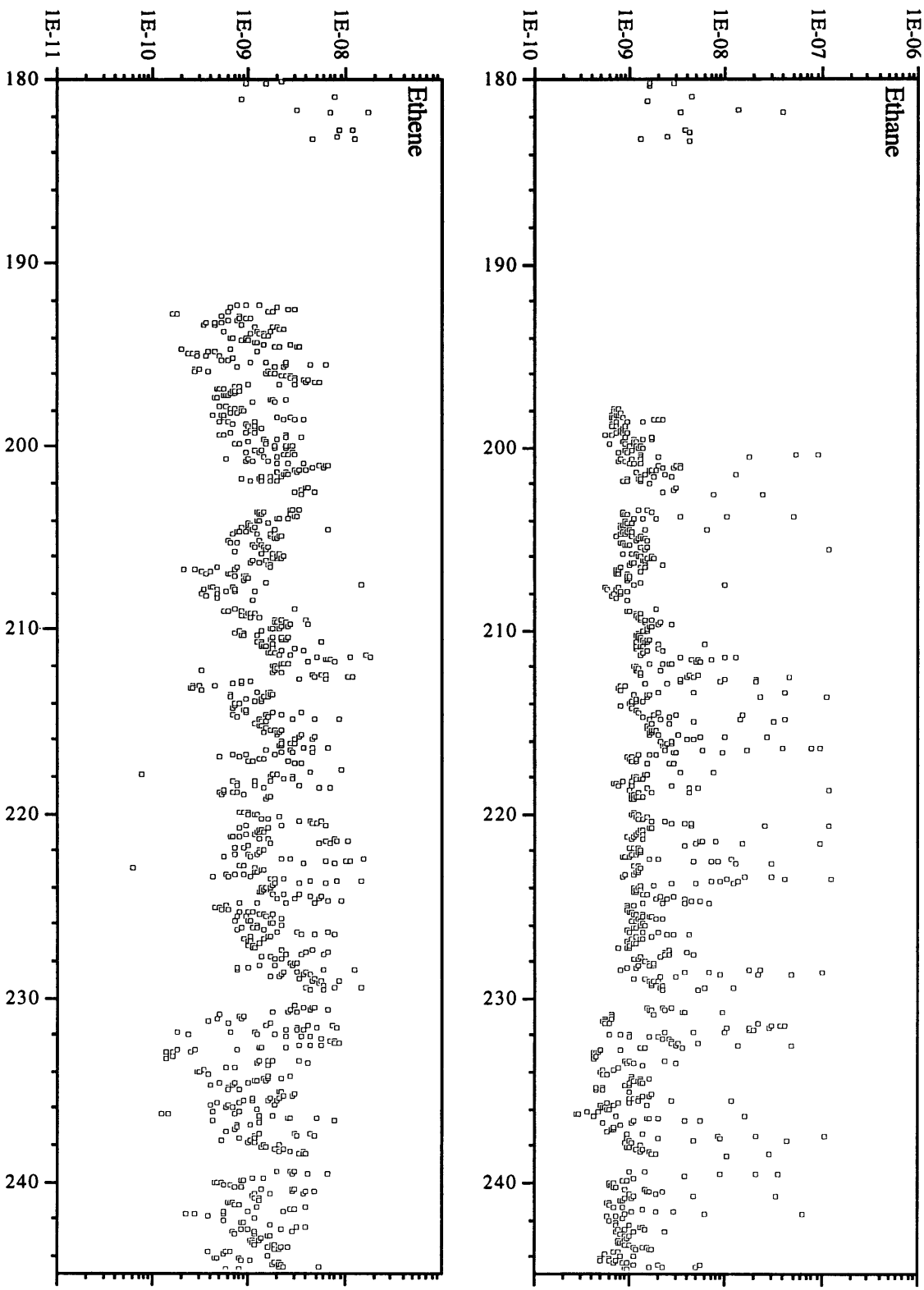
Ethene
1E-11
1E-10
1E-09
1E-08
180
190
200
210
220
230
240
Ethane
1E-10
1E-09
1E-08
1E-07
1E-06
180
190
200
210
220
230
240

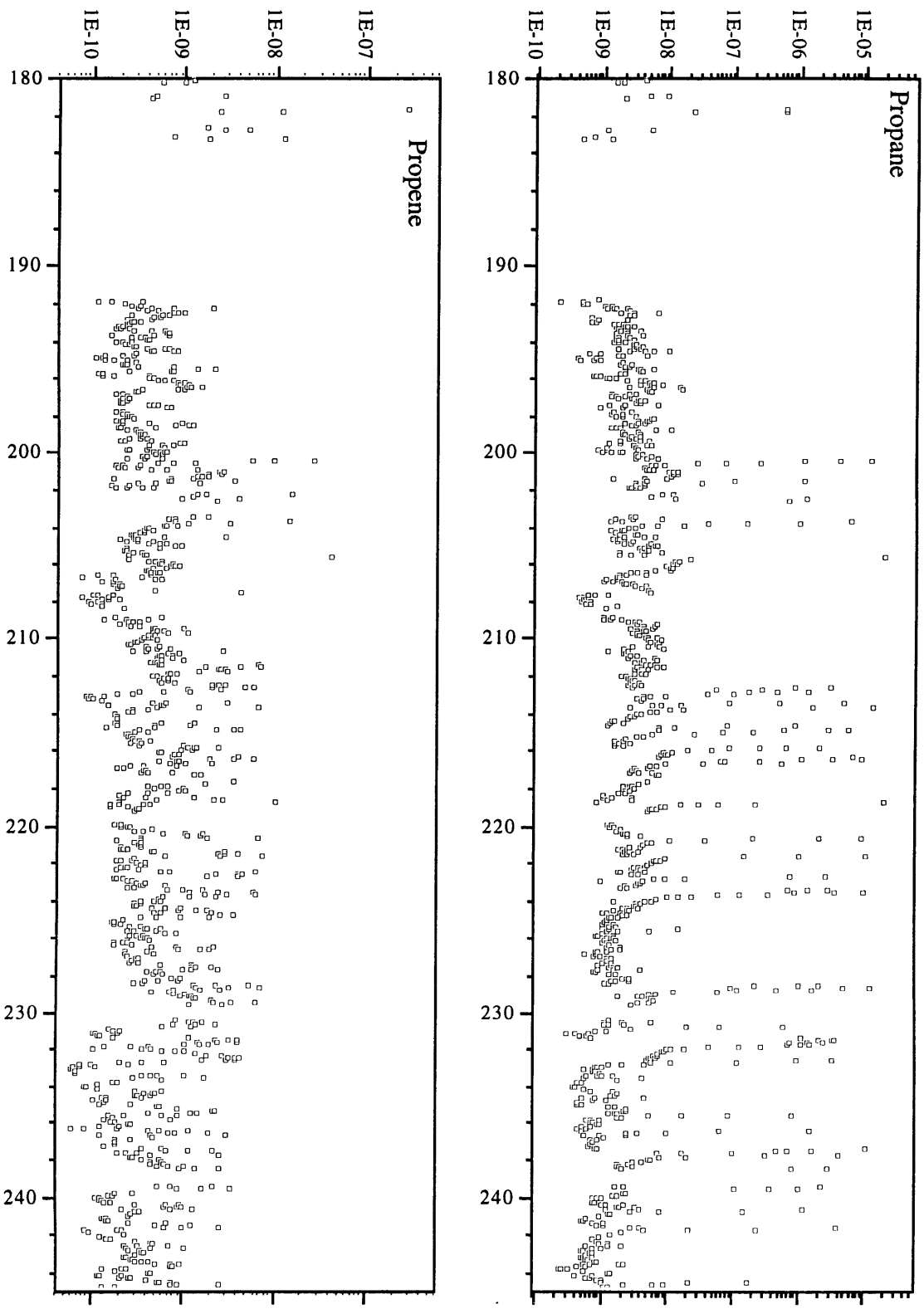
Propene
Propane
1E-10
1E-09
1E-08
1E-07
1E-06
1E-05
180
190
200
210
220
230
240

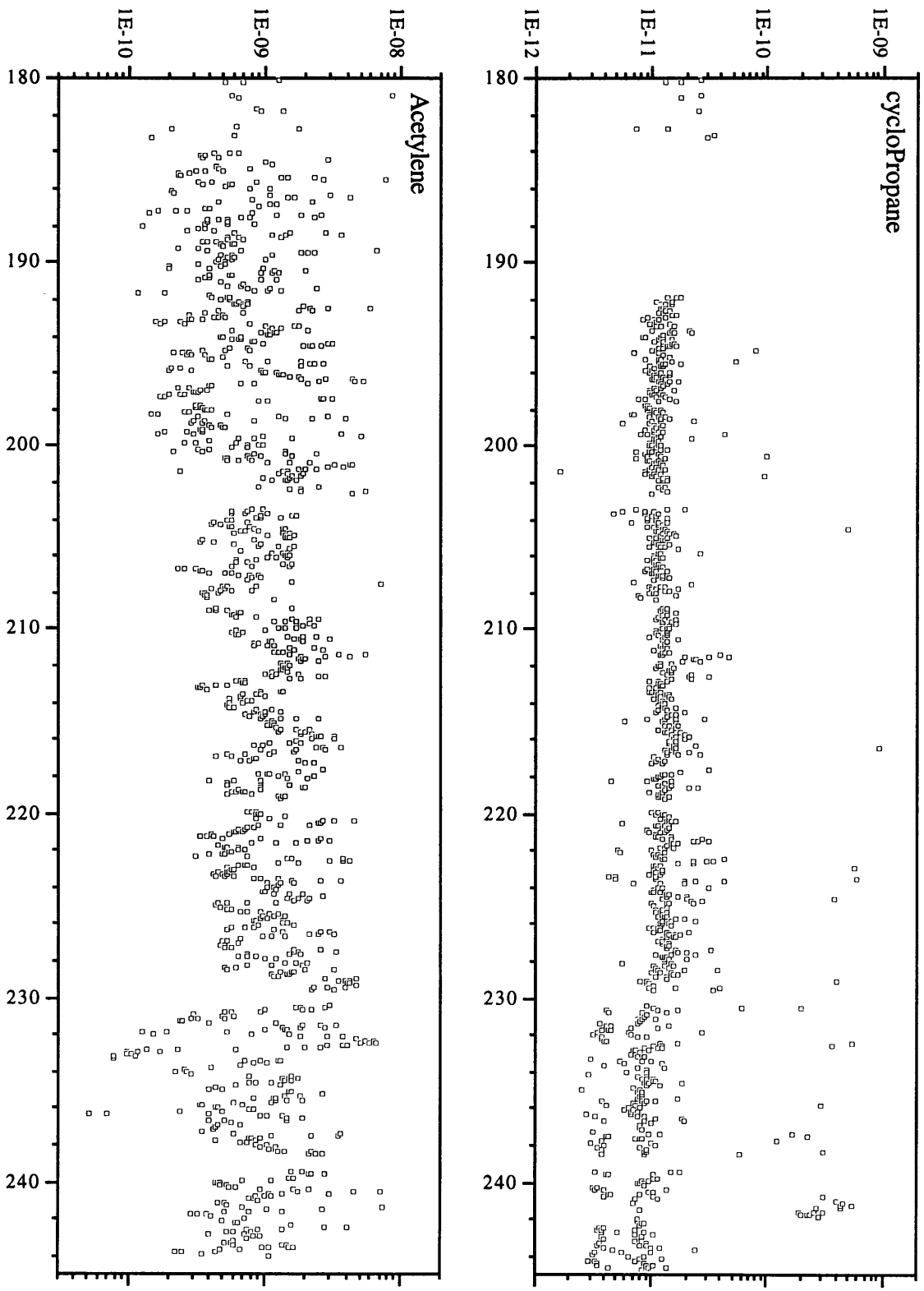
Acetylene
cycloPropane
1E-08
1E-09
1E-10
1E-11
1E-12
180
190
200
210
220
230
240

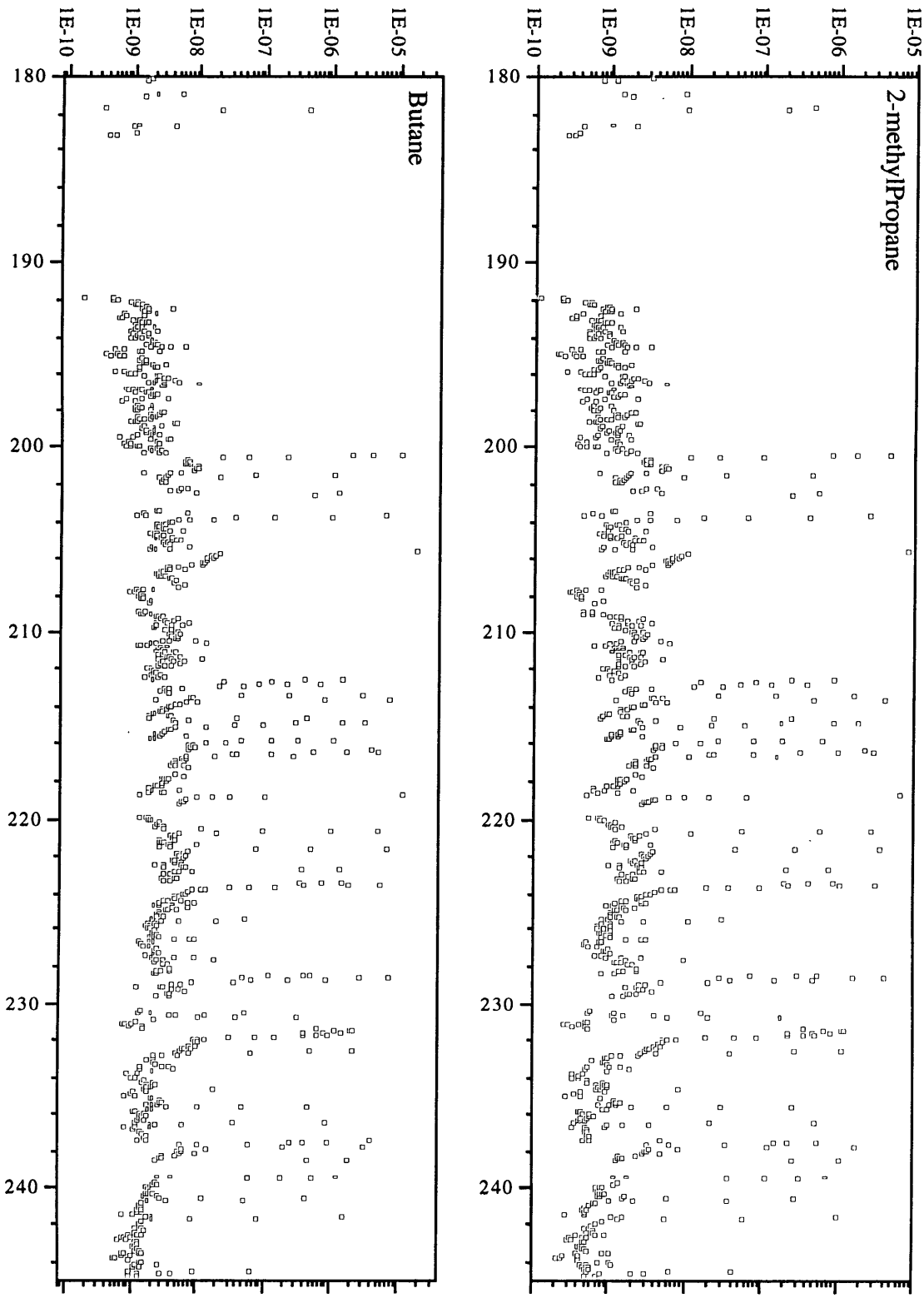
Butane
2-methylPropane
1E-10
1E-09
1E-08
1E-07
1E-06
1E-05
180
190
200
210
220
230
240

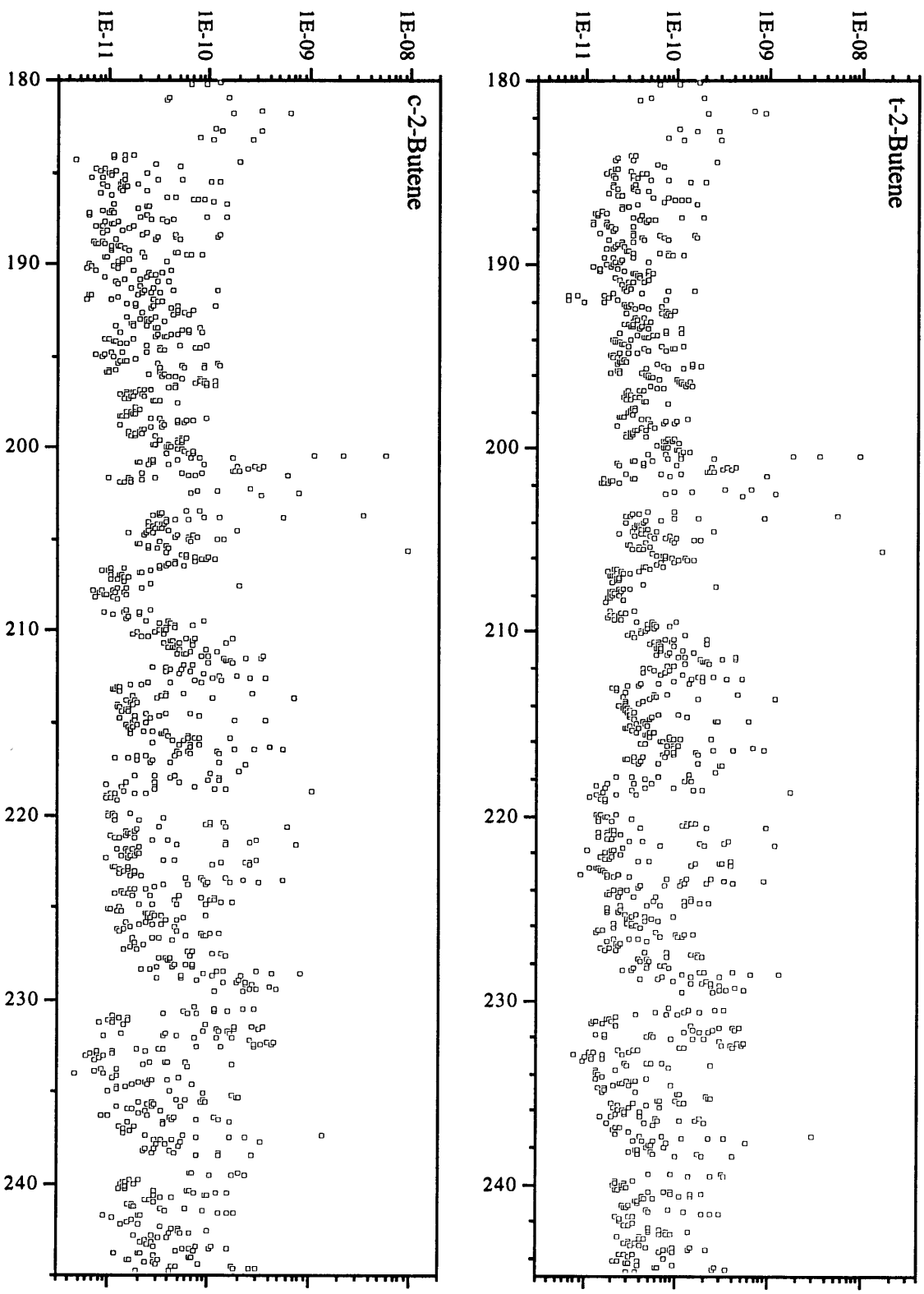
1E-11
1E-10
1E-09
1E-08
180
190
200
210
220
230
240
c-2-Butene
t-2-Butene

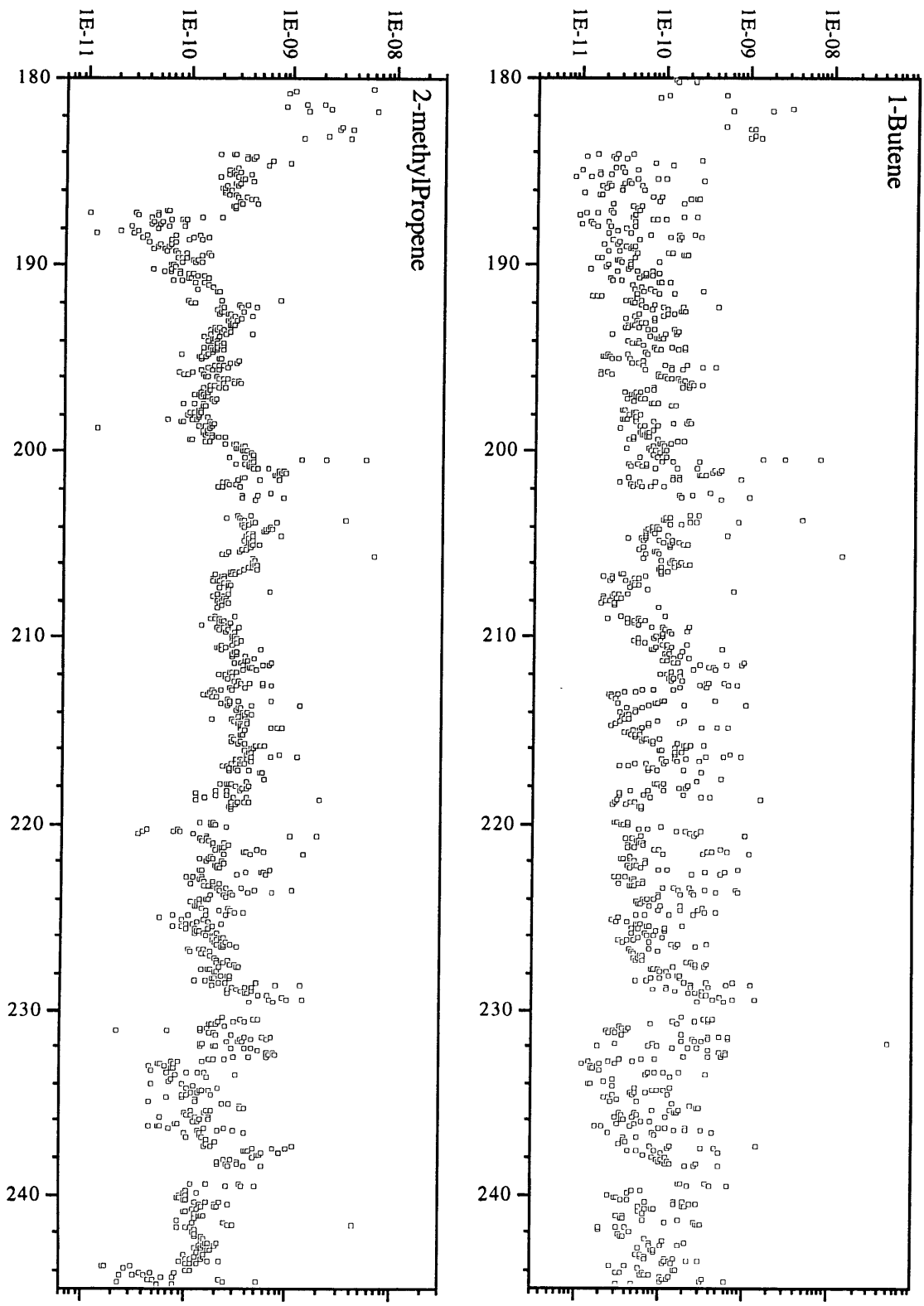
1E-11
1E-10
1E-09
1E-08
180
190
200
210
220
230
240
2-methylPropene
1-Butene

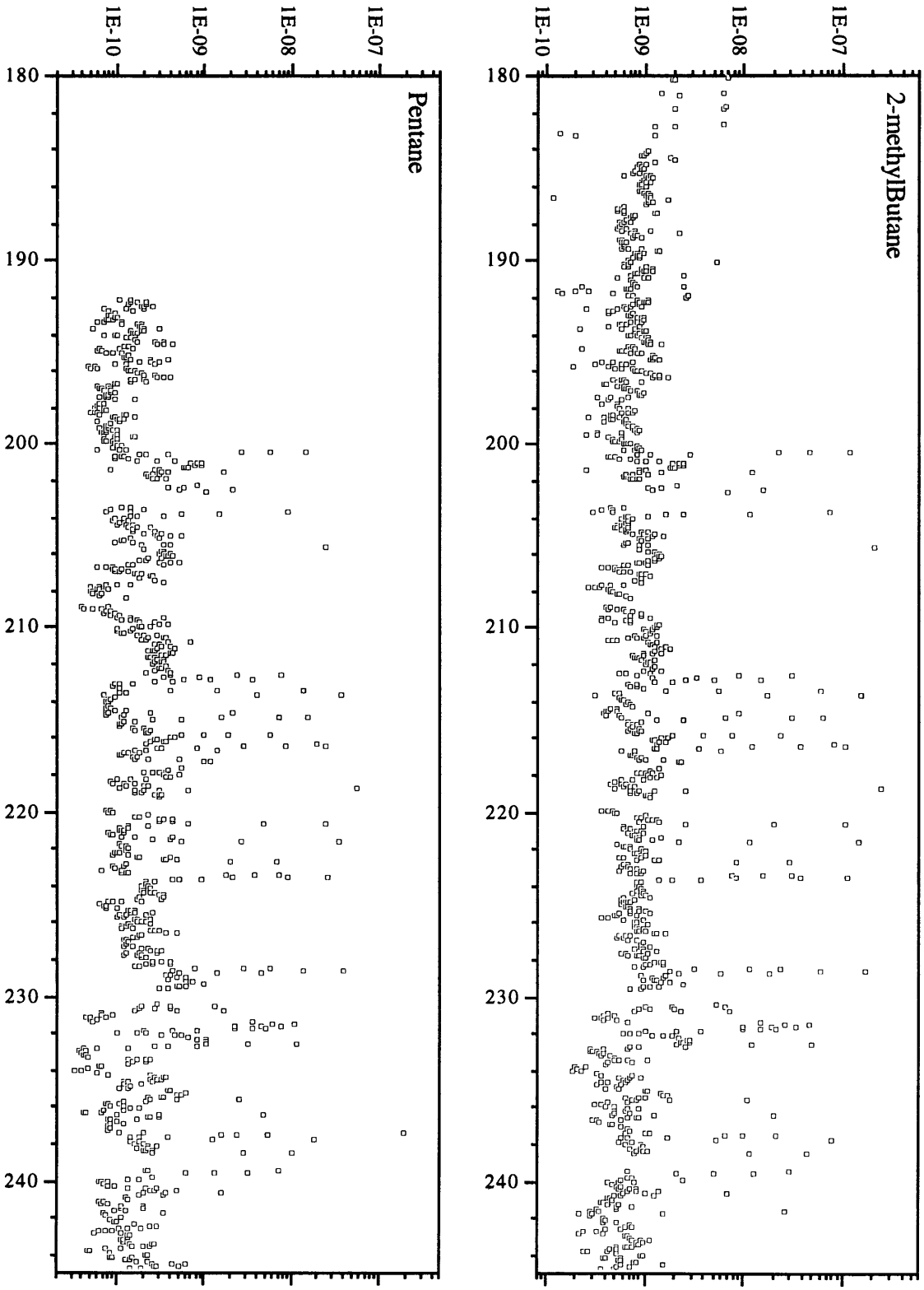
Pentane
2-methylButane
1E-10
1E-09
1E-08
1E-07
180
190
200
210
220
230
240

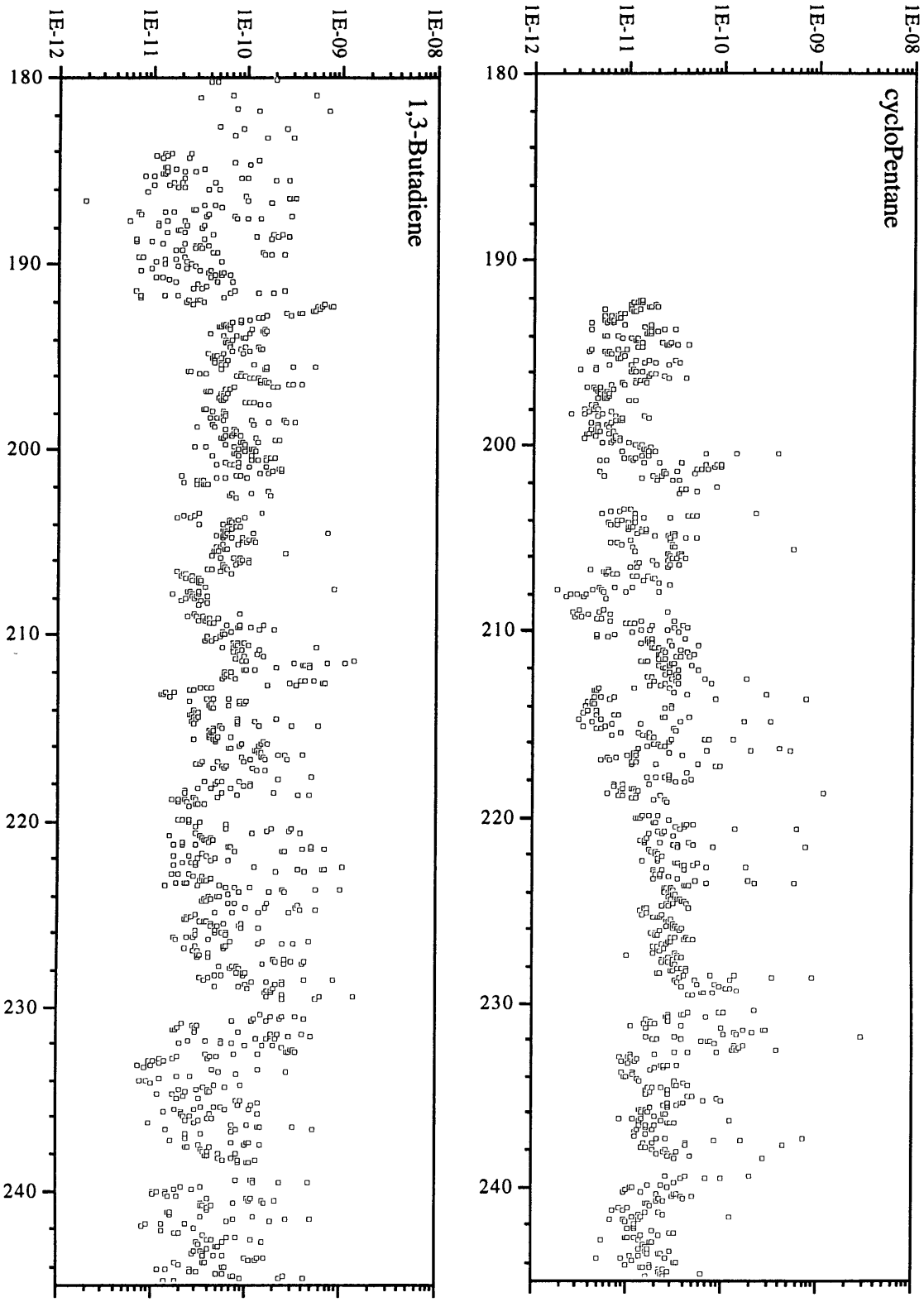
1E-12
1E-11
1E-10
1E-09
1E-08
180
190
200
210
220
230
240
1,3-Butadiene
cycloPentane

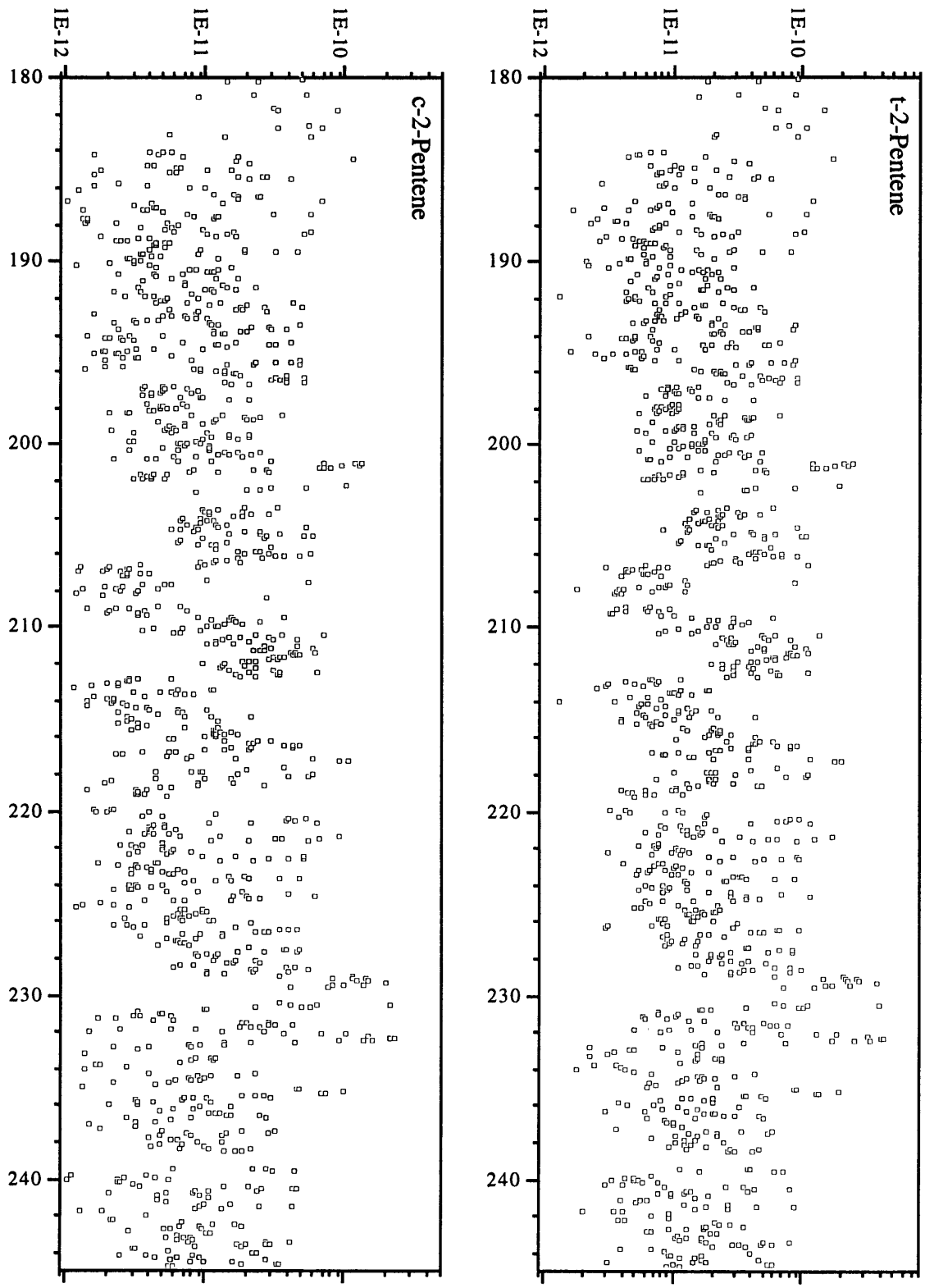
1E-12
1E-11
1E-10
180
190
200
210
220
230
240
c-2-Pentene
t-2-Pentene

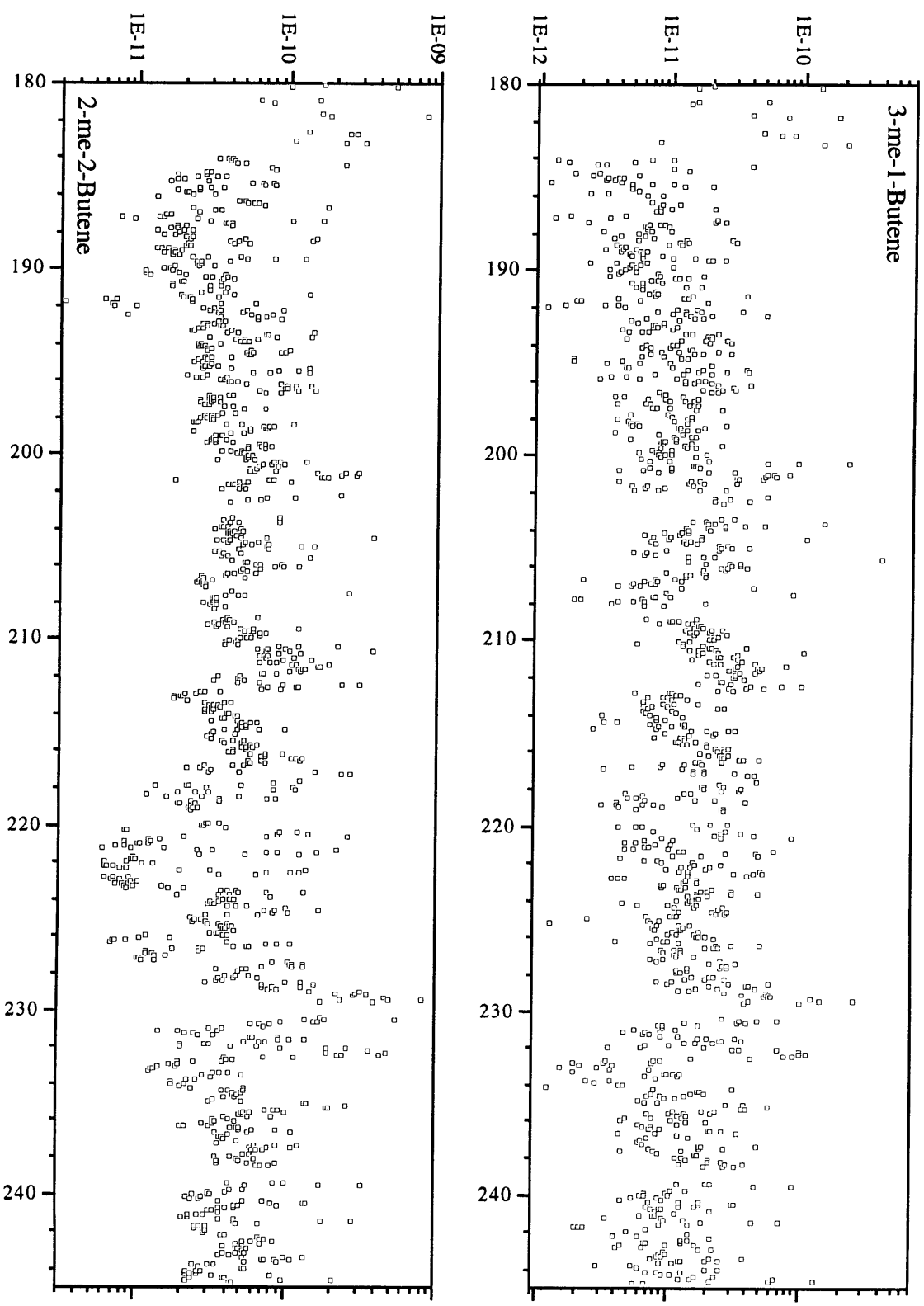
2-me-2-Butene
3-me-1-Butene
1E-09
1E-10
1E-11
1E-12
180
190
200
210
220
230
240

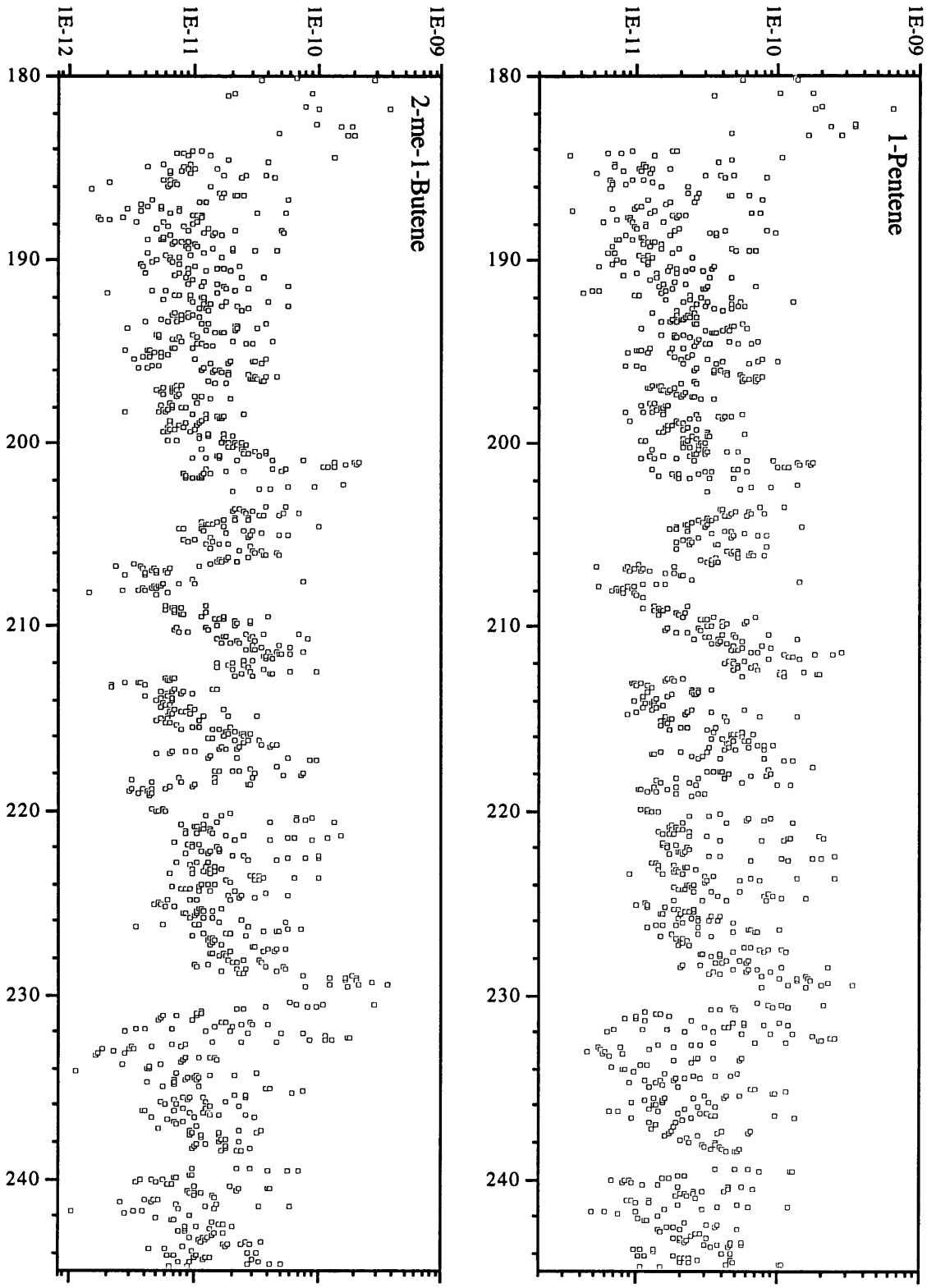
1E-12
1E-11
1E-10
1E-09
180
190
200
210
220
230
240
2-me-1-Butene
1E-11
1E-10
1E-09
180
190
200
210
220
230
240
1-Pentene

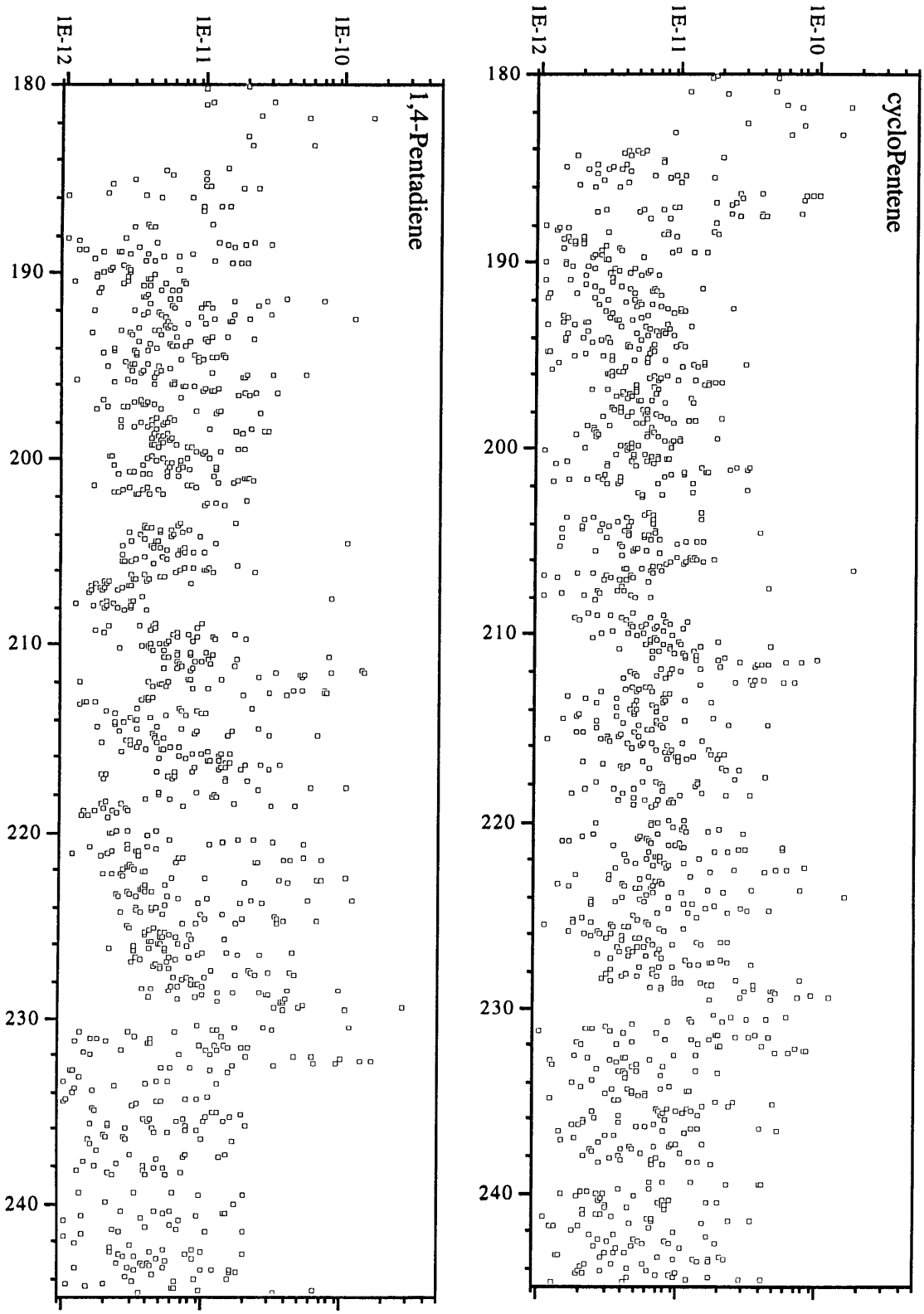
1E-12
1E-11
1E-10
180
190
200
210
220
230
240
1,4-Pentadiene
cycloPentene

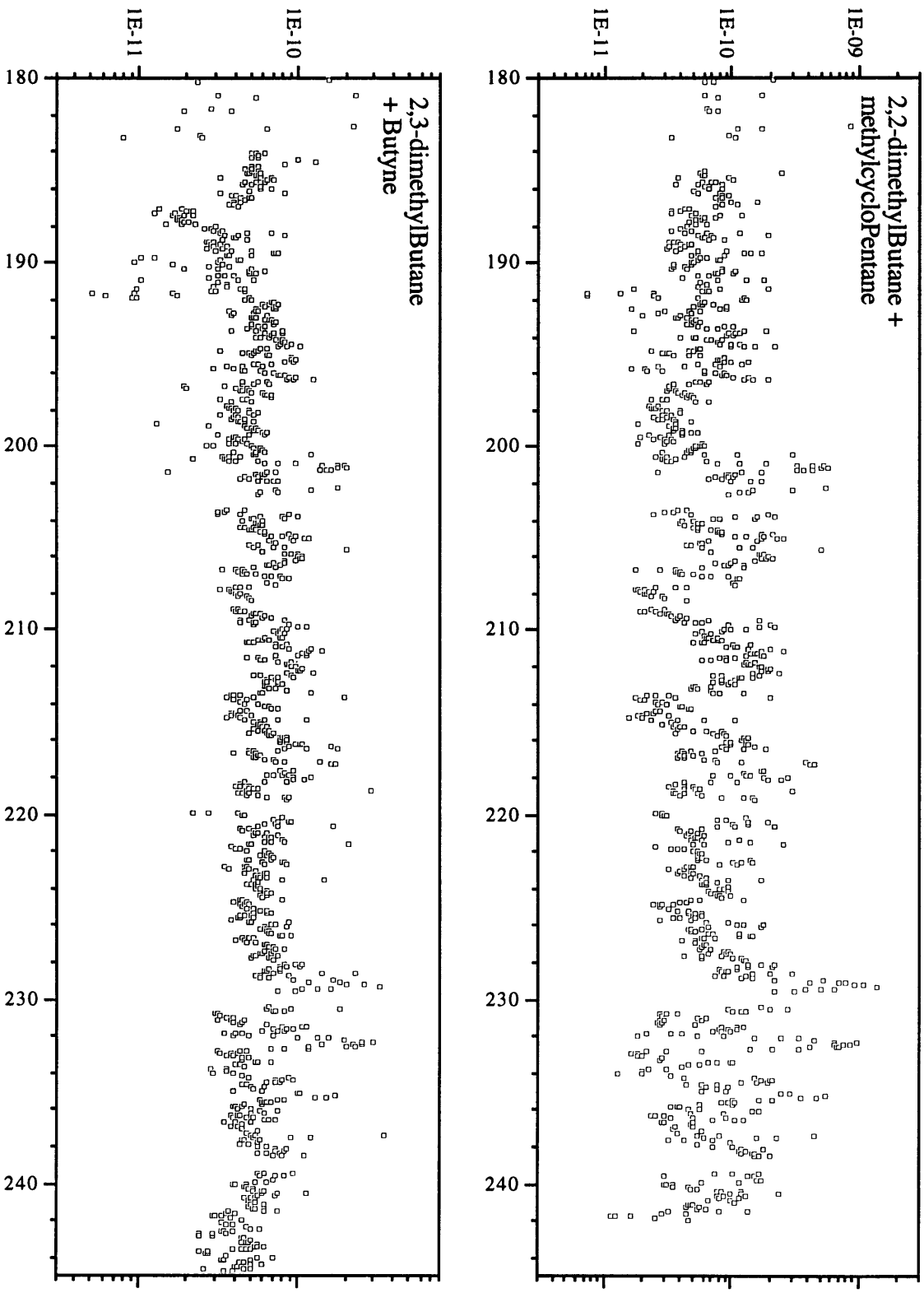
2,2-dimethylButane +
methylcycloPentane
2,3-dimethylButane
+ Butyne
1E-09
1E-10
1E-11
180
190
200
210
220
230
240

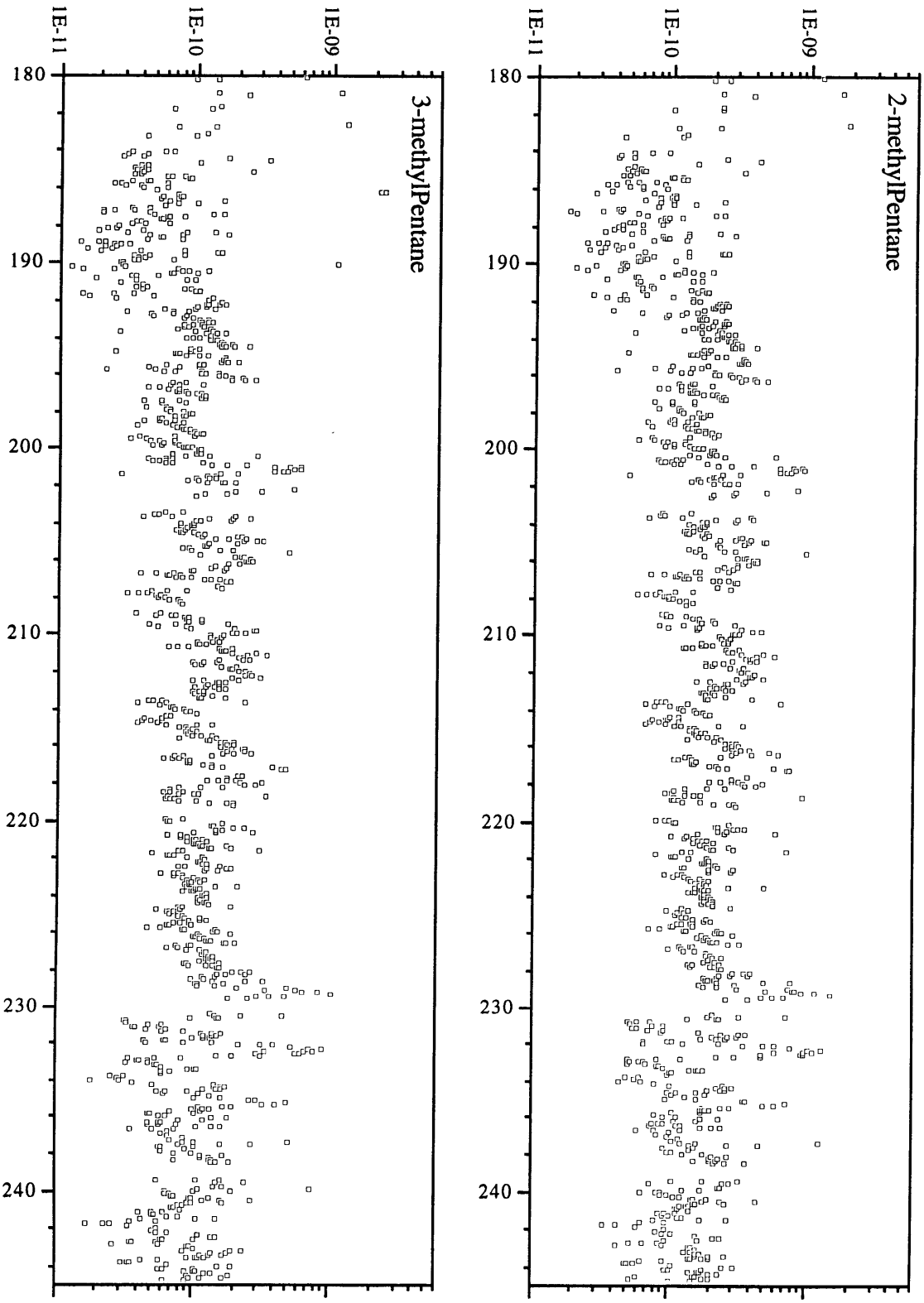
1E-11
1E-10
1E-09
180
190
200
210
220
230
240
3-methylPentane
2-methylPentane

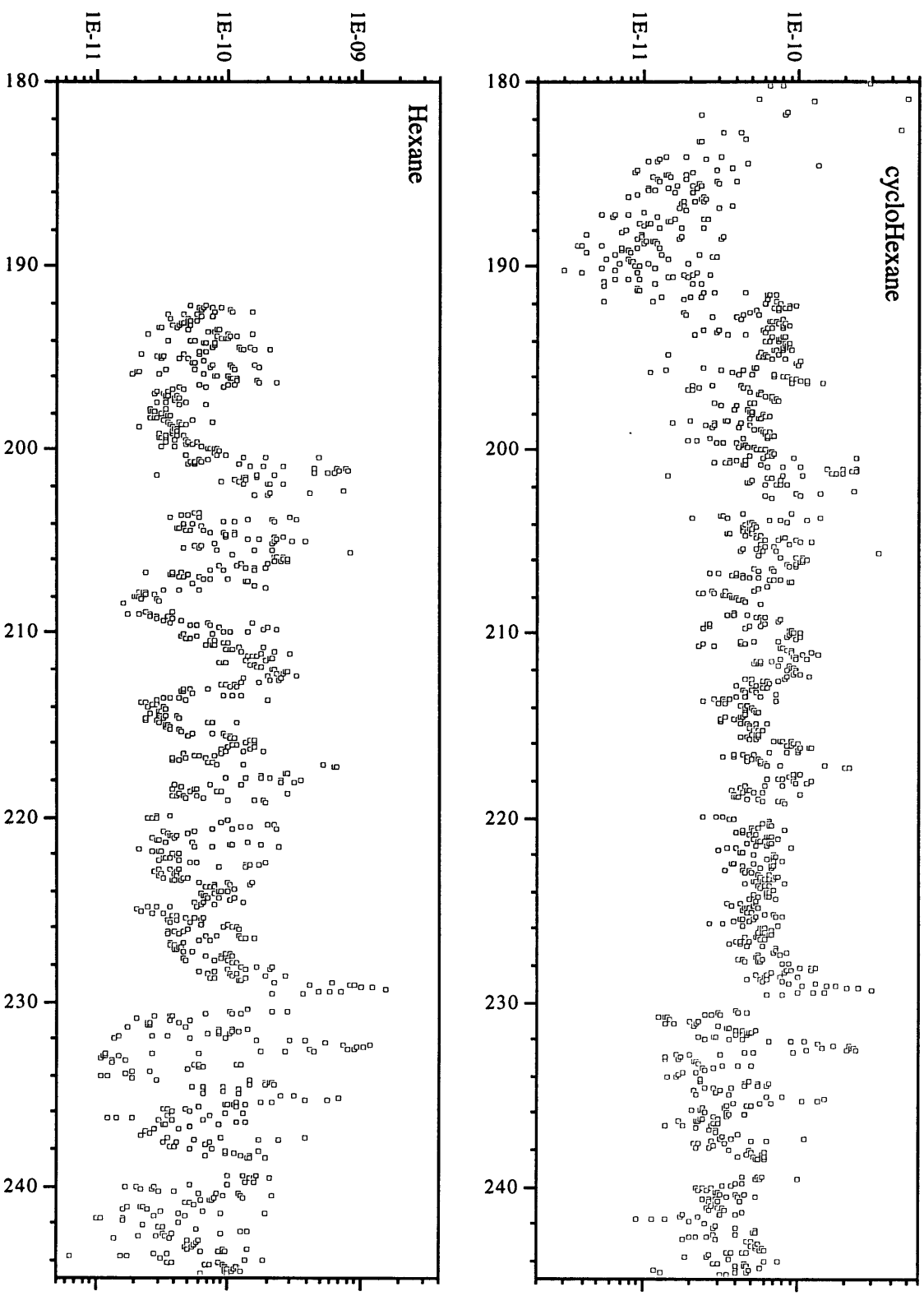
Hexane
cycloHexane
1E-11
1E-10
1E-09
180
190
200
210
220
230
240

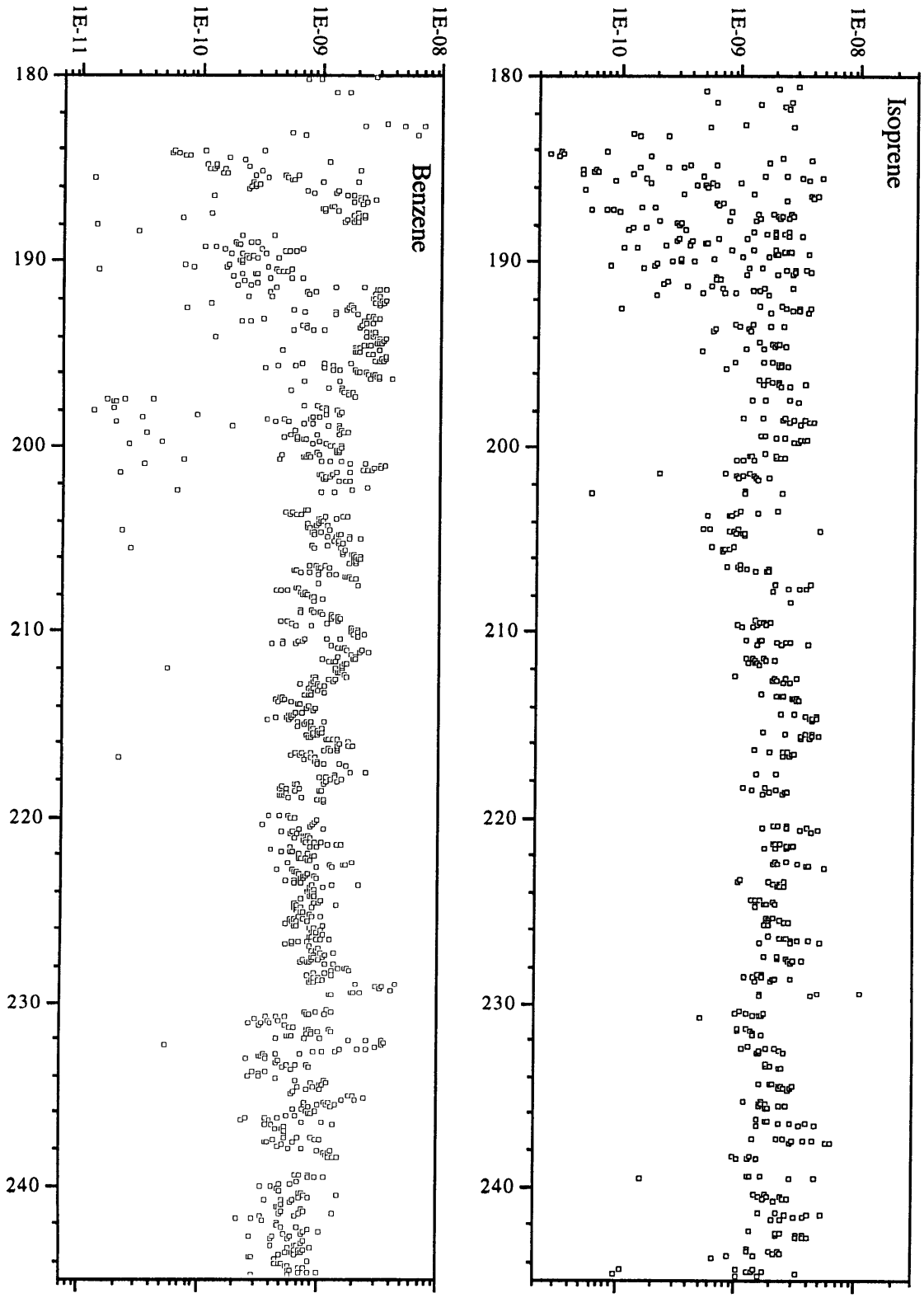
Benzene
Isoprene
1E-11
1E-10
1E-09
1E-08
180
190
200
210
220
230
240

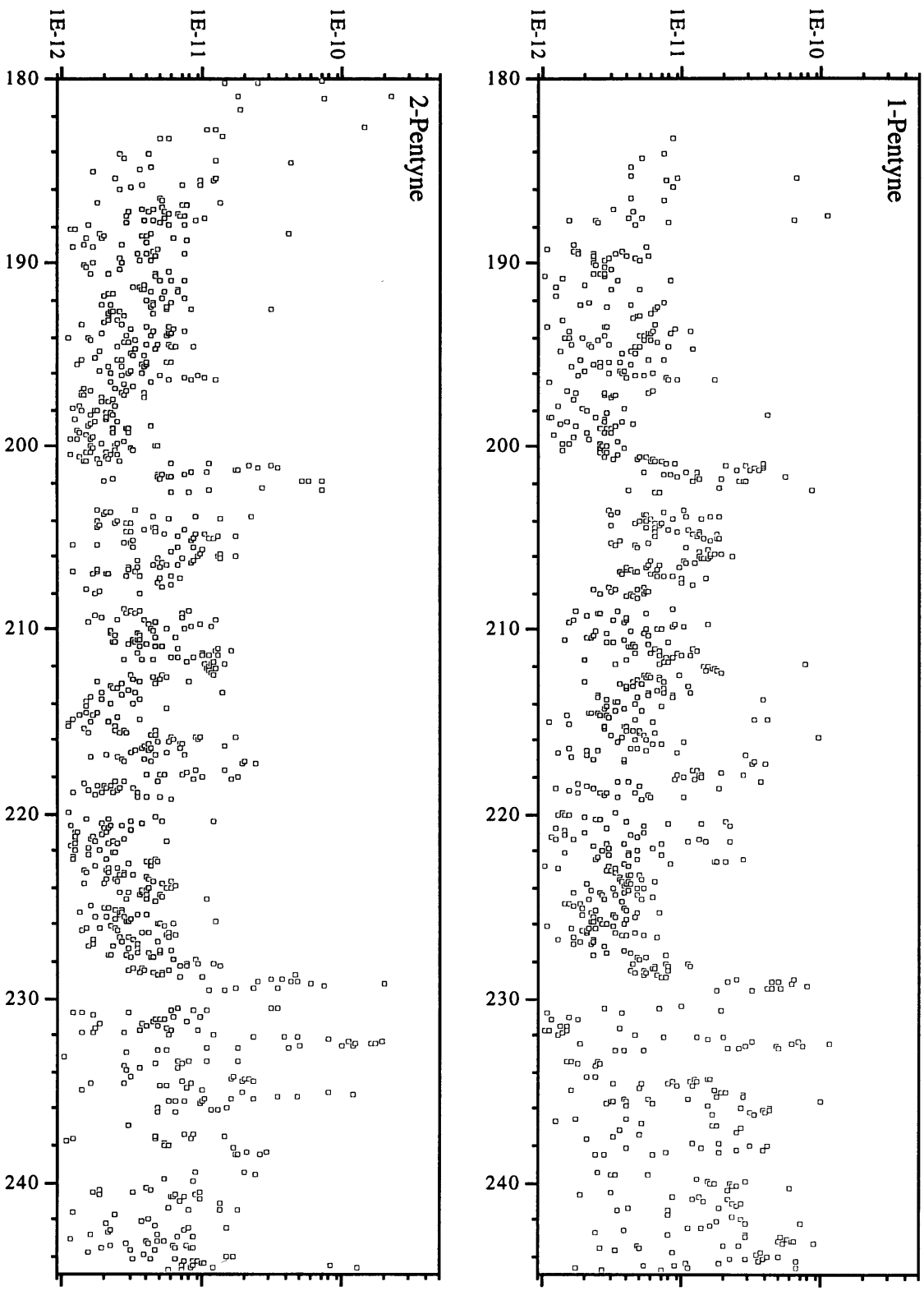
1E-12
1E-11
1E-10
180
190
200
210
220
230
240
2-Pentyne
1-Pentyne

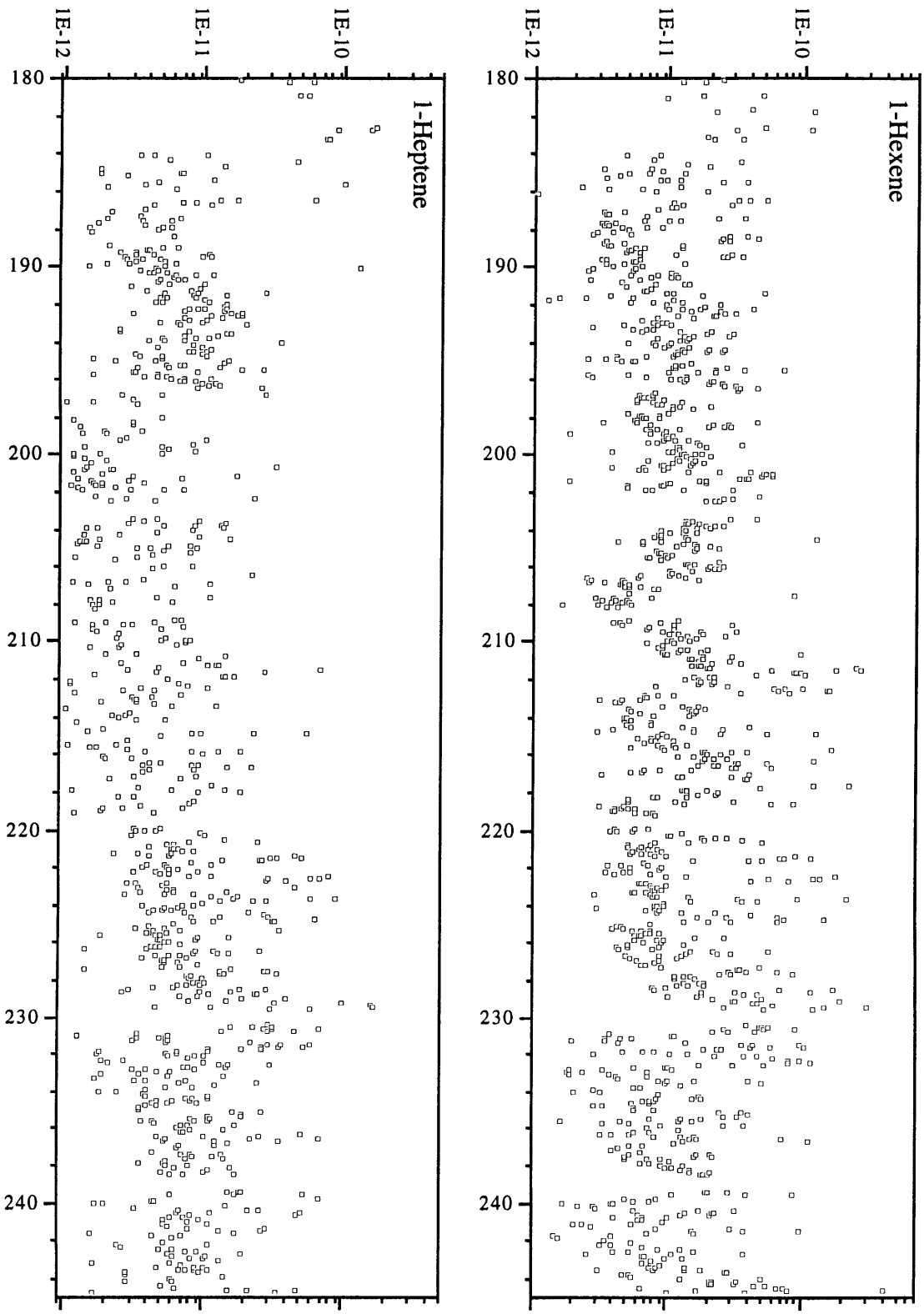
1E-12
1E-11
1E-10
180
190
200
210
220
230
240
1-Heptene
1-Hexene

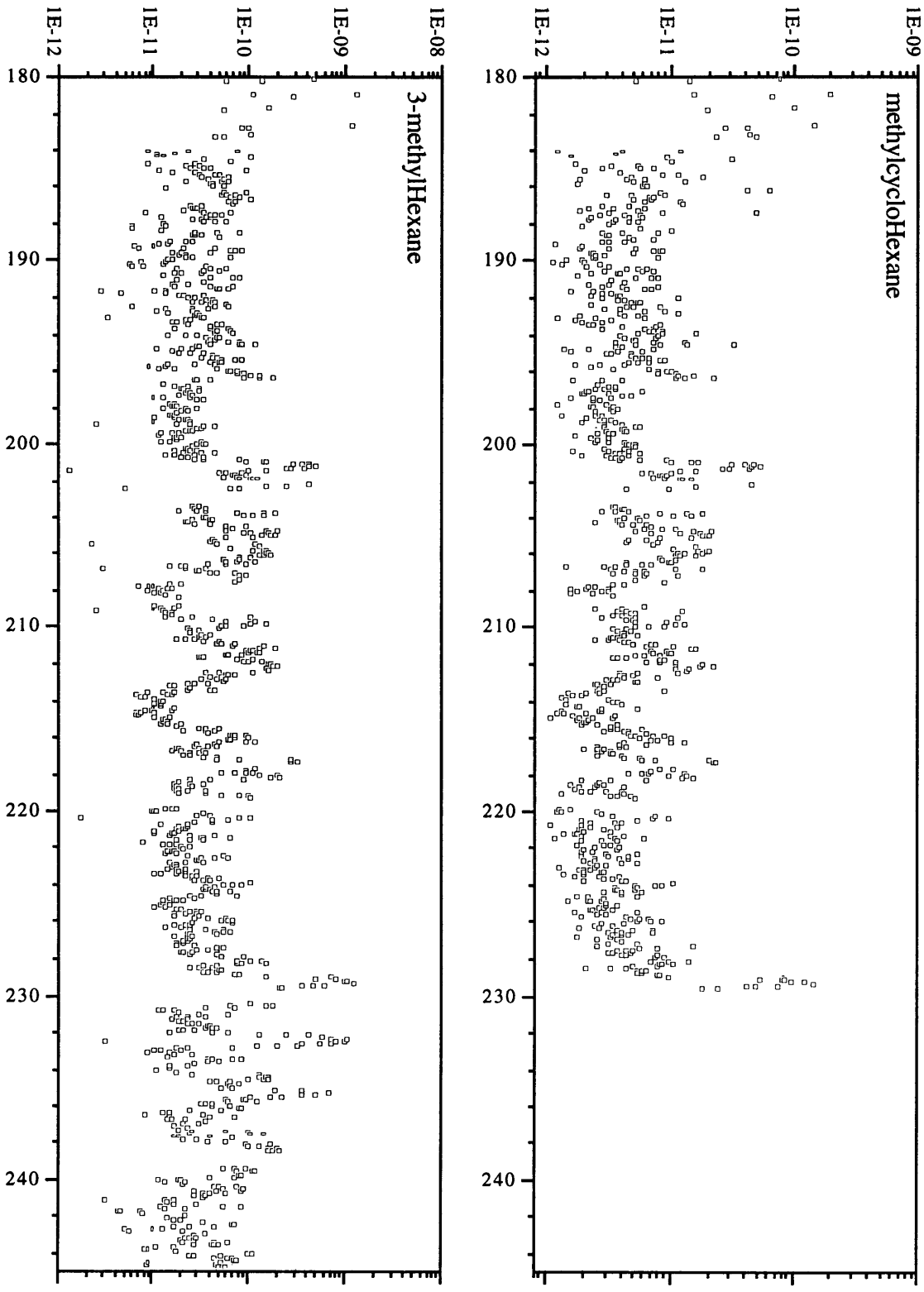
1E-12
1E-11
1E-10
1E-09
1E-08
180
190
200
210
220
230
240
3-methylHexane
1E-12
1E-11
1E-10
1E-09
180
190
200
210
220
230
240
methylcycloHexane

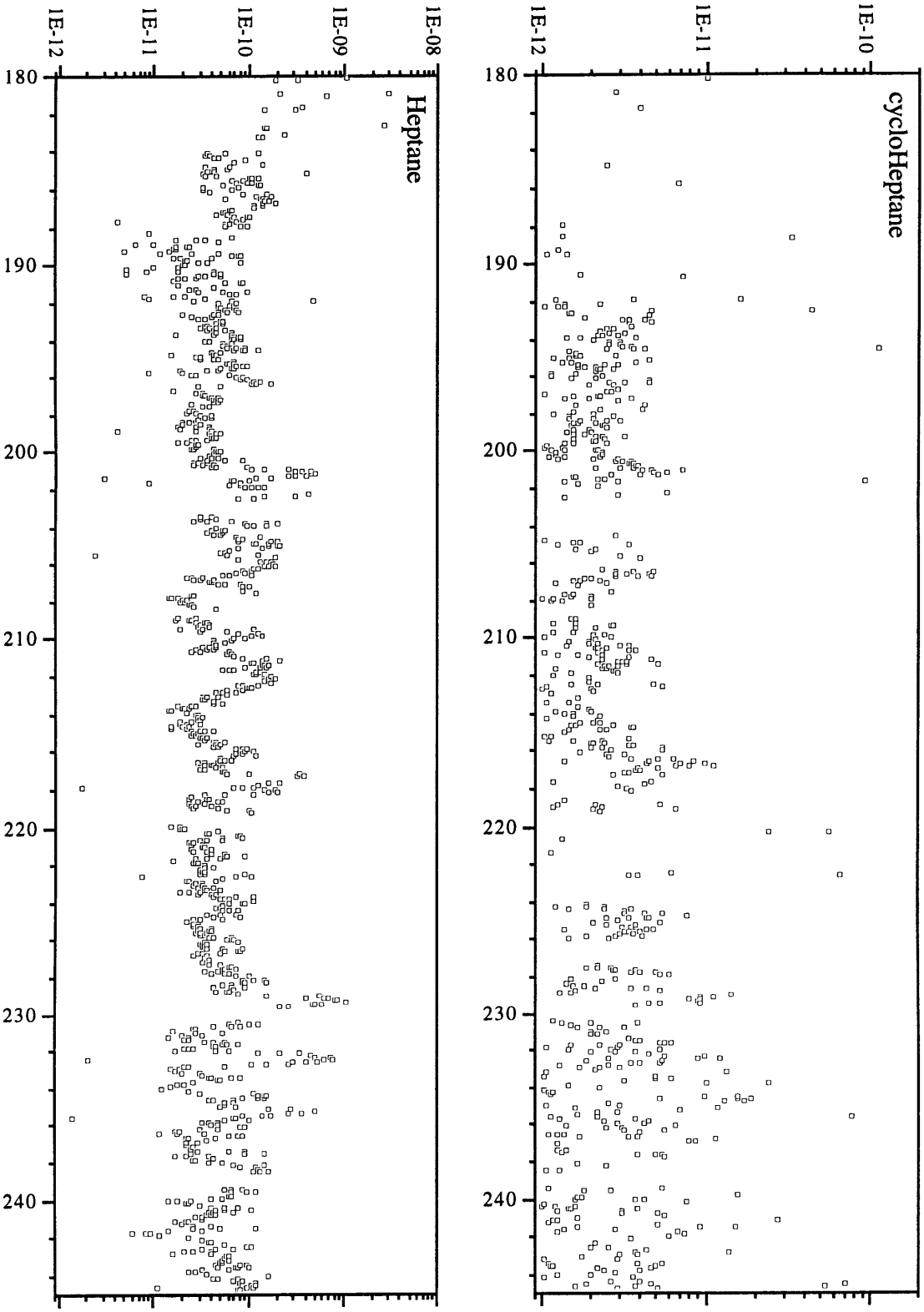
Heptane
cycloHeptane
1E-12
1E-11
1E-10
1E-09
1E-08
180
190
200
210
220
230
240

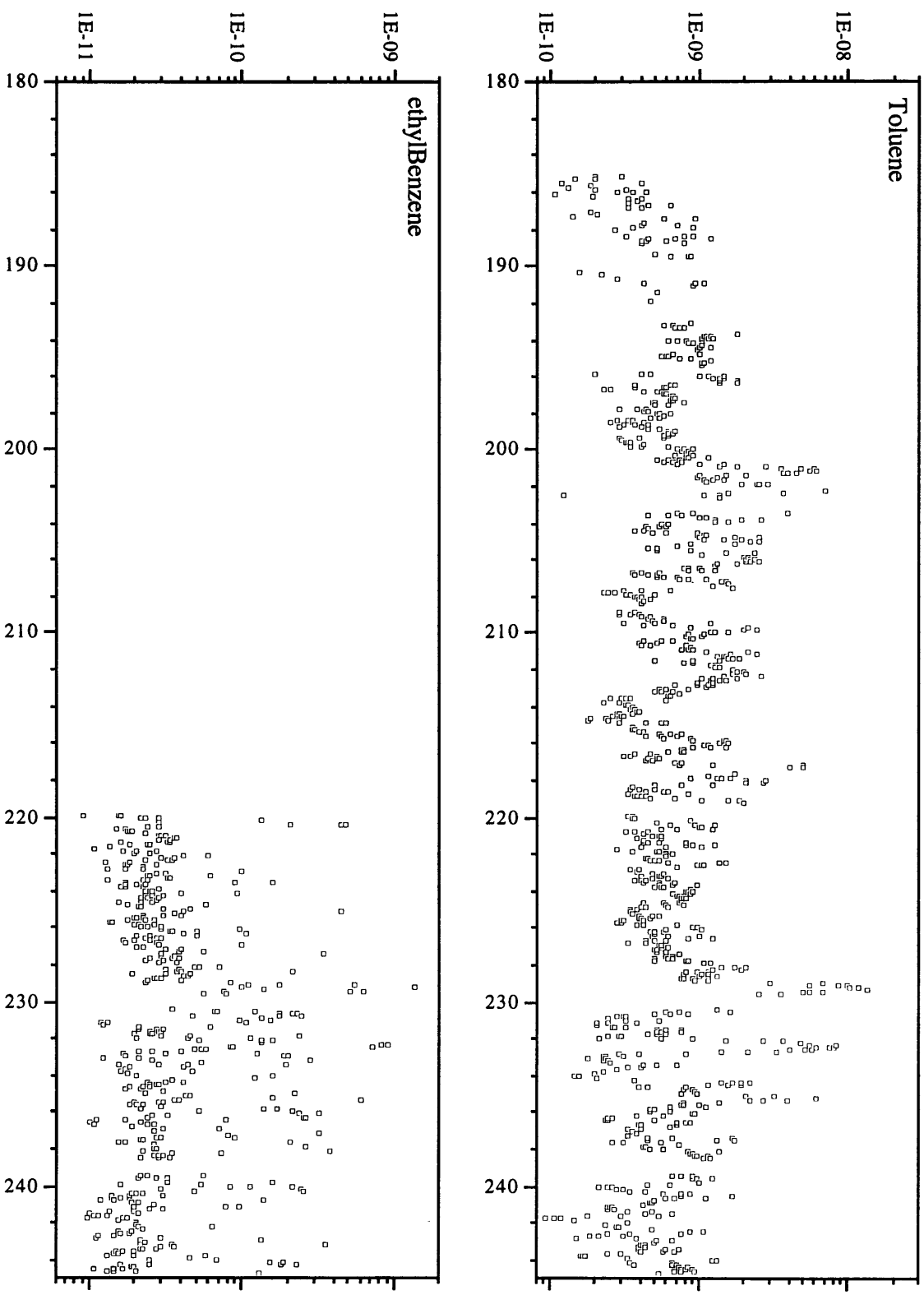
ethylBenzene
1E-11
1E-10
1E-09
180
190
200
210
220
230
240
Toluene
1E-10
1E-09
1E-08
180
190
200
210
220
230
240

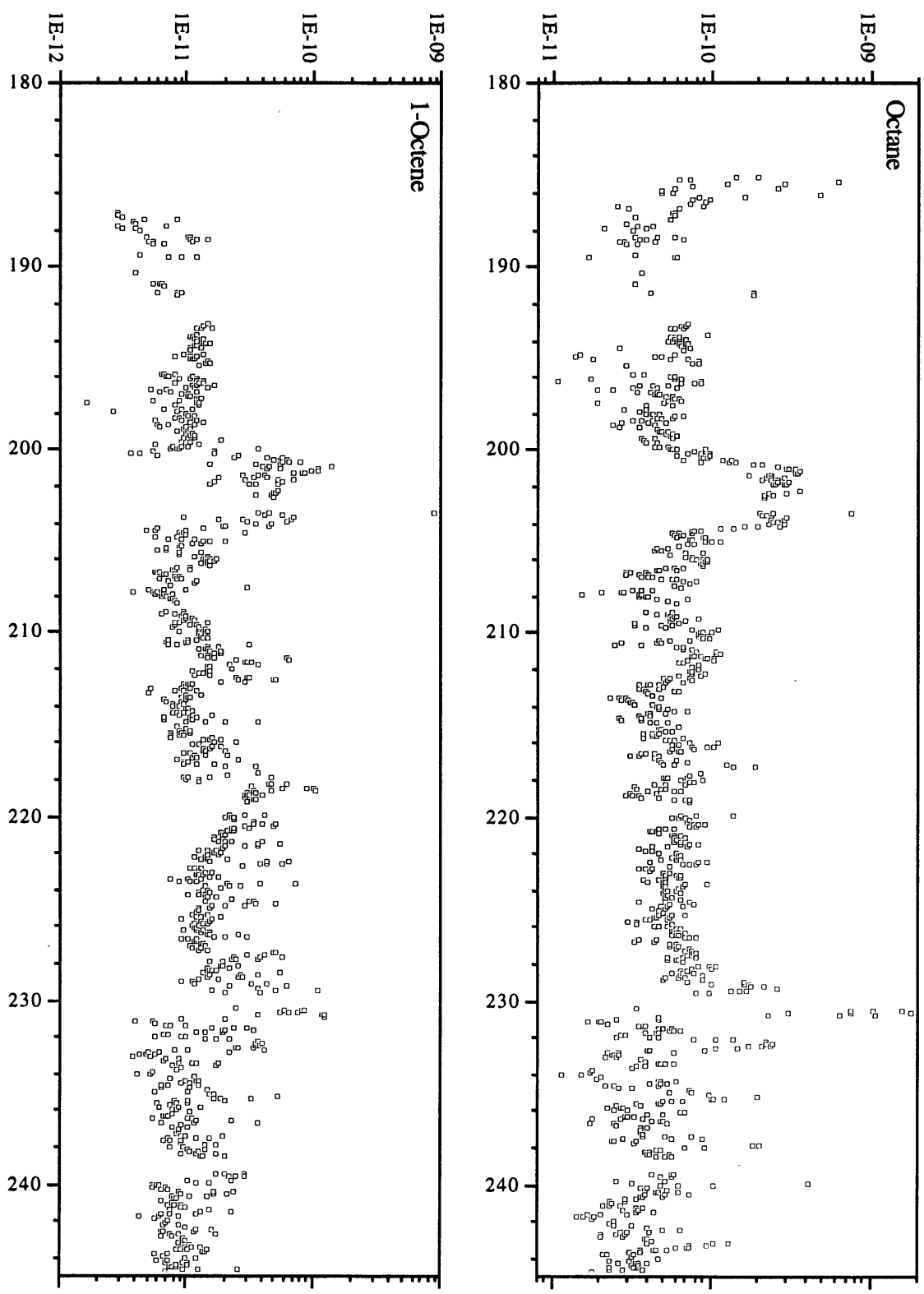
1-Octene
Octane
1E-12
1E-11
1E-10
1E-09
180
190
200
210
220
230
240

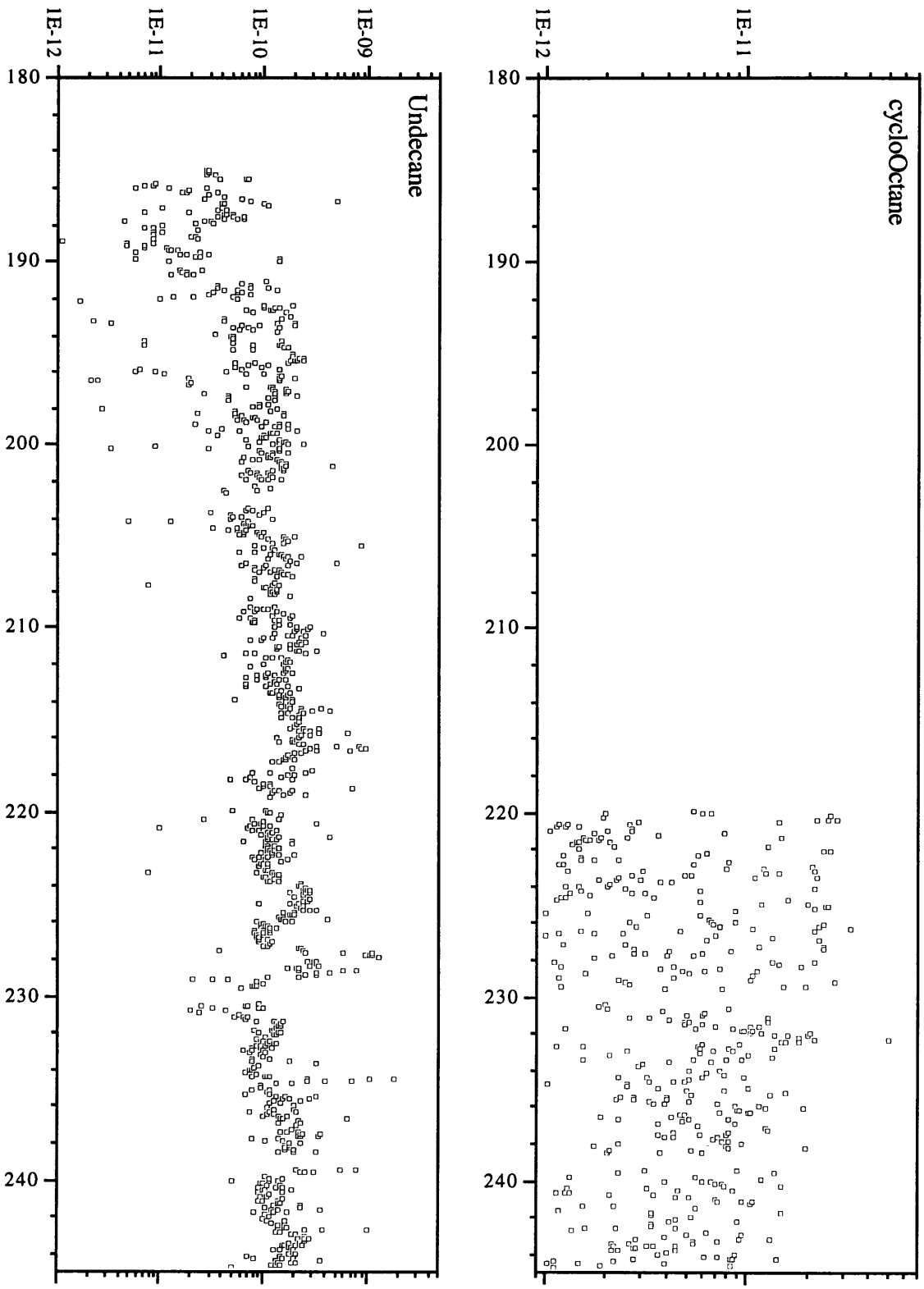
Undecane
cycloOctane
1E-12
1E-11
1E-10
1E-09
180
190
200
210
220
230
240

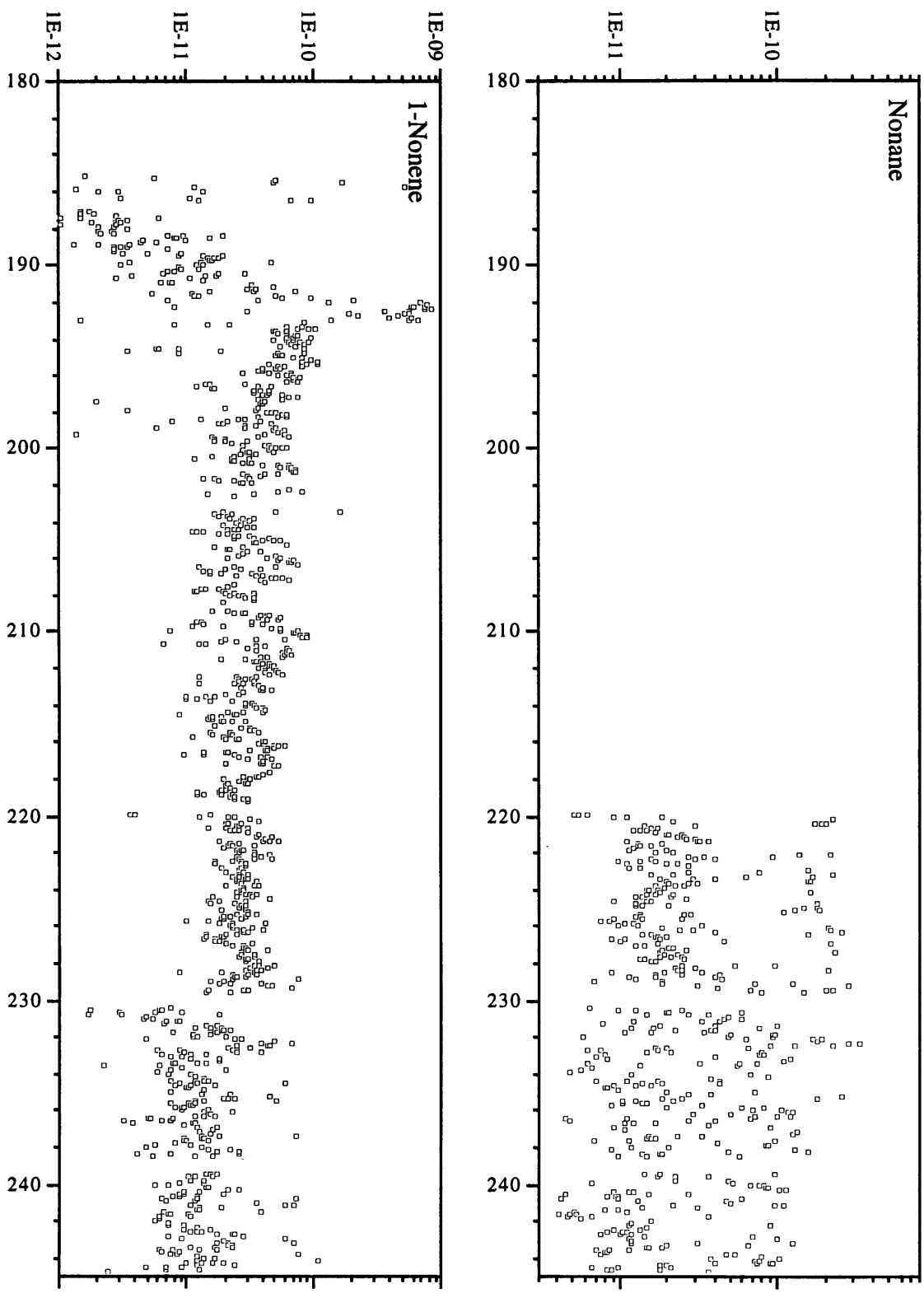
1E-12
1E-11
1E-10
1E-09
180
190
200
210
220
230
240
1-Nonene
1E-11
1E-10
180
190
200
210
220
230
240
Nonane

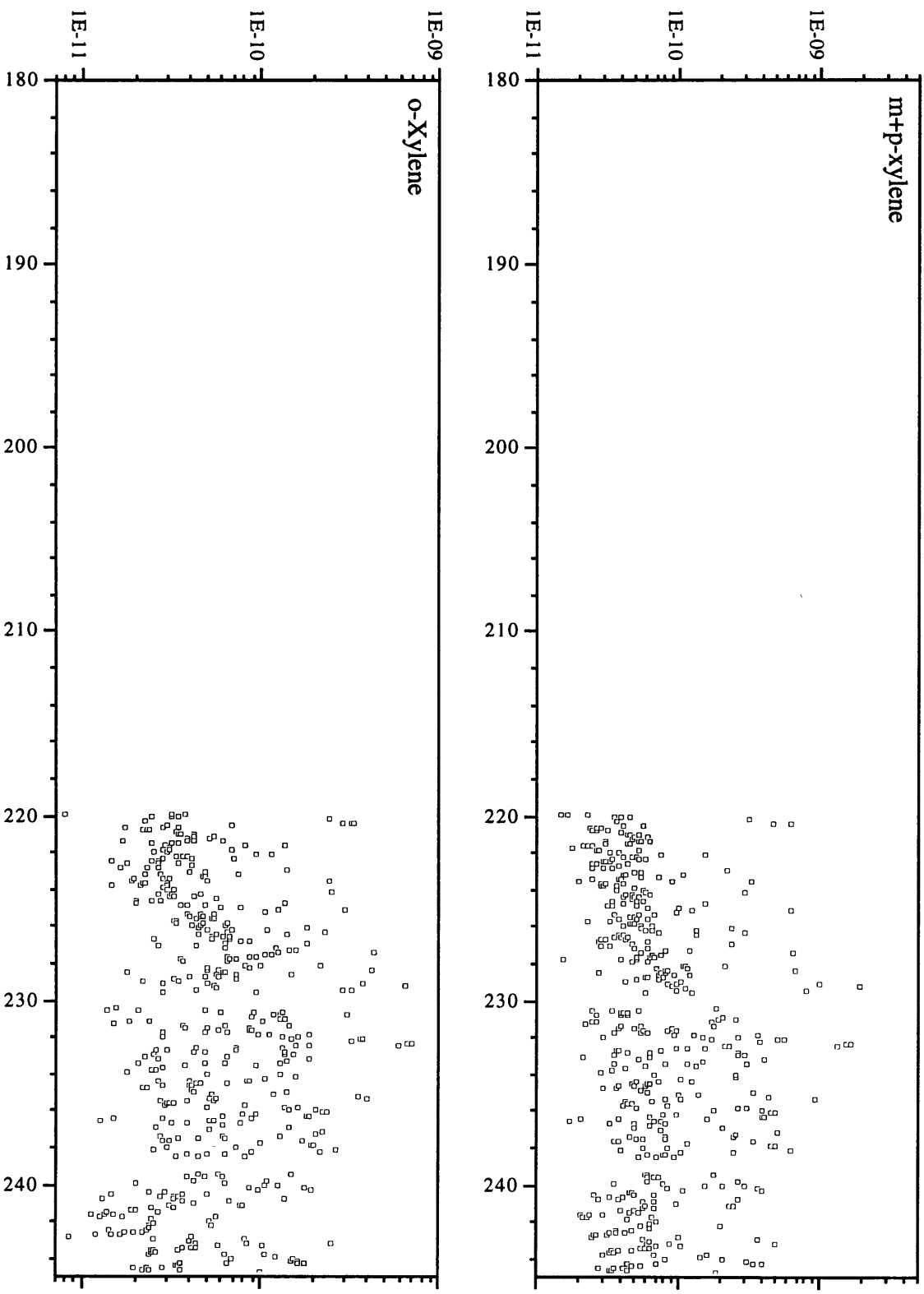
1E-11
1E-10
1E-09
180
190
200
210
220
230
240
o-Xylene
m+p-xylene

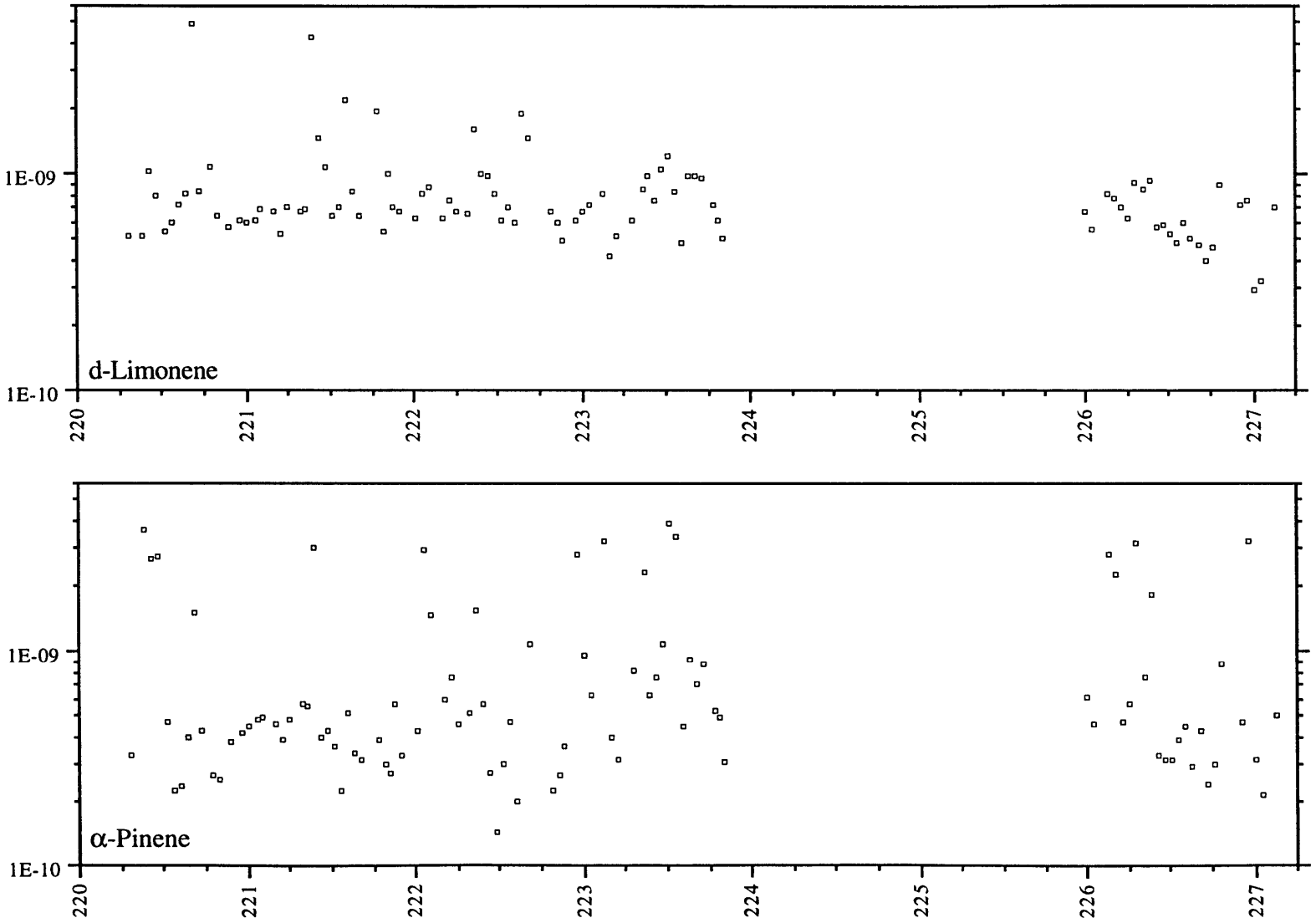
1E-09
1E-10
d-Limonene
220
221
222
223
224
225
226
227
1E-09
1E-10
α-Pinene
220
221
222
223
224
225
226
227

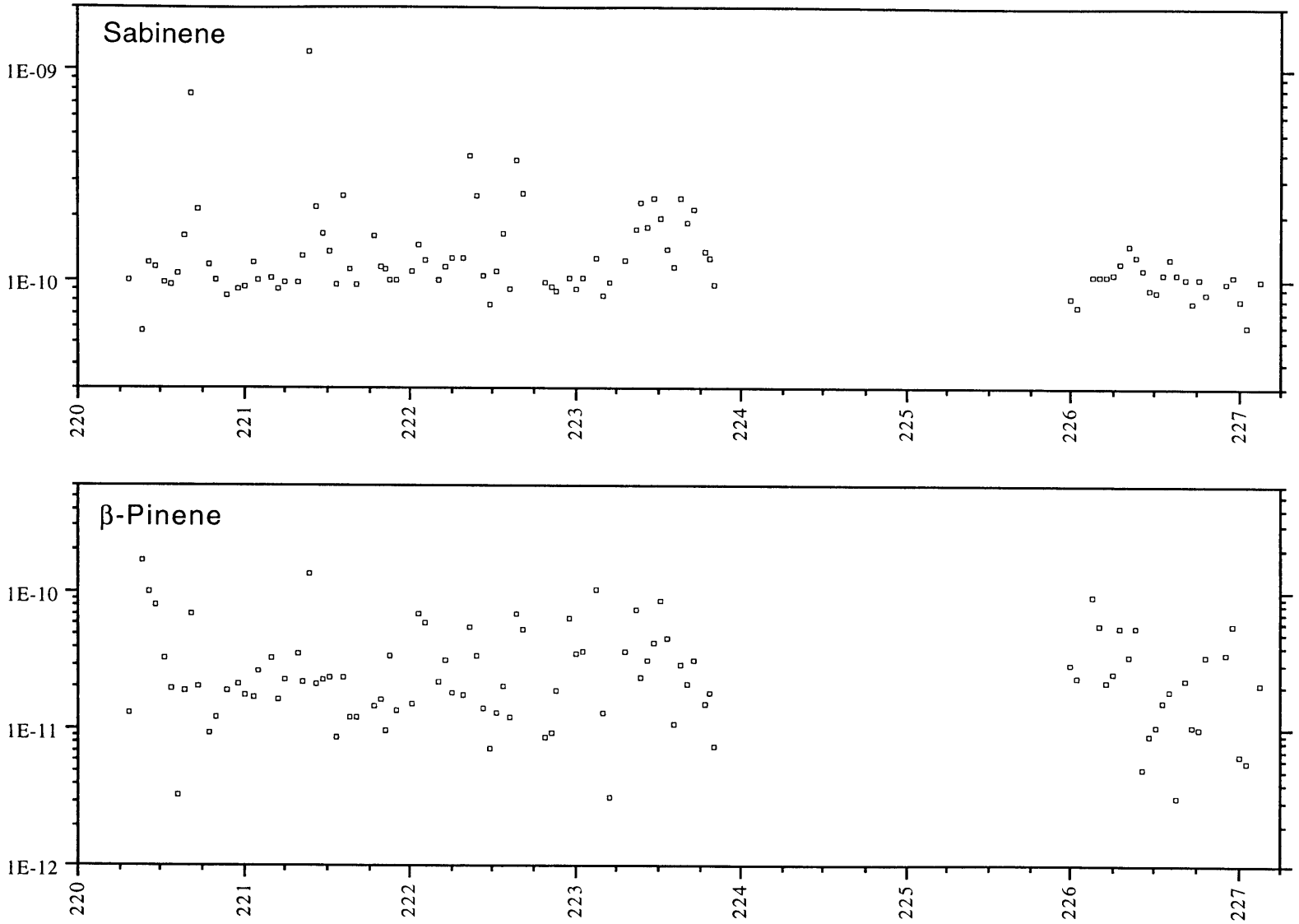
Sabinene
1E-09
1E-10
220
221
222
223
224
225
226
227
β-Pinene
1E-10
1E-11
1E-12
220
221
222
223
224
225
226
227

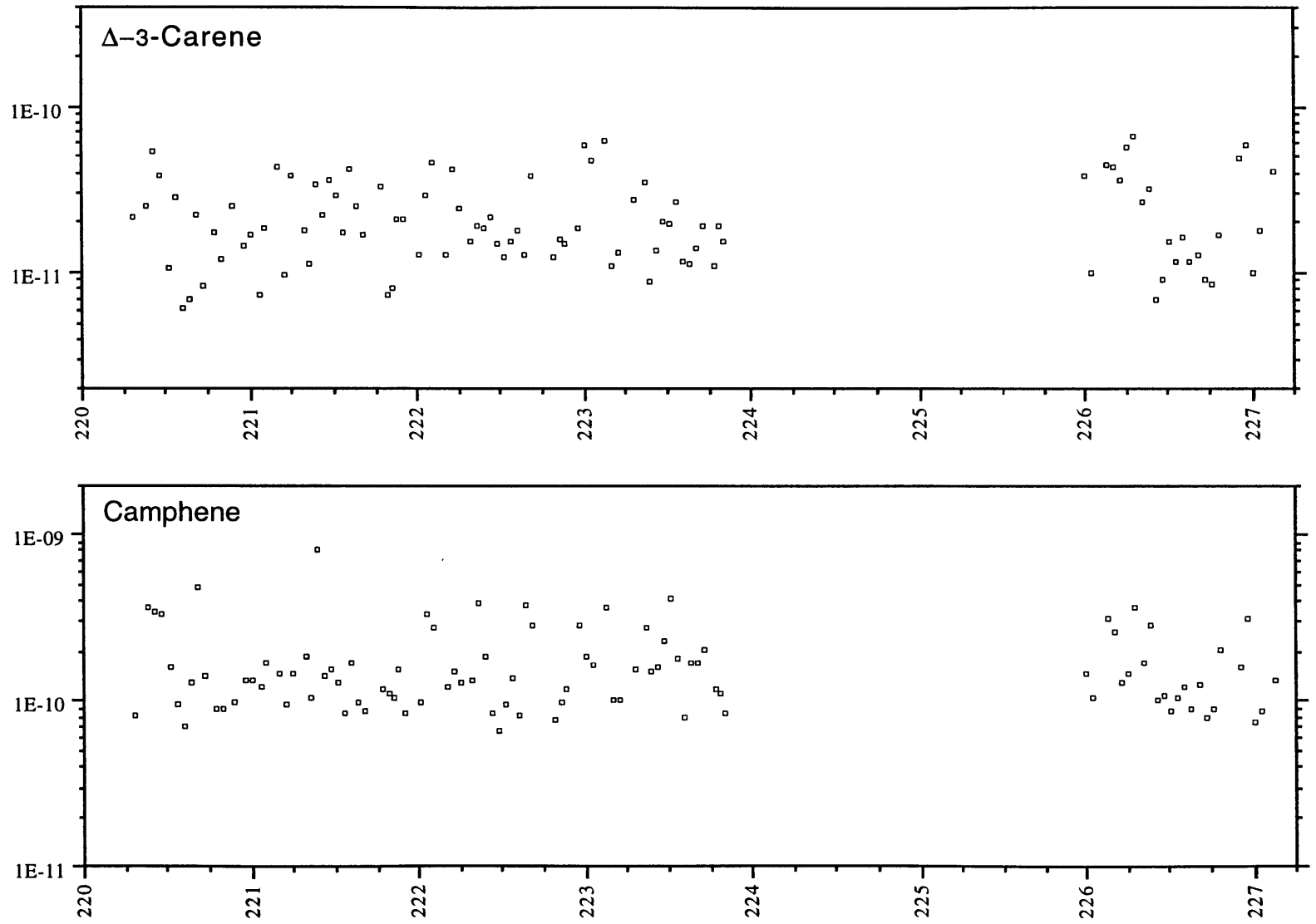
Δ–3-Carene
1E-10
1E-11
220
221
222
223
224
225
226
227
Camphene
1E-09
1E-10
1E-11
220
221
222
223
224
225
226
227

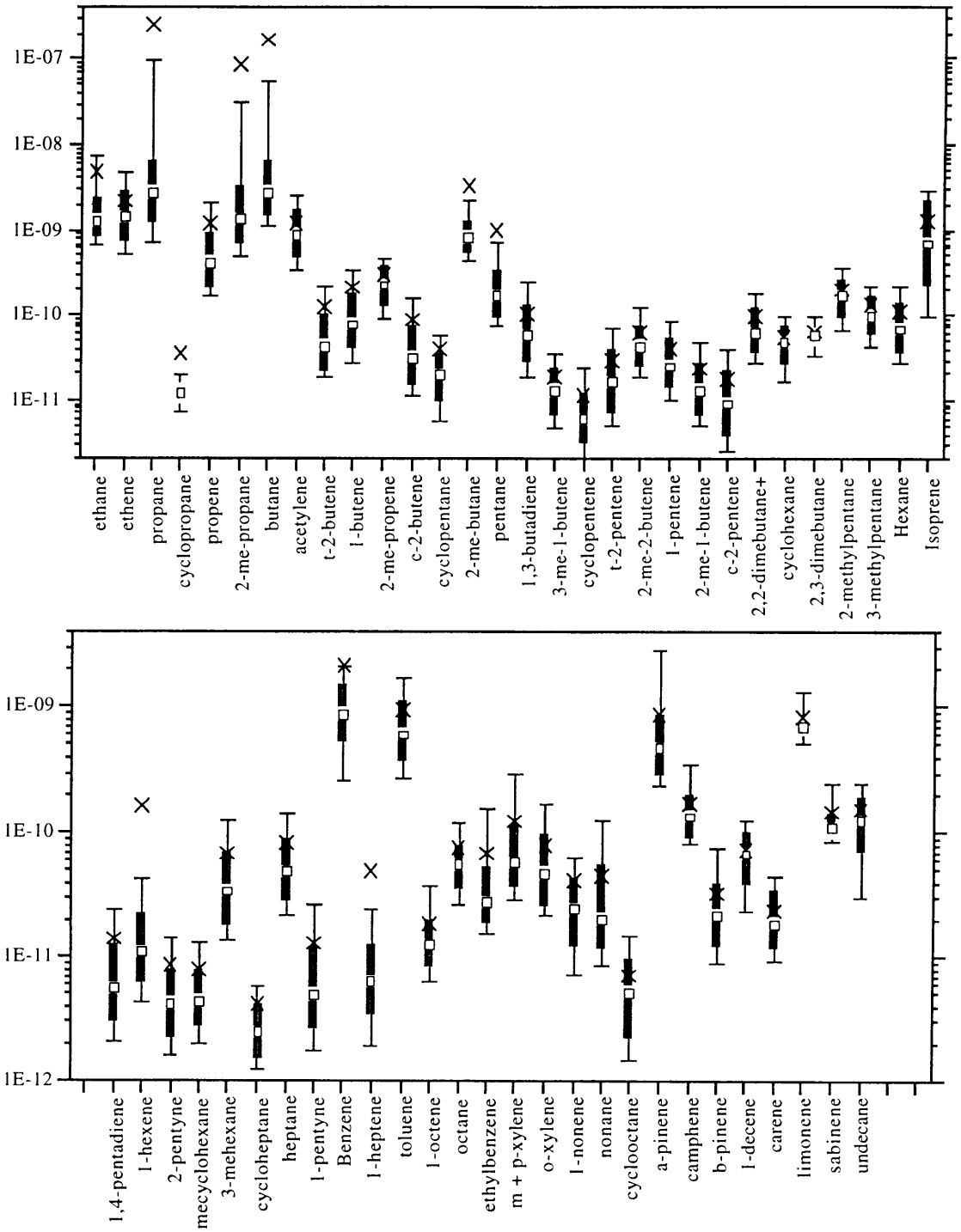

Figure 3.5.2 Box and whisker plots for summer 1996 data. The square is the median value with the solid rectangle showing the interquartile range. Tenth and ninetieth percentiles are given by the whiskers. The x marks the average value. Note for some species the average is even greater than the ninetieth percentile due to a few points orders of magnitude above the rest.

includes only those data where no Nafion dryer was used. It is interesting to note the relative ranges of benzene and toluene. Most published concentrations for these species show toluene levels a factor of two greater than benzene. For our data set, they are comparable. This could be due to the influence of local biomass burning or some other source relatively high in benzene. Ethene levels may also be influenced by biomass burning. There did not seem to be increased levels of ethene when propane values spiked yet the mixing ratio is quite high at times. Blake et al. (1994) report that relative to ethane, ethene may be enhanced by a factor of four in biomass burning plumes and benzene levels are more than two times those of toluene. We tabulate some other representative hydrocarbon values for comparison (Table 3.5.1).

We measured a wide variety of hydrocarbons at Dinghushan and determined a subset of the data which was representative of background values as outlined in section 3.6.4. Analysis of these background values revealed some diurnal variation for certain groups. Light alkenes, including the butenes, propene and ethene and ethane all showed maximum concentrations during the early afternoon. Factors of two to four increases from nighttime lows were observed. This could point to a biogenic source for these species. Similar variations were seen for the seven pentene isomers detected with afternoon concentrations as much as 3 times greater than those found at night. The primary difference is that the pentenes reached maximum concentrations before noon while the lighter species increased into the early afternoon.

Other species behaved in an opposite manner. The hexane isomers had maximum concentrations before dawn which were roughly 50% greater than the minimum values in the late afternoon. Benzene, toluene and 3-methylhexane had similar variation. The light alkanes did not display diurnal trends. Concentrations for those species had no distinct pattern. This may be due to the influences of the local propane source. Since decay from a propane emission event may take place over half a day, our filtering methods may not have been sufficient to remove all influence from our "background" air. For hydrocarbons with shorter lifetimes, this effect would be less of an issue.

The results of our biogenic hydrocarbon in situ measurements after day 192 are somewhat disappointing. With isoprene, prior to day 192, we are quite confident in the data. After we switched the inlet line from stainless steel to Teflon, there was a decided change in the behavior of the isoprene. A number of explanations can be put forward but none is really satisfying. First, it might seem that there could be either production in the line or degassing from the Teflon. To our knowledge, no one has reported problems of this sort for isoprene. Goldstein et al. (1995) reveal that their Teflon sampling line had occasional contamination but it was on the order of 20-30 pptv, not on the order of 600 pptv that is necessary to explain our results. In any case, if it were degassing, we would

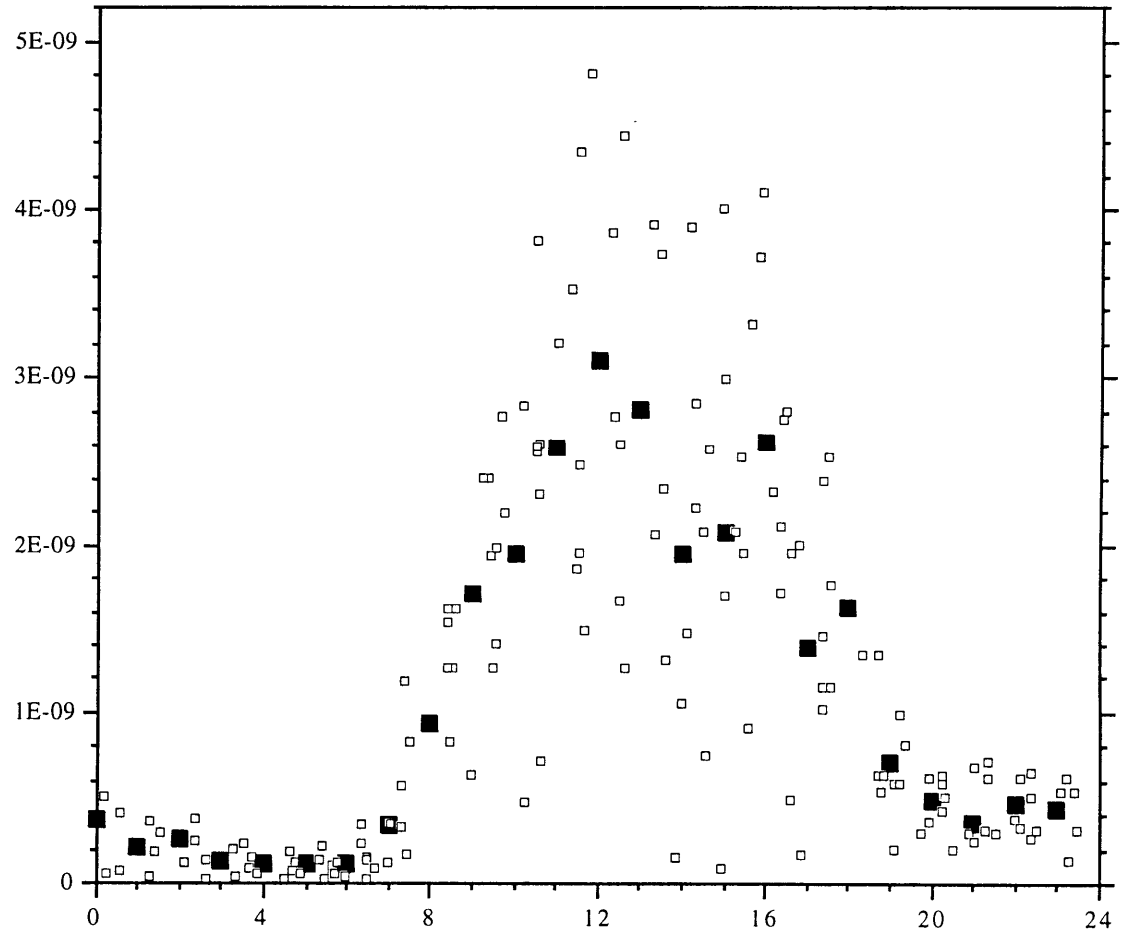

Figure 3.5.3 Diurnal isoprene data from days 180 through 192. The horizontal axis is diurnal hour and vertical axis is ppbv. The open squares represent individual data measurements. The solid squares are the average for that diurnal hour. An afternoon maximum in isoprene mole fractions is clearly apparent.

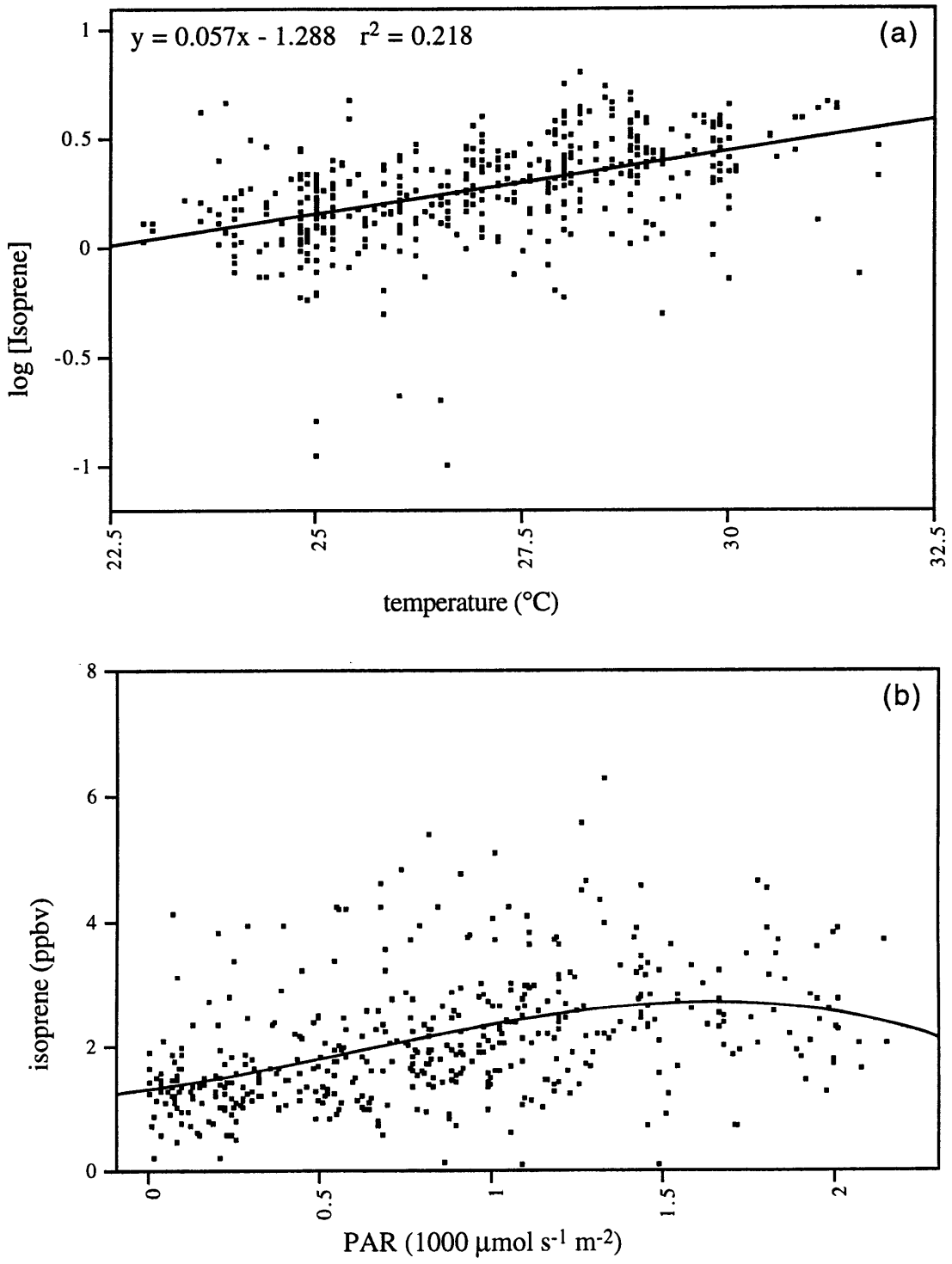

Figure 3.5.4 In (a) we show the relationship between log [isoprene (ppbv)] and temperature. The slope agrees well with values obtained by other researchers (see Table 2.1.1). The bottom graph (b) gives the plot of isoprene concentration versus PAR. Light saturation of leaf emission is reported to occur between 1000 and 1500 µmol s^{-1} m^{-2} (Fehsenfeld et al. 1992). This saturation is evident here as shown by the solid line (a cubic polynomial fit to the data).

expect that the isoprene levels would decay into the evening as temperature and the amount of adsorbed isoprene declines. That is not the case. We see gradually increasing levels of isoprene from early evening into the next morning. Production within the line would be unheard of, as no researcher has reported isoprene sources during the night.

Another possibility is that some compound was coeluting with isoprene. We have no reason to believe this to be the case. First, we should have seen it before the line switch if the compound was in the atmosphere. Second, if a compound was degassing from the Teflon, it is reasonable to expect over the course of the summer that the levels would decrease. The most definitive proof that coelution is not to blame is mass spectrometry runs performed on flask samples in our MIT laboratory (Hewlett Packard model 5972 Mass Selective Detector). The flasks had been filled with air that came through the same inlet as in our intensive samples. There were no other ion fragments detected with isoprene. It is possible that the potential coeluter was not present during the daytime as all flasks were filled between 8 AM and 2 PM. The daytime data before and after the line change does look very similar.

The variation is such that sometime shortly after sunrise we see a decline in the levels of isoprene. This corresponds to a change in the local wind direction most often and also is possibly related to ventilation as the boundary layer develops. Between the hours of 8 AM and 7 PM the variation is as we would expect, peaking in mid-afternoon and declining into the evening as emissions from vegetation decay with the declining PAR. After sundown, we observe a recovery in the isoprene levels. The local wind direction reverses at this time coming mainly from the southwest. Similar values to the nighttime mixing ratios we see after day 192 have been reported in the past in the boundary layer. Vertical profiles of isoprene recorded by Zimmerman et al. (1988) in the Amazon show that isoprene concentration remains high aloft throughout the night relative to the surface. Mixing ratios above 1 ppbv at the surface during the night have been reported before, but the levels always are decreasing from higher afternoon values

(Montzka et al., 1993). It could be that at night we are seeing air from aloft which has subsided.

We plot all of the isoprene data points taken during daylight hours to investigate temperature and PAR dependencies of isoprene concentration. The results are given in Figure 3.5.4. The curve fit in Figure 3.5.4 has a slope of 0.057 for all points and 0.059 for those points taken before day 192. These values agree with those reported by other researchers as summarized earlier in Table 2.1.1. Figure 3.5.4(b) also agrees qualitatively with previous observations. Fehsenfeld et al. (1992) state that the isoprene emission rate at a given temperature increases with increasing PAR until light saturation is reached around 1500 $\mu mol\ m^{-2}\ s^{-1}$. From our data it is apparent that the cubic fit line reaches a maximum just above 1500 and starts to decline thereafter. This effect may be more pronounced were we to plot PAR and isoprene for specific temperatures rather than including values taken over a ten degree range.

We report measurements of six terpenes between day 220 and 227. The time series of α-pinene and d-limonene demonstrate the effect of the Nafion dryer on the terpenes. We performed analyses without the dryer from day 220 to late in the evening on day 223 when we switched back to using a dryer. At that point, a dramatic drop is seen in the level of pinene detected. The dryer was removed once again on day 226 and a clear increase in concentrations is seen for pinene and limonene. Sabinene shows a slight increase in mixing ratio when the dryer is in line while the other three species show no discernible effect one way or the other. There is a fair amount of scatter which is typical of terpene measurements reported in the literature (Yokouchi et al., 1983). Consistent diurnal changes are not apparent. For α-pinene, the nighttime concentrations on days 222, 223, 226 and 227 on average are higher than the daytime levels. There are some high peaks during the daytime as well. Initially we suspected that some of this behavior was due to coelution because it appeared that these afternoon peaks were corresponding with the local propane pollution. In reality, they lag the pollution plumes by a couple hours. This trend is true for other species not found in the pollution source as well. It

may also be that the local chemistry is disturbed by the huge concentrations of light hydrocarbons such that other reactive species with local sources are allowed to build up in the boundary layer. Competition for the OH radical becomes greater when some background hydrocarbon values increase by three or four orders of magnitude.

3.6 Intensive Phase: Interpretation

3.6.1 Indirect determination of OH concentrations

Although the frequent light hydrocarbon releases from near the sample inlet made determination of true background concentrations of those species difficult, they did afford a chance to measure OH. We assume that the source is highly local and short-lived since initially we see a large spike in concentrations which gradually dissipates. By assuming we can separate the effects of transport and chemistry as in equation 2.2.1, we can calculate OH. We will use the fact that hydrocarbons react at different rates with OH to ascertain OH levels in the forest. It is necessary to designate a tracer hydrocarbon, one whose reaction with OH is very slow in comparison to the effects of transport. This tracer will provide information on the nature of advection and turbulence. Once the K_m is determined, the equation can be solved for OH using knowledge of the time evolution of other hydrocarbons.

We solve first for K_m using ethane, propane and sometimes propene concentrations at time zero and time t; the time step ends up being about an hour as our measurement frequency was roughly hourly. It is necessary to know the background concentration of hydrocarbons entering the sample area, as they will influence the time evolution of local hydrocarbon levels. To minimize the effects of the background (of whose level we are somewhat uncertain), we tried to choose pollution spikes which were orders of magnitude above background. Depending on the compound, we can follow the decay in concentration over several hours until they approach background. Unfortunately, the calculation is quite sensitive to the value chosen for K_m which is why we use three separate calculated values. Ethane background concentrations and maximum

concentrations at the initial time differ by two orders of magnitude while propane background and maximum concentrations differ by as many as four orders of magnitude. The source of the polluted plumes was rich primarily in propane, 2-methylpropane and butane, so these three gases all have very large differences between the peak measured mole fractions and the background level. We therefore use calculations for K_m from propane when deriving OH levels for 2-methylpropane and butane. We took the 25th percentile value from all measurements as being true background levels for the forest. Since many of the measurements used in compiling percentiles were from the polluted plumes, it is quite possible that the 10th percentile value would be even more appropriate. The magnitude of the difference between background and maximum ethane are similar to those for the butenes, propene and the pentanes so the K_m values used for those species were calculated using ethane. In the August 8 case, propene was used to determine K_m for the butenes.

The solution to equation 2.2.1 is

$$[HC]_t = C + ([HC]_o - C) \cdot \exp(-t \cdot (K_m + k_{HC}[OH])) \qquad (3.6.1)$$

where

$$C = \frac{K_m[HC_b]}{K_m + k_H[OH]} \qquad (3.6.2)$$

Solving for K_m is simplified if we assume that $K_m >> k_{HC}[OH]$. In that case, the constant C simplifies to $[HC]_b$ which is the hydrocarbon mixing ratio of the background. K_m is on the order of 4×10^{-4} s^{-1} or larger for most cases and [OH] can be conservatively given a maximum concentration of 1×10^7 molecules cm^{-3}. For ethane, we expect K_m to be more than 100 times $k_{HC}[OH]$ and solving for K_m is trivial. For propane, the factor drops to 50 and the error in [OH] from the assumption that $K_m >> K_{propane}[OH]$ is about 1%. Propene is not an ideal candidate for determining K_m since its reaction rate with OH times [OH] is of the same order as K_m (about half). To determine K_m accurately from

propene, it is necessary to use a calculated value of [OH] from other longer-lived hydrocarbons in equations 3.6.1 and 3.6.2.

Once we have determined the value for K_m, we proceed to solve for [OH] using eight species which were seen to jointly increase as they apparently had a common source. The results of several of these calculations for different times are given in Table 3.6.1. Often a trend for the estimated OH values arises from this type of analysis such that the more reactive species indicate lower OH levels than the less reactive ones (McKeen et al, 1990 and references therein). In their theoretical study of the problem, McKeen et al. (1990) demonstrate that it is not valid to separate the transport and chemistry processes in many cases. They specifically label vertical mixing and horizontal diffusion as inseparable from chemistry when the hydrocarbon source is continuous in time; spatial gradients caused by chemistry also play a role. They claim separability should be acceptable for single pulse emissions. They also state that the

Table 3.6.1 Results of OH calculations based on time evolution of reactive hydrocarbon concentrations. Ten species are used: the eight listed here in addition to ethane and propane from which the mixing coefficients were derived. The average value for [OH] is given here (molecules cm^{-3}). The slight increase in PAR may indicate more radiation available for OH production through photolysis of ozone, yielding a greater concentration on August 28 versus August 8. Wind velocity is an instantaneous measurement at the hour nearest to the sampling time.

Compound	August 5		August 8		August 28	
	[OH]	K_m specie	[OH]	K_m specie	[OH]	K_m specie
propene	1.9	ethane			8.0	ethane
2-methylpropane	9.6	propane	6.1	propane	5.2	propane
butane	10.0	propane	8.4	propane	9.3	propane
t-2-butene	2.9	ethane	2.5	propene	2.6	ethane
1-butene	5.4	ethane	4.2	propene	10.4	ethane
c-2-butene	3.0	ethane	2.7	propene	2.9	ethane
2-methylbutane	8.1	propane	6.2	ethane		
pentane	4.0	propane	6.3	ethane		
Average value	$5.6 \pm 3.2 \times 10^6$ molecules cm^{-3}		$5.2 \pm 2.2 \times 10^6$ molecules cm^{-3}		$6.4 \pm 3.3 \times 10^6$ molecules cm^{-3}	
Wind Velocity	0.6 m s^{-1} west		calm		0.6 m s^{-1} west southwest	
PAR	Not available		1.28 μmol s^{-1} m^{-2}		1.38 μmol s^{-1} m^{-2}	

results of this indirect OH radical determination method are most accurate when the time period studied is short and the OH reactivity of the sampled hydrocarbon is low. Other researchers conclude that the discrepancy is due to unaccounted for chemical interactions (Blake et al., 1993). The latter authors also note that predicted OH levels from hydrocarbons with significant O_3 reaction rates will be lower than those determined by considering chemical loss through reaction with OH alone. Kramp and Volz-Thomas (1997) follow a plume and take advantage of an approximate Lagrangian reference frame which largely eliminates the advective part of the flux divergence. We tried to minimize these transport effects by choosing sample times with low wind values.

Our results show the trend found in earlier studies to some extent with the more reactive species predicting lower OH levels The criteria outlined by McKeen et al. (1990) for OH agreement among a set of reactive hydrocarbons seem to be met for our case. The sampling time is short and the source should also be short-lived as it is derived from a local propane stove. Possibly the assumption of a short-lived source is in error or a second puff emission occurred. Also, since the spatial gradients of species within the plume may change with time due to chemistry, the diffusion characteristics may not be exactly the same for the relatively non-reactive specie used to determine K_m and the reactive compounds. Quantitatively, our results show fair agreement with OH predictions made for a region outside of London (Blake et al., 1993) and in Germany (Kramp et al., 1997). The predicted concentrations were 1.7-4.1 x 10^6 and 5-8 x 10^6 molecules cm^{-3} respectively. Model studies of the Amazon predicted lower levels of OH in the boundary layer, with a maximum of 2.4 x 10^6 molecules cm^{-3} reached mid-afternoon (Jacob and Wofsy, 1990). Our average value was 5.7 x 10^6 molecules cm^{-3} with a range of 1.9-10.4 x 10^6 molecules cm^{-3} and standard deviation of 2.8 x 10^6 molecules cm^{-3}.

3.6.2 Estimation of Isoprene Flux

We can use our estimates of OH concentrations along with our isoprene measurements to calculate the isoprene flux from the surface by equating the flux to the

column destruction rate due to OH and O_3 We must make an assumption about the height of the boundary layer as well. The equation to be solved is

$$\Phi = \int_0^h (k_{OH}[OH] + k_{O_3}[O_3]) \cdot [Is] dz \qquad (3.6.3)$$

$$\cong (k_{OH}\overline{[OH]} + k_{O_3}\overline{[O_3]}) \cdot \overline{[M]} h \chi_{Is} \qquad (3.6.4)$$

where

k_{OH}, k_{O_3}= isoprene rate constants for reaction with OH and O_3
h = height of the mixing layer

$\overline{[\ ]}$ represents average value over the altitude range 0 to h

We take h to be 1.5 ± 0.5 kilometers. We only have surface measurements of isoprene and predicted OH (5.7 ± 2.8 x 10^6 molecules cm^{-3}). Using vertical profiles of isoprene from Ayers and Gillett (1988) and Zimmerman et al. (1988), we assume that isoprene concentrations at h will be roughly half those seen at the surface. The average value and standard deviation of isoprene concentrations from our daytime measurements are 1.91 ± 1.19 ppbv. We estimate average isoprene levels in the boundary layer will be 75% of that value. Our experiments measuring OH occurred in mid-afternoon and would be representative of maximum daytime OH concentrations. A reasonable estimate of the daytime average OH would be half of our maximum measured concentration. The altitude average of molecular density [M] is about 2.42 x 10^{25} molecules m^{-3}. Rate constants for reaction of isoprene with OH and O_3 are 1.01 x 10^{-10} and 1.43 x 10^{-17} cm^3 $molecules^{-1}$ s^{-1} respectively (Atkinson, 1990). Evaluation of equation 3.6.4 yields an isoprene flux of 5.6 ± 4.9 mg C m^{-2} h^{-1}. If there are other processes causing the removal of isoprene, such as deposition or other chemical loss pathways, the flux could be underestimated. At the same time, the OH values we have estimated may be near maximum values for a typical afternoon, which could bias the result high. Despite the

many assumptions used to determine OH with equation 3.6.4, our value determined by this method compares remarkably well to our estimate of 8.6 ± 6.1 mg C m^{-2} h^{-1} which we derived from the enclosure experiment.

3.6.3 Impact of biogenic NMHC on local OH

Nonmethane hydrocarbons play an important role in the HO_x budget of the troposphere and partitioning within the family between OH and peroxy radicals. Modeling studies of the 1993 Tropospheric OH Photochemistry Experiment gave 110% greater OH than the in situ measurements when the runs included only CO and CH_4 hydrocarbon chemistry. This highlights the importance of NMHC as an OH sink in the troposphere (Mount and Williams, 1997; Goldan et al., 1997). Young et al. (1997) report that isoprene can reduce the oxidative capacity of the local atmosphere in the boreal forest they studied when NO_x levels are low. The chemical loss rate of OH outweighs its production and recycling through HO_2 + NO. Results from a second modeling study (Fehsenfeld et al., 1992) confirm that in low NO_x environments, a reactive NMHC like isoprene can lead to a five-fold decrease in OH. At appreciable NO_x levels the reduction in OH is less than 50%. Modeling of terpene chemistry in a coniferous forest revealed that near surface OH levels could be suppressed by a factor of five when terpenes were included (Hov et al. 1983).

We can assess the impact of biogenic nonmethane hydrocarbons on local atmospheric chemistry by investigating the loss frequency of OH due to each species. The reaction rate times the concentration of each hydrocarbon gives this loss frequency. In Figure 3.6.1 we have plotted the relative impacts of 52 species that were measured at Dinghushan. Hydrocarbon concentrations were taken as the mean values obtained over the summer. Those species whose OH removal frequency was low were grouped with other like species. The Figure displays the ratio of the loss rate due to an individual hydrocarbon or group of hydrocarbons to the loss rate obtained for CO at its median value of 152 ppbv. The relative impact of isoprene and the terpenes is quite large.

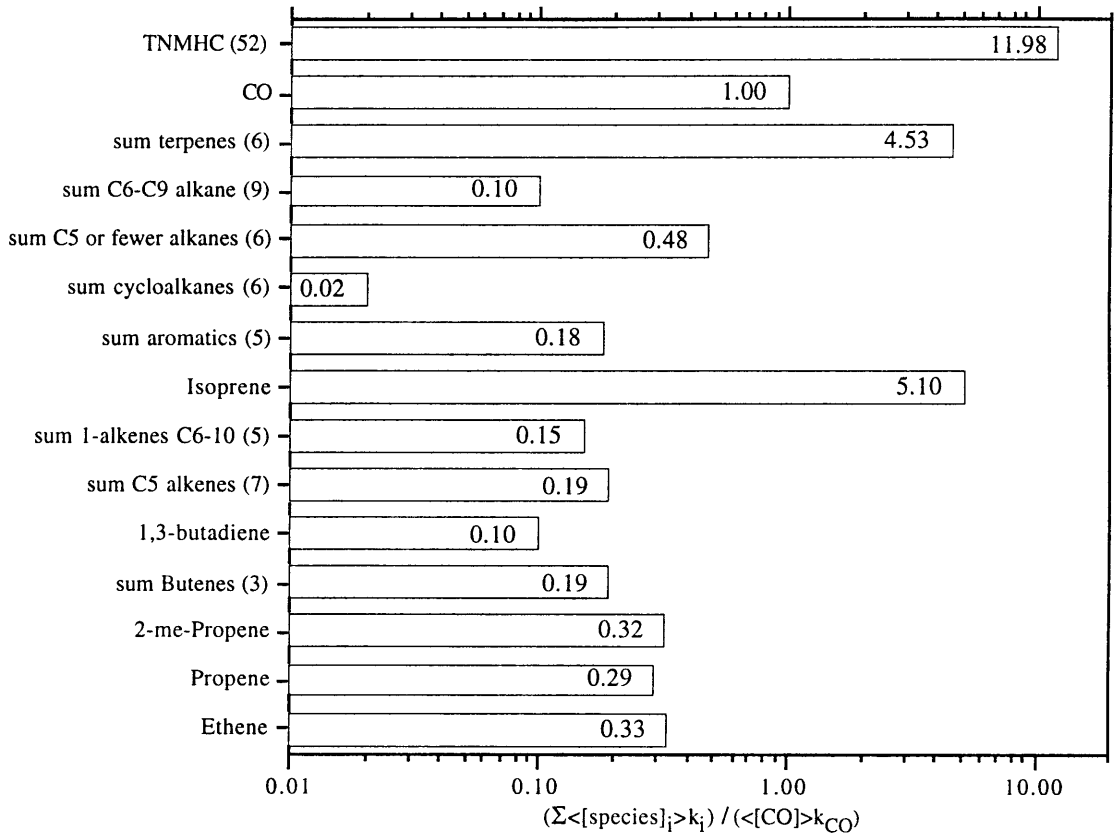

Figure 3.6.1 Ratio of the loss frequency of OH (s^{-1}) with the median value(s) of an individual or sum of hydrocarbons to loss frequency with median CO concentration 152 ppbv. Loss frequency is caluculated as <[trace gas]>k where k is the rate constant for reaction with OH (from Atkinson, 1990) and <[trace gas]> is the mean concentration detected. The Y-axis shows the specie(s) included with the total number of species in parentheses. TNMHC is total non methane hydrocarbons. Note that isoprene and the terpenes account for over 80% of the potential OH loss from hydrocarbons. This percentage would be even higher were the median concentrations of anthropogenics reflective of "background" air.

Isoprene is five times more efficient at removing OH than CO. In sum, isoprene and terpenes account for over 80% of the loss frequency for all hydrocarbons combined; they are five times more effective than CO at OH removal. The impact of these biogenic hydrocarbons may actually be even greater than that for two reasons. First, the frequent pollution events raised the median level of many of the anthropogenic hydrocarbons. We would expect the real background median for non-terpenic and non-isoprene NMHC to be considerably lower. If this is true, the relative biogenic impact would obviously be heightened. Second, the isoprene OH reaction products methylvinylketone (MVK) and methacrolein also efficiently consume OH, further amplifying the impact of isoprene. In

addition, much of the carbon in the NMHC may end up as CO, which will further react with OH.

3.6.4 Multi-gas Correlations

High frequency in situ measurements have a distinct advantage over flask measurements. Many different gases can be measured simultaneously as we have done in this study. Since ozone and nitrogen oxides are not stable in canisters, those species are not appropriate for a flask sampling effort. We observed several different categories of air masses as determined by a variety of correlations between measured species. We classify the main types as background, regional anthropogenic pollution, local propane pollution and biomass burning. Figures 3.6.2 and 3.6.3 display nineteen hydrocarbons, NO_X, and CO over a six and five day period respectively.

We used several approaches to identify air masses of different origins. Inspection of the trace gas plots over time provided an initial indication of which species were related. Also, correlation coefficients were determined for each pair of species, indicating groups of compounds that moved in concert. A third technique, principle component analysis was performed on a subset of seventeen representative species. The final piece of information used was wind data from NCAR reanalyzed wind fields. These four means of data inspection were used to identify the different types of air masses observed at DHSBR.

The simplest method, aligning all species in time, gave the first indication that we sampled several distinct air mass types. The first most obvious features were the data spikes for the alkanes, propene and the butene isomers. There were little or no changes seen for NO_X, CO or the aromatic compounds. These episodes were undoubtedly due to an immediately local propane source as our inspection of the local area within several hundred meters of our sample inlet revealed that propane was used for cooking. The second relevant features were NO and CO pollution spikes. The largest of these were accompanied by increased concentrations of a broad variety of hydrocarbons: aromatics, hexane isomers, light alkenes and acetylene. These air masses based on their duration and

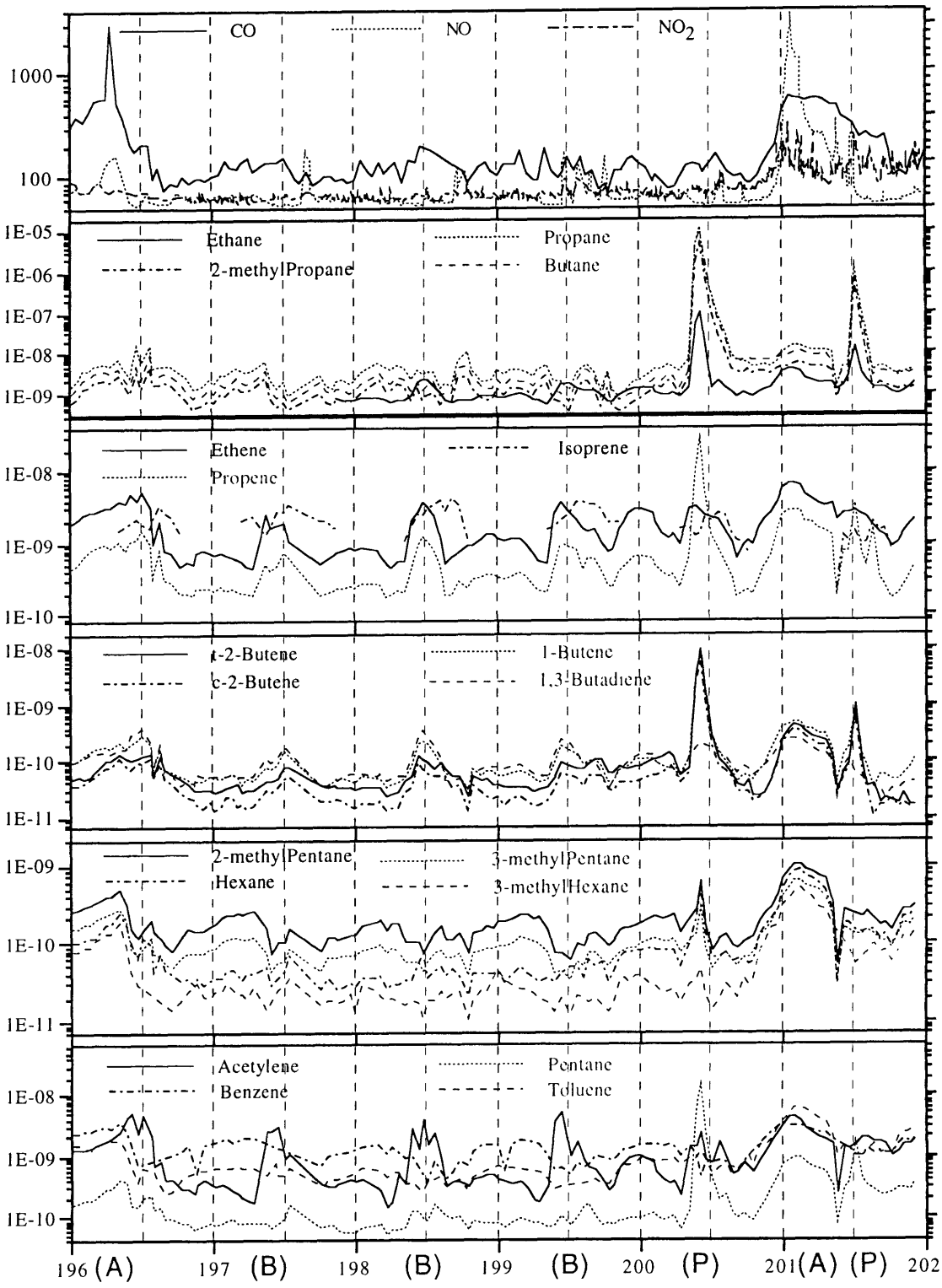

Figure 3.6.2 Time series plot with JD on the horizontal axis and mole fraction on the vertical except for CO, where the unit of the vertical axis is ppbv. NO_X are uncalibrated for this period. Along the time axis, (A) represents a regional anthropogenic episode, (B) shows biomass burning episodes and (P) indicates a high propane period.

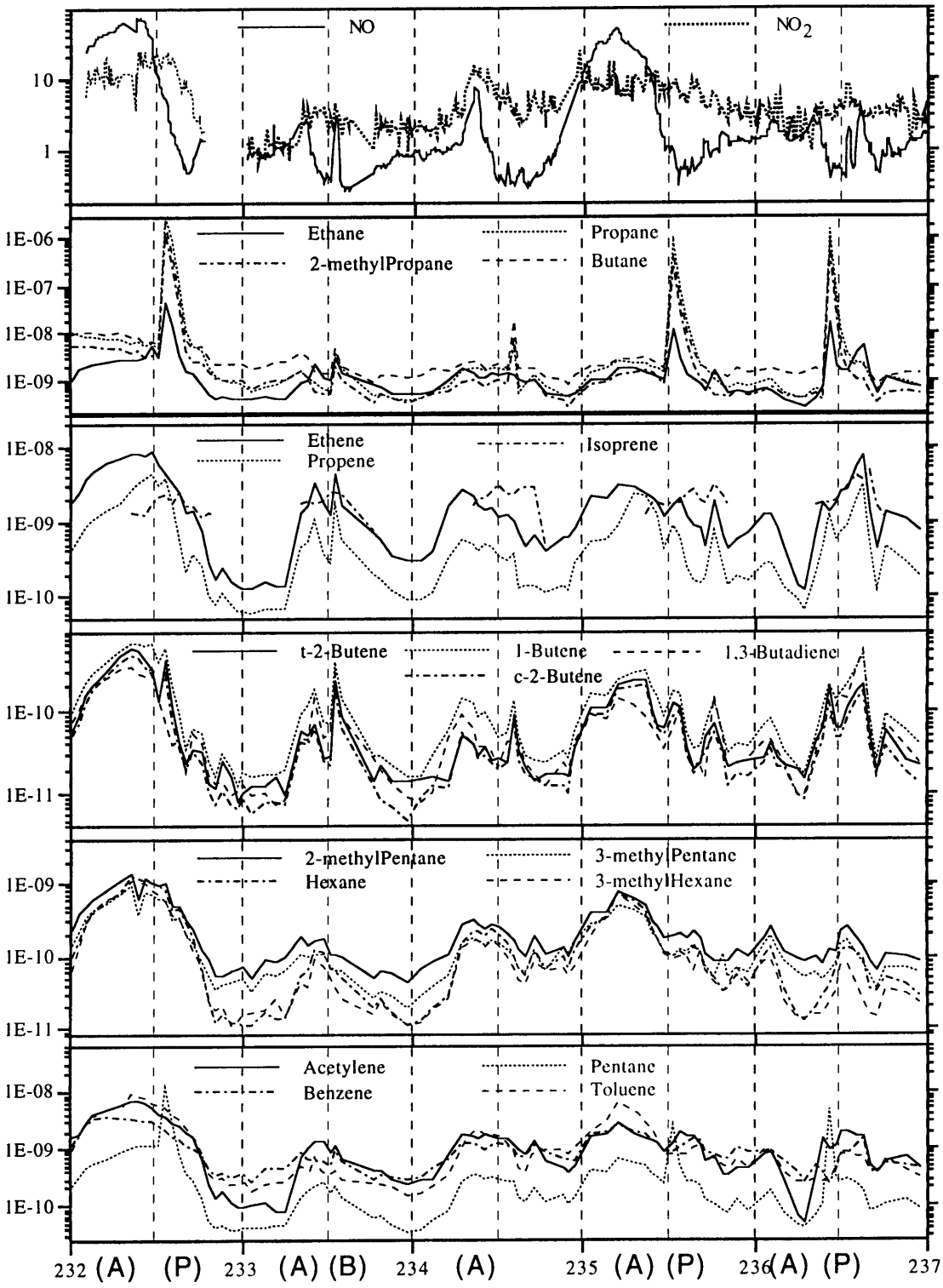

Figure 3.6.3 Time series plot with JD on the horizontal axis and mole fraction on the vertical, with the exception of NO_x, where the vertical unit is ppbv. As in the previous Figure, (A), (B) and (P) refer to anthropogenic, biomass burning and high propane episodes respectively.

composition seemed to be derived from a broad anthropogenic source, most likely from the coastal cities of Guangzhou and Hong Kong. Our wind data confirms this. A third group of related species was also observed which contained many of the same compounds as the anthropogenic air masses. The major differences were that the concentrations of methylpentanes were not enhanced and increases in CO and NO were not as pronounced. Based on reports of the most common hydrocarbons present in biomass burning plumes (Ayers and Gillett, 1988, Blake et al, 1994; Mauzerall et al., 1998) and the knowledge that local residents collect leaf litter and branches for fuel, we identified these samples as air influenced by biomass burning. Those measurements that were not identified as one of the above three categories are assumed to be background. We chose the days for Figures 3.6.2 and 3.6.3 to reflect the three major pollution types. As a result, very little of the plotted points are representative of background air.

We next performed correlations between each pair of species. To investigate the propane pollution events, we split the data into two groups, one with propane levels above 4 ppbv (365 points) and the other with propane below that level (657 points). In the high propane group, the correlation coefficients (ρ) between the light alkanes ethane, propane, 2-methylpropane, butane, and 2-methylbutane were all above 0.87. This compares to a ρ less than 0.4 for the relationship in the low propane group. For c-2-butene and t-2-butene, the ρ value is 0.6-0.7 with the light alkanes in the high propane case and is close to 0.2 in the low propane case except for ethane, whose correlation rises to almost 0.8. In contrast, ρ is generally less than 0.1 between the alkanes and ethene, propene, 1-butene, 1,3-butadiene, acetylene, NO_X and CO. The correlation between these two groups is greater (as high as 0.3) in the low propane case, though only for ethane do the coefficients reach values greater than 0.5. For the other species, in general, the correlations are stronger in the low propane case. We take the strong correlations seen among the light alkanes and to a lesser extent, between alkanes and the 2-butenes for the high propane samples as an indication that these species are all derived from a common source.

We also split our CO observations into three regimes, very clean air (CO<110 ppbv with 69 samples), average background CO (110ppbv < CO <200 ppbv with 122 samples) and polluted air (CO>200 ppbv with 79 samples). The first two cases had $\rho < 0.2$ between CO and all hydrocarbons and NO. For the polluted cases, significant

	Biomass Average $\Delta HC/\Delta C_2H_2$	Biomass s.d.	Anthropogenic Average $\Delta HC/\Delta C_2H_2$	Anthropogenic s.d.
ethane	3.36	3.11	0.87	0.66
ethene	4.23	3.64	1.78	1.16
propane	0.92	1.15	0.76	1.85
propene	1.68	1.62	0.67	0.73
2-methylpropane	0.44	0.69	0.35	0.89
butane	1.35	2.40	0.73	1.92
t-2-butene	0.12	0.12	0.08	0.11
1-butene	0.26	0.27	0.12	0.13
c-2-butene	0.09	0.09	0.09	0.17
2-methylbutane	0.03	0.18	0.29	0.35
pentane	0.07	0.08	0.15	0.16
1,3-butadiene	0.33	0.33	0.08	0.08
3-me-1-butene	0.02	0.05	0.01	0.01
cyclopentene	0.02	0.02	0.01	0.02
t-2-pentene	0.03	0.04	0.06	0.09
2-me-2-butene	0.08	0.16	0.06	0.11
1-pentene	0.07	0.07	0.04	0.02
2-me-1-butene	0.02	0.04	0.03	0.03
c-2-pentene	0.02	0.02	0.01	0.04
cyclohexane	0.00	0.01	0.03	0.05
2-methylpentane	0.00	0.04	0.17	0.17
3-methylpentane	0.00	0.02	0.12	0.15
hexane	0.02	0.02	0.17	0.17
3-methylhexane	0.01	0.02	0.10	0.11
benzene	0.21	0.46	0.13	0.64
toluene	0.09	0.23	0.80	0.96
NO	0.35	0.81	3.67	4.38

Table 3.6.2 Ratio summary for biomass and regional anthropogenic episodes. The ratio is determined by taking the difference between peak and minimum episode concentration for each species divided by the difference in acetylene concentrations for the same two samples. This "enrichment factor" aids in the characterization of both air mass types. Shaded values indicate a higher factor, representative of the particular air mass type. Relative enhancements of the light species are seen in biomass samples. Greater enhancements of the heavier alkanes, toluene and NO are observed for anthropogenic samples. Note the ratio of benzene to toluene in the biomass average is 2.3 which is similar to that observed by Blake et al. (1994). The standard deviations (s.d.) for the ratios are quite high, which may limit the significance of these results.

correlations ($\rho > 0.6$) were seen between CO, NO, the pentene isomers, the hexane isomers, 3-methylhexane and toluene. This category corresponds to our regional anthropogenic air masses.

Principle component analysis was performed with seventeen species (16 hydrocarbons and NO). The first three eigenvalues/eigenvectors accounted for almost 90% of the variance. The primary eigenvector (59% of the variance) had essentially the same weightings for each species. The three primary axes showed three consistent groupings: (1) propane, 2-methylpropane and butane; (2) ethene, propene and 1-butene; (3) hexane, 3-methylhexane, toluene and NO. This information confirms our groupings of these species from the simple time series analysis.

To better understand the differences between those events that we labeled as regional anthropogenic and biomass burning, we looked at hydrocarbon ratios derived from samples of both types. The first step was to identify a species that had similar behavior for both types of events. We looked at two points in each individual event, the sample with maximum concentrations and one with minimum concentrations. The maximum is relatively easy to determine. The sample chosen as minimum may not have been the true minimum as there was no definite way to identify the true beginning or end of an episode. We took the difference in acetylene concentrations between the two points and determined that the relative enrichment factor of acetylene for both biomass and anthropogenic events were similar (1.96 ± 1.59 ppbv for 12 biomass episodes and 1.93 ± 1.60 ppbv for 16 anthropogenic episodes, where the uncertainty is one standard deviation). We then took the difference in concentrations for each hydrocarbon in the same maximum and minimum samples to obtain $\Delta HC/\Delta C_2H_2$.

The results of our ratio analysis are shown in Table 3.6.2. The average ratio plus the standard deviation is given for both biomass and anthropogenic episodes. Shaded values in the Table indicate a high enrichment factor for that hydrocarbon relative to the enrichment factor for the other episode type. For biomass burning episodes, the species ethane, ethene, propene, 1-butene, 1,3-butadiene, butane and 1-pentene all show higher

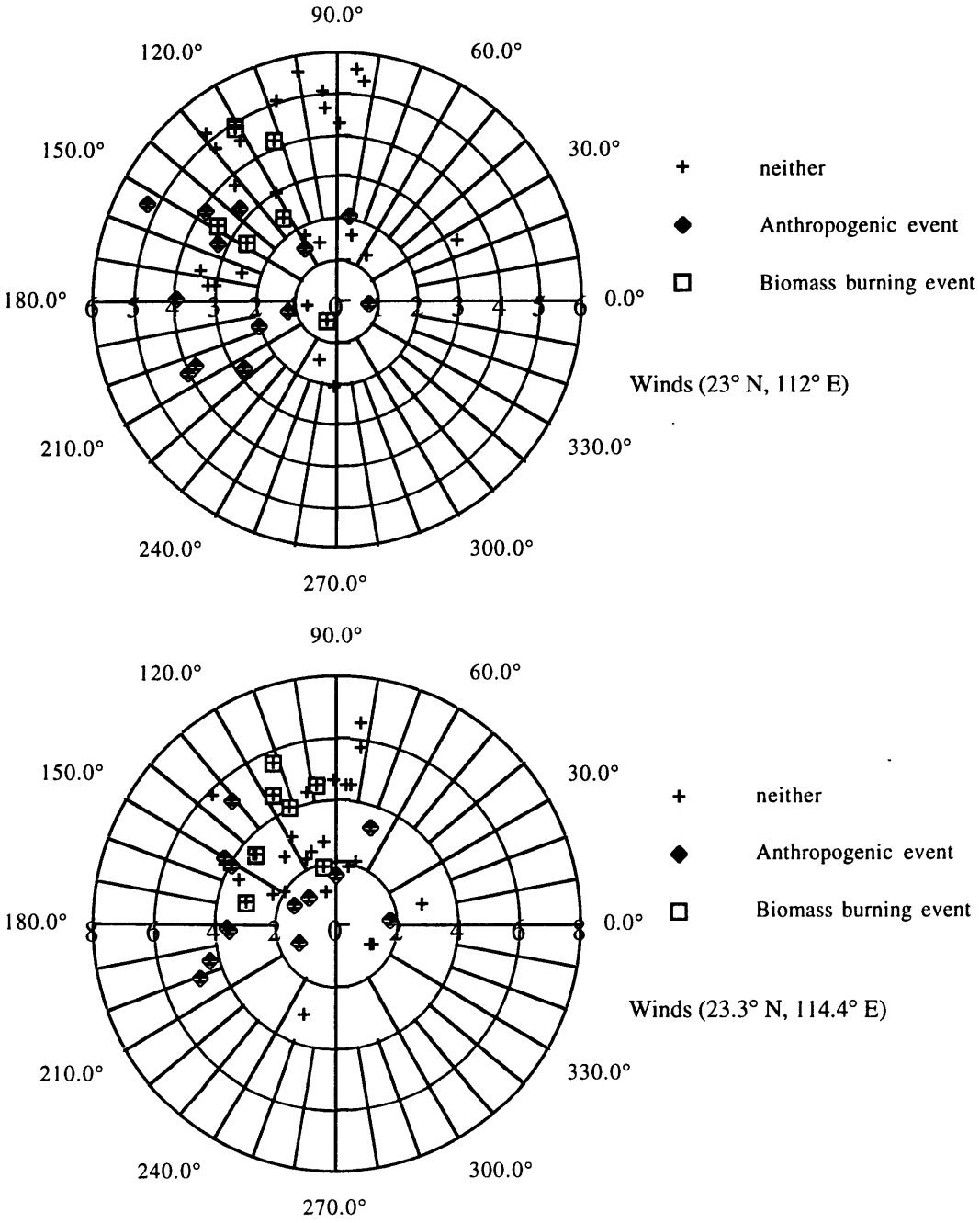

Figure 3.6.4 NCAR reanalyzed winds for JD 196-202 and JD 232-237 at 0, 6, 12 and 18 z. The top polar plot are winds from just west and south of DHSBR. The bottom plot are winds from just north and east of Guangzhou. Triangles are winds corresponding to anthropogenic events as labeled in Figures 3.6.2 and 3.6.3. Squares correspond to biomass burning events. The crosses are winds when neither designation is made. In general, when the wind is a primarily easterly (between 150° and 210°) from the near Guangzhou wind measurement site, there is a corresponding easterly at the near DHS wind measurement site. Pollution is derived from either Guangzhou or Hong Kong in those cases. The point in the top graph that is a westerly corresponds to the brief event around 6 AM on JD 236. This could represent pollution from Zhaoqing. The biomass burning points are primarily associated with local winds (top graph). The southeasterly direction would be consistent with pollution from the temple or the town of Dinghushan at the base of the mountain near the entrance to the biosphere reserve.

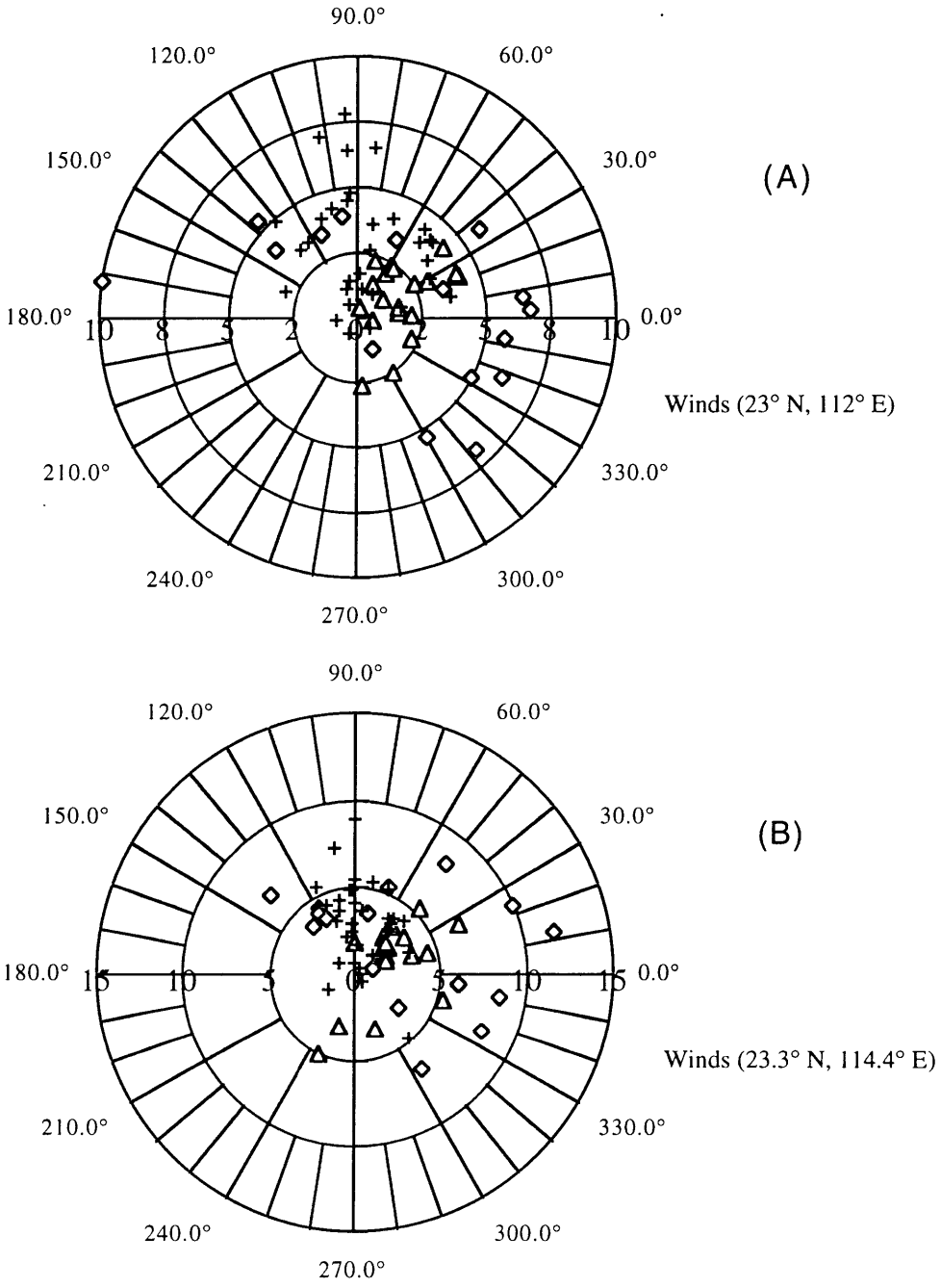

Figure 3.6.5 NCAR reanalyzed winds for three muliple day periods of "background" air masses at DHSBR (8 day period given by plusses, 4 day period by diamonds and 5 day period by triangles). (A) gives the magnitude and direction of winds just west of the reserve while (B) gives the winds east of Guangzhou. Primarily, the local winds are southwesterly.

ratios than their anthropogenic episode counterparts. Enhancement of all of these species is noted by Blake et al. (1994) in their analysis of biomass burning plumes in Canada. The enhancement in biomass samples of benzene to toluene (a factor of 2.3) also agrees with that seen in the Canadian study. The heavier alkanes, toluene and NO all have greater enhancements in the anthropogenic events.

The final indicator that we used to look at air mass origins was wind velocity. We made use of NCAR's reanalyzed winds for two sites (23.3° N, 114.4° E; 23.0° N, 112.0° E). Recall that the biosphere reserve is at 23.16°N, 112.5° E with Zhaoqing, a city of roughly 200,000 inhabitants 19 km to the west, and Guangzhou, with over 2 million people 86 km to the east. Hong Kong is also close by, to the south and east of Guangzhou. The winds are given as instantaneous values four times daily (0, 6, 12 and 18z) We have plotted these values on a polar graph for the eleven days of measurements given in Figures 3.6.2 and 3.6.3 (Figure 3.6.4). In general, winds were easterly at both analysis locations when NO levels were observed to be much higher than background values (refer to Figures 3.3.1a and 3.3.1b for these high NO periods). Figure 3.6.5 displays wind information for three periods where background air masses were measured. It is apparent that the local wind direction at DHSBR for those times are primarily southwesterly.

Figure 3.6.2 shows two regional anthropogenic episodes, three biomass burning periods and two high propane events. The first event on JD 196 has winds from the southeast in the early morning. These could be bringing air masses that originated around Hong Kong. For the three biomass burning events on JDs 197, 198 and 199, the winds at both stations were from the south or southeast which imply the observed air masses would have traveled over the town of Dinghushan at the entrance to the reserve. The NO spike on day 201 is likely due to pollution from the Guangzhou region. Winds from the station nearby are eastsoutheasterly and easterly at 18 z on day 200 and 0 z on day 201. Wind speed is about 4 m s^{-1} which would imply a six hour travel time between the populated coastal region and our sampling site. The maximum NO occurs roughly six

hours after the winds blow directly over the cities toward DHSBR. Local winds are also eastsoutheasterly or easterly for the period.

The situation in Figure 3.6.3 is much the same. Here we have five periods listed as regional anthropogenic. The first four all have similar wind patterns implying air masses passing over the coastal cities as they move inland and over our observation site at the biosphere reserve. The final event on day 236 has local winds from the west. This implies sampled air had recently passed over Zhaoqing City. The increases in concentrations are much less than increases observed for coastal city influence.

In summary, we were able to categorize our measurements at DHSBR due to our high frequency sampling of many trace gases. Wind data helped to confirm our belief that high NO periods were a result of regional anthropogenic pollution. Enrichment ratios aided in our identification of air masses likely influenced by biomass burning. Our correlation analysis showed that the light alkanes had very strong relationships when propane levels were well above background, with a ρ more significant than the lower propane periods. The periods not corresponding to these three categories may be considered background levels for the Dinghushan region and represented 38% of the measurements. The breakdown for the polluted samples were 30% propane, 20% urban and 12% biomass burning.

3.7 Comparison of flask and in situ measurements

We were able to take flask samples during the intensive campaign which were sent to MIT for future analysis. In Figure 3.7.1 we show the results of two flask samples taken on August 1 in comparison to the bracketing real time measurements. Not every specie reported for the seasonal flask measurements is reported on this Figure. Since the flask runs were performed without a Nafion dryer, we were able to obtain results for the terpenes camphene, carene and α-pinene. Also, the xylenes suffered from contamination problems at Dinghushan on the day these samples were taken. We can see from the graphs that some results compare quite favorably while others do not. It

should be recalled that the time to fill a flask is about two minutes whereas the real time sample was collected over a sixteen minute interval. Additionally, there is some difference in the time of sampling, as the flasks were filled sometime between the real time runs.

Alkanes show the most consistent results, with flask concentrations differing at most 20% from the range of the bracketing in situ runs when the concentration did not fall between the two in situ runs. The results for the cyclic species except for cyclohexane were not as consistent, sometimes falling 50% outside of the in situ bracketing range. Butadiene was lower in the flask than in situ, raising the issue of its stability in the sampling canisters. Isoprene, on the other hand, showed higher values in the flasks. Other alkene species show varied results. For 2-methylpropene, the flask results were lower but this difference could be made up for by subtracting possible contamination from the in-line traps used in Dinghushan. The mole fractions for the 1-alkenes and methyl-1-butenes tend to be higher in the flasks while 2-methyl-2- butene is lower. Gong and Demerjian (1995) report that Nafion dryers may cause rearrangement in alkenes having four and five carbons when the dryer is heat cleaned between collections. We did not heat our Nafion dryer but some of the variation seen might be caused by interactions with the dryer. The results for our standard analyses in China which included runs with and without the dryer did not reveal problems for those species in the standard, namely the butenes and 1-pentene. However, we cannot rule out interactions with the other alkenes as being responsible for the above discrepancies in concentration determination between flask and real time samples. Finally, those species near the detection limit (20 pptC) tend to display higher levels of disagreement. For example, the detection limit for ethane is about 10 ppt whereas for pentane it is closer to 2 ppt. This is a result of the FID response toward carbon. Since our accuracy near these detection limits is only ± 50%, this is not surprising.

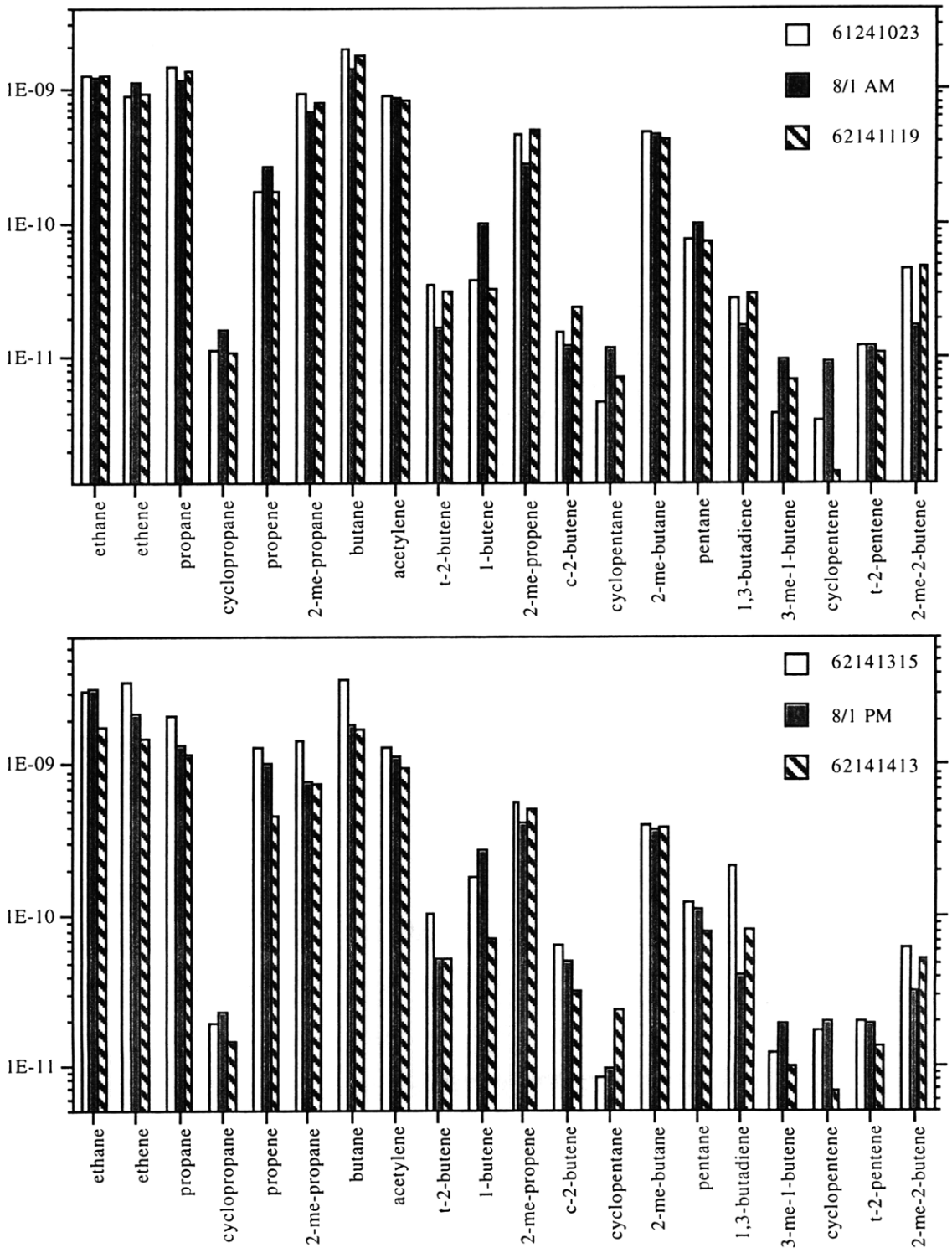

Figure 3.7.1a Shown is the result of a comparison between two flasks filled at Dinghushan and sent to MIT for analysis and two real time runs which took place immediately before and after each flask collection. The samples were taken around 11 AM for the top graph and 2 PM for the bottom.

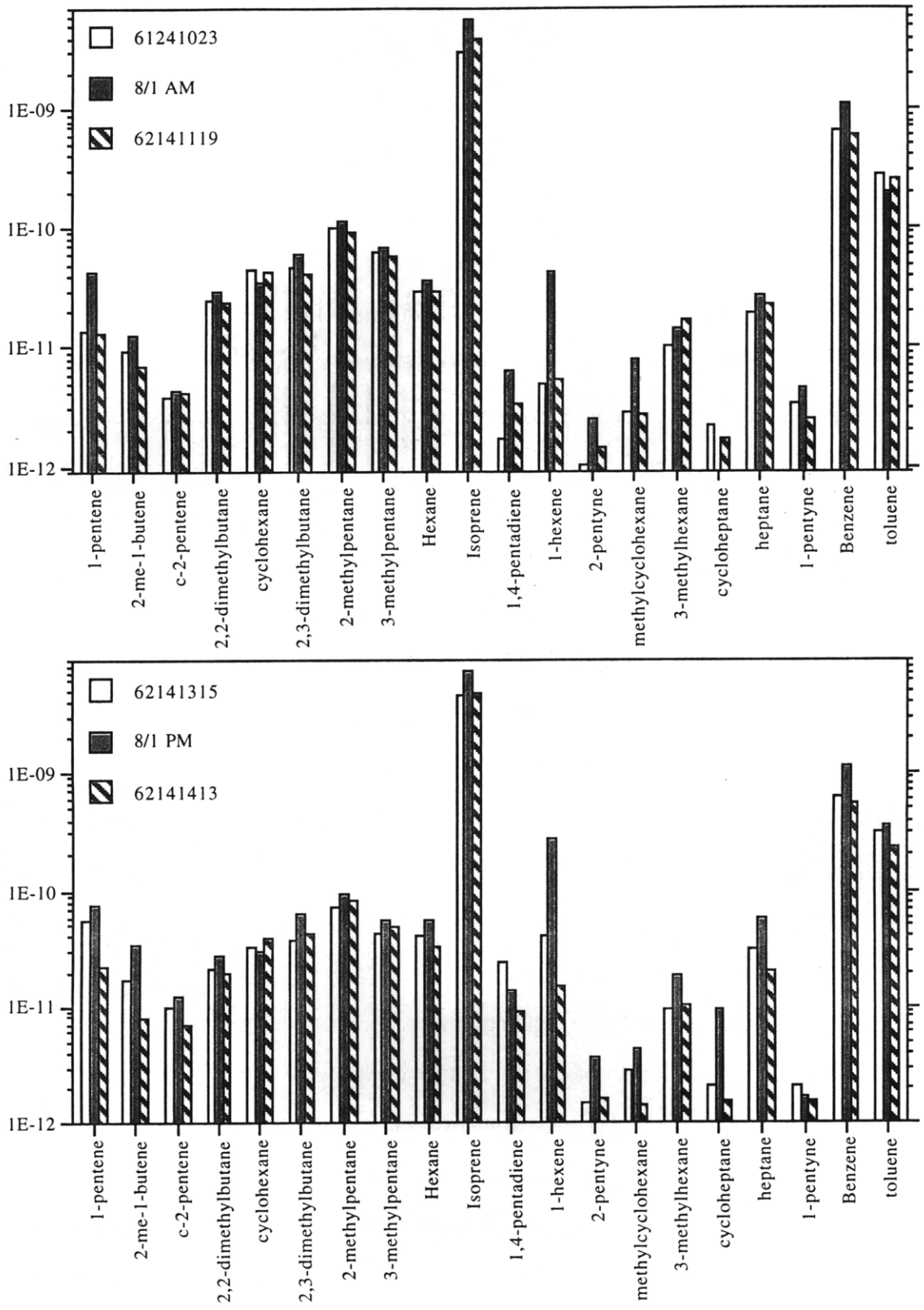

Figure 3.7.1b As Figure 3.7.1a

Chapter 4: Conclusions

Nonmethane hydrocarbons play a significant role in the chemistry of the troposphere. This thesis has focused on vegetative emissions from a heretofore uninvestigated subtropical evergreen broad-leafed forest in Southern China. Our preliminary measurements in June 1994 indicated that biogenic emissions could dominate the chemistry in the local forest. With the advent of more sophisticated chemical and transport models, accurate regional emissions estimates for biogenic hydrocarbons have become a necessity. We set out to assess through multi-gas measurements the extent that biogenic NMHC influence the local tropospheric chemistry in rural Southern China.

To begin our study, we initiated a flask sampling campaign in June 1995. Bi-monthly samples were obtained over a fifteen month period at the Dinghushan Biosphere Reserve in Guangdong, China and analyzed at MIT with a GC-FID. The end of this study was overlapped by an in situ measurement effort over the summer of 1996 which included the hourly measurements of NMHC, CO, temperature, relative humidity and wind velocity. In addition, continuous monitoring of NO_x, and PAR was performed. An enclosure study allowed us to estimate the emission rates of important biogenic NMHC from the dominant local vegetation.

The nine weeks of high frequency measurements we report for this ecosystem are unique both in the length of the study and in the wide array of species observed, including alkanes, alkenes, alkynes, aromatics and cyclic hydrocarbons. In addition to detailed information on locally emitted biogenic species, a variety of anthropogenic hydrocarbons were identified (and certain species have both biogenic and anthropogenic sources). The reactivities of these hydrocarbons vary widely and the presence of appreciable levels for many short-lived alkenes indicates a source near our sampling area. To accurately portray the regional chemistry in the terrestrial boundary layer it is vital

to know the abundance of the reactive NMHC. This data set will prove invaluable to chemical modelers of this region by providing information on the concentrations of such a wide variety of hydrocarbons. During the summertime, our results indicate significant biogenic emissions may dominate the hydrocarbon chemistry. During colder months we would expect anthropogenic hydrocarbons to play a greater role.

Seasonal variations in both biogenic and light NMHC were observed at DHSBR. Isoprene and terpenes exhibited maximum concentrations (7 ppbv and 3 ppbv respectively) during the warm summer months and minimums (100 pptv and 40 pptv) during the cooler winter season as we would expect from their emission dependence upon temperature. We plotted log [isoprene (ppbv)] versus temperature which gave a regression line slope of 0.072 per °C. This corresponds to a doubling of isoprene concentration for an increase of four degrees Celsius which agrees quite well with measurements of other investigators for U. S. ecosystems (Fehsenfeld et al., 1992). The concentrations of biogenic gases reported from this ecosystem are near the maximum values reported from any biome. The terpene concentrations are consistent with measurements performed in Japan whereas isoprene concentrations are much greater at DHSBR (Yokouchi and Ambe, 1988; Yokouchi et al., 1983). This result is most likely due to the species compositions of the respective forests studied. Summertime levels of isoprene at DHSBR are also much greater than those found in boreal regions (Jobson et al., 1994) but are only somewhat above levels reported in the Amazon (Jacob and Wofsy 1988) and similar to those found in a mid-latitude forest (Goldan et al., 1995).

Unlike the biogenic hydrocarbons, background mole fractions of light NMHC showed wintertime maxima and summertime minima. The magnitude of the seasonal cycle at DHSBR is not as great as that observed at higher latitudes (Goldstein et al, 1994b; Laurila and Hakola, 1996) as would be expected due to their different seasonal OH variations. We used ratios of light hydrocarbon measurements to investigate the photochemical age of sampled air masses and to determine the relative effects of transport and chemistry on the species concentrations. Our results compared favorably

with those obtained by other researchers (Table 2.2.3). Plotted ratios do not fall along either the pure chemistry or the pure dilution slopes. Our analysis showed that mixing processes were responsible for about 70% of the changes in hydrocarbon ratios. When investigating two species with like chemical loss with OH, it was apparent that two distinct sources were present for the butane isomers, apparently there was a local source relatively more rich in i-butane than n-butane.

We conducted dynamic flow through enclosure experiments of six different species in the DHSBR to determine the emission fluxes of isoprene and terpenes from the forest. Two of the tree species had significant standard isoprene emission rates over 50 $\mu g\ C\ g^{-1}\ h^{-1}$. These values are on a par with those reported for oak species which are considered high isoprene emitters (König et al. (1995). Total standard terpene emission rates for species measured ranged from 0.05-0.55 $\mu g\ C\ g^{-1}\ h^{-1}$. Our calculated biomass factor of $1410 \pm 170\ g\ m^{-2}$ was used to estimate the emission from the forest region. The flux of isoprene and terpenes from DHSBR over the summer of 1996 was 8.6 ± 6.1 and $0.08 \pm 0.10\ mg\ C\ m^{-2}\ h^{-1}$ respectively. The isoprene emission rate reported from the Amazon was $3.2 \pm 1.2\ mg\ C\ m^{-2}\ h^{-1}$ and from Alabama, $3.9 \pm 2.9\ mg\ C\ m^{-2}\ h^{-1}$ (Davis et al., 1994). The terpene flux from the same study in Alabama was $2.2 \pm 1.4\ mg\ C\ m^{-2}\ h^{-1}$ which agrees with the estimate of Hov et al. (1983) for a coniferous forest in Norway. Our emission estimate for terpenes is not truly representative of the forest at DHSBR as our in situ measurement system did not properly measure the three most abundant terpene species measured from flasks. We obtained a second estimate of isoprene emission from the forest by an alternative method. By computing the column rate of destruction of isoprene, we determined the isoprene flux to be $5.6 \pm 4.9\ mg\ C\ m^{-2}\ h^{-1}$, which compares favorably to our direct measurement from vegetation.

Hourly in situ measurements of NMHC enabled us to get a clearer picture of the different types of air masses prevalent at DHSBR which was not possible from our infrequent flask analyses. Measurements of CO and NO were also helpful in determining air mass histories. In addition to background air (or non-polluted), we

observed three other distinct types: local propane pollution plumes, biomass burning plumes and anthropogenic pollution plumes. The propane plumes were characterized by high levels of propane and other light NMHC without significantly increased levels of NO or CO. The primary difference between the biomass burning plumes and anthropogenic plumes were in the relatively higher levels of NO, toluene and hexane isomers in the latter.

The local propane pollution plumes afforded us the opportunity to indirectly determine OH concentrations using a simplified equation to represent the effects of chemistry and mixing processes on the hydrocarbons in the plume. By designating relatively unreactive NMHC as tracers, we were able to estimate [OH] from as many as eight different hydrocarbons on three separate occasions. According to our calculations, afternoon [OH] is $5.7 \pm 2.8 \times 10^6$ molecules cm^{-3}. This result is near those obtained by similar methods in Europe (Blake et al., 1993; Kramp et al., 1997).

We have determined that biogenic emissions from this ecosystem are significant. Based on a simple analysis of the loss frequency of OH, we can see that the biogenic NMHC may dominate the local boundary layer tropospheric chemistry, accounting for over 80% of OH removal. This local OH depletion may enable transport of other less reactive anthropogenic hydrocarbons farther afield. Sufficient NO_X exists (sources are both natural and anthropogenic) such that the biogenic hydrocarbons may contribute to increased local ozone. Jacob and Wofsy (1988) report that vegetative NMHC in the tropics account for increased ozone levels of 30-40 ppbv. They also found that isoprene oxidation enhanced local CO by up to 70 ppb. In addition, the biogenic hydrocarbons may act to sequester nitrogen oxides and enable long distance transport of NO_X. For these reasons, it is important that we continue to investigate the natural background emissions of NMHC so we may improve our understanding of tropospheric chemistry.

In this investigation, we have determined that high frequency measurements are necessary to obtain an accurate picture of local background levels of NMHC at DHSBR. In situ measurements, though more demanding in resources than flask samples, yield a

much greater wealth of information. Further investigation at DHSBR could prove useful. The most advantageous approach would be to move the monitoring station below the existing meteorological observation tower. Since this tower is hundreds of meters further away from the temple complex and the living quarters of the residents, the number of high local pollution measurements that we observed would be minimized. This is extremely important as a high percentage of our light hydrocarbon measurements were directly affected by this pollution and other measurements may have been indirectly affected. The tower should be equipped with anemometers and other meteorological instruments to properly characterize ambient conditions. Our estimates of significant biogenic emissions indicate a more in depth study of fluxes would be productive. Such an effort would better constrain the emission flux than our simple approach. The tower could be used for this flux estimation by relaxed eddy accumulation or another micrometeorological method. Additionally, chemical modeling should be employed to help better understand the impact of local biogenic emissions on tropospheric chemistry.

References

Aiken, A., J. Herman, E. Maier, and C. McQuillan, Atmospheric Chemistry of Ethane and Ethylene, *J. Geophys. Res.*, 87, 3105-3118, 1982.

Aiken, A., C. Gallagher, C. Spicer, and M. Holdren, Measurements of Methane and Other Light Hydrocarbons in the Troposphere and Lower Stratosphere, *J. Geophys. Res.*, 92, 3135-3138, 1987.

Allwine, G., B. Lamb, and H. Westberg, Application of Atmospheric Tracer Techniques for Determining Biogenic Hydrocarbon Fluxes from an Oak Forest, The Forest-Atmosphere Interaction, 361-382, 1985.

Altshuller, A. P., Review: Natural Volatile Organic Substances and Their Effect on Air Quality in the United States, *Atmos. Environ.*, 17, 2131-2165, 1983.

Altshuller, A. P., Chemical Reactions and Transport of Alkanes and Their Products in the Troposhere, *J. Atmos. Chem.*, 12, 19-61, 1991.

Anastasi, C., L. Hopkinson, and V. Simpson, Natural Hydrocarbon Emission in the United Kingdom, *Atmos. Environ.*, 25A, 1403-1408, 1991.

Andreani-Aksoyoglu, S., and J. Keller, Estimates of Monoterpene and Isoprene Emissions from the Forests in Switzerland, *J. Atmos. Chem.*, 20, 71-87, 1995.

Apel, A. E., and J. G. Calvert, The nonmethane hydrocarbon intercomparison experiment (NOMHICE): Task 1 and 2, *J. Geophys. Res.*, 99, 16,651-16,664, 1994.

Arey, J., A. Winer, R. Atkinson, S. Aschmann, W. Long, C. Morrison, and D. Olszyk, Terpenes Emitted from Agricultural Species Found in California's Central Valley, *J. Geophys. Res.*, 96, 9329-9336, 1991.

Arey, J., D. Crowley, M. Crowley, M. Resketo, and J. Lester, Hydrocarbon Emissions from Natural Vegetation in California's South Coast Air Basin, *Atmos. Environ.*, 29, 2977-2988, 1995.

Arnts, R., W. Peterson, R. Seila, and B. Gay, Estimates of α-Pinene Emissions from a Loblolly Pine Forest Using an Atmospheric Diffusion Model, *Atmos. Environ.*, 16, 2127-2137, 1982.

Arnts, R. R., and S. Meeks, Biogenic Hydrocarbon Contribution to the Ambient Air of Selected Areas, *Atmos. Environ.*, 15, 1643-1651, 1981.

Atherton, C., and J. Penner, The Effects of Biogenic Hydrocarbons on the Tansformation of Nitrogen Oxides in the Troposphere, *J. Geophys. Res.*, 95, 14,027-14,038, 1990.

Atkinson, R., Gas-Phase Tropospheric Chemistry of Organic Compounds: a Review, *Atmos. Environ.*, 24A, 1-41, 1990.

Ayers, G., and W. Gillett, Isoprene Emissions from Vegetation and Hydrocarbon Emissions from Bushfires in Tropical Australia, *J. Atmos. Chem.*, 7, 177-190, 1988.

Barrie, L., and R. Hoff, Five Years of Air Chemistry Observations in the Canadian Arctic, *Atmos. Environ.*, 19, 1995-2010, 1985.

Beine, B., D. Jaffe, D. Blake, E. Atlas, and J. Harris, Measurements of PAN, alkyl nitrates, ozone, and hydrocarbons during spring in interior Alaska, *J. Geophys. Res.*, 101, 12,613-12,619, 1996.

Benoit, R., On the Integral of the Surface Layer Profile-Gradient Functions, *Journal of Applied Meteorology*, 16, 859-860, 1977.

Beverland, I. J., R. Milne, C. Boissard, D. H. ONeill, J. B. Moncrief, and C. N. Hewitt, Meaurement of

carbon dioxide and hydrocarbon fluxes from a sitka spruce forest using micrometeorological techniques, *J. Geophys. Res.*, 101, 22,807-22,815, 1996.

Blake, D., and F. S. Rowland, Global Atmospheric Concentrations and Source Strength of Ethane, *Nature*, 321, 231-233, 1986.

Blake, D., D. Hurst, T. Smith, W. Whipple, T. Chen, N. Blake, and F. S. Rowland, Summertime Measurements of Selected Nonmethane Hydrocarbons in the Arctic and Subarctic during the 1988 Arctic Boundary Layer Expedtion (ABLE 3A), *J. Geophys. Res.*, 97, 16,559-16,588, 1992.

Blake, D., T. W. Smith, T.-Y. Chen, W. J. Whipple, and F. S. Rowland, Effects of biomass burning on summertime nonmethane hydrocarbon concentrations in the Canadian wetlands, *J. Geophys. Res.*, 99, 1699-1719, 1994.

Blake, D., N. Blake, T. Smith, O. Wingenter, and F. S. Rowland, Nonmethane hydrocarbon and halocarbon distributions during Atlantic Stratocumulus Transition Experiment/Marine Aerosol and Gas Exchange, June 1992., *J. Geophys. Res.*, 101, 4501-4514, 1996.

Blake, N., S. Penkett, K. Clemitshaw, P. Anwyl, P. Lightman, A. Marsh, and G. Butcher, Estimates of Atmospheric Hydroxyl Radical Concentrations from the Observed Decay of Many Reactive Hydrocarbons in Well-defined Urban Plumes, *J. Geophys. Res.*, 98, 2851-2864, 1993.

Boissard, C., B. Bonsang, M. Kanakidou, and G. Lambert, TROPOS II: Global Distributions and Budgets of Methane and Light Hydrocarbons, *J. Atmos. Chem.*, 25, 115-148, 1996.

Bonsang, B., and G. Lambert, Nonmethane Hydrocarbons in an Oceanic Atmosphere, *J. Atmos. Chem.*, 2, 257-271, 1985.

Bonsang, B., M. Kanakidou, and G. Lambert, Nonmethane Hydrocarbons Chemistry in the Atmosphere of an Equatorial Forest: A Case of Indirect Photochemical Production of OH Radicals, *Geophys. Res. Lett.*, 14, 1250-1253, 1987.

Bonsang, B., M. Kanakidou, G. Lambert, and P. Monfray, The Marine Source of C_2-C_6 Aliphatic Hydrocarbons, *J. Atmos. Chem.*, 6, 3-20, 1988.

Bonsang, B., M. Kanakidou, and G. Lambert, NMHC in the Marine Atmosphere: Preliminary Results of Monitoring at Amsterdam Island, *J. Atmos. Chem.*, 11, 169-178, 1990.

Bonsang, B., D. Martin, G. Lambert, M. Kanakidou, J. Le Roulley, and G. Sennequier, Vertical Distribution of Nonmethane Hydrocarbons in the Remote Marine Boundary Layer, *J. Geophys. Res.*, 96, 7313-7324, 1991.

Bottenheim, J., and M. Shepherd, C_2-C_6 Hydrocarbon Measurements at Four Rural Locations across Canada, *Atmos. Environ.*, 29, 647-664, 1995.

Bottenheim, J., P. Brickell, T. Dann, D. Wang, F. Hopper, A. Gallant, K. Anlauf, and H. A. Wiebe, Non-Methane Hydrocarbons and CO during Pacific '93, *Atmos. Environ.*, 31, 2079-2087, 1997.

Boudries, H., G. Toupance, and A. L. Dutot, Seasonal Variation of Atmospheric Nonmethane Hydrocarbons on the Western Coast of Brittany, France, *Atmos. Environ.*, 28, 1095-1112, 1994.

Brewer, D., T. Augustsson, and J. Levine, The Photochemistry of Anthropogenic Nonmethane Hydrocarbons in the Troposhere, *J. Geophys. Res.*, 88, 6683-6695, 1983.

Brice, K., and R. Derwent, Emissions Inventory for Hydrocarbons in the United Kingdom, *Atmos. Environ.*, 12, 2045-2054, 1978.

Brooks, J., and W. Sackett, Sources, Sinks, and Concentrations of Light Hydrocarbons in the Gulf of

Mexico, *J. Geophys. Res.*, 78, 5248-5258, 1973.

Bufler, U., and K. Wegman, Diurnal Variation of Monoterpene Concentrations in in Open-Top Chambers and in the Welzheim Forest Air, F.R.G., *Atmos. Environ.*, 25A, 251-256, 1991.

Burns, w., D. Tingey, and R. Evans, Problems with a Nafion membrane dryer for drying chromatographic samples, *J. Chromatography*, 1, 269, 1983.

Cao, X. L., C. Boissard, A. J. Juan, and C. N. Hewitt, Biogenic emissions of volatile organic compounds from gorse (*Ulex europaeus*): Diurnal emission fluxes at Kelling Heath, England, *J. Geophys. Res.*, 102, 18,903-18,915, 1997.

Carter, W., and R. Atkinson, Atmoshperic Chemistry of Alkanes, *J. Atmos. Chem.*, 3, 377-405, 1985.

Chameides, W. L., and R. J. Cicerone, Effects of Nonmethane Hydrocarbons in the Atmosphere, *J. Geophys. Res.*, 83, 947-952, 1978.

Clarkson, T. S., R. J. Martin, and J. Rudolph, Ethane and Propane in the Southern Marine Troposphere, *Atmos. Environ.*, 31, 3763-3771, 1997.

Clement, B., M. Riba, Leduc R., M. Haziza, and L. Torres, Concentraion of Monoterpenes in a Maple Forest in Quebec, *Atmos. Environ.*, 24A, 2513-2516, 1990.

Cofer, W., Methane and Nonmethane Hydrocarbon Concentrations in the North and South Atlantic Marine Boundary Layer, *J. Geophys. Res.*, 87, 7201-7205, 1982.

Cofer, W., Trace Gas Emissions from Chaparral and Boreal Fores Fires, *J. Geophys. Res.*, 94, 2255-2259, 1989.

Cofer, W., J. Levine, E. Winstead, P. LeBel, A. Koller, and C. Hinkle, Trace Gas Emissions from Burning Florida Wetlands, *J. Geophys. Res.*, 95, 1865-1870, 1990.

Cronn, D., and W. Nutmagul, Analysis of Atmospheric Hydrocarbons during Winter MONEX, *Tellus*, 34, 159-165, 1982.

Crutzen, P., and P. Zimmermann, The changing photochemistry of the troposphere, *Tellus*, 43AB, 136-151, 1991.

Darnall, K., A. Lloyd, A. Winer, and J. Pitts, Reactivity Scale for Atmospheric Hydrocarbons Based on Reaction with Hydroxyl Radical, *Environ. Sci. Technol.*, 10, 692-696, 1976.

Das, T. N., Terpenes in a Conifer Forest: Detection at Sub-parts per Billion Level without Sample Preconcentration, *Atmos. Environ.*, 26A, 2853-2857, 1992.

Davis, K. J., D. H. Lenschow, and P. R. Zimmerman, Biogenic nonmethane hydrocarbon emissions estimated from tethered balloon observations, *J. Geophys. Res.*, 99, 25,587-25,598, 1994.

Derwent R.G.M. E. Jenkin, Hydrocarbons and the Long-range Transport of Ozone and Pan across Europe, *Atmos. Environ.*, 25A, 1661-1678, 1991.

Donahue, N., and R. Prinn, Nonmethane Hydrocarbon Chemistry in the Remote Marine Boundary Layer, *J. Geophys. Res.*, 95, 18,387-18,411, 1990.

Donahue, N., Nonmethane Hydrocarbon Chemistry in the Remote Marine Atmosphere, Ph.D. Thesis, Massachusetts Institute of Technology, 1991.

Donoso, L., R. Romero, A. Rondon, E. Fernandez, P. Oyola, and E. Sanhueza, Natural and Anthropogenic C_2 to C_6 Hydrocarbons in the Central-Eastern Venezuelan Atmosphere During the Rainy

Season, *J. Atmos. Chem.*, 25, 201-214, 1996.

Eichmann, R., P. Neuling, G. Ketseridis, J. Hahn, R. Jaenicke, and C. Junge, n-Alkane Studies in the Tropopsphere-I: Gas and Particulate Concentrations in North Atlantic Air, *Atmos. Environ.*, 13, 587-599, 1979.

Eichmann, R., G. Ketseridis, G. Schebeske, R. Jaenicke, J. Hahn, P. Warneck, and C. Junge, N-Alkane Studies in the Troposphere-II: Gas and Particulate Concentrations in Indian Ocean Air, *Atmos. Environ.*, 14, 695-703, 1980.

Enhalt, D., J. Rudolph, F. Meixner, and U. Schmidt, Measurements of Selected C_2-C_5 Hydrocarbons in the Background Troposphere: Vertical and Latitudinal Variations, *J. Atmos. Chem.*, 3, 29-52, 1985.

Evans, R., D. Tingey, M. Gumpertz, and W. Burns, Estimates of Isoprene and Monoterpene Emission Rates in Plants, *Bot. Gaz.*, 143, 304-310, 1982.

Fehsenfeld, F., J. Calvert, R. Fall, P. Goldan, A. Guenther, C. Hewitt, B. Lamb, S. Liu, M. Trainer, H. Westberg, and P. Zimmerman, Emissions of Volatile Organic Compounds from Vegetation and the Implications for Atmospheric Chemistry, *Global Biogeochem. Cycles*, 6, 389-430, 1992.

Field, R., M. Goldstone, J. Lester, and R. Perry, The Sources and Behavior of Tropospheric Anthropogenic Volatile Hydrocarbons, *Atmos. Environ.*, 26A, 2983-2996, 1992.

Fuentes, J. D., D. Wang, G. D. Hartog, H. H. Neumann, T. F. Dann, and K. J. Puckett, Modelled and Field Measurements of Biogenic Hydrocarbon Emissions from a Canadian Deciduous Forest, *Atmos. Environ.*, 29, 3003-3017, 1995.

Fuentes, J. D., D. Wang, H. H. Neumann, T. J. Gillespie, G. D. Hartog, and T. F. Dann, Ambient Biogenic Hydrocarbons and Isoprene Emissions from a Mixed Deciduous Forest, *J. Atmos. Chem.*, 25, 67-95, 1996.

Gao, W., M. L. Wesely, and P. V. Doskey, Numerical Modeling of the Turbulent Diffusion and Chemistry of NO_x, O_3, Isoprene, and Other Reactive Trace Gases in and Above a Forest Canopy, *J. Geophys. Res.*, 98, 18,339-18,353, 1993.

Geron, C., A.Guenther and T.Pierce, An improved model for estimating emissions of volatile organic compounds from forests in the eastern United States, *J. Geophys. Res.*, 99,12,773-12,792, 1994.

Geron, C., D. Nie, R. Arnts, T. Sharkey, E. Singsaas, P. Vanderveer, A. Guenther, J. Sickles II, and T. Kleindienst, Biogenic isoprene emission: Model evaluation in a southeastern United States bottomland deciduous forest, *J. Geophys. Res.*, 102, 18,889-18,901, 1997.

Goldan, P., W. Kuster, F. Fehsenfeld, and S. Montzka, Hydrocarbon measurements in the southeastern United States: The Rural Oxidants in the Southern Environment (ROSE) Program 1990, *J. Geophys. Res.*, 100, 25,945-25,963, 1995.

Goldan, P., W. Kuster and F. Fehsenfeld, Nonmethane hydrocarbon measurements during the Tropospheric OH Photochemistry Experiment, *J. Geophys. Res.*, 102, 6315-6324, 1997.

Goldstein, A., B. Daube, J. Munger, and S. Wofsy, Automated In-Situ Monitoring of Atmospheric Non-Methane Hydrocarbon Concentrations and Gradients, *J. Atmos. Chem.*, 21, 43-59, 1995.

Goldstein, A., S. Wofsy, and C. Spivakovsky, Seasonal variations of nonmethane hydrocarbons in rural New England: Constraints on OH concentrations in northern midlatitudes, *J. Geophys. Res.*, 100, 21,023-21,033, 1995.

Gong, Q., and K. Demerjian, Measurement and Analysis of C_2-C_{10} Hydrocarbons at Whiteface Mountain, New York., *J. Geophys. Res.*, 102, 28,059-28,069, 1997.

Gong, Q., and K. Demerjian, Hydrocarbon Losses on a Regenerated Nafion Dryer, *Journal of the Air and Waste Management Association*, 45, 490-493, 1995.

Greenberg, J., and Zimmerman. P., Nonmethane Hydrocarbons in Remote, Tropical, Continental and Marine Atmospheres, *J. Geophys. Res.*, 89, 4767-4778, 1984.

Greenberg, J., Zimmerman. P., L. Heidt, and W. Pollack, Hydrocarbon and Carbon Monoxide Emissions from Biomass Burning in Brazil, *J. Geophys. Res.*, 89, 1350-1354, 1984.

Greenberg, J., Zimmerman. P., and R. Chatfield, Hydrocarbons and Carbon Monoxide in African Savannah Air, *Geophys. Res. Lett.*, 12, 113-116, 1985.

Greenberg, J., Zimmerman. P., and P. Haagenson, Tropospheric Hydrocarbon and CO Profiles over the U.S. West Coast and Alaska, *J. Geophys. Res.*, 95, 14,015-14,026, 1990.

Greenberg, J. P., P. Zimmerman, W. Pollock, R. Lueb, and L. Heidt, Diurnal Variability of Atmospheric Methane, Nonmethane Hydrocarbons, and Carbon Monoxide at Mauna Loa, *J. Geophys. Res.*, 97, 10,395-10,413, 1992.

Greenberg, J. P., D. Helmig, and P. R. Zimmerman, Seasonal measurements of nonmethane hydrocarbons and carbon monoxide at the Mauna Loa Observatory during the Mauna Loa Observatory Photochemistry Experiment 2, *J. Geophys. Res.*, 101, 14,581-14,598, 1996.

Gregory, G. L., Air Chemistry Over the Tropical Forest of Guyana, *J. Geophys. Res.*, 91, 8603-8612, 1986.

Grosjean, D., E. Williams, and J. Seinfeld, Atmospheric Oxidation of Select Terpenes and Related Carbonyls: Gas-Phase Carbonyl Products, *Environ. Sci. Technol.*, 26, 1526-1532, 1992.

Gschwend, P., O. Zafirou, and R. Gagosian, Volatile Organic Compounds in Seawater from the Peru Upweeling Region, *Limnology Oceangraphy*, 25, 1044-1053, 1980.

Guenthar, A., C. N. Hewitt, D. Erickson, R. Rall, C. Geron, T. Graedel, P. Harley, L. Klinger, M. Lerdau, W. McKay, T. Pierce, B. Scholes, R. Steinbrecher, R. Tallamraju, J. Taylor, and P. Zimmerman, A global model of natural volatile organic compound emissions, *J. Geophys. Res.*, 100, 8873-8892, 1995.

Guenthar, A., W. Baugh, K. Davis, G. Hampton, P. Harley, L. Klinger, L. Vierling, P. Zimmerman, E. Allwine, S. Dilts, B. Lamb, H. Westberg, D. Baldocchi, C. Geron, and T. Pierce, Isoprene fluxes measured by enclosure, relaxed eddy accumulation, surface layer gradient, mixed layer gradient, and mixed layer mass balance techniques, *J. Geophys. Res.*, 101, 18,555-18,567, 1996.

Guenthar, A., L. Otter, P. Zimmerman, J. Greenberg, R. Scholes, and M. Scholes, Biogenic hydrocarbon emissions from southern African savannas, *J. Geophys. Res.*, 101, 25,859-25,865, 1996.

Guenthar, A., P. Zimmerman, L. Klinger, J. Greenberg, C. Ennis, K. Davis, W. Pollock, H. Westberg, G. Allwine, and C. Geron, Estimates of regional natural volatile organic compound fluxes from enclosure and ambient measurements, *J. Geophys. Res.*, 101, 1345-1359, 1996.

Guenthar, A. B., R. K. Monson, and R. Fall, Isoprene and Monoterpene Emission Rate Variability : Observations With Eucalyptus and Emission Rate Algorithm Development, *J. Geophys. Res.*, 96, 10,799-10,808, 1991.

Guenthar, A. B., P. Zimmerman, P. Harley, R. K. Monson, and R. Fall, Isoprene and Monoterpene Emission Rate Variability : Model Evaluations and Sensitivity Analyses, *J. Geophys. Res.*, 98, 12,609-12,617, 1993.

Hagerman, L., V. Aneja, and W. Lonneman, Characterization of Non-methane Hydrocarbons in the Rural Southest United States, *Atmos. Environ.*, 31, 4017-4038, 1997.

Hanst, P., J. Spence, and E. Edney, Carbon Monoxide Production in Photooxidation of Organic Molecules in the Air, *Atmos. Environ.*, 14, 1077-1088, 1980.

Haszpra, L., I. Demeter, T. Turanyi, and T. Berces, Non-Methane Hydrocarbon and Aldehyde Measurements in Budapest, Hungary, *Atmos. Environ.*, 25A, 2103-2110, 1991.

Hatakeyama, S., K. Izumi, T. Fukuyama, H. Akimoto, and N. Washida, Reactions of OH with a-Pinene and b-Pinene in Air: Estimate of Global CO Production from the Atmospheric Oxidation of Terpenes, *J. Geophys. Res.*, 96, 947-958, 1991.

Heikes, B., M. Lee, D. Jacob, R. Talbot, J. Bradshaw, H. Singh, D. Blake, B. Anderson, H. Fuelberg, and A. Thompson, Ozone, hydroperoxides, oxides of nitrogen, and hydrocarbon budgets in the marine boundary layer over the South Atlantic, *J. Geophys. Res.*, 101, 24,221-24,234, 1996.

Hoffmann, T., J. Odum, F. Bowman, D. Collins, D. Klockow, R. Flagan, and J. Seinfeld, Formation of Organic Aerosols from the Oxidation of Biogenic Hydrocarbons, *J. Atmos. Chem.*, 26, 189-222, 1997.

Holdren, M., H. Westberg, and P. Zimmerman, Analysis of Monoterpene Hydrocarbons in Rural Atmospheres, *J. Geophys. Res.*, 84, 5083-5088, 1979.

Hov, O., J. Shjoldager, and B. Wathne, Measurement and Modeling of the Concentrations of Terpenes in Coniferous Forest Air, *J. Geophys. Res.*, 88, 10,679-10,688, 1983.

Hov, O., S. A. Penkett, I. S. A. Isaken, and A. Semb, Organic Gases in the Norwegian Arctic, *Geophys. Res. Lett.*, 11, 425-428, 1984.

Hov, O., N. Schmidbauer, and M. Oehme, Light Hydrocarbons in the Norwegian Arctic, *Atmos. Environ.*, 23, 2471-2482, 1989.

Hov, O., N. Schmidbauer, and M. Oehme, C_2-C_5 Hydrocarbons in Rural South Norway, *Atmos. Environ.*, 25A, 1981-1999, 1991.

Hov, O., A. Sorteberg, N. Schmidbauer, S. Solberg, F. Stordal, D. Simpson, A. Lindskog, H. Aerskoug, P. Oyola, H. Lattila, and N. Heidam, European VOC Emission Estimates Evaluated by Measurements and Model Calculations, *J. Atmos. Chem.*, 28, 173-193, 1997.

Hov., O., Atmospheric Concentrations of Nonmethane hydrocarbons at a North European Coastal Site, *J. Atmos. Chem.*, 14, 515-526, 1992.

Isodorov, V., I. Zenkovich, and B. Ioffe, Volatile Organic Compounds in the Atmospheres of Forests, *Atmos. Environ.*, 19, 1-8, 1984.

Jacob, D., and S. Wofsy, Photochemistry of Biogenic Emissions Over the Amazon Forest, *J. Geophys. Res.*, 93, 1477-1486, 1988.

Jacob, D., and S. Wofsy, Budgets of Reactive Nitrogen, Hydrocarbons, and Ozone Over the Amazon Forest during the Wet Season, *J. Geophys. Res.*, 95, 16,737-16,754, 1990.

Jacob, D. J., Chemistry of OH in Remote Clouds and Its Role in the Production of Formic Acid and Peroxymonosulfate, *J. Geophys. Res.*, 91, 9807-9826, 1986.

Janson, R., Monoterpene Concentrations in and Above a Forest of Scots Pine, *J. Atmos. Chem.*, 14, 385-394, 1992.

Jobson, B. T., H. Niki, Y. Yokouchi, J. Bottenheim, F. Hopper, and R. Leaitch, Measurements of C_2-

C_6 hydrocarbons during the Polar Sunrise 1992 Experiment: Evidence for Cl atom and Br atom chemistry, *J. Geophys. Res.*, 99, 25,355-25,368, 1994.

Jobson, B. T., Z. Wu, H. Niki, and L. A. Barrie, Seasonal trends of isoprene, C_2-C_5 alkanes, and acetylene at a remote boreal site in Canada, *J. Geophys. Res.*, 99, 1589-1599, 1994.

Juttner, F., Analysis of Organic Compounds (VOC) in Forest Air of the Southern Black Forest, *Chemosphere*, 15, 985-992, 1986.

Juttner, F., Quantitative Analysis of Monoterpenes and Volatile Organic Pollution Products (VOC) in Forest Air of the Southern Black Forest, *Chemosphere*, 17, 309-317, 1988.

Juuti, S., J. Arey, and R. Atkinson, Monoterpene Emission Rate Measurements from a Monterey Pine, *J. Geophys. Res.*, 95, 7515-7519, 1990.

Kamens, R., H. Jeffries, M. Gery, R. Wiener, K. Sexton, and G. Howe, The Impact of a-Pinene on Urban Smog Formation: An Outdoor Smog Chamber Study, *Atmos. Environ.*, 15, 969-981, 1981.

Kanakidou, M., B. Bonsang, and G. Lambert, Light Hydrocarbons, Vertical Profiles and Fluxes in a French Rural Area, *Atmos. Environ.*, 23, 921-927, 1989.

Kanakidou, M., H. B. Singh, K. Valentin, and Crutzen P.J., A Two-Dimensionsal Study of Ethane and Propane Oxidation in the Troposphere, *J. Geophys. Res.*, 96, 15,395-15,413, 1991.

Kaplan, W., S. C. Wofsy, M. Keller, and J. M. Da Costa, Emission of NO and Deposition of O_3 in a Tropical Forest System, *J. Geophys. Res.*, 93, 1389-1395, 1988.

Kasting, J. F., and H. B. Singh, Nonmethane Hydrocarbons in the Troposhere: Impact on the Odd Hydrogen and Odd Nitrogen Chemistry, *J. Geophys. Res.*, 91, 13,239-13,256, 1986.

Khalil, M., R. Rasmussen, M. Wang, and L. Ren, Emission of Trace Gases from Chinese Rice Fields and Biogas Generators: CH_4, N_2O, CO, CO_2, Chlorocarbons and Hydrocarbons, *Chemosphere*, 20, 207-226, 1990.

Khalil, M., and R. A. Rasmussen, Forest Hydrocarbon Emissions: Relationships Between Fluxes and Ambient Concentrations, *J. Air Waste Manage. Assoc.*, 42, 810-813, 1992.

Klemp, D., D. Kley, F. Kramp, H. Buers, G. Pilwat, F. Flocke, H. Patz, and A. Volz-Thomas, Long-Term Measurements of Light Hydrocarbons (C_2-C_5) at Schauinsland (Black Forest), *J. Atmos. Chem.*, 28, 135-171, 1997.

Klinger, L., P. Zimmerman, J. Greenberg, L. Heidt, and A. Guenthar, Carbon trace gas fluxes along a successional gradient in the Hudson Bay lowland, *J. Geophys. Res.*, 99, 1469-1494, 1994.

Knoerr, K., and F. Mowry, Energy Balance/Bowen Ratio Technique for Estimating Hydrocarbon Fluxes, Atmospheric Biogenic hydrocarbons, 35-54, 1981.

Kong, G., L. Chun, H. Wu and Z. Huang, *Dinghushan Biosphere Reserve Ecological Reasearch History and Perspective*. Science Press, Beijing 1993.

Konig, G., M. Brunda, H. Puxbaum, C. N. Hewitt, S. C. Duckham, and J. Rudolph, Relative contribution of Oxygenated Hydrocarbons to the Total Biogenic VOC Emissions of Selected Mid-European Agricultural and Natural Plant Species, *Atmos. Environ.*, 29, 861-874, 1995.

Koppmann, R., R. Bauer, F. Johnen, C. Plass, and J. Rudolph, The Distribution of Light Nonmethane Hydrocarbons over the Mid-Atlantic: Results of the *Polarstern* Cruise ANT VII/1, *J. Atmos. Chem.*, 15, 215-234, 1992.

Kotzias, D., K. Fyutianos, and F. Geiss, Reaction of Monoterpenes with Ozone, Sulphur Dioxide and Nitrogen Dioxide--Gas-Phase Oxidation of SO_2 and Formation of Sulphuric Acid, *Atmos. Environ.*, 24A, 2127-2132, 1990.

Kramp, F., and A. Volz-Thomas, On the Budget of OH Radicals and Ozone in an Urban Plume from the Decay of C_5-C_8 Hydrocarbons and NO_x, *J. Atmos. Chem.*, 28, 263-282, 1997.

Lamb, B., H. Westberg, G. Allwine, and T. Quarles, Biogenic Hydrocarbon Emissions from Deciduous and Coniferous Trees in the United States, *J. Geophys. Res.*, 90, 2380-2390, 1985.

Lamb, B., H. Westberg, and G. Allwine, Isoprene Emission Fluxes Determined by an Atmospheric Tracer Technique, *Atmos. Environ.*, 20, 1-8, 1986.

Lamb, B., A. Guenthar, D. Gay, and H. Westburg, A National Inventory of Biogenic Hydrocarbon Emissions, *Atmos. Environ.*, 21, 1695-1705, 1987.

Lamontagne, R., J. Swinnerton, and V. Linnenbom, C_1-C_4 Hydrocarbons in the North and South Pacific, *Tellus*, XXVI, 7177, 1974.

Lerdau, M., S. Dilts, H. Westberg, B. Lamb, and E. Allwine, Monoterpene emission from ponderosa pine, *J. Geophys. Res.*, 99, 16,609-16,615, 1994.

Lindskog, A., and J. Moldanova, The Influence of the Origin, Season and Time of the Day on the Distribution of Individual NMHC Measured at Rorvik, Sweden, *Atmos. Environ.*, 28, 2383-2398, 1994.

Liu, S. C., M. Trainer, F. Fehsenfeld, D. Parrish, E. Williams, D. Fahey, G. Hubler, R. Martin, H. Westberg, E. Allwine, J. Ashman, J. Farmer, and B. Lamb, Measurements of Isoprene and its Atmospheric Oxidation Products in a Central Pennsylvania Deciduous Forest, *J. Atmos. Chem.*, 13, 1-31, 1991.

Logan, J., M. Prather, S. Wofsy, and McElroy M., Tropospheric Chemistry: A Global Perspective, *J. Geophys. Res.*, 86, 7210-7254, 1981.

Lonneman, W., S. Kopczynski, P. Darley, and F. Sutterfield, Hydrocarbon Composition of Urban Air Pollution, *Environ. Sci. Technol.*, 8, 229-236, 1974.

Lonneman, W., R. Seila, and J. Bufalini, Ambient Air Hydrocarbon Concentrations in Florida, *Environ. Sci. Technol.*, 12, 459-463, 1978.

Lopez, A., S. Prieur, J. Fontan, and M. Barthomeuf, Modelisation de la Chimie d'une Couche Limite Atmospherique non Polluee Influence des Hydrocarbures *Nature*ls Emis par la Vegetation, *Atmos. Environ.*, 21, 671-685, 1987.

Lopez, A., M. O. Barthomeuf, and M. L. Huertas, Simulation of Chemical Processes Occurring in an Atmosphere Boundary Layer. Influence of Light and Biogenic Hydrocarbons on the Formation of Oxidants., *Atmos. Environ.*, 23, 1465-1478, 1989.

MacKenzie, A. R., R. Harrison, I. Colbreck, and C. Hewitt, The Role of Biogenic Hydrocarbons in the Production of Ozone in Urban Plumes in Southeast England, *Atmos. Environ.*, 25A, 351-359, 1991.

Mauzerall, D., J. Logan, D. Jacob, B. Anderson, D. Blake, J. Bradshaw, B. Heikes, G. Sachse, H. Singh, and B. Talbot, Photochemistry in biomass burning plumes and implications for the tropospheric ozone over the tropical South Atlantic, *J. Geophys. Res.*, 103, 8401-8423, 1998.

McKeen, S., M. Trainer, E. Hsie, K. Tallartaju and S. C. Liu, On the Indirect Determination of Atmospheric OH Radical Concentrations From Reactive Hydrocarbon Measurements, *J. Geophys. Res.*, 95, 7493-7500, 1990.

McKeen, S., E. Hsie, and S. C. Liu, A Study of the Dependence of Rural Ozone on Ozone Precursors in the Eastern United States, *J. Geophys. Res.*, 96, 15,377-15,394, 1991.

McKeen, S. and S. C. Liu, Hydrocarbon ratios and photochemical history of air masses, *Geophys. Res. Lett.*, 20,2363-2366, 1993.

McKeen, S., S. Liu, E. Hsie, X. Lin, J. Bradshaw, S. Smyth, G. Gregory and D. Blake, Hydrocarbon ratios during PEM-WEST A: A model perspective, *J. Geophys. Res.*, 101, 2087-2109, 1996.

Moller, D., Production of Free Radicals by an Ozone-Alkene Reaction-A Possible factor in the New-Type Forest Decline?, *Atmos. Environ.*, 22, 2607-2611, 1988.

Molnar, A., Estimation for Volatile Organic Compounds (VOC) Emissions for Hungary, *Atmos. Environ.*, 24A, 2855-2860, 1990.

Monson, R., M. Lerdau, T. Sharkey, D. Schimel, and R. Fall, Biological Aspects of Constructing Volatile Organic Compound Emission Inventories, *Atmos. Environ.*, 29, 2989-3002, 1995.

Montzka, S., M. Trainer, P. Goldan, W. Kuster, and F. Fehsenfeld, Isoprene and its oxidation products, methyl vinyl ketone, and methacrolein, in the rural troposphere, *J. Geophys. Res.*, 98, 1101-1111, 1993.

Mount, G. and E. Williams, An overview of the Tropospheric OH Photochemistry Experiment, Fritz Peak/Idaho Hill, Colorado, fall 1993, *J. Geophys. Res.*, 102, 6171-6186, 1997.

Mowrer, J., and A. Lindskog, Automatic Unattended Sampling and Analysis of Background Levels of C_2-C_5 Hydrocarbons, *Atmos. Environ.*, 25A, 1971-1979, 1991.

Munger, J. W., S. Wofsy, P. Bakwin, S.-M. Fan, M. Goulden, B. Daube, A. Goldstein, K. Moore, and D. Fitzjarrald, Atmospheric depostion of reactive nitrogen oxides and ozone in a temperate deciduous forest and a subarctic woodland 1. Measurements and mechanisms, *J. Geophys. Res.*, 101, 12,639-12,657, 1996.

Murphy, P., Ozone Production in the Rural Troposphere and the Implications for Regional and Global Ozone Distributions, *J. Geophys. Res.*, 92, 4191-4207, 1987.

National Research Council, China and Global Change: Opportunities for Collaboration, 1992.
Navas, M. J., A. M. Jimenez, and G. Galan, Air Analysis: Determination of Nitrogen Compounds by Chemiluminescence, *Atmos. Environ.*, 31, 3603-3608, 1997.

Nelson, P., and S. Quigley, Non-Methane Hydrocarbons in the Atmosphere of Sydney, Australia, *Environ. Sci. Technol.*, 16, 650-655, 1982.

Nelson, P., S. Quigley, and Y. Smith, Sources of Atmospheric Hydrocarbons in Sydney: A Quantitative Determination Using a Source Reconciliation Technique, *Atmos. Environ.*, 17, 439-449, 1983.

Nieuwstadt, F., The Computation of the Friction Velocity u* and the Temperature scale T* from Temperature and Wind Velocity Profiles by Least-Square Methods, *Boundary-Layer Meteorology*, 14, 235-246, 1978.

Pandis, S. N., S. Paulson, J. Seinfeld, and R. Flagan, Aerosol Formation in the Photooxidation of Isoprene and β–Pinene, *Atmos. Environ.*, 25A, 997-1008, 1991.

Pandit, G., and A. Rao, Evaluation of Auto Exhaust Contribution to Atmospheric C_2-C_5 Hydrocarbons at Deonar, Bombay, *Atmos. Environ.*, 24A, 811-813, 1990.

Parrish, D., C. Hahn, E. Williams, R. Norton, F. Fehsenfeld, H. B. Singh, J. Shetter, B. Gandrud, and B. Ridley, Indicatinos of Photochemical Histories of Pacific Air Masses from Measurements of

Atmospheric Trace Species at Point Arena, California, *J. Geophys. Res.*, 97, 15,883-15,901, 1992.

Peterson, E., and D. Tingey, An Estimate of the Possible Contribution of Biogenic Sources to Airborne Hydrocarbon Concentraions, *Atmos. Environ.*, 14, 79-81, 1980.

Pierotti, D., S. Wofsy, D. Jacob, and R. A. Rasmussen, Isoprene and Its Oxidation Products: Methacrolein and Methyl Vinyl Ketone, *J. Geophys. Res.*, 95, 1871-1881, 1990.

Plass-Dulmer, C., A. Khedim, R. Koppmann, F. Johnen, J. Rudolph, and H. Kuosa, Emissions of Light Nonmethane Hydrocarbons from the Atlantic into the Atmosphere, *Global Biogeochem. Cycles*, 7, 211-228, 1993.

Pleil, J., K. Oliver, and W. McClenny, Enhanced Performance of Nafion Dryers in Removing Water from Air Samples Prior to Gas Chromatographic Analysis, *J. Air Poll. Control Assoc.*, 37, 244-248, 1987.

Rasmussen, R., Isoprene: Identified as a Forest-type Emission to the Atmosphere, *Environ. Sci. Technol.*, 4, 667-671, 1970.

Rasmussen, R. A., M. Khalil, and R. Dalluge, Atmospheric Trace Gases in Antarctica, *Science*, 211, 285-287, 1981.

Rasmussen, R. A., and M. Khalil, Atmospheric Benzene and Toluene, *Geophys. Res. Lett.*, 10, 1096-1099, 1983.

Rasmussen, R. A., M. Khalil, and R. Fox, Altitudinal and Temporal Variation of Hydrocarbons and Other Gaseous Tracers of Arctic Haze, *Geophys. Res. Lett.*, 10, 144-147, 1983.

Rasmussen, R. A., and M. Khalil, Isoprene Over the Amazon Basin, *J. Geophys. Res.*, 93, 1417-1421, 1988.

Riba, M., J. Tathy, N. Tsiropoulos, B. Monsarrat, and L. Torres, Diurnal Variation in the Concentration of a- and b-Pinene in Landes Forest (France), *Atmos. Environ.*, 21, 191-193, 1987.

Riba, M., N. Tsiropoulous, B. Clement, A. Golfier, and L. Torres, Preconcentration and Analysis of Atmospheric Isoprene and Monoterpenes System Automation, *J. Chromatography*, 456, 165-173, 1988.

Rinsland, C., R. Zander, C. Farmer, R. Norton, and J. Russell, Concentrations of Ethane (C_2H_6) in the Lower Stratosphere and Upper Troposphere and Acetylene (C_2H_2) in the Upper Troposphere Deduced From Atmospheric Trace Molecule Spectroscopy/Spacelab 3 Spectra, *J. Geophys. Res.*, 92, 11,951-11,964, 1987.

Roberts, J., F. Fehnsenfeld, D. Albritton, and R. Sievers, Measurements of Monoterpene Hydrocarbons at Niwot Ridge, Colorado, *J. Geophys. Res.*, 88, 10,667-10,678, 1983.

Roberts, J., F. Fehnsenfeld, D. Albritton, and R. Sievers, Sampling and Analysis of Monoterpene Hydrocarbons in the Atmosphere with Tenax Gas Chromatographic Porous Polymer in Identification and Analysis of Organic Pollutants in Air, 1984.

Roberts, J., C. Hahn, F. Fehsenfeld, J. Warnock, D. Albritton, and R. Slevers, Monoterpene Hydrocarbons in the Nighttime Troposphere, *Environ. Sci. Technol.*, 19, 364-369, 1985.

Robinson, E., Hydrocarbons in the Atmosphere, *Pure Applied Geophysics*, 116, 372-384, 1978.

Rudolph, J., and D. H. Enhalt, Measurements of C_2-C_5 Hydrocarbons over the North Atlantic, *J. Geophys. Res.*, 86, 11,959-11,964, 1981.

Rudolph, J., Two-Dimensional Distibution of Light Hydrocarbons: Results from the STRATOZ III Experiment, *J. Geophys. Res.*, 93, 8367-8377, 1988.

Rudolph, J., A. Khedim, and D. Wagenbach, The Seasonal Variation of Light Nonmethane Hydrocarbons in the Antarctic Troposphere, *J. Geophys. Res.*, 94, 13,039-13,044, 1989.

Rudolph, J., and F. J. Johnen, Measurements of Light Atmospheric Hydrocarbons Over the Atlantic in Regions of Low Biological Activity, *J. Geophys. Res.*, 95, 20,583-20,591, 1990.

Rudolph, J., A. Khedim, and B. Bonsang, Light Hydrocarbons in the Tropospheric Boundary Layer Over Tropical Africa, *J. Geophys. Res.*, 97, 6181-6186, 1992.

Rudolph, J., A. Khedim, T. Clarkson, and D. Wagenbach, Longterm measurements of light alkanes and acetylene in the Antarctic troposphere, *Tellus*, 44B, 252-261, 1992.

Scanlon, J., and D. Willis, Calculation of Flame Ionization Detector Relative Response Factors using the Effective Carbon Number Concept, *J. Chrom. Sci.*, 23, 333-340, 1985.

Schuh, G., A. Heiden, T. Hoffmann, J. Kahl, P. Rockel, J. Rudolph, and J. Wildt, Emissions of Volatile Organic Compounds from Sunflower and Beech: Dependence on Temperature and Light Intensity, *J. Atmos. Chem.*, 27, 291-318, 1997.

Shaw, R., A. Crittenden, R. Stevens, D. Cronn, and V. Titov, Ambient Concentrations of Hydrocarbons from Conifers in Atmospheric Gases and Aerosol Particles Measured in Soviet Georgia, *Environ. Sci. Technol.*, 17, 389-395, 1983.

Sillman, S., J. Logan, and S. Wofsy, The Sensitivity of Ozone to Nitrogen Oxides and Hydrocarbons in Regional Ozone Episodes, *J. Geophys. Res.*, 95, 1837-1851, 1990.

Simo, R., M. Colom-Altes, J. Grimalt, and J. Albaiges, Background Levels of Atmospheric Hydrocarbons, Sulphate and Nitrate Over the Western Mediterranean, *Atmos. Environ.*, 25A, 1463-1471, 1991.

Simon, V., B. Clement, M.-L. Riba, and L. Torres, The Landes experiment: Monoterpenes emitted from the maritime pine, *J. Geophys. Res.*, 99, 16,501-16,510, 1994.

Singh, H. B., and L. Salas, Measurements of Selected Light Hydrocarbons over the Pacific Ocean: Latitudinal and Seasonal Variations, *Geophys. Res. Lett.*, 9, 842-845, 1982.

Singh, H. B., and J. F. Kasting, Chlorine-Hydocarbon Photochemistry in the Marine Troposphere and Lower Stratosphere, *J. Atmos. Chem.*, 7, 261-285, 1988.

Singh, H. B., W. Viezee, and L. Salas, Measurements of Selected C_2-C_5 Hydrocarbons in the Troposphere: Latitudinal, Vertical and Temporal Variations, *J. Geophys. Res.*, 93, 15,861-15,878, 1988.

Skov, H., J. Hjorth, C. Lohse, N. Jensen, and G. Restelli, Products and Mechanisms of the Reactions of the Nitrate Radical (NO_3) with Isoprene, 1,3-Butadiene and 2,3-Dimethyl-1,3-Butadiene in Air, *Atmos. Environ.*, 26A, 2771-2783, 1992.

Solberg, S., C. Dye, N. Schmidbauer, A. Herzog, and R. Gehrig, Carbonyls and Nonmethane Hydrocarbons at Rural European Sites from the Mediterranean to the Arctic, *J. Atmos. Chem.*, 25, 33-66, 1996.

Sprengnether, M., An Active Titration Method for the Local Measurement of Tropospheric Hydroxyl Radical, Ph. D. Thesis, Massachusetts Institute of Technology, 1992.

Swinnerton, J., and R. Lamotagne, Oceanic Distribution of Low Molecular Weight Hydrocarbons Baseline Measurements, *Environ. Sci. Technol.*, 8, 657-663, 1974.

Tille, K., M. Savelsberg, and K. Bachmann, Airborne Measurements of Nonmethane Hydrocarbons over

Western Europe: Vertical Distributions, Seasonal Cycles of Mixing Ratios and Source Strengths, *Atmos. Environ.*, 19, 1751-1760, 1985.

Trainer, M., E. Hsie, S. McKeen, R. Tallamraju, D. Parrish, F. Fehsenfeld, and S. C. Liu, Impact of Natural Hydrocarbons on Hydroxl and Peroxy Radicals at a Remote Site, *J. Geophys. Res.*, 92, 11,879-11,894, 1987.

Trainer, M., E. Williams, D. Parrish, M. Burh, E. Allwine, H. Westberg, F. Fehsenfeld, and S. C. Liu, Model and Observations of the Impact of Natural Hydrocarbons on Rural Ozone, *Nature*, 329, 705-707, 1987.

Walton, S., M. Gallagher, and J. Duyzer, Use of a Detailed Model to Study the Exchange of NO_x and O_3 above and below a Deciduous Canopy, *Atmos. Environ.*, 31, 2915-2931, 1997.

Warneck, P., Chemistry of the Natural Atmosphere. Academic Press, Inc., San Diego, CA, 1988.

Wayne, R., Chemistry of Atmospheres. 1991.

Wei, M. H., D. Ward, G. Olbu, and S. Baker, Emissions of CO_2, CO, and hydrocarbons from fires in diverse African savanna ecosystems, *J. Geophys. Res.*, 101, 23,577-23,584, 1996.

Westberg, H., R. Rasmussen, and M. Holdren, Gas Chromatographic Analysis of Ambient Air for Light Hydrocarbons Using a Chemically Bonded Stationary Phase, *Anal. Chem.*, 46, 1852-1854, 1974.

Yokouchi, Y., T. Fujii, Y. Ambe, and K. Fuwa, Determination of Monoterpene Hydrocarbons in the Atmosphere, *J. Chromatography*, 209, 293-298, 1981.

Yokouchi, Y., M. Okaniwa, Y. Ambe, and K. Fuwa, Seasonal Variation of Monoterpenes in the Atmosphere of a Pine Forest, *Atmos. Environ.*, 17, 743-750, 1983.

Yokouchi, Y., and Y. Ambe, Factors Affecting the Emission of Monoterpenes from Red Pine (Pinus densiflora), *Plant Physiol.*, 75, 1009-1012, 1984.

Yokouchi, Y., and Y. Ambe, Aerosols Formed From the Chemical Reaction of Monoterpenes and Ozone, *Atmos. Environ.*, 19, 1271-1276, 1985.

Yokouchi, Y., and Y. Ambe, Diurnal Variations of Atmospheric Isoprene and Monoterpene Hydrocarbons in an Agricultural Area in Summertime, *J. Geophys. Res.*, 93, 3751-3759, 1988.

Young, V.L., B. Kieser, S. Chen and H. Niki, Seasonal trends and local influences on nonmethane hydrocarbon concentrations in the Canadian boreal forest, *J. Geophys. Res.*, 102,5913-5918, 1997.

Zainal, A., Relationship of Non-Methane Hydrocarbons and NO_x to Ozone Formation in the Atmosphere of Bahrain, *Atmos. Environ.*, 24A, 1915-1922, 1990.

Zimmerman, P., R. Chatfield, J. Fishman, P. Crutzen, and P. Hanst, Estimates on the Production of CO and H_2 from the Oxidation of Hydrocarbon Emissions from Vegetation, *Geophys. Res. Lett.*, 5, 679-682, 1978.

Zimmerman, P., J. Greenberg, and C. Westberg, Measurements of Atmospheric Hydrocarbons and Biogenic Emission Fluxes in the Amazon Boundary Layer, *J. Geophys. Res.*, 93, 1407-1416, 1988.

Appendix

A. Absolute Calibration Methods:

In order to accurately measure atmospheric hydrocarbons, one needs to calibrate the analysis system with appropriate standards. We used two different standards for this purpose: 34 liter standard tanks produced by volumetric static dilution, and permeation devices. Each standard preparation method possesses advantages and disadvantages. By using both, they offer independent calibrations of the system which, if in agreement, help verify the quality of the calibration. Ideally, the concentration of compounds in the standards will be orders of magnitude greater than that in the field (on the order of 100 ppbv). This allows us some flexibility in the field when running standards. We are able to dynamically dilute the standard to whatever level observed in the field. We try to mimic actual atmospheric hydrocarbon levels in our standard runs, treating them as if they are whole air samples. In this way we hope to minimize unanticipated effects of sample collection which may vary with the hydrocarbon mixing ratio in the sample gas stream. A second advantage of these higher standard concentrations relates to long-term stability concerns. Standard concentrations near the detection limit could effectively disappear due to wall interactions for unstable compounds; higher concentrations allow tracking of unstable species over time and with close monitoring of these possible losses, accurate calibration is still possible. Luckily, previous work has shown that most hydrocarbons up to C_6 are stable over time (Donahue, 1991; Sprengnether, 1992). My standards build on this previous work to show long term stability (on the order of a year) of all of our standard hydrocarbons.

Permeation devices, which are essentially a pure reservoir of a compound in a two phase equilibrium between gas and liquid (or solid) phases contained in a small, inert, permeable walled capsule, offer flexibility in standard sample mixture and concentration. You can change the mix of hydrocarbons sampled with permeation tubes

as needed. Also, by varying their storage temperature or the exposed teflon area, you can alter the relative concentrations of hydrocarbons in your standard gas stream. On the other hand, once the tank mixture is produced, you are limited to changing mole fraction uniformly. The primary uncertainties associated with these two types of standards are distinctly different. For the tank mixture at 100 ppb levels, uncertainly is dominated by limitations in the pressure measurements during production. Permeation tube uncertainty in contrast arises from the mass loss measurements. In general, these uncertainties in both cases are greater for heavier NMHC since their volatility is lower. Pressure differentials in tank standard production are lower for heavy hydrocarbons as are mass loss rates in the permeation devices.

A.1 Tank Mixtures

A static dilution system developed by Sprengnether (1992) was used to prepare absolute mixtures of hydrocarbons in tanks. The stainless steel tanks used are 34 liter, type 304 military oxygen tanks, cleaned and electropolished commercially (Electromatic, CA). The filling procedure commenced with a series of UHP N_2 flushes and evacuations. The tanks were monitored for leaks and then weighed empty. Water vapor (roughly 10 Torr) introduced into the tanks neutralized (but does not wet) the walls. The tanks were hooked up to the manifold and each hydrocarbon was added successively as follows:

1. The manifold and mixing volume were evacuated.
2. The liquid constituents were prepared for addition by placing a few milliliters in a glass bulb attached to the manifold, followed by alternating UHP nitrogen flushes and evacuations. After three flushes, the liquid was degassed and allowed to boil for a short time. The bulb was then evacuated twice more to ensure that only hydrocarbon was present. Gases at room temperature were added directly from the gas cylinder which was attached to the manifold. All

volumes were evacuated up to the valve between pure hydrocarbon vapor and the manifold before addition.

3. After addition to the mixing volume and manifold, the pressure was monitored for fifteen minutes to detect pressure changes due to wall adsorption.
4. Once pressure stablilty was confirmed and recorded, the mixing volume was closed off and the manifold was again evacuated and flushed three times with UHP N_2.
5. Next, the manifold and mixing volume were filled to approximately 350 Torr with UHP nitrogen.
6. The volume was isolated from the manifold which was then evacuated. The mixture was allowed to homogenize for one hour.
7. The mixture was reintroduced to the manifold, pressure recorded (allowing calculation of moles of nitrogen added in the previous step), and the two chambers were again isolated.
8. A small quantity of the mixture was injected into the tank via an isolated tee and the resulting pressure change in the manifold was noted. For some compounds, this step was repeated to obtain the desired tank mole fraction.
9. After all of the desired species were added, the tank was pressurized to about 400 psig with UHP nitrogen and weighed again.

This procedure relies on accurate measurements of the mixing manifold volume and pressure. These measurements contribute most to the uncertainty of the mole fraction of tank constituents. Other significant errors may have been introduced due to a small leak in the teflon valve used to connect the addition bulb with the manifold. The leak should not have signficantly effected concentrations of the more volatile liquids but may have been sufficient to contribute to bulb pressure as heavier hydrocarbons, particularly $>C_7$, were volatilized. (Leak rate, though very slow, was a function of differential pressure between atmospheric and internal bulb pressure). Another factor for certain

Table A.1 Manufacturers' listed purity of hydrocarbons introduced into standard tanks.

COMPOUND	PURITY (%)
myrcene	90
1-decene	94
3-carene	95
cyclopentane	95
γ-terpinene	95
limonene	97
cycloheptane	98
1-octene	98
α-pinene	98

hydrocarbons was the available purity levels. With the exception of those values noted in Table A.1, the stated manufacturer's purity was >99%.

Following Sprengnether (1992), we can formally estimate the mixing ratio uncertainty for each individual hydrocarbon in our standard by using the expression:

$$(\frac{\partial \chi_f}{\chi_f})^2 = (\frac{\partial \chi_i}{\chi_i})^2 + \frac{(\partial P_i)^2 + (\partial P_f)^2}{(P_i - P_f)^2} + (\frac{\partial V}{V})^2 + (\frac{\partial n}{n})^2 + (\frac{\partial T}{T}) \qquad \text{(A.1)}$$

where

χ_f = final molar mixing ratio of an individual hydrocarbon
χ_i = molar mixing ratio of hydrocarbon at stage one dilution
P_i = initial manifold pressure
P_f = final manifold pressure after addition to tank
V = manifold volume
n = mass of nitrogen added to tank
T = temperature

The first term on the right hand side of equation A.1 is the most complicated and also contributes the greatest uncertainty to our final mixing ratio assignment. This term can be expanded further yielding:

$$\left(\frac{\partial \chi_i}{\chi_i}\right) = \left(\frac{\partial P_a}{P_a}\right)^2 + \left(\frac{\partial P_b}{P_b}\right)^2 + \left(\frac{\partial T_a}{T_a}\right)^2 + \left(\frac{\partial T_b}{T_b}\right)^2$$

where the subscripts a and b refer to the initial measurements with only hydrocarbon in the bulb and final measurements after the addition of nitrogen. The pressure sensor used

Table A.2 Comparison of original and recalibrated mole fractions of NMHC in standard tanks 5199 and 5200 Percent deviation is calculated as the difference between original and new mole fraction (X) assignments divided by the original. The new values were obtained by using the average RMR of compounds through toluene based on standard analyses over a one year period.

Compound	Tank 5200			Tank 5199		
	original X assignment	*new X assignment*	*% Deviation*	*original X assignment*	*new X assignment*	*% Deviation*
Ethane	2.03E-06	2.28E-06	-12%	1.66E-06	1.78E-06	-7%
Ethene	1.78E-06	1.87E-06	-5%	2.29E-06	2.29E-06	0%
Propane	1.64E-06	1.77E-06	-8%	1.31E-06	1.40E-06	-7%
Propene	1.25E-06	1.25E-06	0%	1.05E-06	1.05E-06	0%
2-mepropane	8.71E-07	9.12E -07	-5%	9.30E-07	9.65E-07	-4%
Butane	8.68E-07	8.95E-07	-3%	9.04E-07	9.32E-07	-3%
t-2-Butene				5.26E-07	5.26E-07	0%
1-Butene	9.88E-07	9.83E-07	1%	9.82E-07	9.87E-07	0%
2-mePropene	9.56E-07	8.89E-07	7%	1.06E-06	9.82E-07	8%
c-2-Butene	5.51E-07	5.40E-07	2%	2.87E-07	2.84E-07	1%
Pentane	8.59E-07	8.88E-07	-3%	5.85E-07	6.18E-07	-6%
CycloPentane	5.41E-07	5.34E-07	1%	5.91E-07	5.70E-07	3%
1-Pentene	3.62E-07	3.71E-07	-2%	3.98E-07	4.14E-07	-4%
Cyclohexane	4.20E-07	3.98E-07	5%	4.58E-07	4.31E-07	6%
Hexane	3.11E-07	3.22E-07	-3%	3.20E-07	3.28E-07	-3%
Isoprene	4.58E-07	4.38E-07	4%	8.45E-07	7.96E-07	6%
1-Hexene	3.83E-07	3.84E-07	0%	3.86E-07	3.86E-07	0%
3-meHexane	2.34E-07	2.48E-07	-6%	2.55E-07	2.63E-07	-3%
Heptane	3.25E-07	3.32E-07	-2%	3.38E-07	3.43E-07	-1%
CycloHeptane	2.07E-07	1.81E-07	13%	2.09E-07	1.91E-07	9%
Benzene	2.97E-07	3.45E-07	-16%	3.14E-07	3.85E-07	-23%
1-Heptene	2.14E-07	2.16E-07	-1%	2.16E-07	2.13E-07	1%
Octane	1.84E-07	1.76E-07	5%	1.81E-07	1.69E-07	7%
cycloOctane	1.11E-07	9.71E-08	12%	1.27E-07	1.00E-07	21%
Toluene	2.64E-07	2.84E-07	7%	2.78E-07	2.50E-07	10%
1-Octene	2.48E-07	2.25E-07	9%	2.58E-07	2.23E-07	13%
Nonane	1.28E-07	1.06E-07	18%	1.31E-07	8.99E-08	32%
α-Pinene	1.45E-07	6.47E-08	55%	1.46E-07	7.28E-08	50%
1-Nonene	1.36E-07	1.22E-07	11%	1.53E-07	1.20E-07	21%
Camphene				2.64E-07	1.30E-07	51%
Carene	1.00E-07	5.01E-08	50%	1.04E-07	3.95E-08	62%
Decane	1.69E-07	1.13E-07	33%	1.76E-07	7.04E-08	60%
Sabinene	1.04E-07	3.27E-08	68%	1.57E-07	3.30E-08	79%
γ-Terpinene	1.08E-07	5.80E-08	46%	1.06E-07	3.86E-08	64%
Limonene	1.76E-07	1.23E-07	30%	1.89E-07	8.29E-08	56%
1-Decene	1.13E-07	9.48E-08	17%	1.33E-07	7.54E-08	43%
Myrcene	1.66E-07	3.46E-08	79%	1.77E-07	3.65E-08	79%
β-Pinene	5.20E-08	7.16E-08	-38%	4.21E-08	8.33E-08	-98%
Undecane	7.31E-08	3.97E-08	46%	8.08E-08	2.44E-08	70%

is rated for +/- 0.5 torr. The percentage error for the final pressure reading should be small (on the order of 0.2%) while that of the initial pressure measurement depends on the vapor pressure of the constituent. The percentage error for volatile compounds (C_2-C_5) is less than one percent. This error grows with increasing carbon number to roughly 3% for C_7 compounds and higher than 10% for some C_{10} species. The percentage error for all temperature terms should contribute less than 0.2%. The pressure drop measurements in A.1 may add as much as 2% error though for most compounds this term is 1% or less. Finally, manifold volume and nitrogen mass terms should both be significantly less than 1%. At best, preparative accuracy is expected to be 2% for the most volatile species and as poor as 15 % for the heavy hydrocarbons. Several of those species have the added error term from initial purity levels.

Based on this analysis we estimate error in the initial standard's mole fractions to be as high as 20-25% for some terpene species. In practice, using the Relative Molar Response Model (RMR), we can estimate errors in our initial NMHC mole fraction assignments within 10 %. Ackman (1968) defines relative molar response as:

$$RMR_i = 100 * C\#_i * \left(\frac{C\%_i}{C\%_{hept}}\right) \qquad \text{(A.2)}$$

where

$C\#_i$ = the carbon number of i
$C\%_i$ = the mass fraction of carbon in i
$C\%_{hept}$ = the mass fraction of carbon in heptane (0.839)

Table A.2 displays the original mole fraction assignments for standard tanks 5199 and 5200. Using RMR it was possible to check the relative assignments. This check is performed by mutiplying the moles of hydrocarbon sampled by its RMR factor and dividing by the area response from the chromatographic peak. If the model is obeyed, the values arrived at by this calculation for each species should be within 10%. Once we were convinced the light hydrocarbons followed RMR, adjustments to the heavier

hydrocarbons could be made. With the exception of benzene (and ethane for tank 5200), the original assignments agreed within 10% of the mole fraction predicted from RMR. The responses from runs performed over a year were averaged for each species in both tanks. The average of all species through toluene was taken, yielding a value of 4.63 x 10^{-14} and 4.71 x 10^{-14} (mole x RMR/Area) for tanks 5200 and 5199 respectively. This average response was then used to calculate the new mole fraction for each hydrocarbon in the tank. We simply multiplied this common factor by the area response for each species and then divided by the appropriate RMR factor to obtain the number of moles hydrocarbon injected. Since we also knew the total volume injected, we can determine the mole fraction in the sampled gas and tank. For the purposes of calibration, the original values were used with hydrocarbons having seven or fewer carbons and the new concentrations based on RMR were used for species with eight or more carbon atoms.

A.2 Permeation Devices

Permeation devices consist of a reservoir of pure compound separated from a dilution flow by a permeable membrane, in our case one made of Teflon. When the device is kept at a constant temperature, the concentration of compound in the dilution flow is controlled by the rate of dilution flow. At constant temperatures we expect that the vapor pressure of the compound, its solubility in Teflon, and its diffusion constant through the teflon are also constant. By measuring the mass loss of the permeation device, the permeation flow out of the device can be determined. Besides changing storage temperature, rate loss can be manipulated by varying the length and wall thickness of the teflon enclosure.

Two designs have been used in the past for permeation devices in our lab. The original design consisted of a stainless steel union filled with the desired liquid with a teflon tube running through. This allowed for permeation into the teflon tubing where the dilution flow passes. Many of these devices may be place in series so any number of constituents may be part of the standard. Unfortunately, difficulty in sealing the device leads to unwanted leaks, sometimes causing as much flow to the atmosphere as to the

dilution flow. Leaks of this type may be detected by enclosing the entire device (capping its ends) and passing a flow over the outside and analyzing the resulting flow. To eliminate this leakage problem, We used a Teflon reservoir capped at the ends. The devices were placed inside another container where the dilution flow passed through. This method guaranteed that all of the compounds lost from the device entered the dilution flow, but thorough, reproducible mixing may not occur. In practice, runs were reproducible providing the permeation tubes were left undisturbed for several hours at a constant permeation flow. The outward flow design also suffers from the constraint of the size of the enclosing volume, limiting the number of compounds which may be sampled at one time. We circumvented this issue by using multiple enclosures. This also allowed us to store the devices at different temperatures, enabling a comparable mole fraction to be achieved for species having from four to ten carbons without requiring extremely large variations in device size.

A distinct advantage of permeation devices is that they are easy to produce and maintain. The mass loss rate is essentially the only thing to be measured. The lighter compound permeation tubes generally need to be replaced every nine months to a year depending on the diffusion rate through the teflon. Some permeation tubes have lasted for 4 years and are still emitting at a constant rate. It is trivial to change the mixture and ratio of hydrocarbons sampled. This versatility enables one to tailor the calibration to the analysis at hand.

Errors in standard concentrations produced using permeation tubes are primarily a function of mass measurement uncertainties. With a Mettler balance (2×10^{-5} g sensitivity), a weekly mass loss of 2×10^{-4} g can be determined. This means for a compound of molecular weight 72, the lower limit of measurable loss rate is on the order of 1×10^{-5} cc per minute. Varying the dilution flow allows a range of concentrations of compounds to be produced. The mole fraction of the resulting standard is given by

$$X_i = \frac{(f_P + X_d f_d)}{f_P + f_d} \qquad \text{or} \qquad X_i \approx \frac{f_P}{f_d} + X_d \tag{A.3}$$

assuming that the dilution flow f_d is much greater than the permeation flow f_p. X_d represents the concentration of hydrocarbon present in the dilution gas. Using UHP Nitrogen, it is generally true that this term is less than 1% of the resultant dilution mole

Table B.1 This table summarizes the results of standard intercalibration runs performed from September 1994 through May 1997. Responses from the entire period for each compound are given as the average value RMR*mole HC/ area. The 95% column shows the the confidence limit in the mean response, calculated as 2*sigma/(sample number)$^{0.5}$.

	Tank 5200		Tank 5199		Tank 5125		Tank 5145		Perm Tubes		Yi Tang Tank	
# of samples	38		35		36		19		8		5	
Date range of samples	Sept. 1994-May 1996		Jan. 1995-May 1997		Sept. 1994-May 1996		June 1995-Nov. 1996		Sept. 1995-March 1996		July 1995	
Compound	Response 5200	95%	Response 5199	95%	Response 5125	95%	Response 5145	95%	Response PT	95%	Response Yi Tang	95%
Ethane	4.14E-14	1%	4.39E-14	4%	5.04E-14	2%	5.06E-14	5%			4.72E-14	1%
Ethene	4.41E-14	1%	4.71E-14	4%	5.39E-14	3%	5.51E-14	4%				
Propane	4.28E-14	1%	4.39E-14	3%	4.90E-14	2%	5.39E-14	4%			4.67E-14	1%
Propene	4.62E-14	1%	4.73E-14	3%	5.80E-14	2%					4.64E-14	1%
Cyclopropane					4.78E-14	3%	5.18E-14	8%				
2-mepropane	4.43E-14	1%	4.55E-14	3%	5.28E-14	3%	5.81E-14	9%			4.70E-14	1%
Butane	4.50E-14	1%	4.57E-14	3%	5.39E-14	3%	5.75E-14	9%			4.70E-14	1%
t-2-Butene			4.71E-14	3%	5.10E-14	3%	5.62E-14	9%			4.66E-14	1%
1-Butene	4.66E-14	1%	4.69E-14	3%							4.47E-14	1%
2-mePropene	4.99E-14	1%	5.11E-14	3%	5.66E-14	3%	6.21E-14	9%			4.66E-14	1%
c-2-Butene	4.73E-14	1%	4.76E-14	5%	5.60E-14	3%	6.09E-14	9%			4.81E-14	1%
2-meButane					5.40E-14	3%	5.61E-14	10%	4.77E-14	23%	5.60E-14	1%
Pentane	4.48E-14	2%	4.46E-14	4%	7.81E-14	3%	8.27E-14	9%	4.58E-14	8%	4.57E-14	2%
CycloPentane	4.70E-14	2%	4.88E-14	3%	6.80E-14	4%	7.99E-14	11%	5.26E-14	9%	5.19E-14	9%
1,3-Butadiene					5.85E-14	3%	5.94E-14	9%				
3-me-1-Butene					5.83E-14	3%	6.18E-14	10%			4.70E-14	1%
Cyclopentene					5.22E-14	10%	6.45E-14	9%				
t-2-pentene					5.75E-14	6%	5.94E-14	10%	4.40E-14	7%	4.79E-14	1%
1-Pentene	4.53E-14	1%	4.53E-14	3%	7.13E-14	7%			4.08E-14	11%	2.61E-14	1%

Compound	Response 5200	95%	Response 5199	95%	Response 5125	95%	Response 5145	95%	Response PT	95%	Response Yi Tang	95%
2-me-2-Butene					8.40E-14	4%	4.76E-14	9%			3.11E-14	1%
2-me-1-Butene					5.64E-14	3%	5.90E-14	10%	5.69E-14	0%	7.17E-14	1%
c-2-Pentene					5.81E-14	3%	5.87E-14	10%	4.82E-14	6%	3.74E-13	2%
2,2-dimebutane									5.13E-14	11%		
2-Butyne					5.84E-14	4%	6.36E-14	9%				
1,4-Pentadiene					7.43E-14	5%	9.13E-14	9%	5.10E-14	2%		
2,3-dimebutane									4.29E-14	24%		
2-me-pentane									3.91E-14	11%		
3-me-pentane									4.44E-14	5%		
Cyclohexane	4.90E-14	2%	5.01E-14	4%					4.84E-14	10%		
Hexane	4.49E-14	2%	4.59E-14	3%					4.66E-14	8%		
Isoprene	4.86E-14	1%	5.01E-14	4%	4.98E-14	3%	6.15E-14	9%	4.25E-14	8%		
cycloHexene									5.13E-14	0%		
1-Hexene	4.63E-14	2%	4.71E-14	3%	3.59E-14	12%	2.22E-14	28%	4.19E-14	16%		
2-Pentyne					7.84E-14	3%	8.46E-14	9%	4.87E-14	7%		
1-Pentyne					2.68E-14	3%	6.23E-14	10%	4.96E-14	6%		
3-meHexane	4.37E-14	2%	4.58E-14	9%					4.46E-14	9%		
Heptane	4.54E-14	3%	4.65E-14	5%					4.53E-14	6%		
CycloHeptane	5.30E-14	5%	5.17E-14	4%					5.14E-14	19%		
Benzene	3.99E-14	3%	3.85E-14	4%	6.62E-14	4%	6.84E-14	9%	5.36E-14	2%		
1-Heptene	4.61E-14	3%	4.78E-14	5%					4.45E-14	13%		
Octane	4.86E-14	6%	5.05E-14	5%					4.32E-14	7%		
cycloOctane	5.30E-14	9%	5.98E-14	10%								
Toluene	4.98E-14	6%	5.24E-14	7%	5.88E-14	7%	5.70E-14	10%	4.52E-14	5%		
Propyl Cyclohexane									4.28E-14	7%		
1-Octene	5.11E-14	5%	5.44E-14	6%								
Nonane	5.63E-14	11%	6.89E-14	12%					4.23E-14	9%		
α-Pinene	1.04E-13	9%	9.44E-14	10%					4.46E-14	15%		
EthylBenzene									4.69E-14	11%		
p-Xylene									4.55E-14	12%		
1-Nonene	5.19E-14	11%	6.00E-14	16%								
Camphene			9.60E-14	13%					6.11E-14	35%		
o-Xylene									4.81E-14	12%		
Carene	9.25E-14	17%	1.24E-13	19%					4.63E-14	8%		
Decane	6.96E-14	17%	1.18E-13	20%					3 83E-14	7%		
Sabinene	1.47E-13	14%	2.25E-13	21%					5.01E-14	53%		
γ-Terpinene	8.63E-14	18%	1.29E-13	26%					4.48E-14	9%		
Limonene	6.65E-14	18%	1.07E-13	22%					4 61E-14	10%		
1-Decene	5.57E-14	32%	8.29E-14	22%								
Myrcene	2.22E-13	16%	2.28E-13	17%								
β-Pinene	3.37E-14	9%	2.38E-14	10%								
Undecane	8.54E-14	19%	1.56E-13	29%								
α-terpinene									6.17E-14	22%		
Average up to Toluene	4.64E-14		4.76E-14		5.77E-14		6.10E-14		4.70E-14		4.78E-14	
Average all	6.04E-14		7.08E-14						4.72E-14		6.51E-14	

The average response of all species for each calibration standard is given in the final row. These values are somewhat higher due to the inclusion of the heavier hydrocarbons. The original calibration scale, which in general had incorrect mole fractions for heavier hydrocarbons, was used in the production of the average responses, yielding response factors well above the average. A more appropriate average was taken using species up through toluene for the first four tanks. The Yi Tang average listed in that column does not include the final four species. Note the average for the permeation tubes is essentially the same for both. This lends credence to the belief that heavy hydrocarbons from tanks 5199 and 5200 have misassigned mole fractions.

fraction. From Donahue (1991), uncertainty can be estimated as:

$$(\partial \ln(X))^2 = (\partial \ln(f_p))^2 + (\partial \ln(fd))^2 + \frac{(\partial Xd)^2}{X^2} \qquad \text{(A.4)}$$

where

$\partial \ln(f_p)$= percentage uncertainty in permeation flow
$\partial \ln(f_d)$= percentage uncertainty in the dilution flow
∂X_d = uncertainty of the contamination level in the dilution gas

Dilution flow is known to better than one percent using mass flow controllers and generally the dilution gas contamination term X_1 is much less than one percent of the actual hydrocarbon mole fractions for UHP N_2 (at most a few ppt). The permeation flow term varies depending on the tube in question. In general, the mass loss rate of our tubes is so great that the percentage uncertainty is no more than one percent. By this analysis, our expected uncertainty for mole fractions in the standard (on the order of 100 ppb) is less than two percent.

B. Standard Intercomparison

B.1 Internal Intercomparison

Our laboratory produced two sets of NMHC standard tanks and maintained a collection of permeation tubes for calibration while I was at MIT. In 1991 tanks 5125 and 5145 were made for the MAGE II field campaign. These tanks contain 28 and 29 hydrocarbons from ethane to toluene. Tanks 5199 and 5200 were made with 39 and 37 species respectively, including eight terpenes and undecane. Fourteen species are in common. For the purposes of this intercomparison, data exists for 39 permeation tubes. Five tubes are common with all four standard tanks and nine are not present in any. In total, we have sixty-four distinct species represented. An additional set of samples was taken from a tank produced prior to my tenure at MIT.

Remarkably, the intercomparisons agree well. Table B.1 summarizes information about the intercomparison. The total number of samples and the sampling time span are listed along with the average RMR*mol HC/area response for each hydrocarbon present in the tanks and permeation tubes. At the bottom of the table, two average values of this response are given, first the best average, which includes compounds from ethane through toluene for all sample types with the exception of the "Yi Tang" tank, where the last four outlier species are removed. The other row shows the true average of all species represented. Since the two permeation tube averages showed no real difference, it was deemed that RMR yields good results over the entire carbon range we consider. Based on this observation, it seemed reasonable that the heavier hydrocarbon mole fractions in tanks 5199 and 5200 were assigned incorrectly. This result is not entirely unexpected based on our error analysis for standard tank production, though the error in mole fraction assignment for some species is outside the bounds that we predicted. Recalibration of those compounds was shown in Table A.2.

B.2 External Intercomparison.

The Nonmethane Hydrocarbon Intercomparison Experiment (NOMHICE) (Apel and Calvert, 1994) was begun in an effort to evaluate the consistency of NMHC analysis results around the globe. The National Center for Atmospheric Research (NCAR) serves as the referee laboratory and prepared several tasks for the participating research groups. Each laboratory was expected to analyze the tank for a given task using its particular detection and calibration system. Our lab performed relatively well in comparison to other labs. One important observation to be made in this experiment is that many researchers use the same National Institute of Standards (NIST) traceable standards in their analyses as used at NCAR whereas our lab prepares our own standard gases.

An example of our performance is shown in Table B.2. Analysis was performed by Dr. Xian Shi using tank 5145 as a standard. The second and third columns give the NCAR analysis for mole fraction in the phase 3 tank, the second column measured

before the tank left their lab and the third upon its return from our analysis. As can be seen, there is very little change in these two measurements. The fourth column gives our results, which are generally higher than those of NCAR; the average percent difference defined as ((NCAR-Our result)/NCAR) of the fifteen compounds is 13.29 and 12.51 for before and after. Before refers to the initial analysis performed at NCAR before sending the tank to our laboratory and after is their analysis upon return of the sample tank. The next two columns give values for the response factors as caluclated with RMR (mole HC*RMR/Area) of standard tanks 5145 and 5199. By taking the response ratios (5199/5145), which on average are 25% higher for tank 5145, and multiplying by the value obtained in Shi's analysis, we can estimate the mole fraction that would have been reported had tank 5199 been used. This value is in the seventh column. The percent differences for recalibration using tank 5199 on average (shown in the final two columns) are a little closer to NCAR values than those obtained with tank 5145. Agreement is better for the light hydrocarbons and isoprene specifically and poorer for the butenes

Table B.2 Phase 3 NOMHICE results comparing our original reported values and recalibrated values calculated using the response ratio from tanks 5145 and 5199. Concentrations listed are in ppbv. The percent difference is calculated as (NCAR result - our result) / (NCAR result). Before and after refer to NCAR's initial analysis before sending the tank and the analysis upon return of the tank. The percent difference is comparing our mole fraction assignment to NCAR's before and after assignments.

Compound	NCAR Before	NCAR After	Shi values with 5145	Response 5145	Response 5199	5199 value	% diff Before	% diff After
Ethane	10.20	10.57	11.52	5.06E-14	4.39E-14	9.99	-2.04	-5.47
Ethene	18.22	19.49	20.94	5.51E-14	4.71E-14	17.90	-1.78	-8.18
Propane	25.29	25.51	31.50	5.39E-14	4.39E-14	25.66	1.46	0.59
Propene	9.59	9.76	11.94	5.52E-14	4.73E-14	10.23	6.64	4.78
2-mePropane	20.28	20.43	22.02	5.81E-14	4.55E-14	17.23	-15.02	-15.64
Butane	30.91	31.17	36.06	5.75E-14	4.57E-14	28.68	-7.23	-8.00
t-2-Butene	9.58	9.62	9.84	5.62E-14	4.71E-14	8.25	-13.84	-14.20
1-Butene	9.39	9.48	10.26	5.62E-14	4.69E-14	8.56	-8.81	-9.68
2-mePropene	9.95	10.07	10.92	6.21E-14	5.11E-14	8.98	-9.80	-10.87
c-2-Butene	7.66	7.69	7.38	6.09E-14	4.76E-14	5.77	-24.67	-24.96
Pentane	12.52	12.62	18.18	8.27E-14	4.46E-14	9.81	-21.63	-22.25
CycloPentane	4.20	4.23	4.73	7.99E-14	4.88E-14	2.89	-31.16	-31.65
Isoprene	5.76	5.24	6.48	6.15E-14	5.01E-14	5.27	-8.44	0.65
Benzene	8.73	8.80	8.46	6.84E-14	5.24E-14	6.48	-25.81	-26.40
Toluene	5.36	5.39	6.00	5.70E-14	5.24E-14	5.52	2.89	2.32

and benzene. One observation can be made about tank 5145 from this table. Using RMR, it would appear that pentane and cyclopentane may have incorrect mole fraction assignments. The response factor for both species is around 8E-14 whereas that for the other hydrocarbons is closer to 6E-14. If you were to use the average response (5.79E-14) of the other compounds in the tank to calibrate, the concentrations would be 12.73 and 3.43 ppbv for pentane and cyclopentane. These numbers are obtained by multiplying the reported value of Shi by the average response and dividing by the reported response factor for pentane and cyclopentane in the response 5145 column. The pentane result is within 1% of NCAR in that case, which is a great improvement in agreement over the actual reported value. However, cyclopentane then would have a negative 19% difference, which is somewhat worse than the 12% difference using the original calibration.

Multiplication of our reported concentrations by the ratios given in Table B.3 converts them to the NCAR (NIST) scale. Those species not represented in the Table

Table B.3 The ratio of NCAR (NIST) to Dinghushan (Tank 5199) concentrations obtained from Phase 3 of NOMHICE. Multiplication of the ratio by reported concentrations in this thesis will convert the mole fraction to the NCAR calibration scale. The mean value may be used to convert species not listed in the Table. This conversion relies on relative molar responses obtained from analysis of MIT standard tanks 5145 and 5199 as summarized in Table B.3.

compound	NCAR/Dinghushan
Ethane	1.04
Ethene	1.05
Propane	0.99
Propene	0.95
2-mepropane	1.18
Butane	1.08
t-2-Butene	1.16
1-Butene	1.10
2-mePropene	1.12
c-2-Butene	1.33
Pentane	1.28
CycloPentane	1.46
Isoprene	1.04
Benzene	1.35
Toluene	0.97
mean	1.14
St. Deviation	0.15

can be multiplied by the mean value. Note that this conversion is at best accurate to ± 15% as that is the variation in the molar response for Tank 5145. This is reflected in the standard deviation for the converstion ratios.

C. Standard Stability

From September 1994 through May 1996, Tank 5200 analyses were performed on the HP-5890a to monitor standard stability and instrumental performance. Thirty-seven measurements were taken on eight different days. All but one were made over the course of the first year, in groups of three to seven reproducible runs. The final analysis occurred in May 1996 just prior to departure for China to show that no significant change in detector response had occurred over the preceding eight months assuming the tank concentrations did not vary. If we make the assumption that detector response did not change, then we can say that no appreciable changes in tank mole fractions occurred for the lighter compounds. It seems unlikely that both detector response and constituent concentrations would have moved in a similar manner, resulting in consistent results. Table C.1 shows the confidence limits for each compound in standard 5200. As can be seen from the table, in general, light NMHC show a more stable area response. Essentially, the results in the Table give a rough measure of precision for our analysis over the period. Variations in integration, separation and peak widths lead to lower precision for the heavier hydrocarbons. On the analysis system, the four peaks from sabinene to 1-decene experience incomplete separation, causing heightened variability in the peak area assigment. Retention time also influenced peak area. Later eluting (heavier) compounds were subject to more deviation and broader peaks. Over the testing period, response to ethane changed on the order of 1%. The variation in the heaviest species is more pronounced. Despite the low precision for those compounds, we can show that the average variation from year to year is not as large by looking at information from all four standard tanks. Figure C.1 displays the trends of area ratios of individual species to ethane over time. An advantage of this comparison is that we may ignore drift in the

instrument response (assuming that such drift affects each species in the same way). We also eliminate uncertainty arising from volume calculations since each ratio arises from an individual run. In Table C.1 we normalized the area responses as some run volumes were different from others, but uncertainty in collected volume could still affect results. Table C.2 gives the percent annual change obtained from the linear fit to the curves in Figure C.1.

Variations in standard tank concentrations are negligible over the two week time span of our in situ measurements. For the flask measurements, performed over one year, we expect variations in standard concentrations to account for less than two percent of error in mole fraction assignments for all reported species with the exception of toluene (within 6%) and α-pinene (within 5%).

Table C.1 Results from the analysis of standard tank 5200 from September 1994 through May 1996. The first three months contain 19 runs and the 20 month span has 38 data points. Shown are the 95% confidence limits for the area response normalized to a one scc injection volume.

Compound	*first 3 months (+/-)*	*21 month span (+/-)*
Ethane	1.1%	1.4%
Ethene	0.9%	1.3%
Propane	1.4%	1.2%
Propene	0.9%	1.1%
2-mepropane	1.1%	1.2%
Butane	1.2%	1.3%
1-Butene	0.9%	1.1%
2-mePropene	1.1%	1.2%
c-2-Butene	1.2%	1.3%
Pentane	1.2%	1.9%
CycloPentane	1.6%	1.6%
1-Pentene	1.3%	1.5%
Cyclohexane	1.6%	2.2%
Hexane	1.0%	1.8%
Isoprene	1.1%	1.5%
1-Hexene	1.1%	1.8%
3-meHexane	1.2%	2.4%
Heptane	1.2%	3.0%
CycloHeptane	1.3%	4.5%
Benzene	1.2%	2.9%
1-Heptene	1.3%	2.7%
Octane	1.7%	5.8%
cycloOctane	4.8%	9.2%
Toluene	2.3%	6.1%
1-Octene	1.7%	5.2%
Nonane	4.0%	10.9%
α-Pinene	5.1%	9.0%
1-Nonene	3.6%	10.7%
Carene	8.8%	16.4%
Decane	10.3%	16.6%
Sabinene	12.6%	13.8%
γ-Terpinene	11.6%	17.8%
Limonene	11.1%	18.2%
1-Decene	9.2%	31.6%
Myrcene	26.3%	15.7%
β-Pinene	13.5%	11.5%
Undecane	27.4%	22.3%

Table C.2 Regression line slopes from Figure C.1

Compound	*% annual change*			
	Tank 5199	Tank 5200	Tank 5125	Tank 5154
Ethene	0.51	0.20	-1.59	-3.78
Propane	-1.92	1.67	-0.84	-4.30
Propene	-0.64	0.54	-3.52	0.00
cycloPropane			-8.73	-15.31
2-mePropane	-1.18	0.25	-8.05	-12.77
Butane	-1.27	0.55	-8.84	-13.26
t-2-Butene	-0.60		-8.36	-13.69
1-Butene	-1.21	-1.16		
2-mePropene	-1.17	0.26	-7.33	-10.52
c-2-Butene	-0.29	0.82	-7.91	-10.09
2-meButane			-2.63	-4.85
Pentane	-1.85	0.87	-6.06	-3.84
cycloPentane	-1.24	0.33	-3.90	-7.49
1,3-Butadiene			-2.55	-3.33
3-me-1-Butene			-8.25	-12.33
cycloPentene			-12.22	-1.54
t-2-Pentene			7.49	-3.17
1-Pentene	-0.61	0.82		
2-me-2-Butene			-16.39	-40.84
2-me-1-Butene			-1.25	2.80
c-2-Pentene			-0.76	-1.31
2-Butyne			-10.75	-9.75
1,4-Pentadiene			-2.98	-37.14
cyclohexane	-1.27	0.01		
Hexane	-0.72	-2.27		
Isoprene	-1.86	1.43	0.20	-0.33
1-Hexene	-0.69	0.47	-8.69	-6.31
2-Pentyne			-1.29	-2.95
1-Pentyne			-6.79	-6.58
3-meHexane	-1.34	-0.39		
Heptane	-1.24	0.18		
CycloHeptane	0.50	-0.87		
Benzene	2.40	2.17	-3.52	-3.44
1-Heptene	-0.79	0.24		
Octane	-0.59	-0.88		
cycloOctane	5.67	-0.88		
Toluene	-6.35	2.08	1.66	-0.61
1-Octene	-1.03	-1.17		
Nonane	-0.33	-1.42		
α-Pinene	-4.95	-2.10		
1-Nonene	-1.50	-2.12		
Camphene	-0.76	0.00		
Carene	-1.06	-1.23		
Decane	-1.73	-1.00		
Sabinene	-0.67	-2.80		
γ-Terpinene	5.08	5.66		
Limonene	-1.49	2.18		
1-Decene	-11.13	1.45		
Myrcene	-4.63	7.44		
Undecane	-17.84	24.12		

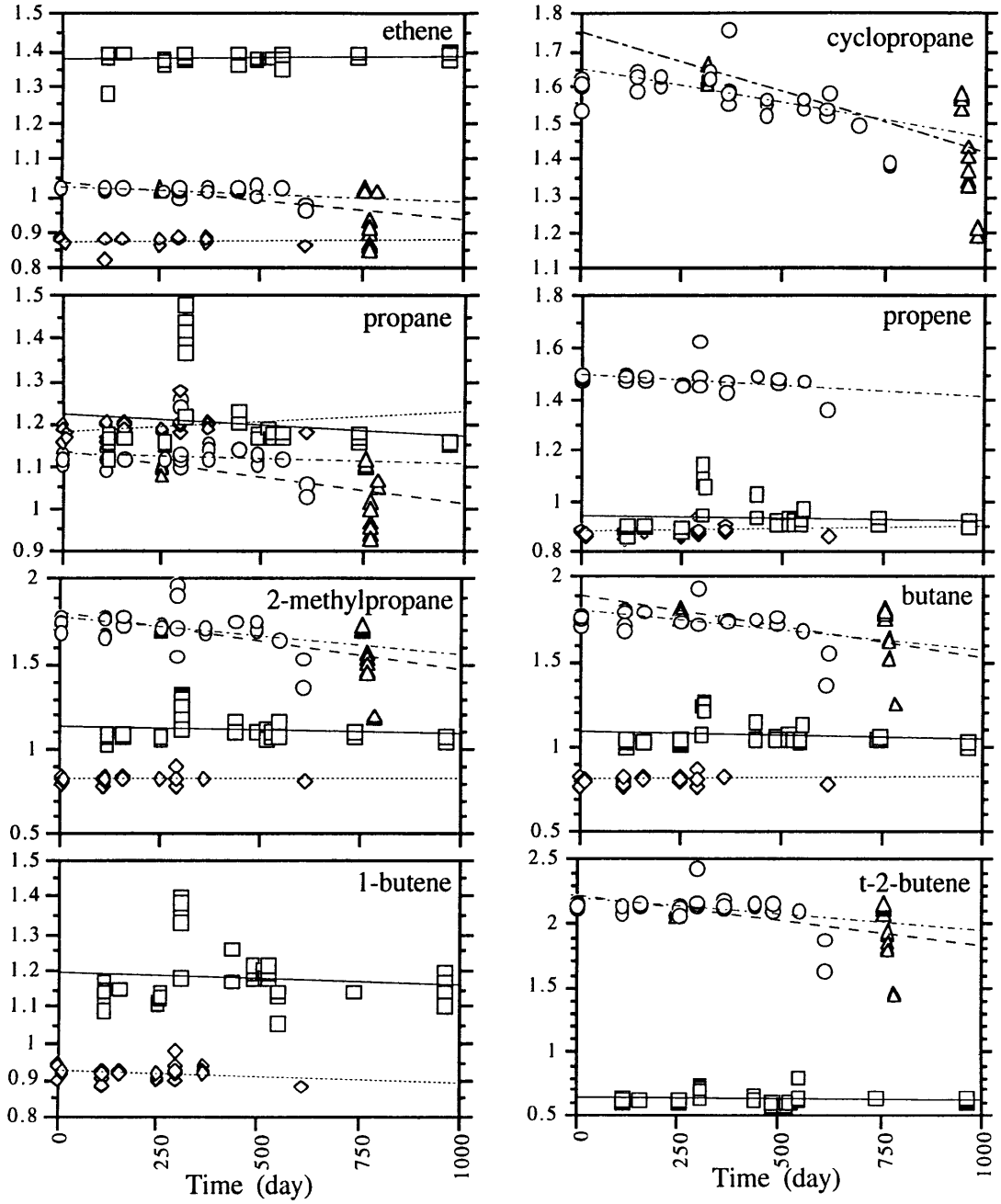

Figure C.1 Shown are peak area ratios of individual hydrocarbon to ethane over the period October 1994 to May 1997. Analyses of four standard tanks were performed on the HP-5890a GC. Symbol and trendline legend is below. The unit of the x-axis is given in days.

Tank 5199

Tank 5200

Tank 5125

Tank 5145

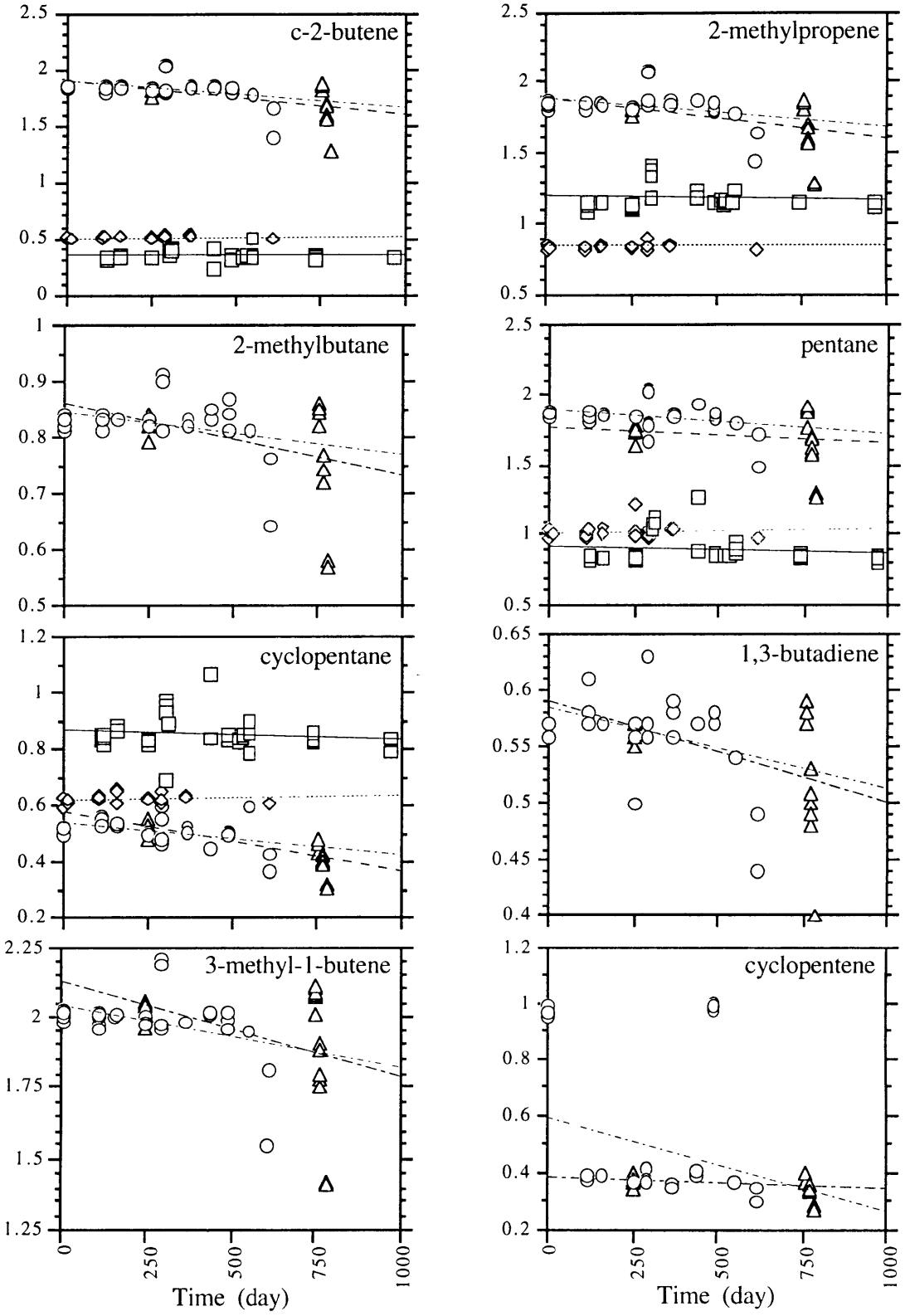
c-2-butene
2-methylpropene
2-methylbutane
pentane
cyclopentane
1,3-butadiene
3-methyl-1-butene
cyclopentene
Time (day)
Time (day)

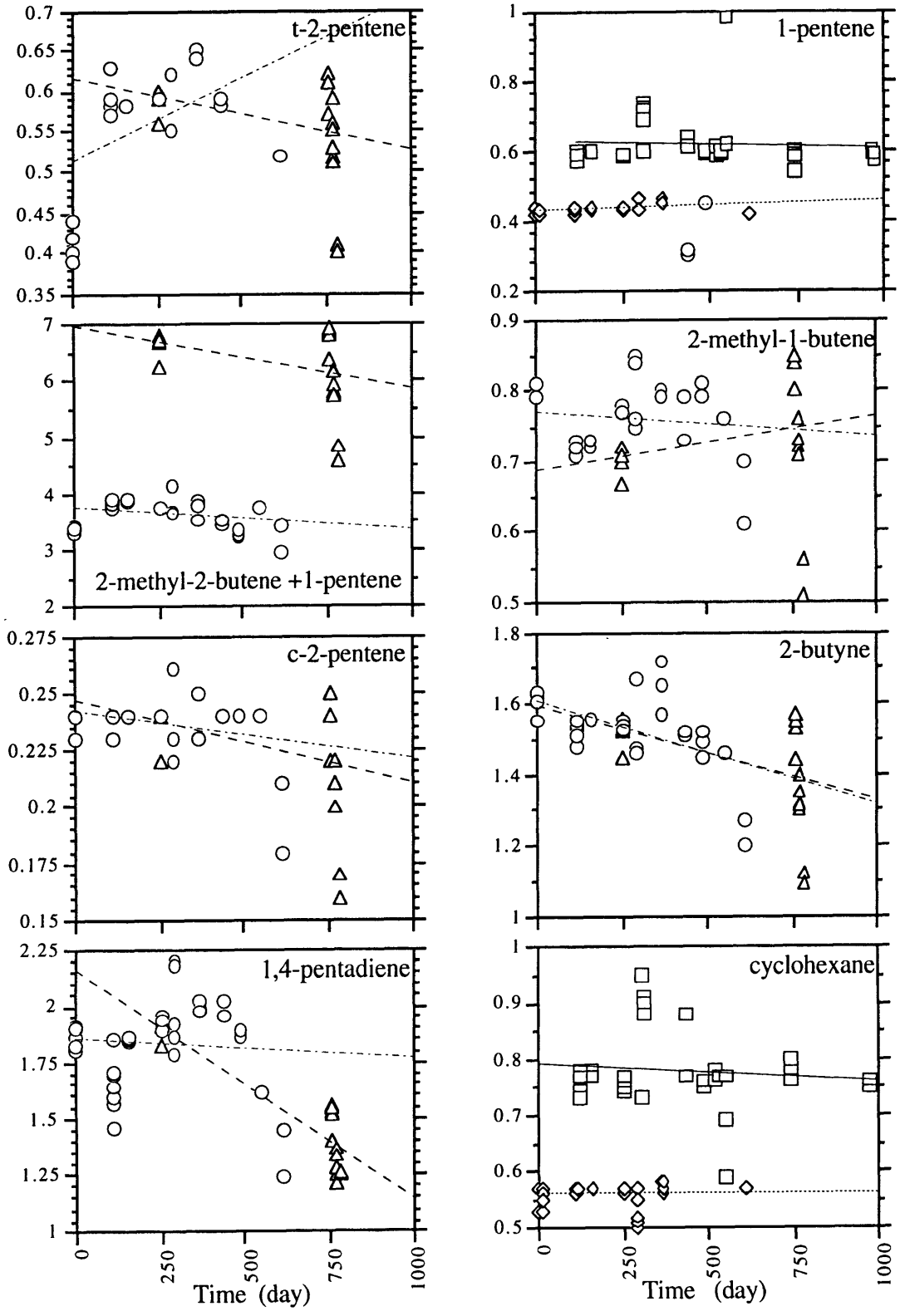
t-2-pentene
1-pentene
2-methyl-2-butene +1-pentene
2-methyl-1-butene
c-2-pentene
2-butyne
1,4-pentadiene
cyclohexane
Time (day)
Time (day)

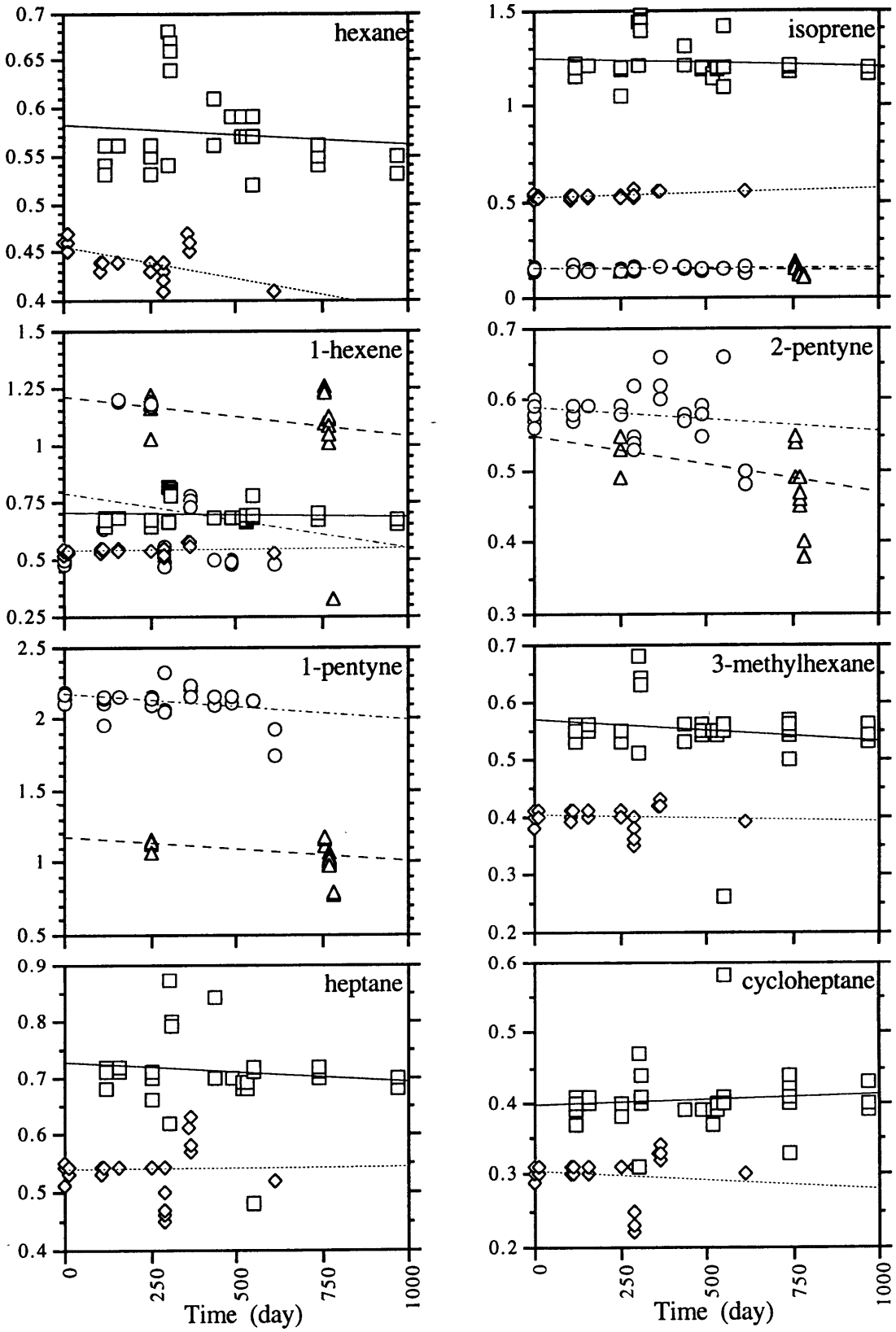
hexane
isoprene
1-hexene
2-pentyne
1-pentyne
3-methylhexane
heptane
cycloheptane
Time (day)
Time (day)

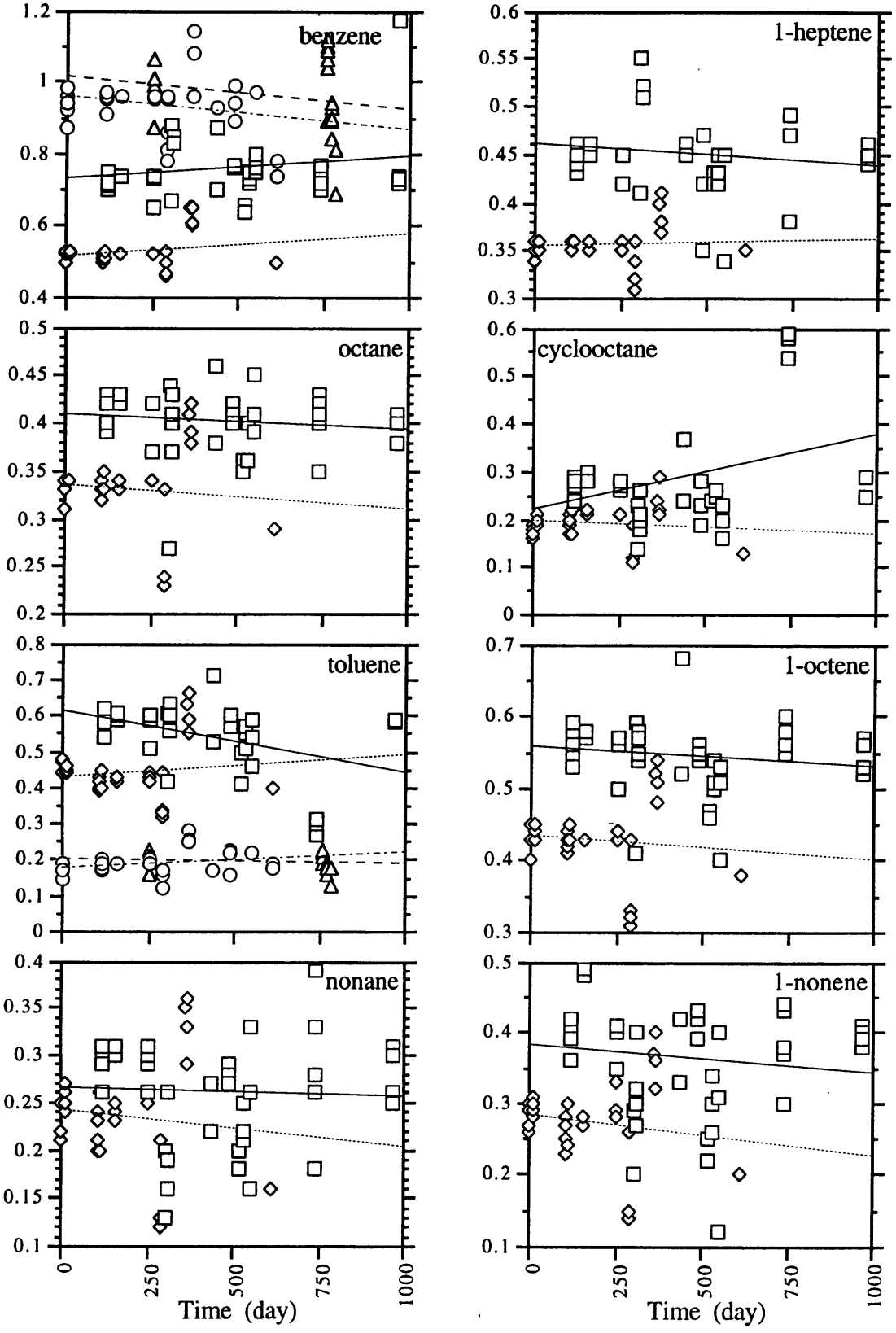
benzene
1-heptene
octane
cyclooctane
toluene
1-octene
nonane
1-nonene
Time (day)
Time (day)

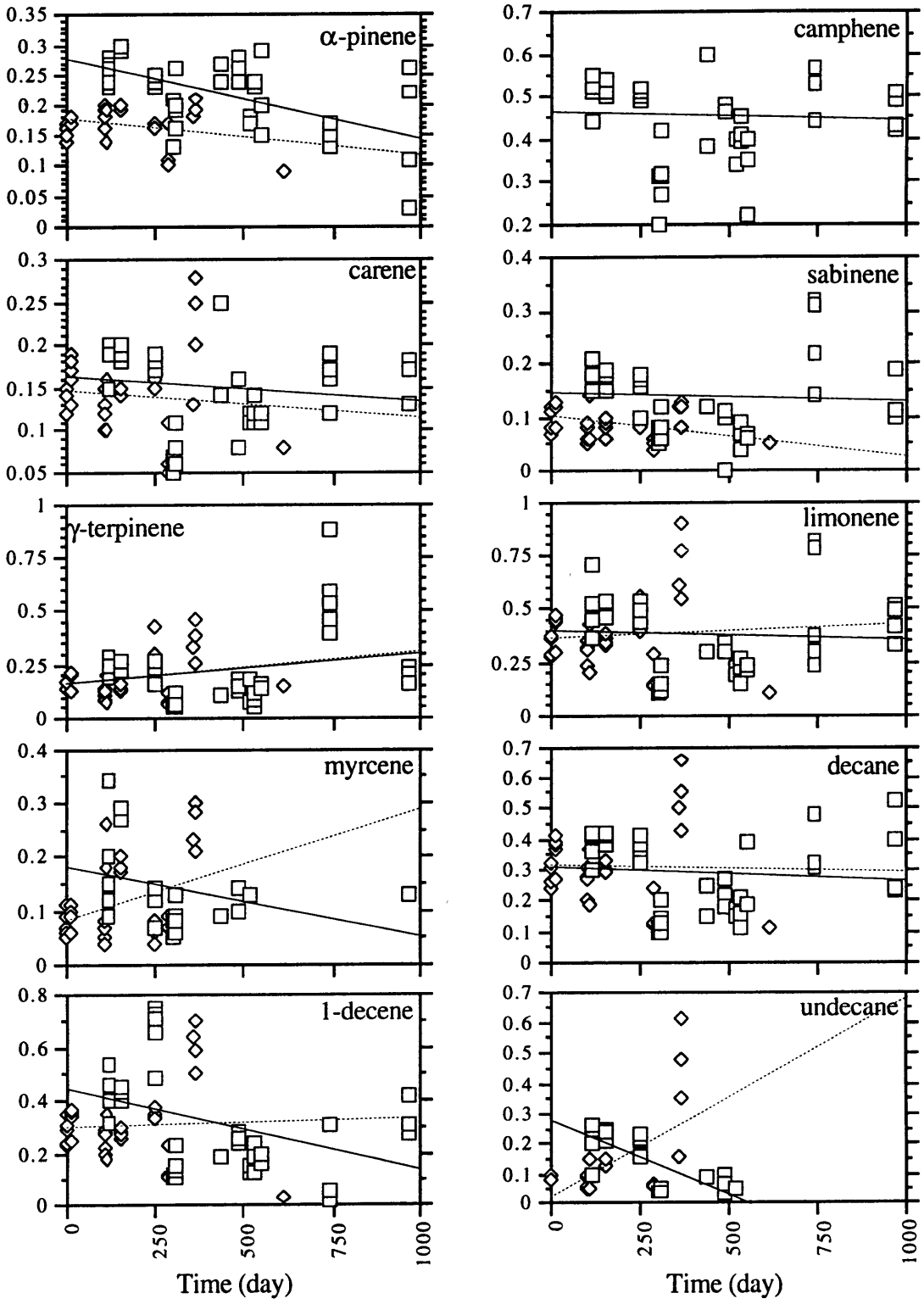
α-pinene
camphene
carene
sabinene
γ-terpinene
limonene
myrcene
decane
1-decene
undecane
Time (day)
Time (day)

5697 - 73